Spring 1993

Hydrodynamic studies of the flow of fine particles through a fluidized dense bed of coarse solids

Jaideep Talukdar
University of New Hampshire, Durham

Order Number 9400400

Hydrodynamic studies of the flow of fine particles through a fluidized dense bed of coarse solids

Talukdar, Jaideep, Ph.D.

University of New Hampshire, 1993

U·M·I
300 N. Zeeb Rd.
Ann Arbor, MI 48106

HYDRODYNAMIC STUDIES OF THE FLOW OF FINE PARTICLES THROUGH A FLUIDIZED DENSE BED OF COARSE SOLIDS

BY

Jaideep Talukdar

B.Tech(Hons.), I.I.T. Kharagpur(India), 1983
M.S., University of New Hampshire, 1987.

A DISSERTATION

Submitted to the University of New Hampshire
in Partial Fulfillment of
the Requirements for the Degree of

Doctor of Philosophy

in

Engineering

May, 1993

This dissertation has been examined and approved.

Virendra K. Mathur

Dissertation Director, Dr. Virendra K. Mathur
Professor of Chemical Engineering

Stephen S.T. Fan

Dr. Stephen S.T. Fan
Professor and Chairman,
Department of Chemical Engineering

Arthur H. Copeland Jr.

Dr. Arthur H. Copeland, Jr.,
Professor of Mathematics

Russell T. Carr

Dr. Russell T. Carr
Associate Professor of Chemical Engineering

Ronald W. Breault

Dr. Ronald W. Breault, Senior Program Manager
Tecogen Inc., Massachusetts.

Dec. 16, 1992

Date

DEDICATED TO MY PARENTS

ACKNOWLEDEGMENTS

The completion of this dissertation was made possible due to the support and guidance of many individuals. While I will not endeavour to acknowledge each and every one of them, I will take this opportunity to express my gratitude to those who were the most instrumental. Dr. V.K. Mathur, the chairman of my committee, has been a guiding influence throughout my graduate studies and I extend my special thanks to him. I also extend thanks to Dr. S.S.T. Fan, Dr. A.H. Copeland, Dr. R.T. Carr and Dr. R.W. Breault for being on my dissertation committee and their helpful suggestions for the improvement of this dissertation. I thank Mr. J. Newell for his help and assistance with a variety of experimental rigs that had to be fabricated at UNH.

I would take this opportunity to thank some of my friends who have contributed to the completion of my dissertation. Their help and support was constant and unwavering over a period of four years. Ms. D. Seiken, Mr. G. Schrager, Ms. H. Buckland, Mr. S. Nagarjuna and Mr. V. Chidgopkar, to name a few, were all involved in this work in some capacity. I extend my heartfelt thanks to their support and I know that this dissertation would not have been completed without their help.

Finally, I would like to thank Riley Stoker Corporation of Worcester, Massachusetts, for funding this research study and also for giving me an opportunity to work with the industry.

Table of Contents

List of Tables

List of Figures

ABSTRACT

HYDRODYNAMIC STUDIES OF THE FLOW OF FINE PARTICLES
THROUGH A FLUIDIZED DENSE BED OF COARSE SOLIDS

by

Jaideep Talukdar
University of New Hampshire, May, 1993

Circulating fluidized bed systems are steadily gaining popularity in the combustion industry. Particular designs, with what appears to be inconsequential differences, have exhibited wide performance variations from SO_2 capture efficiency to carbon burnout. A leading cause of these discrepancies is the lack of fundamental understanding of the hydrodynamics of such systems. This study explains the hydrodynamics of one such CFB system, the Battelle Multi-Solids Fluidized Bed System (MSFB). It consists of a circulating fluidized bed of fine particles superimposed on a bubbling bed of coarse solids.

One way to characterize such a system is to describe the mechanism of gas-solid flow through the bed. The gas flow in systems like these is through bubbles or slugs (regions of voids containing little or no solids). Bubbles are typically characterized by their size (length or diameter), their rise velocity, and their frequency. As part of the initial phase of experimentation, an attempt is made to visually observe bubble phenomena.

Another task of the initial phase of this study is to characterize an L-valve, a solids-recirculating device commonly used in an MSFB. Solids fractions and total pressures near the bend of an L-valve are measured as a function of solids mass fluxes.

Next , the mechanism of fine particle movement through a bubbling region of coarse fluidized solids is studied in considerable detail. Bubble characteristics are studied in a variety of systems of coarse particles with fines passing through at high velocity.

Amongst numerous optical, electrical and other techniques available for the study of the passage of bubbles, the pressure fluctuation technique is the most robust. In this investigation, pressure probes are connected to pressure transducers which are in turn linked to an on-line data acquisition system supported on a microcomputer. A commercially available software package (Notebook) is used to sample pressure at specified points in the fluidized bed at extremely fast rates, of up to 200 Hz. This resulted in pressure-time traces which are analysed to give bubble length, bubble rise velocity, and bubble frequency. The experimentation is done in two bench scale units at the university and a small pilot plant scale model in the industry.

Another important objective of this study is to estimate the fine particle residence time in the dense bed section. A defluidization technique is utilized in experimentally measuring the solids holdup in the dense bed.

A mathematical model is developed from first principles, based on a momentum balance on the fine particles. An empirical correlation is also developed, so that the residence time of fine particles may be predicted for any fine particle- coarse particle system, based on system dependent parameters. The model is in fair agreement with experimental data.

The 'gross' or macroscopic aspects of an MSFB are also investigated. These include pressure drop in the dense bed of coarse particles, dense bed height and dense bed voidage variation, with the passage of fines.

Chapter 1

INTRODUCTION

From the time circulating systems gained popularity with catalyzed gas phase reactions, like catalytic cracking of heavier petroleum products to produce gasoline, enormous advances in such systems have been made. The circulating fluidized bed technology has made inroads into the combustion industry since the late 1970s, and appears to have excellent prospects in the future. The success of the circulating fluidized bed (CFB) boiler is due to the many advantages it offers over conventional bubbling fluidized beds and pulverized combustors. Among them are its superior carbon burn-out efficiency, a lowered temperature operation resulting in less nitrogen oxide emissions, efficient capture of sulfur oxides, excellent turn-down capabilities, and its ability to burn a variety of fuels. These factors have led to many competing designs of circulating fluidized bed coal combustors each operating on the same basic principles and yet having some unique features.

As with any technology, the industry has rapidly forged ahead in the manufacture and operation of CFB coal combustors. However there is lack of understanding of fundamental hydrodynamic and heat transfer phenomena. This weakness in knowledge manifests itself in scale-up, from pilot plant operation to a full scale combustor. For example, the carbon efficiency may be lower in a larger unit than an smaller sized prototype plant, due to the use of improper scaling parameters. Unlike bubbling fluidized beds which are well understood, CFBs are relatively new, and their behavior and operation need further study. Most of the problems in CFB operation stem from a lack of understanding of fundamental hydrodynamic and associated heat transfer phenomena. Prediction of regimes of flow, of

the mixing of gas and solids and of heat transfer coefficents thus becomes considerably more difficult. Fairly extensive work over the last decade on the hydrodynamics of CFBs have been performed, enabling us to better understand the movement of gas and solids in the riser, the solids recirculating devices, and the mechanics of flow in the standpipe. Pneumatic conveying experience has been utilized to analyze the phenomena of choking, and the distribution of gas and solids in the riser. Still, considerable work on the fundamental transport mechanisms need to be done before a more complete understanding of the behavior of CFBs emerges.

As mentioned earlier, boiler manufacturers worldwide have joined in the race for finding efficient coal burning CFB systems. The major manufacturers are Ahlstrom/Pyropower of Finland, Lurgi (Germany), Studsvik of Sweden and Keeler/ Dorr-Oliver and Battelle in the USA (Figs.1.1,1.2). The Battelle system has been licensed by companies like Senior Greens, Riley Stoker , and Mitsui of Japan. The systems mentioned above other than Battelle all employ conventional CFB technology. This consists of a bed of fast moving solids in the lean phase in the riser section, a gas-solids separation system, a standpipe containing a very large part of the solids inventory, and a solids recirculting device. The Battelle technology utilizes a multi-solids fluidized bed (MSFB) design, with a dense bed of bubbling inert materials superimposed on a circulating bed of fine particles. This dense bed acts as a resistance to the fast-moving circulating coal particles, slowing them down by the repeated collisions and friction. This allows for increased residence times of the fines resulting in more complete combustion. The Battelle MSFB is a special case of the CFB systems. Understanding the hydrodynamics of this system was the primary objective of this study, with particular emphasis on the bubbling (dense) bed region of the combustor.

The hydrodynamic behavior of any fluidized bed may be viewed and analyzed from a gross (or macroscopic) viewpoint and a fine (or microscopic) scale. The gross behavior of a fluidized bed is characterized by the pressure drop across the bed, the average bed voidage, and the bed expansion. The fine behavior of the bed is typically an analysis of

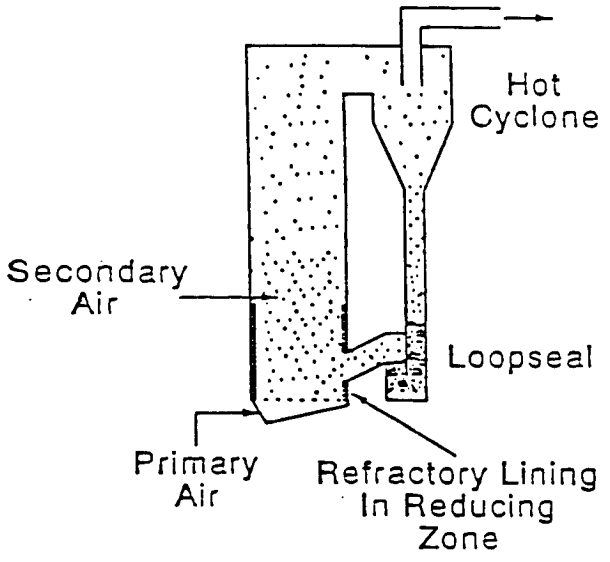

Ahlstrom CFB boiler.

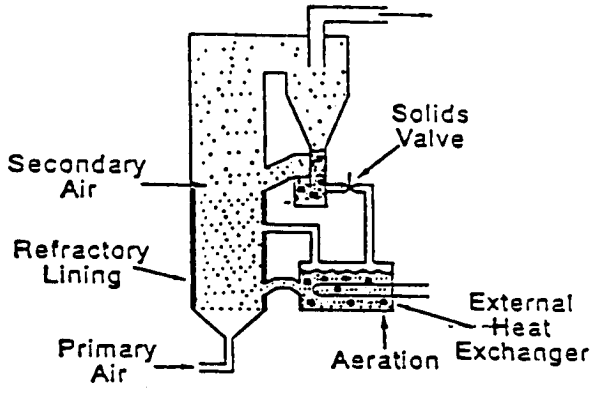

Lurgi CFB system.

Figure 1.1: The Ahlstrom and Lurgi CFB Systems

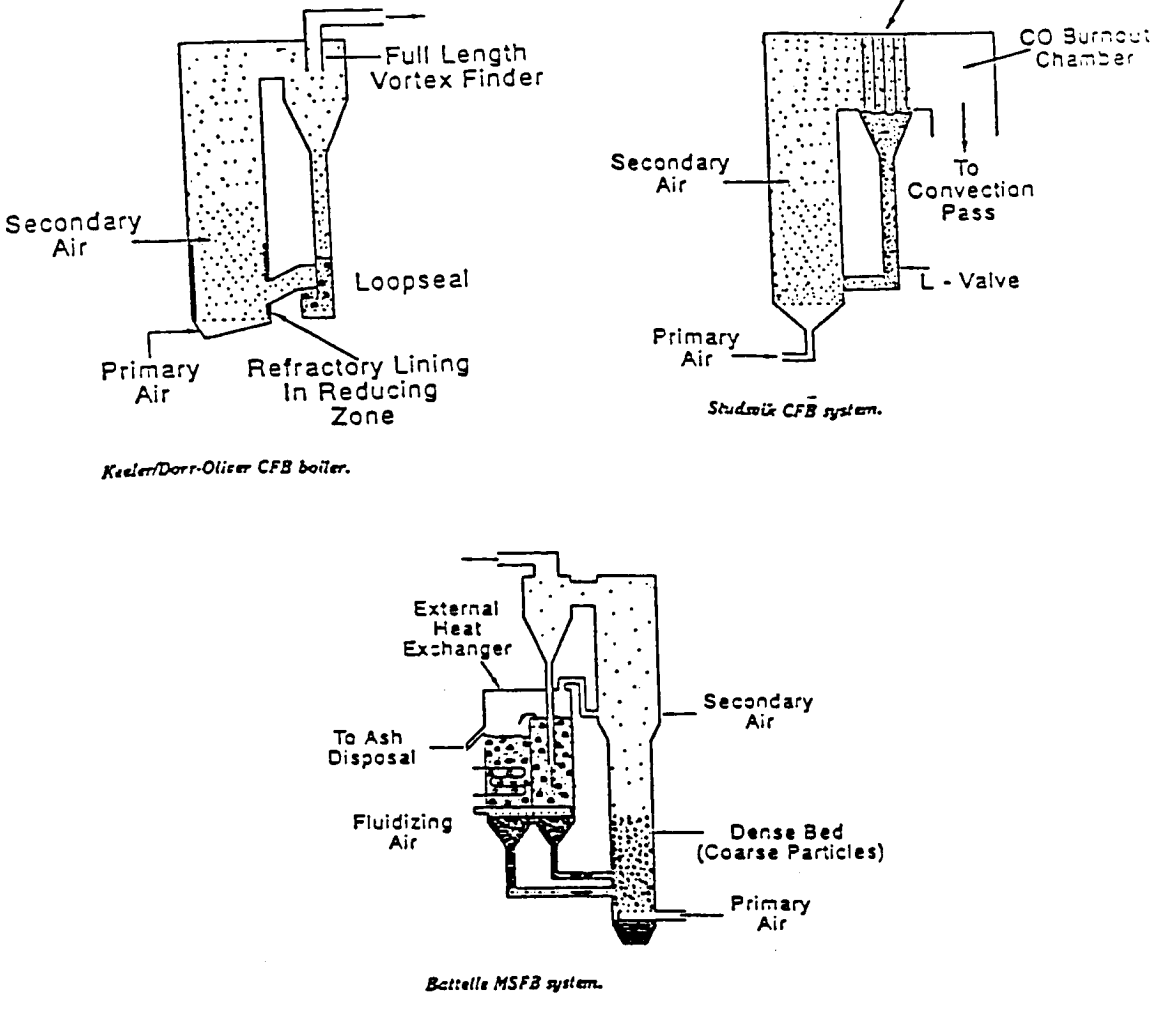

Figure 1.2: The Keeler/Dorr-Oliver, Studsvik and Battelle CFB Systems

the movement of gas and solids in a microscopic sense. Foremost in such a description is the bubble behavior, characterized by three bubble properties - bubble rise velocity, bubble diameter (or length), and bubble frequency.

This study was undertaken with the objective of characterizing the bubbling dense bed section of a MSFB. The primary focus was towards understanding the microscopic behavior of the circulating fine particles as they passed through the dense bed of coarse particles. The significance of this study is twofold. From a purely academic viewpoint, there are few data/models available to analyze the behavior of coarse particle systems, particularly those systems which have fine solids passing through. The interactions of the fine particles-coarse particles-wall are complex and poorly understood. From an industrial point of view, the Battelle design utilizes a coarse particle system with fast circulating fines passing through. Thus, an enhancement in the knowledge of the hydrodynamic behavior of a coarse particle system with fines passing through, would represent important progress, both in academia as well as the industry.

Two experimental units of diameters 0.038m (1.5") and 0.102m (4") were built and operated at UNH to get bubble characteristic data. The pressure fluctuation technique was used for that purpose, together with a microcomputer based on-line data acquisition system. Additional bubble data was obtained from a 0.229m (9") square fluidizing column operated at the Riley Stoker facility in Worcester, MA. Bubble behavior was studied using a number of solid systems . Solid materials chosen were those actually used in a hot combustor as well as materials based on a 'scaling law analysis', that allowed the simulation of a hot combustor while operating a cold unit. An additional microscopic characteristic, the residence time of fines, was experimentally determined. A defluidization technique was used to measure fine particle holdup in the dense bed section, and residence time values were obtained from the holdup data. A mathematical model was developed to predict the residence time of fines in any MSFB unit, from the physical characteristics of the gas-solid system. The macroscopic behavior (pressure drop and bed voidage) was also studied. The L-valve, a robust solids

recirculating device employed in the Battelle MSFB system, was also characterized and its behavior with various independent parameters studied in an effort to calibrate the device.

Chapter 2

LITERATURE REVIEW

This study was conducted with the objective of investigating the behavior of fine particles as they passed through a bed of bubbling coarse solids. Such a system exists in the industry. As an alternate to a circulating fluidized bed boiler, Battelle Memorial Institute of Columbus, Ohio, developed the Multi- solids fluidized bed (MSFB) process. The MSFB process consists of a dense bed of bubbling inert coarse solids superimposed on a circulating fluidized bed of fine particles. The coarse material does not circulate but remains at the base of the riser section. This is the major difference between a CFB and the MSFB. As this process entails both a bubbling fluidized bed and a pneumatic transport bed, a literature search was conducted with the objective of reviewing the existing *hydrodynamic* information relating to both areas. Literature pertinent to solids recirculating devices was also reviewed as part of this study was devoted towards characterizing such a device.

2.1 Bubbling Fluidized Beds

Ever since the petroleum industry implemented the first fluidized-bed catalytic cracking units, the growth of fluidized bed technology and processes have been phenomenal. There has been extensive research into the dynamics of a fluidized bed as an efficient method of contacting granular solids and a fluid. Fig 2.1 reproduced from Kunii et al.[1] shows the various kinds of contacting possible in a fluid-solid system. As the gas velocity is increased the bed of fixed particles expands till it is loosely supported by the fluid. This is the minimum fluidization condition. Further increase in fluid velocity results in the fluid escaping

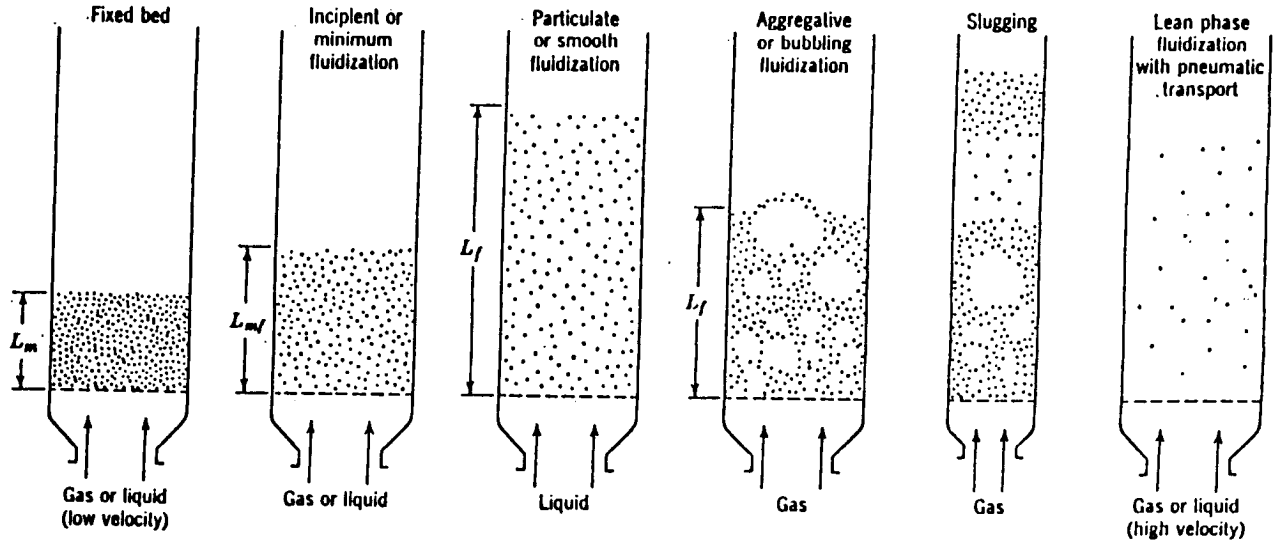

Figure 2.1: Various Kinds of Contacting of a Batch of Solids by Fluid [1]

in the form of bubbles or slugs, and ultimately if the fluid superficial velocity exceeds the terminal velocity of the solids, the solids are entrained. This results in a transport bed, and if the solids are recyled it is called a circulating fluidized bed (CFB). Various models have been developed during the past thirty years to understand the interaction between the bubbles and the fluid. The rheological behavior of fluidized solids has been investigated thoroughly. Geldart [2] was the first to classify a particular solids-gas system in a methodical way. He devised a system by which the fluidization characteristics of various solids could be predicted. The classification resulted in four groups of solids A, B, C, D and each group had its own fluidization characteristic. The solids are placed in a particular group according to the density ratio with respect to the fluidizing medium and their size.

The Davidson [3] model was the first to describe the dynamics of a fluidized gas-solids system. This simplistic model accounted for the behavior of a single bubble rising through the dense or the emulsion phase. Fig 2.2, also adapted from Kunii et al., shows the gas stream lines near a single rising bubble for various ratios of bubble rise velocites to superficial gas velocites. Of particular importance is the slow rising bubbles, as these occur in coarse particle systems. When $\frac{U_{br}}{U_f}$ is in the range of 0 to 1, the gas escapes through the bubbles since it is the shortest path. This mechanism was visually observed in the UNH dense bed unit, as the fines entrained through the bubbles along with the gas. Exhaustive lists of existing models and correlations relating to minimum fluidization velocities, minimum bubbling velocities , bed expansion and bubble characteristics such as bubble length, bubble velocity and bubble frequency may be found in Davidson et al. [4] and Cheremisnoff et al. [5]. It must be mentioned, however, that most of these correlations and models were developed for fine particle systems.

2.1.1 Coarse Particle Systems

Large particles (> 1mm) have different fluidizing characteristics from fine powdered solids. The passage of gas through these coarse particles typically occurs in the form of

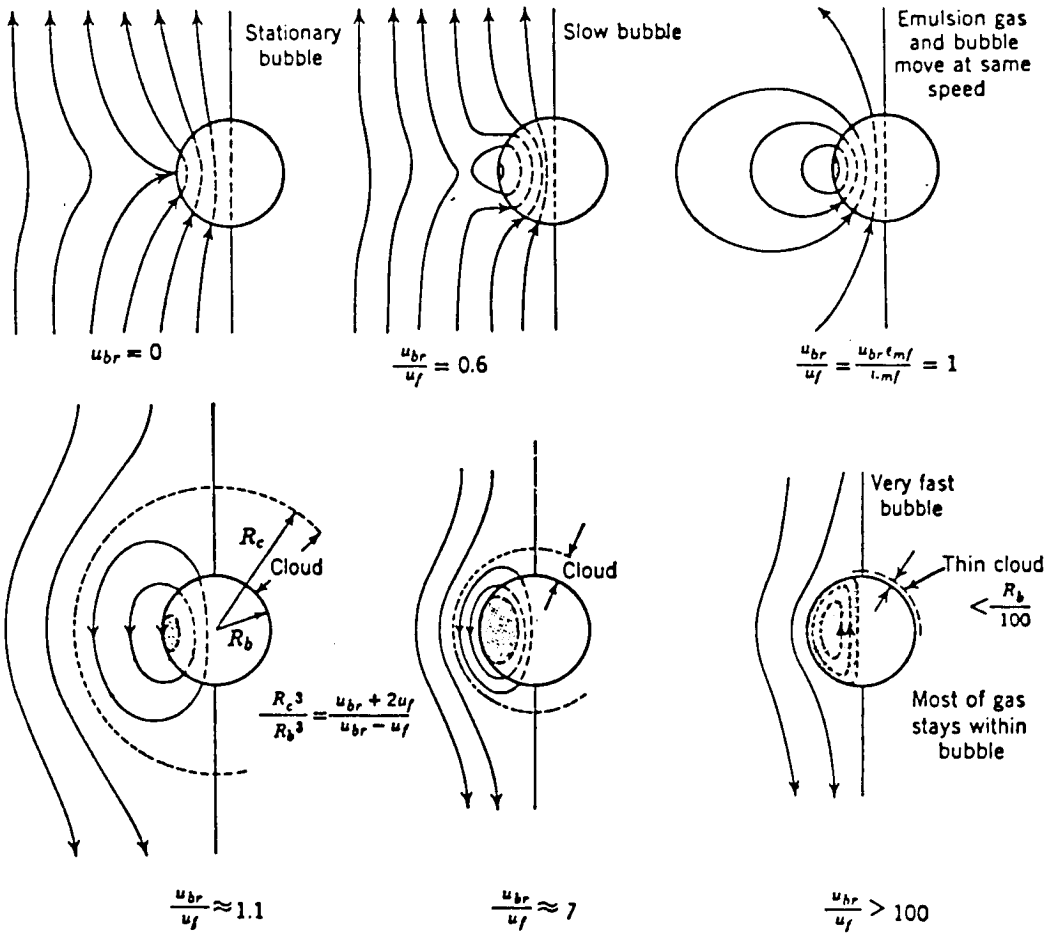

Figure 2.2: Streamlines of Gas Near a Single Rising Bubble, from the Davidson Model. Only Flow on the Left Side is Shown; the Right Side is Symmetric [1]

slow rising bubbles [4]. As mentioned earlier the dense bed of the MSFB is a bubbling bed of coarse solids, and this part of the literature search was conducted to review the existing literature on behavior of fluidized large particles.

There have been relatively few studies in coarse particle systems, with respect to bubble characteristics, gas solids mixing etc. Interestingly, there is no model available as of today, that predicts bubble behavior in a system of coarse particles with fines passing through them. There are very few data available in the literature for such a system. For the sake of completeness, a few pertinent studies available for coarse particle systems are reviewed here.

As in fine particle systems, the bubble phenomena in coarse particle systems are characterized by bubble length or diameter, bubble rise velocity and bubble frequency. Several models have been developed to fit the experimental data. Cranfield et al.[6] and McGrath et al. [7] developed correlations for bubble diameters based on superficial gas velocity, particle characterisitics and height of the bed. Glicksman et al.[8] , Davidson et al. [1], and McGrath et al. [7] modeled bubble rise velocities based on bubble diameters. These models are , briefly, as follows:

Cranfield and Geldart [6] proposed the following equations for calculating bubble characteristics:

$$
\begin{aligned}
d_b &= 0.326(U - U_{mb})^{1.11} h^{0.81} \\
U_b &= 16.3\sqrt{d_b}, 2 - D \\
U_b &= 22.5\sqrt{d_b}, 3 - D \\
f_b &= 16.7 h^{-0.72}
\end{aligned}
$$

where d_b, U_b, and f_b are bubble diameter, rise velocity and frequency, respectively. U_{mb} is the minimum bubbling velocity, h is the height of the fluidized bed, U is the superficial gas velocity, and D is the dimension of the bed.

McGrath and Streatfield [7] proposed the following for estimating bubble rise velocity, U_b and bubble diameter, d_b :

$$U_b = 0.711\sqrt{gd_b}$$
$$d_b = \frac{2}{g}R^2(\frac{U-U_0}{R-1})^2$$

where $R = \frac{H}{H_0}$, the ratio of expanded bed height to height of bed at minimum fluidization conditions, and U_0 is the minimum fluidization velocity.

Glicksman [8] proposed the following for calculating bubble rise velocity:

$$U_b = \phi\sqrt{gd_b} + U - U_{mf}$$

where d_b is the diameter of the bubble, U is the superficial gas velocity, U_{mf} is the minimum fluidization velocity, and ϕ is a fitting coefficient that varies between 0.4-0.6 .

2.2 Circulating Fluidized Beds (CFBs)

A CFB unit consists of a riser where solids are entrained by a high velocity gas, then separated using a gas-solids separation device and recycled at the bottom of the riser. The term 'fast bed' was coined by the researchers of City College NY . This pioneering work by Yerushalmi et al.[9] resulted in some understanding of the hydrodynamics of dilute phase transport, the phenomena of choking etc. Avidan et al.[10] extended the work to include the bed expansion aspects of high velocity fluidization. Fairly extensive work on the hydrodynamics of solids-gas flow in a CFB have been performed. Geldart et al.[11] have critically reviewed the hydrodynamic aspects of all types of fluidized beds, from bubbling beds to pneumatic transport beds. Some microscopic gas-solids behavior like boundary layer growth and attrition, onset of choking etc. in a fast fluidized bed have been studied by Brereton et al.[12]. Glicksman [13] propounded the 'scaling law hypothesis' for circulating

fluidized beds and experimentally verified his hypothesis with data from both hot and cold circulating fluidized bed units. Breault [14] investigated the pressure profile in the entire loop of a loop fluidized bed system (a slight variant of the CFB), and proposed a correlation for estimating solids friction in the riser. Knowlton et al.[15] pioneered the use of an L-valve as a robust, non-mechanical solids return device. Dry et al.[16] have given an excellent review of the state of circulating fluidized beds as applied to the combustion industry. The classical theory of CFBs are described in texts such as Kunii et al.[1] , Davidson et al.[4] , and Cheremisinoff et al.[5]. Thus a substantial amount of work has been done over the past ten years to enhance the understanding of the hydrodynamics of the CFB. This literature review is by no means complete, but highlights the important works done in this area.

2.3 Hydrodynamics of a CFB with a Dense Bed Superimposed - the MSFB Process

The Multi-solids fluidized bed process consists of a dense bed at the base of the riser superimposed on a circulating bed of fine particles. A very limited number of studies have been undertaken about this particular system. The hydrodynamics of the flow of fines through the dense bed were not well understood and hence was the main focus of this investigation. Fan et al.[17,18] have studied this system for two modes of the dense bed - a packed bed, and a fluidized (bubbling) bed. Solids holdup have been measured using an instantaneous shutter technique, and a mathematical model was developed to fit the data. The work of Fan et al.[17,18] is also described in more detail elsewhere in this thesis. Nack et al.[19] of Battelle Memorial Institute (the inventors of this process) have also published some preliminary hydrodynamic work done towards the estimation of residence time of fines in the dense bed.

2.4 Experimental Techniques

The main objective of this study was to characterize the dense bed section, with fines passing through it. Investigating the bubble dynamics was part of the characterization process. A pressure fluctuation technique was adopted for that purpose, described again in more detail in the Theory chapter of this dissertation. This technique was based on the investigations of Lirag et al.[20] and Fan et al.[21,22] . Wisecarver et al.[23] have used the pressure fluctuation technique to demarcate the transition from the slugging to the turbulent regime in a multi- solid pneumatic transport bed. Their work uses the same experimental assembly as that used by Fan et al.[21,22], being part of the same research team. The experimental limitations of the Fan et al. work thus apply there identically. Other pertinent literature are reviewed in detail in the Theory chapter to avoid repetition. The L-valve designed on the basis of the pioneering studies by Knowlton et al.[15] was studied in detail, and is discussed in the Results and Discussion chapter.

Chapter 3

THEORY AND PROPOSED MODEL DEVELOPMENT

3.1 Hydrodynamics of Circulating Fluidized Beds

Circulating fluidized bed systems are steadily becoming popular in the combustion industry. The first step towards understanding the combustion phenomena occurring in such systems is to gain an insight of the hydrodynamics. Considerable research has been done on the mechanics of flow behavior in CFBs. A typical CFB is shown in Fig. 3.1. It consists of a riser section, AB, where the gas and solids move upward in cocurrent flow. This is followed by a gas-solid disengaging section, BC, typically consisting of a cyclone. The solids are recirculated to the bottom of the riser by a solids recirculating device, either a loop-seal or an L-valve. The cyclone-standpipe section, CD, controls the solids inventory of the system. Superificial fludization velocites in such systems are high, of the order of 4 - 10 m/s, compared to bubbling fluidized beds employing gas velocities of 1 - 3 m/s. Thus, the term 'fast fluidized bed' has often been used to describe circulating fluidized bed systems. The hydrodynamics of the various sections of a CFB have been studied by a large number of researchers. Yerushalmi et al. [9] did some pioneering work towards understanding the gas-solid flow behavior in such systems. Fundamental pressure drop studies in a loop-fluidized bed and modifications to existing correlations for pneumatic transport were conducted by Breault [14] at the University of New Hampshire. Several other researchers including Liu

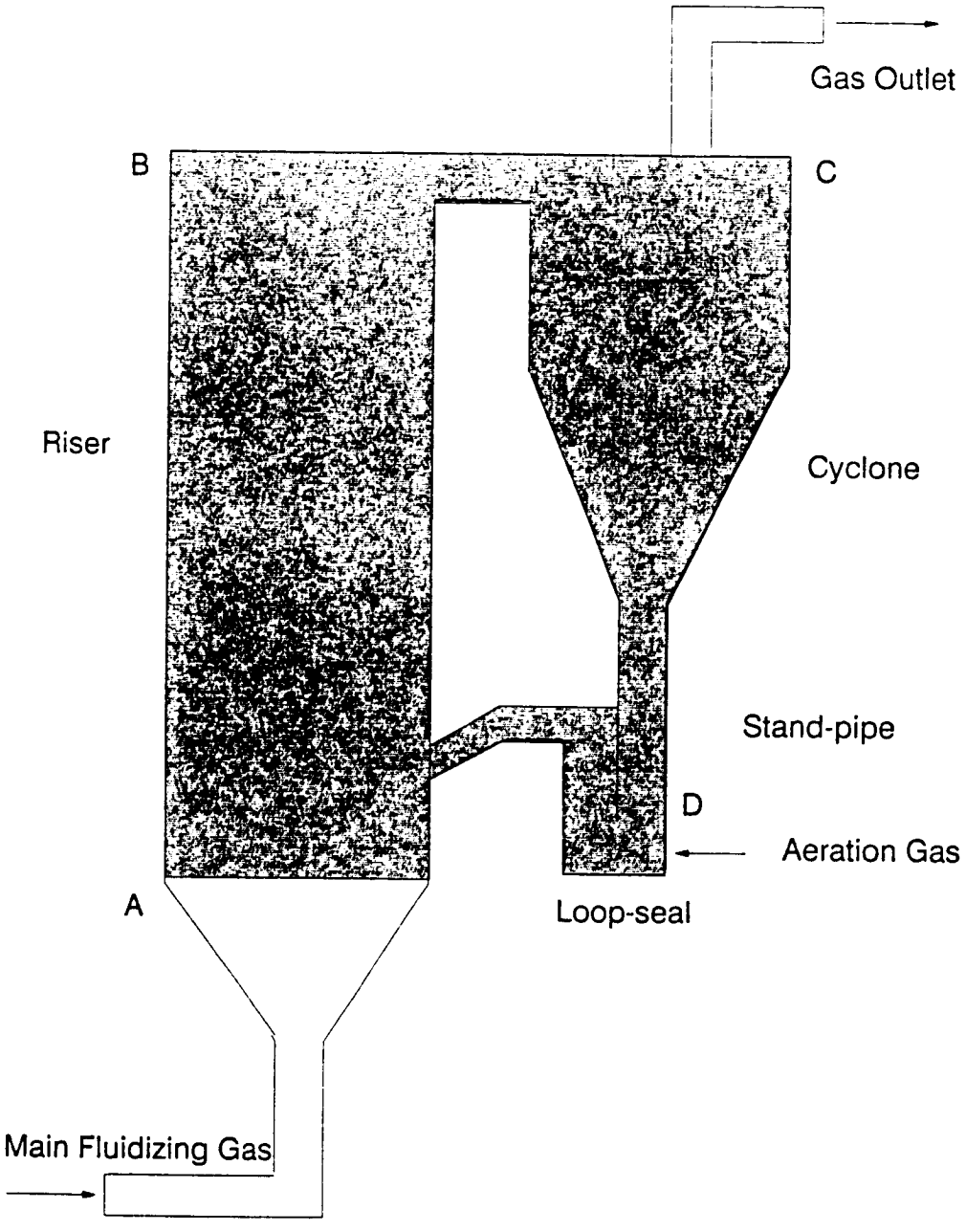

Figure 3.1: A Circulating Fluidized Bed

et al.[24], van Deemter [25] and Lee et al. [26] have contributed towards understanding the gas-solid flow behavior including solids mixing, gas mixing, and choking in circulating systems.

3.1.1 The Multi-solid Fluidized Bed Process with a Dense Bed

Of all the current CFBs in operation, as reviewed by Dry et al. [16], the multi-solid fluidized bed is a unique process developed by the Battelle Memorial Institue in Columbus, OH. This is shown in Fig. 3.2. It consists primarily of a dense bed of inert large particles superimposed on a circulating fluidized bed of fine particles. The coarse particles remain at the bottom of the riser section and serve a number of purposes. They tend to slow down both the circulating coal and sand particles, tend to grind the larger lumps of freshly fed coal, and also act as a zone of intense gas solid mixing for efficient combustion. The superficial gas velocity is maintained such that it far exceeds the terminal velocity of the fines; it is however greater than the minimum fluidization velocity of the large inert particles but less than their terminal velocity. Thus, the fines entrain once they pass through the dense bed. The coarse particles remain in a bubbling mode at the lower end of the riser section.

The primary objective of this investigation is to understand the mechanics of flow behavior of the fines particles as they passed through the bubbling bed of coarse solids. Flow behavior is characterized by bubble properties of the dense bed. Solids residence times are measured and a mechanistic model developed based on the gas-fine particle-coarse particle interactions.

3.2 Theory of Bubble Characteristics, and Measurement Techniques

The behavior of fluidized beds can be categorized into two broad groups - their gross behavior, referring to the dynamics in the macro scale, and the finer behavior relating to

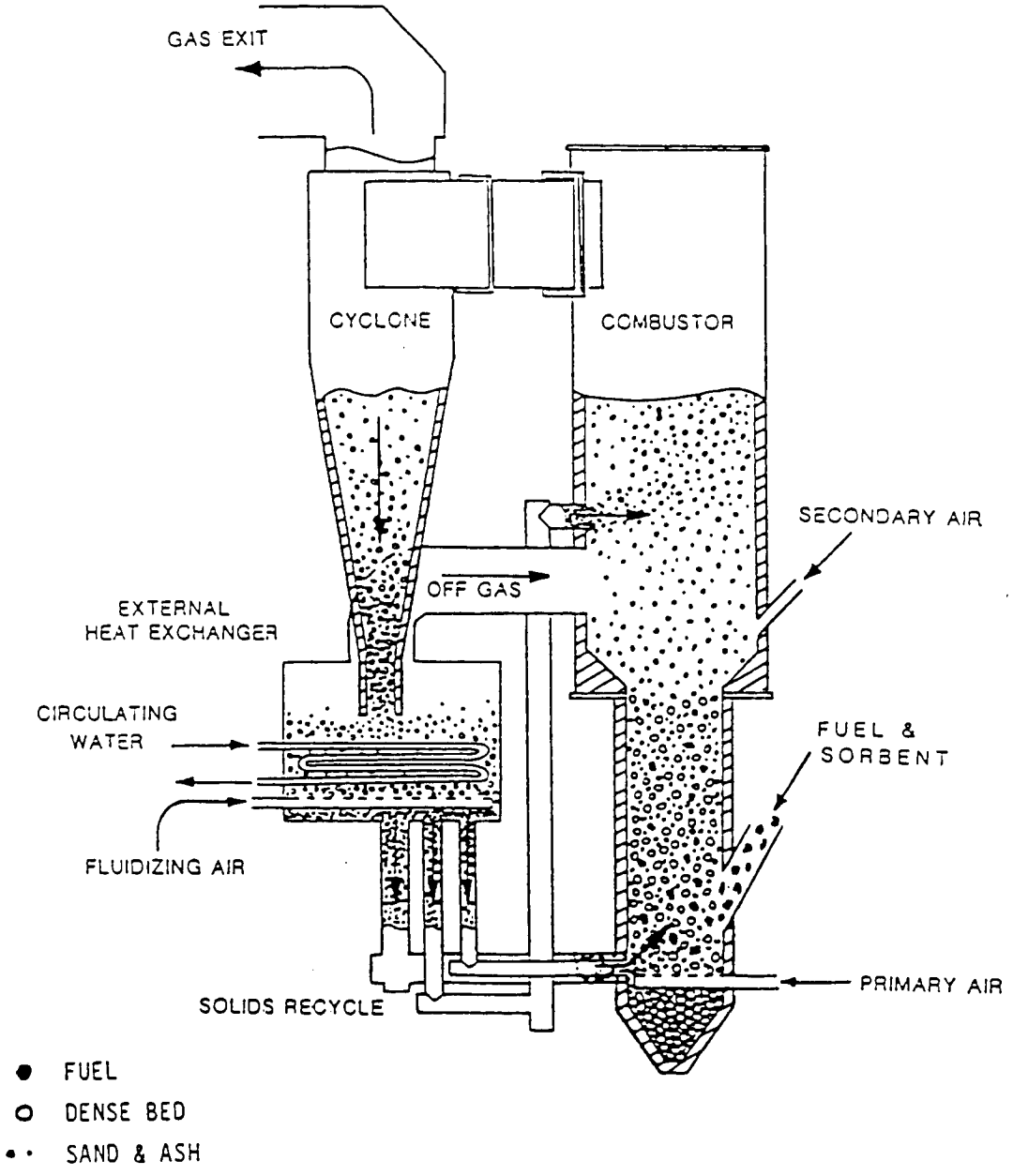

Figure 3.2: The Multi-Solid Fluidized Bed Process [27]

the micro scale. The gross behavior of fluidized beds are described by characteristics such as pressure drop across the bed, the bed expansion and the average bed voidage. The fine behavior - or the specific interactions between gas and solids - are best described by the characteristics of bubbles (regions of void spaces containing little or no solids). Bubble behavior in the bed can be described by three main parameters : bubble size, bubble rise velocity and bubble frequency.

Bubbles are an important means of gas escape in bubbling fluidized beds and are also the primary cause of gas-solids mixing in the bed. As a gas bubble rises, solids come in from the regions surrounding the bubble to occupy its space. This phenomena is repeated as successions of bubbles rise, and causes a vigorous churning action of the bed, resulting in intense gas-solids mixing. Thus, as the first step in an attempt to describe observations on heat transfer, mass transfer and solid-catalyzed reactions, substantial efforts have been devoted towards the understanding of the movement of bubbles in a fluidized bed. A vast majority of the studies, however, have been done on fine powders.

The presence of the dense bed, which is a coarse particle bed, gives rise to the existence of bubbles in that region. Large particle systems are characterized by 'slow' rising bubbles. As noted earlier, considerable efforts have been made in the last twenty years towards understanding bubbling fluidized beds. At present there is substantial information on the size of bubbles, their rise velocity and frequency, gas and solids mixing patterns and the various modes of fluidization possible, in a bubbling bed of fine particles. However, there are limited data available in the literature about bubbles in a coarse particle system. Moreover there are virtually no data or models available about bubble characteristics in a coarse particle system with fines passing through them. Various different experimental techniques have been used to characterize bubbles in fine particles; it is envisaged that most could possibly be extended to study bubble behavior in coarse particle systems. These include pressure fluctuation technique, high speed photography, X-ray photography, light probe techniques, electroresistivity methods, capacitance techniques, and Laser Doppler anemometry. All the

above methods rely on differentiating between specific physical properties between bubbles (lean phase or region of void) and the dense phase. Accuracy depends on the level of sophistication of the data acquisition system (resolution) and the ability to analyze and process large amounts of raw data.

3.2.1 The Pressure Fluctuation Technique and Analysis of the Pressure Signals

Of all the methods used to detect and characterize bubbles mentioned earlier, the pressure fluctuation technique is the most robust. The optical methods are best suited for two-dimensional configurations. The electroresistivity and capacitance techniques fail if the materials being fiuidized are strong conductors of electricity and Laser Doppler works well only in dilute phase systems.

The pressure fluctuation technique used by Fan et al.[21,22] to effectively measure bubble properties was selected for this study. Pressure probes connected to pressure transducers were used to continuously measure absolute pressure in the dense bed. As a region of void (bubble or slug) passed by the probe mouth, there was a decrease in pressure. This was followed by the dense phase coming back across the probe, inducing a rise in pressure. This phenomena repeated continuously as the bubbles/slugs travelled upwards, thus giving rise to fluctuating pressure signals. The origin of such pressure-time traces is further described by Lirag et al.[20] and Fan et al.[21,22]. To use these pressure signals to study bubble properties, the dense bed pressure was measured at two points along the bed length, separated by a distance L (Fig. 3.3). The time taken by the bubble to traverse the distance L is the lag time between the two pressure time traces, obtained from the two probes. This was termed τ_m. Another time of importance was the average horizontal distance between the troughs (or peaks) in the pressure trace. This time τ was the time needed by the bubble to pass by a single pressure probe. In this study, the traces were photocopied onto a square grid paper. The lag-time, τ_m was then estimated as the average lag between the two traces.

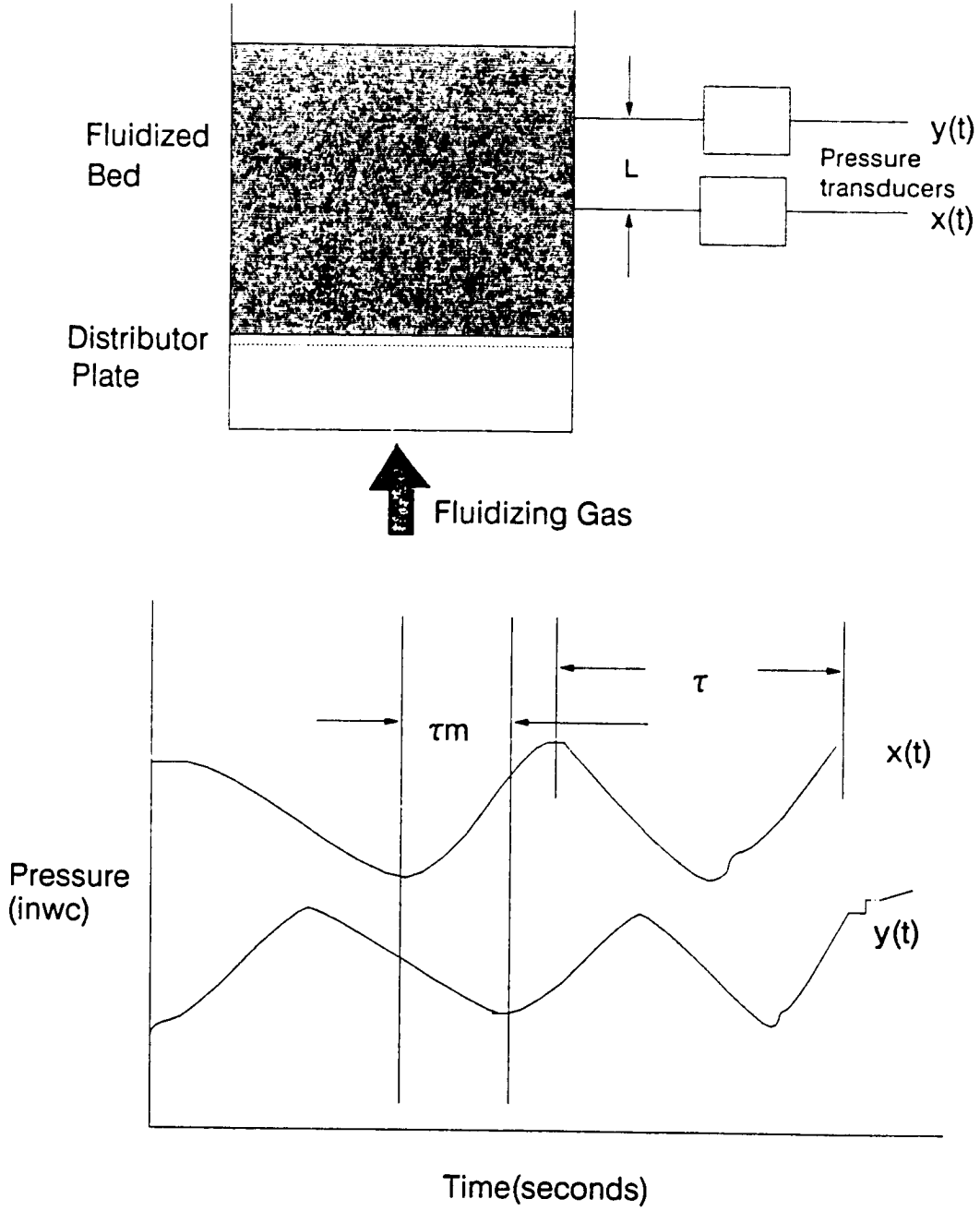

Figure 3.3: The Pressure Fluctuation Technique and Traces

All peaks on the graph were used for the averaging process. The time τ was determined as the average duration of a bubble, from a single trace; this was an average peak-to-peak distance. Once these times were obtained from a trace, bubble lengths and bubble rise velocities were determined easily. The distance L divided by the lag time τ_m is a measure of the rise velocity of the bubble. The pierced length of bubble, or more simply bubble length is a product of the time τ and the bubble rise velocity. Thus,

$$U_b = \frac{L}{\tau_m} \tag{3.2.1}$$

and

$$L_b = \tau U_b \tag{3.2.2}$$

where U_b is the bubble rise velocity and L_b is the bubble length. Bubble frequencies were evident from the number of such fluctuations per unit time, and estimated from the pressure trace. One set of calculations from the fluctuating pressure signals yielding bubble length, bubble rise velocity and bubble frequency is shown in Appendix A.

An alternate route of estimating the lag time τ_m is by the use of certain statistical functions. Statistical analysis of the pressure signals were used by Swinehart [28] , Kang et al. [29], Lirag et al. [20], and Fan et al. [21,22]. The analyses primarily aimed at estimating the lag time, τ_m by obtaining the peak of the cross-correlation function of two pressure-time traces. The other statistical functions calculated were the mean of the signal, variance, the auto-correlation function, and the power spectral density function (this is the Fourier Transform of the Auto-correlation function). If $x(t)$ and $y(t)$ are the two pressure-time traces from the two successive pressure probes (Fig.3.3), then these functions can be defined as follows:

$$\mu_x = \lim_{T\to\infty} \frac{1}{T} \int_0^T x(t)dt \tag{3.2.3}$$

$$\sigma_x{}^2 = \lim_{T\to\infty} \frac{1}{T} \int_0^T (x(t) - \mu)^2 dt \tag{3.2.4}$$

$$\phi_{xx}(\tau) = \lim_{T\to\infty} \frac{1}{T} \int_0^T x(t)x(t+\tau)dt \tag{3.2.5}$$

$$\phi_{xy}(\tau) = \lim_{T\to\infty} \frac{1}{T} \int_0^T x(t)y(t+\tau)dt \tag{3.2.6}$$

$$S_{xx}(\omega) = \int_{-\infty}^{\infty} \phi_{xx}(\tau)e^{-j(\omega)t}dt \tag{3.2.7}$$

Here, μ_x and ${\sigma_x}^2$ are the mean and variance of the signal $x(t)$, $\phi_{xx}(\tau)$ is the auto-correlation function, $\phi_{xy}(\tau)$ is the cross-correlation function, and $S_{xx}(\omega)$ is the power spectral density function.

As mentioned earlier, the cross-correlation function gives a measure of the average lag between the two traces and the power spectral density function indicates the average frequency. Values of these functions may also be obtained using an FFT (Fast Fourier Transform) analyzer and/or a cross-correlation analyzer, which are hardware devices. In this study the cross-correlation technique was tried using a software approach; the results are within + 5% of those obtained using the graphical technique.This is supported by a recent investigation in Japan. Ishii et al. [30] showed that the mean delay time obtained from original fluctuating signals (light intensity in their case) agreed fairly well with that obtained by the FFT analyser and the cross correlation approach.

3.3 Rationale for the choice of Fluidizing Materials - Scaling Law Hypothesis

Three fine particle-coarse particle systems were chosen for this study. The fluidizing medium in each case was air at ambient temperature and pressure. The systems were sand circulating through rocks, sand through spherical alumina balls, and copper dust through steel shots. The first two systems are materials used in an actual combustor, operating at elevated temperatures. The last system (copper-steel) is a result of the scaling law

hypothesis as proposed and experimentally verified by Nicastro et al. [31]. The laws were derived from the non-dimensional equations of conservation of mass and momentum, of both the particulate and the gas phase. These non-dimensional continuity and Navier-Stokes equations when coupled with Ergun's equation of flow through a porous medium, result in a set of dimensionless 'scaling groups'. The following groups are important for scaling of gas-solids fluidized bed : Re_p, the particle Reynolds number, $\frac{\rho_s}{\rho}$, the ratio of solid density to gas density, Ar, the Archimedes number, Fr, the Froude number, $\frac{H}{d_p}$, and $\frac{D}{d_p}$. H and D are the column height and diameter, respectively and d_p is the mean particle diameter. In the scaling method, the cold flow model is so designed that the model values of these scaling groups are similar to the values for the full scale hot combustor. In this way the gas and solids inertia, buoyancy, and viscous drag forces are balanced between the cold model and the full scale combustor [13]. Ake and Glicksman [27] have chosen materials that have similar scaling group values after applying the scaling method. This is shown in Table 3.1 and 3.2 adapted from Ake et al.

Table 3.1 gives the results of the scaling law analysis. Table 3.2 shows the values of the important scaling groups for fuel, recycle material and dense bed material. As mentioned earlier Nicastro et al.[31] have verified experimentally the validity of the scaling law method as applied to fluidized beds. They analyzed pressure signals from three different units - a hot combustor burning coal, a cold flow unit using hot bed materials, and a cold flow unit using materials chosen as a result of the scaling method. The pressure signals were transformed into the power spectral density function, which gives the average frequency of fluidization. This function is considered to be indicative of the quality and type of fluidization behavior of a gas-solids system. The plot of power spectral density function versus dimensionless frequency as shown by Nicastro and Glicksman [31] is reproduced here (Fig. 3.4) . It shows there is a distinct shift in frequency (or general mode of fluidization), when hot bed materials are used in the cold flow unit, although the shape remains similar. Details of other statistical functions used in the verification of the theory are given by Nicastro et al.

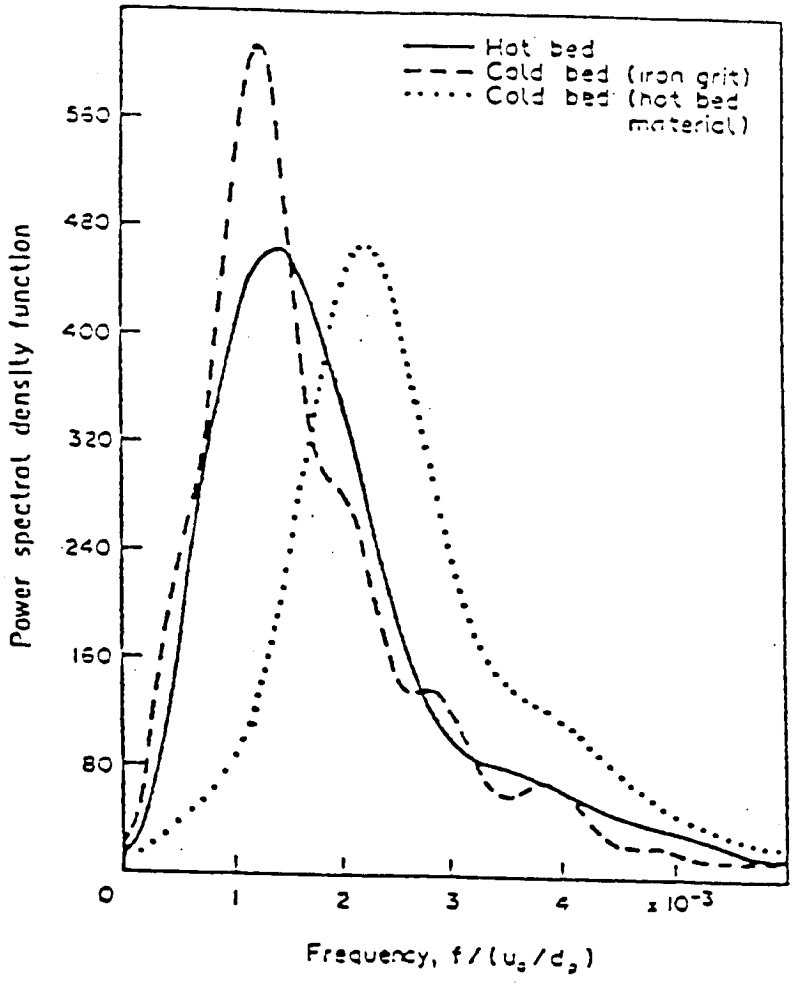

Figure 3.4: Comparison of Dimensionless Power Spectra of Differential Pressure Fluctuations [31]

Table 3.1: Scaling Factors for Proper Modeling of Hot Bed Performance [27]

Variable	Full Scale Combustor	Scaled Model
–	$1600°F$	$75°F$
Superficial Velocity	u'	$0.5u'$
Particle Diameter	d_p'	$0.25d_p'$
Particle Density	ρ_s'	$3.5\rho_s'$
Bed Height	H'	$0.25H'$
Bed Diameter	D'	$0.25D'$
Time	t'	$0.5t'$
Frequency	f'	$2f'$
Solids Flux	G_s'	$1.75G_s'$

and will not be elaborated upon here.

Therefore, the data subsequently presented in this study are much more useful than those obtained from a cold flow unit using 'unscaled' materials.

3.4 Available models and Evaluation

3.4.1 Models for Bubble Properties in the Dense Bed

Till the present date, there is no available model which describes bubble characteristics of a coarse particle bubbling bed with fines circulating through it. A literature review shows that there is substantial information about fine particle bubbling beds starting with Davidson's model [3]. There are a few empirical models that predict bubble diameter, bubble rise velocity and bubble frequency in coarse particle bubbling beds. The important ones are by Cranfield et al. [6], McGrath et al. [7] and Glicksman [8]. These models have been

Table 3.2: Scaling Groups Used to Design the Cold Flow Model [27]

Prototype Solids	Model Solids	Scaling Group	Full Scale Value	Model Value
Fuel : Coal	*Fuel : Iron Ore*	Re_p	63	69
		ρ_s/ρ	4530	4250
		Ar	8400	8400
		Fr	5400	5400
		H/d_p	950	950
		D/d_p	1333	1333
Recycle Material : Sand	*Recycle Material : Copper Powder*	Re_p	8.4	9.2
		ρ_s/ρ	8418	6667
		Ar	30.4	28.8
		Fr	43140	43140
		H/d_p	7600	7600
		D/d_p	10668	10668
		F	$4.88 * 10^{-4}$	$4.68 * 10^{-4}$
Dense Bed : Gravel	*Dense Bed Steel Pellets*	Re_p	1075	1175
		ρ_s/ρ	8418	6667
		Ar	$30.4 * 10^6$	$29.4 * 10^6$
		Fr	431	431
		H/d_p	76	100
		D/d_p	106	106

reviewed by Mathur [32] and their performance was numerically evaluated with data from this study in an internal report to Riley Stoker. This showed that the models developed for coarse particle systems deviate from experimentally measured values as much as 400% in their prediction of bubble lengths and bubble velocities, when applied to this system of coarse particles with fines passing through them [32]. As a result of the current investigation there is substantial data available of bubble parameters as measured by the pressure fluctuation technique. These bubble characteristics portray the microscopic behavior of the bed and are indicative of the quality of fluidization. Moreover, additional information like solids residence times may be generated by modeling the bubble characteristics data and incorporating it with a solids mixing model. In this study an alternate experimental route was chosen that directly generated solids residence times. The data was then checked against a model developed from first principles, based on a momentum balance of the fine particles.

One of the reasons of the existence of the dense bed superimposed on a circulating fluidized bed of fines is its ability to slow down the fine particles. The major thrust of the investigation was to analyze the fine particle behavior in the dense bed, and get estimates of the fine particle residence times in the dense bed section. As mentioned earlier, accurate analysis and modeling of the bubble rise velocites will give an insight into the residence time behavior of fines. An alternate approach would be to develop or modify any existing model for predicting the residence time of fines . The latter route was chosen and a robust mathematical model was developed from a fundamental momentum balance on the fines. The current model draws upon the work by Boothroyd [33], Klinzing [34], and Fan et al. [17,18].

3.4.2 Models for the Residence Time of Fine Particles in the Dense Bed

An exhaustive literature search shows only one available model for the prediction of the residence time of fine particles through a coarse particle bubbling bed. This was the

result of the investigation by Fan et al. [18]. An earlier work by the same researcher [17] resulted in the basic formulation of the momentum balance on the fines, upon which the later model is based. The two studies differed only in the mode of operation of the dense bed. In the first study the dense bed was a packed bed, and in the second it was a fluidized bubbling bed. Both studies had fine particles circulating through the dense bed, and in both the dense bed section was located near the upper part of the riser. The physical location of the dense bed is quite different from that used in this study; the dense bed section here was always at the lower end of the riser, in accordance with the Battelle MSFB process. The model by Fan et al. is briefly reviewed here. Comparision with the proposed model developed in this study can be found in the Results and Discussion chapter of this thesis.

Model of the Hold-up of Fines by the Dense Bed of the CFB unit by Fan et al. [18] is presented below:

$$U_p \frac{dU_p}{dz} = \frac{3}{4} C_{DM} \frac{\rho_a (U_a - U_p)^2}{\rho_p d_p} - (1 - \frac{\rho_a}{\rho_p}) g - 2 f_k \frac{U_p^2}{D} \tag{3.4.8}$$

The Boundary Condition is: $U_p = U_{p0}$, at $z = 0$. Here, U_p refers to the fine particle velocity, d_p is the mean diameter of the fine particles, U_a is the air velocity, C_{DM} is the modified drag coefficient, ρ_p is the fine particle density, ρ_a is the air density, f_k is the interaction coefficient, z is the upward direction (of motion of particles) , and D is the column diameter. The term $U_p \frac{dU_p}{dz}$ is the net force per unit mass acting on the fine particles. The terms on the right hand side of the above equation are , in order, the drag force per unit mass, the net gravitational force per unit mass, and the net frictional force on the fine particles per unit mass. The unit of each term is thus m^2/sec, the unit of acceleration (or force per unit mass). The average fine particle hold-up is then calculated from the axial particle velocity, U_p by:

$$\epsilon_p = \frac{W_{mp}}{\rho_p A U_p} \tag{3.4.9}$$

where, W_{mp} is the mass flow rate of the circulating fines, A is the cross-sectional area of the empty tower, and U_p is the linear particle velocity of the fines.

3.5 Development of a Proposed Mathematical Model to Predict Residence Times of Fine Particles in the Dense Bed Section of a MSFB

Residence time data for fines circulating through the dense bed were experimentally obtained at the UNH unit , using a defluidization technique. Details of the technique are available elsewhere in this thesis. This data did not check with the Fan et al. expression. The single most important reason for this anomaly is the Fan model contains no explicit dependance of circulating solids mass flux in the velocity expression (momentum balance). The experimental finding of this study clearly shows such a dependance, hence the need to incoporate this in the model. Further discussion of the modifications of the Fan et al. model is given in the Results and Discussion chapter of this thesis.

Thus, a mathematical model is proposed to account for the behavior of fine particles circulating through the dense bed. The model is based on a force balance approach and follows a development similar to that of Fan et al. [17,18].

3.5.1 Model Development

Consider the flow of gas and fine particles through a bubbling (dense) bed of coarse solids as shown in Fig. 3.5. A force balance on the fines across the differential length dL may be represented as:

$$dm_2 \frac{dU_{p_2}}{dt} = dF_{drag} - dF_{gravity} - dF_{friction} - dF_{collision} \qquad (3.5.10)$$

Here, dm_2 is the effective weight of the fine particles in the section dL. Subsequently, subscripts 1 and 2 will refer to the coarse and fine particles, respectively. Thus, U_{p_2} refers to the velocity of fine particles as they move upwards through the dense bed.

It has been noted by Fan et al.[18] that fine particles quickly achieve their steady state velocity within a fraction of a millimeter from being introduced into the dense bed. Thus

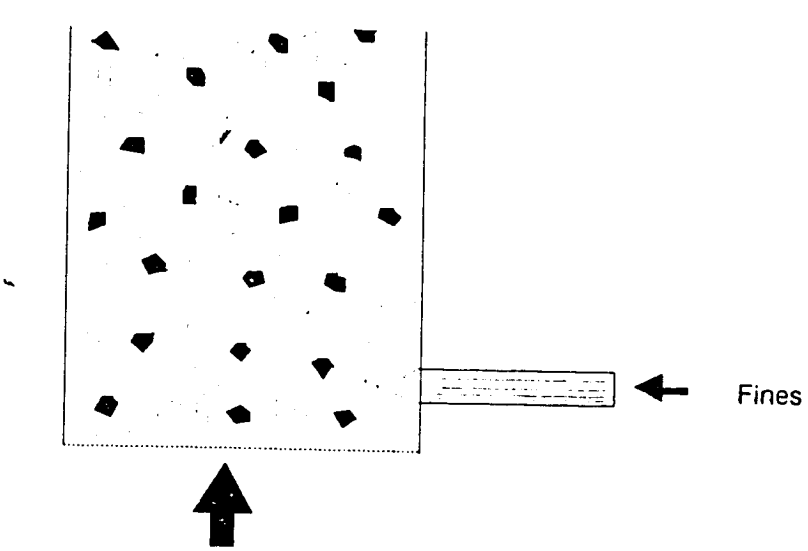

Figure 3.5: Flow of Fines in a Bed of Coarse Particles

the term $\Delta m_2 \frac{dU_{p2}}{dt}$ is equal to 0. Therefore equation (1) becomes a balance between the upward drag force and the downward gravitational, frictional and collision forces.

$$dF_{drag} - dF_{gravity} - dF_{friction} - dF_{collision} = 0 \tag{3.5.11}$$

Considering the individual terms in equation(2) in more detail, dF_{drag} is the drag force acting on all the fine particles by the fluidizing medium(air). This is also equal to the sum of the drag forces acting on one single particle. This may be represented as:

$$dF_{drag} = \frac{\frac{3}{4} C_{DM} \rho_a (U_a - U_{p_2})^2}{\rho_{p_2} d_{p_2}} \Delta m_2 \tag{3.5.12}$$

where, $U_a = \frac{U_0}{\epsilon}$, and C_{DM} is the multi-particle drag coefficient.

Yang [35] suggested a relationship between C_{DM} and C_{DS}, the single- particle drag coefficient as follows:

$$C_{DM} = \epsilon^{-4.7} C_{DS} \tag{3.5.13}$$

In this model, the void fraction used is ϵ_f, which is the void fraction in the phase containing primarily fine particles. Thus,

$$C_{DM} = \epsilon_f{}^{-4.7} C_{DS} \tag{3.5.14}$$

where,

$$\begin{aligned} C_{DS} &= \frac{24}{Re_{p_2}}, Re_{p_2} \leq 2 \\ &= \frac{18.5}{Re_{p_2}{}^{0.6}}, 2 \leq Re_{p_2} \leq 500 \\ &= 0.44, Re_{p_2} \geq 500 \end{aligned}$$

The gravitational force term is

$$dF_{gravity} = g(1 - \frac{\rho_a}{\rho_{p_2}})dm_2 \tag{3.5.15}$$

The frictional term accounts for the friction between small particles and large particles, between small particles themselves, and between small particles and the wall;

$$dF_{fric} = dF_{fric,1-2} + dF_{fric,2-2} + dF_{fric,2-wall} \tag{3.5.16}$$

Breault [14] developed an expression to account for these effects. However, his expression has been modified here to account for the different physical system. The mass-flux dependance of velocity has been included in the friction term, which gives it a certain degree of empiricity. The above individual frictional effects have been combined, resulting in the following expression for the frictional force term:

$$dF_{fric} = 10(\frac{(1-\epsilon)}{\epsilon})^n U_{p_2} D \frac{1}{\phi d_{p_1}} (\frac{W_g}{W_{p_2}})^p dm_2 \tag{3.5.17}$$

where $\frac{W_g}{W_{p_2}}$ is the ratio of mass flux of gas to small particles, p is a fitting parameter, ϕ is the sphericity, and ϵ is the void fraction of the dense bed, and n is a system-dependent

parameter that can be evaluated based on system properties. A discussion of n and p follows later on, in the Results and Discussion chapter of this thesis. Note, ϵ is not equal to ϵ_f.

An expression for the collision force has been derived by Marble [36], from first principles, considering elastic collisions between small and large rigid spherical bodies. The collision force term is a major addition to the ideas presented in earlier models, and enhances the understanding of the fine particle flow behavior through the dense bed. This term implies momentum changes to the fine particles as a result of elastic collisions between the small and large particles. The original expression is modified here to include the effect of mass flux:

$$dF_{collision} = \frac{6(U_{p_1} - U_{p_2})^2(1-\epsilon)}{\phi d_{p_1}}(\frac{W_g}{W_{p_2}})^p dm_2 \qquad (3.5.18)$$

Now , collecting all the terms and substituting in equation(2.5.11), and noting that Δm_2 cancels out, we have:

$$\begin{aligned}\frac{\frac{3}{4}C_{DS}\epsilon_f^{-4.7}\rho_a(U_a - U_{p_2})^2}{\rho_{p_2}d_{p_2}} - g(1-\frac{\rho_a}{\rho_{p_2}}) &- 10(\frac{(1-\epsilon)}{\epsilon})^n U_{p_2} D\frac{1}{\phi d_{p_1}}(\frac{W_g}{W_{p_2}})^p \\ &- \frac{6(U_{p_1} - U_{p_2})^2(1-\epsilon)}{\phi_1 d_{p_1}}(\frac{W_g}{W_{p_2}})^p = 0\end{aligned}$$

or,

$$\begin{aligned}\frac{\frac{3}{4}C_{DS}\epsilon_f^{-4.7}\rho_a(U_a - U_{p_2})^2}{\rho_{p_2}d_{p_2}} &= g(1-\frac{\rho_a}{\rho_{p_2}}) \\ &+ 10(\frac{(1-\epsilon)}{\epsilon})^n U_{p_2} D\frac{1}{\phi d_{p_1}}(\frac{W_g}{W_{p_2}})^p \\ &+ \frac{6(U_{p_1} - U_{p_2})^2(1-\epsilon)}{\phi_1 d_{p_1}}(\frac{W_g}{W_{p_2}})^p\end{aligned}$$

For any specified small particle-large particle-gas system, the system-dependent parameters n and p may be evaluated. The above equation can then be solved for the small-particle velocity, U_{p_2}. Once U_{p_2} is determined , the residence time in seconds per meter of the dense bed can be determined from

$$\tau_r = \frac{1}{U_{p_2}} \tag{3.5.19}$$

if U_{p_2} is in m/sec. The model described above has been put in the form of a computer code, for the evaluation of residence times with varying independent parameters. The computer code is presented in Appendix A.

Chapter 4

EXPERIMENTAL APPARATUS AND PROCEDURE

This study has been conducted with the objective of analyzing the behavior of fine particles circulating through a bubbling dense bed of coarse solids. A systematic investigation was undertaken, and the various stages of the experimental work are described in this chapter.

Briefly, the study was conducted as follows: the first stage consisted of building bench scale two-dimensional models and visually observing the hydrodynamic behavior of bubbling coarse particles. This was followed by the design, fabrication and operation of 0.038m (1.5") and 0.102m (4"),n.d., cold circulating fluidized bed units, with the objective of studying bubble dynamics. The fluctuating pressure signal technique was used to obtain bubble characteristics. A sophisticated on-line data acquisition system with associated software was utilized for that purpose. The next phase consisted of obtaining data from a pilot unit which had a very similar experimental data acquisition system. This consisted of a 0.229m x 0.229m (9" x 9") square cross section and was used to obtain bubble characteristics data. As a final step in trying to understand the dynamics of the dense bed region, a thorough study was conducted to obtain fine particle residence time data. A defluidization technique was used in the 0.102m UNH unit to get residence time values of fine particles in the dense bed. This is of critical importance for the MSFB boiler, as it is a measure of how long burning coal particles stay in the dense bed section of the combustor.

4.1 Experimental Apparatus

4.1.1 Visual Studies in a Two Dimensional Plexiglass Model

In an attempt to visually observe 'bubble dynamics', a two dimensional bubbling fluidized bed was designed (Fig. 4.1). It is so called because one of the dimensions is significantly smaller than the other two (0.2mx0.2mx0.038m). Thus, there is a physical suppression of the third dimension because of the construction of the bed, resulting in two dimensional flow phenomena. The bed was filled to a height of about 0.076m (3") with $6.35 * 10^{-3}$m (1/4") steel pellets and fluidized with air in the bubbling mode. Fines , consisting of 80μ average diameter were injected using a syringe. The behavior of the bed both with and without fines passing through it was observed. The bed appeared to fluidize in the 'free bubbling' state. The fluidizing air passed through in the form of relatively slow bubbles; upon introduction of fines, the motion of the bubbles became more random and chaotic. The bubbles appeared to escape faster.

During a later stage of experimentation with the UNH cold flow circulating unit, an attempt was made to record the passage of the bubbles and accompanying fines through the dense bed using a high-speed motion picture camera. This did not prove very successful; curvature effects and the passage of fines near the wall prevented a clear picture of the phenomena inside the bed.

4.1.2 The UNH Circulating Fluidized Bed Experimental Unit with a Computer -aided Data Acquisition System

A cold circulating fluidized bed unit was designed, fabricated and operated at the UNH facility (Fig. 4.2). This experimental unit was constructed primarily of cast plexiglass tubing and was designed to operate at atmospheric pressure and temperature. The system consisted of an Ingersoll-Rand air compressor as the primary source of fluidizing air. This was a reciprocating machine equipped with an 80 gallon tank capable of supplying $0.019 Sm^3/s$ (2400 SCFH) of air at 446.1 kPa (50 psig). The main air line from the com-

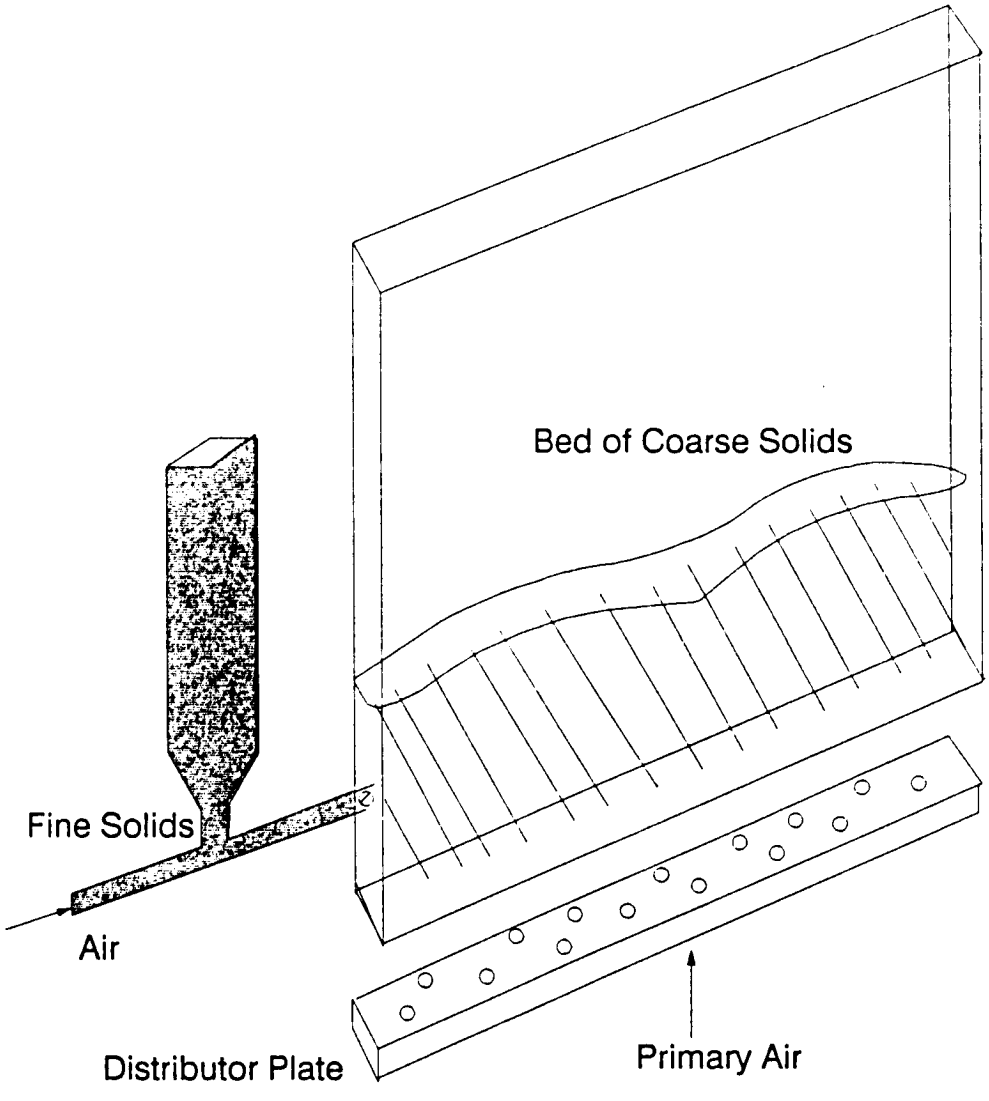

Figure 4.1: Two Dimensional Bubbling Fluidized Bed with Injection of Fines

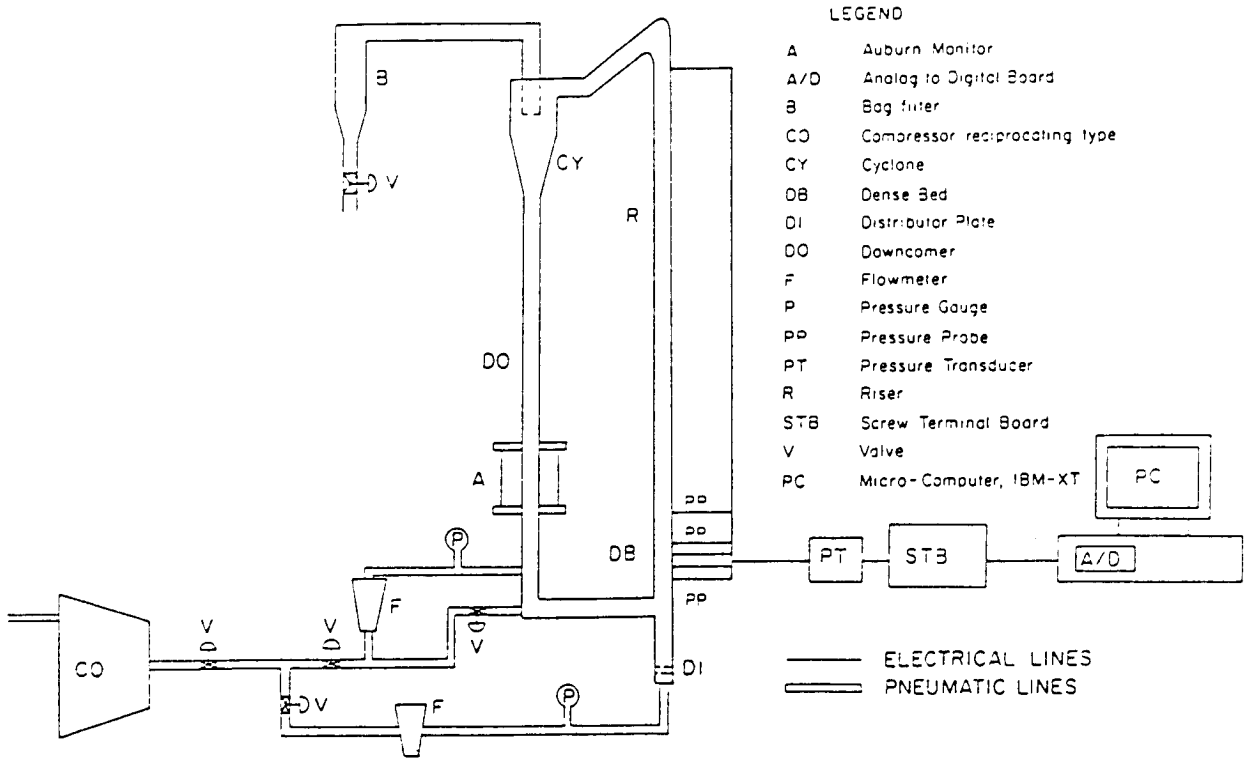

Figure 4.2: Schematic Diagram of the UNH MSFB Unit with Computer Aided Data Acquisition System

pressor passed through a pressure regulator, whose outlet pressure was adjusted to about 274 kPa. This system resulted in minimal air pressure fluctuations. Air was supplied to the bottom of the riser section, below the distributor, DI. Air was also supplied to the L-valve in the form of motive and assist air. The L-valve is a non- mechanical device to recirculate solids. It can also be used to measure solids flow rate ; in this phase , however, it was used primarily as a solids recirculating device. Details of the L-valve aeration are provided in the results and discussion section. Additional air was sometimes needed for effective fluidization of a large bed inventory of steel shots. This was provided by a Rotron manufactured cyclonair positive- displacement blower, capable of delivering 0.033 Sm^3/s (4200 SCFH) at 12.16 kPa pressure. The solids loop consisted the riser section, R, a gas-solids disengaging device in the form of a cyclone,CY, a downcomer, DO and a solids return device (L-valve).

The principal region under investigation was the dense bed, DB . This section, was located at the lower end of the riser. The riser diameter could be changed from 0.038 m to 0.102 m ; columns of both diameters were tested using a variety of solid materials. The pressure probes consisted of $3.175 * 10^{-3}m$ (1/8") diameter steel tubes, that were 0.152 m (6") long and 'snubbed' with glass wool at the active end. Four such probes were inserted into the dense bed such that their tips lay on the central axis of the riser. A rib attached to the wall of the plexiglass column by glue avoided direct attachment of the probes onto the bed wall, and helped maintain their rigidity. The other ends of the probes were connected by $6.35 * 10^{-3}m$ (1/4") flexible tygon tubing to high speed pressure transducers. A battery of 4 transducers was mounted close to the pressure probes to minimize pressure signal lag time.

The On-line High-speed Data Acquisition System

Details of the on-line data acquisition system are shown in Fig. 4.3. It consisted of fast acting pressure transducers of the type PX 240-005G (manufacted by Omega Engineering, Inc.) with the ability to measure absolute pressure in the range 14.7 - 19.7 psia. The

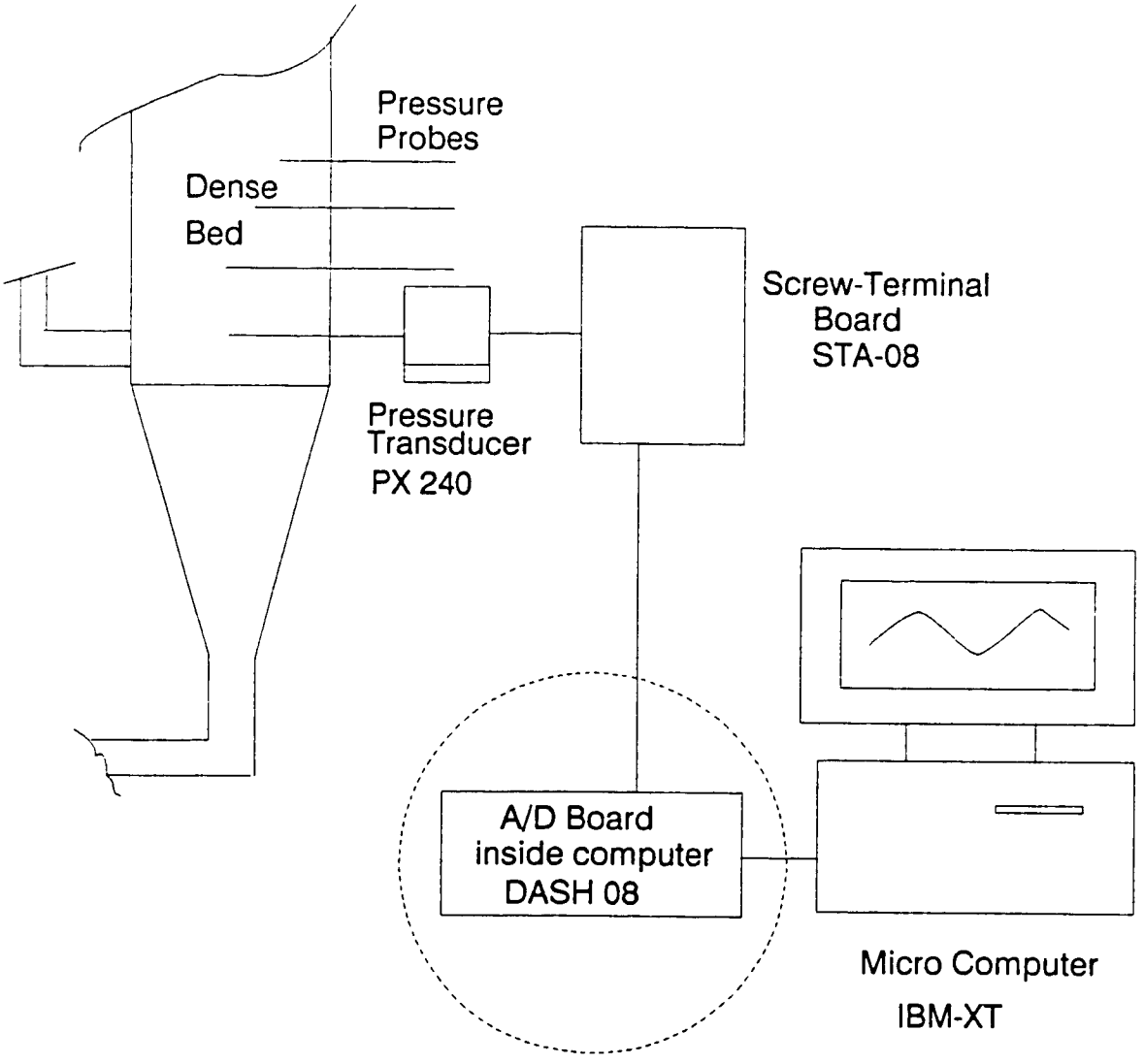

Figure 4.3: Details of the Data Acquisition System at the UNH Facility

transducers were powered by 8V D.C. from a Hewlett Packard D.C. power supply unit . The transducer output was in the 1 - 6 V D.C. range, with a response time of 1 millisecond. This analog electrical signal was transmitted by a thin gauge electrical wire to a screw-terminal board, STA-08; this had the ability to simultaneously sample upto 8 channels. This feature could be improved to accomodate an additional 16 channels by using the EXP-16, a multiplexer board. However, since only 4 signals were processed in this set-up the multiplexer board was not necessary. The signal from the screw terminal board went to the analog-to-digital board via a ribbon cable. This board, the DASH-08, digitized the analog electrical signal. From the A/D board that was installed in the microcomputer (an earlier generation IBM-XT) , the digitized signal was processed by the data acquisition software NoteBook. After a run was made, the data from notebook was 'imported' into a Lotus worksheet; data manipulation and plotting was then subsequently performed in Lotus. Some software preparation was done in advance. Channels for data acquisition were set up for data sampling . Data were sampled at frequencies ranging from 25 Hz to 100 Hz. Typical Notebook Setups are presented in Tables 4.1 and 4.2. Table 4.1 shows the data acquisitions setups for two channels sampling pressure. These channels contained information such as the type of channel (analog or digital), input range in volts, duration of a run , the sampling rate and the number of interface devices. The third channel was 'Time' and the fourth and fifth achannels were calculated channels of the average values of records in channels 1 and 2. Table 4.2 shows the files setup. This setup determined the number of channels being sampled, the mode of data storage and the file used to store the raw data. The file 'dnsbed.prn' was the file used for data storage during a run and later 'exported' to a lotus worksheet for plotting the pressure time traces.

The data acquisition software was supplied by Labtech Corporation. All the hardware boards were supplied by Metrabyte Corporation.

Table 4.1: Notebook Channel(s) Setup of the UNH Data Acquisition System

```
Current Value: 1

                    NORMAL DATA ACQUISITION / CONTROL SETUP
Number of Channels                                        5
Current Channel(s) [n or n..m]                            1
Channel Type                                  Analog Input
Channel Name                                     press,bat
Interface Device                                 1: Dash-8
Interface Channel Number [0..143]                         1

Input Range                                             ±5V
Scale Factor                                         27.690
Offset Constant                                      -0.690
Buffer Size                                            2048
Number of Iterations                                      1
Number of Stages [1..4]                                   1

Sampling Rate, Hz                                    25.000
Stage Duration, sec. [0.0..1.0E+08]                   4.000
Start/Stop Method                                    Normal
Trigger Channel                                           1
Trigger Pattern to AND [0..255]                           1
Trigger Pattern to XOR [0..255]                           0
Time Delay, sec. [0.0..1.0E+08]                       0.000

Current Value: 2

                    NORMAL DATA ACQUISITION / CONTROL SETUP
Number of Channels                                        5
Current Channel(s) [n or n..m]                            2
Channel Type                                  Analog Input
Channel Name                                     press,top
Interface Device                                 1: Dash-8
Interface Channel Number [0..143]                         2

Input Range                                             ±5V
Scale Factor                                         27.690
Offset Constant                                      -0.927
Buffer Size                                            2048
Number of Iterations                                      1
Number of Stages [1..4]                                   1

Sampling Rate, Hz                                    25.000
Stage Duration, sec. [0.0..1.0E+08]                   4.000
Start/Stop Method                                    Normal
Trigger Channel                                           1
Trigger Pattern to AND [0..255]                           1
Trigger Pattern to XOR [0..255]                           0
Time Delay, sec. [0.0..1.0E+08]                       0.000
```

Table 4.2: Notebook File(s) Setup of the UNH Data Acquisition System

Current Value: 1

FILES SETUP

Number of Data Files [0..12]	1				
Current Data File [1..1]	1				
Data File Name	dnsbed.prn				
Storage Mode	ASCII Real				
Number of Header Lines [0..4]	4				
Header Line 1	Dense bed Data				
Header Line 2	from UNH circulating fluidized bed cold				
Header Line 3	flow unit				
Header Line 4					
Num. of Channels in File [0..100]	5				
File Channel Number	1	2	3	4	5
Channel Number	1	2	3	4	5
Channel Name	dns1	dns2	time	p1,avg	p2.avg
Channel Units	inwc	inwc	sec	inwc	inwc
Field Width (ASCII Files)	12	12	12	12	12
Decimal Places (ASCII Real Files)	4	4	4	4	4

NOTEBOOK Global Setup Checking MODE: Normal

4.1.3 The Riley Stoker Cold Circulating Fluidized Bed Unit

The Riley Stoker unit consisted of a 0.229m x 0.229m (9"x9") square fluidizing column constructed of steel with plexiglass windows for visual observations as shown in Fig. 4.4. The air supply source was a large Roots Blower with a capacity of about 0.275 Sm^3/s (35000 SCFH). The solids loop consists of a riser, a proprietary gas-solid separation device (based on the impingement separation principle) , a simulated external heat exchanger, a downcomer and two solids recirculating L-valves. The unit was designed based on 'scaling laws' proposed by Glicksman et al.[31]. This resulted in linear dimensions being one-quarter scale of the actual Multi- Solids Fluidized Bed (MSFB) package boiler that this unit simulates. The package boiler is a small skid-mounted steam/power generating unit that uses MSFB technology in burning coal. The rationale for the choice of fluidization materials is based on scaling law analysis. Solids are initially charged into the system with the help of a screw feeder. The on-line data acquisition system to study bubble dynamics of the dense bed is very similar to the one used in the UNH cold flow unit. A schematic diagram of the data acquisition system is shown in Fig. 4.5. Hardware differences consisted of a different screw-terminal board (an STB-HL instead of an STA-08) , a different A/D board (RTI 815 instead of the DASH-08) and a faster 286 based Compaq microcomputer instead of the IBM-XT used at UNH. The pressure transducers were Omega manufactured P163 series with a 1 -6 V D.C. output. The software used at the Riley facility was identical (NoteBook for data acquisition, and Lotus for data manipulation and plotting); however, the high speed mode of the channel setup was used. Typical channel setups and hardware device lists are shown in Tables 4.3 and 4.4 respectively.

Four pressure probes consisted of $9.525 * 10^{-3}m$ (3/8") diameter stainless steel tubes with swagelok fittings to secure them in place on the bed wall. The pressure probes were aligned to the central axis of the column, and connected by equal lengths of tygon tubing to the pressure transducers. Signals from the pressure transducers were transmitted to the A/D board inside the Compaq microcomputer and subsequently analysed in a manner

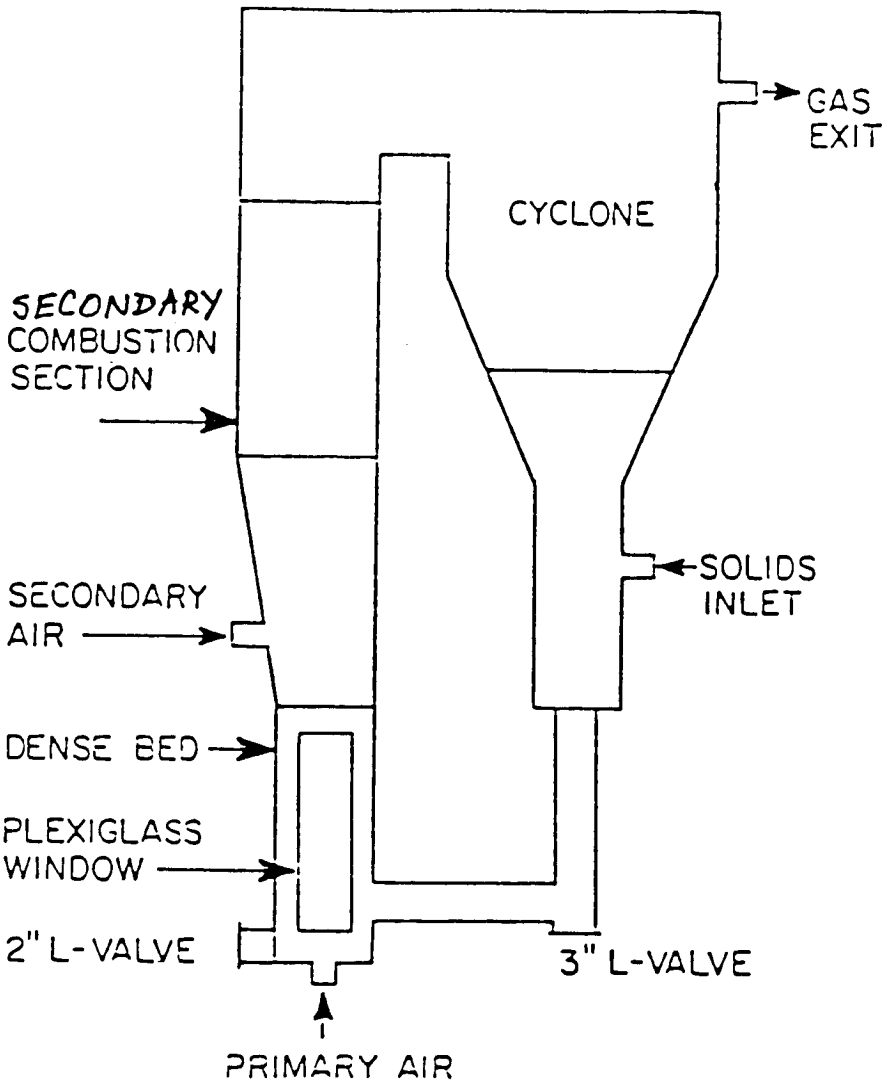

Figure 4.6: The Multi-Solids Fluidized Bed Cold Flow Unit at the Riley Stoker Facility

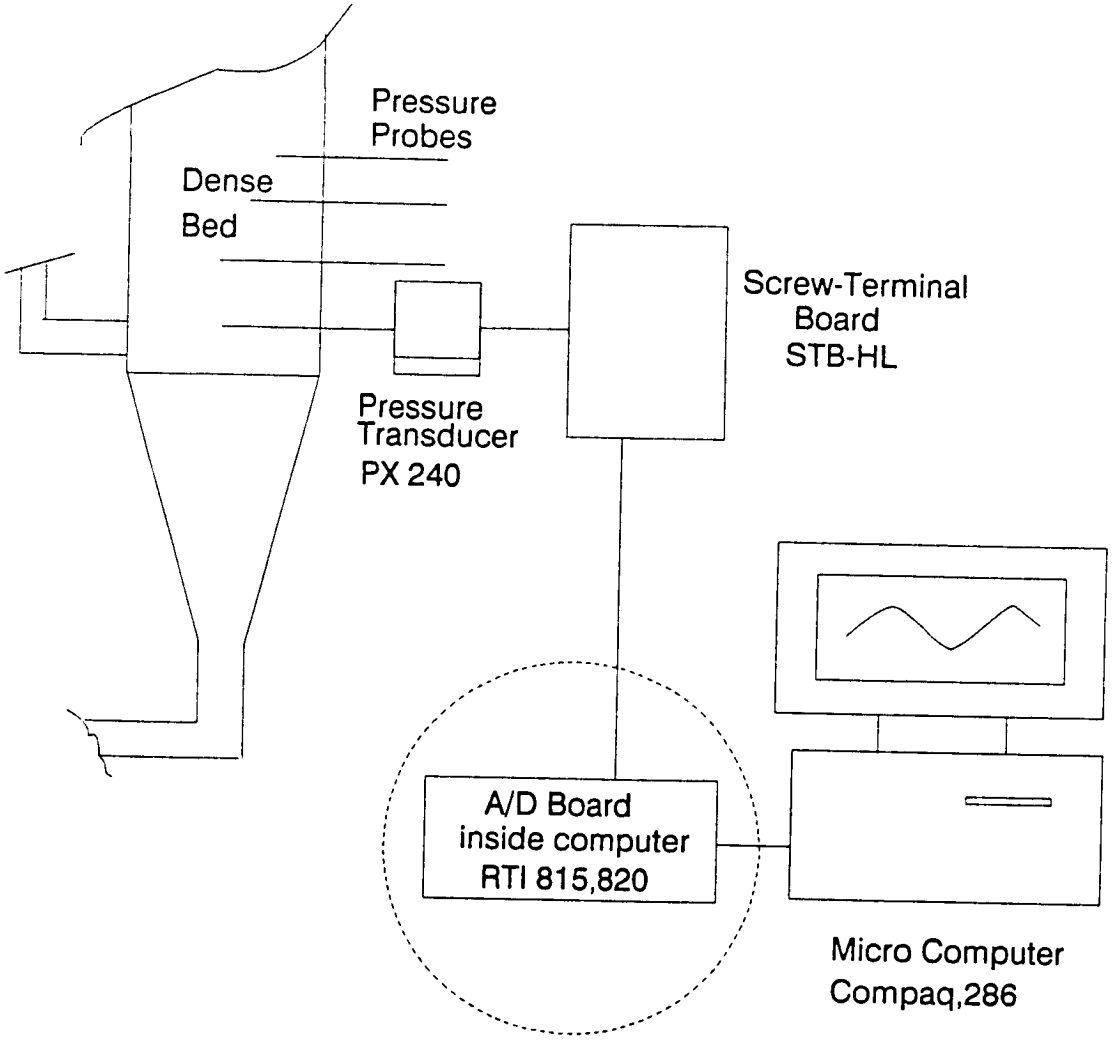

Figure 4.7: Details of the Data Acquisition System at the Riley Stoker Facility

Table 4.3: Notebook Channel(s) Setup of the Riley Stoker Data Acquisition System

Current Value: 4: RTI-815

HIGH SPEED DATA ACQUISITION SETUP

Interface Device	4: RTI-815	
Starting Channel Number [0..31]	0	
Ending Channel Number [0..31]	3	
Channel Name		
Input Range	±10 V	
Scale Factor	1.000	
Offset Constant	0.000	
Sampling Rate, Hz	100.000	CLOCKED
Run Duration, sec.	4.000	
Start Method	Normal	
Trigger Interface Device [0..5]	0	
Trigger Interface Channel [0..0]	0	
Trigger Pattern to AND [0..255]	1	
Trigger Pattern to XOR [0..255]	0	
Time Delay, sec. [0.0..1.0E+08]	0.000	
Analog Trigger Value	0.000	
Trigger Polarity	High	

Channels: 4 Maximum sampling rate for clocked timing:

6250.000 Hz

Table 4.4: Hardware Device List of the Riley Stoker Data Acquisition System

NOTEBOOK HARDWARE INSTALLATION Current installed devices are as follows:

Device Number	Base Addr. (hex)		Device Description (AD: Analog Input, DA: Analog Output)
0	0	DEMO BOARD	AD: ch. 0-3: demos - AD & DA chs. 4 & 6: echos
1	300	RTI-820	STB-HL, 64 AD chans, ±10V; 16 DA chans, ±5V
2	300	RTI-820	STB-HL, 64 AD chans, ±10V; 16 DA chans, ±5V
3	300	RTI-820	STB-TC Thermocouple Panel
4	340	RTI-815	32/16 AD chans, ±10V; 2 DA chans, ±10V
5	300	RTI-820	STB-HL, 64 AD chans, ±10V; 16 DA chans, ±5V

similar to that at UNH.

4.2 Experimental Procedures and Processing of Data

4.2.1 Experimental Procedures to Determine Bubble Characteristics

This section describes the method adopted in obtaining data pertaining to bubble properties. The procedures used at the UNH and Riley facilities were almost identical. The method used at UNH is described in detail here and any difference from the procedure adopted at Riley is highligted at the end of this section. The CFB was charged with circulating and dense bed material. Air flow from the compressor and blower were started. This resulted in the dense bed material being fluidized in a bubbling or slugging mode. L-valve motive and assist air was then introduced, thereby starting solids circulation. The L-valve served as a control for solids mass flux. This parameter was fixed by primarily adjusting the motive air flow. Steady state was reached within two to five minutes of startup, and the solids flowrate measured in the downcomer by following one particle down in a stick-slip fashion over a specified distance. Once steady state was attained, all the electronics were switched on to get bubble data from the dense bed for a period of 4 seconds. Details of solids movement procedures including calibration of the L-valve are discussed in the Results and Discussion chapter of this thesis. The theory behind processing of the pressure signals to obtain bubble length, bubble rise velocity and bubble frequency is as follows: as a bubble or a slug passes a pressure probe a sinusoidal trace is obtained, showing the pressure changes surrounding the bubble or slug. The regions of lowest solids density, as in the centre of the bubble constitute the trough of the signal, while the region of high solid density outside the bubble constitutes the peak. Such fluctuations in pressure can only be seen if the pressure is sampled at a high enough frequency of the order of 100 Hz. A typical pressure trace is shown in Fig. 4.6. Details of this method of digital signal analysis has been explained in the Theory chapter of this thesis. As mentioned earlier,the procedures adopted for the measurement of bubble parameters for both UNH and Riley Stoker units

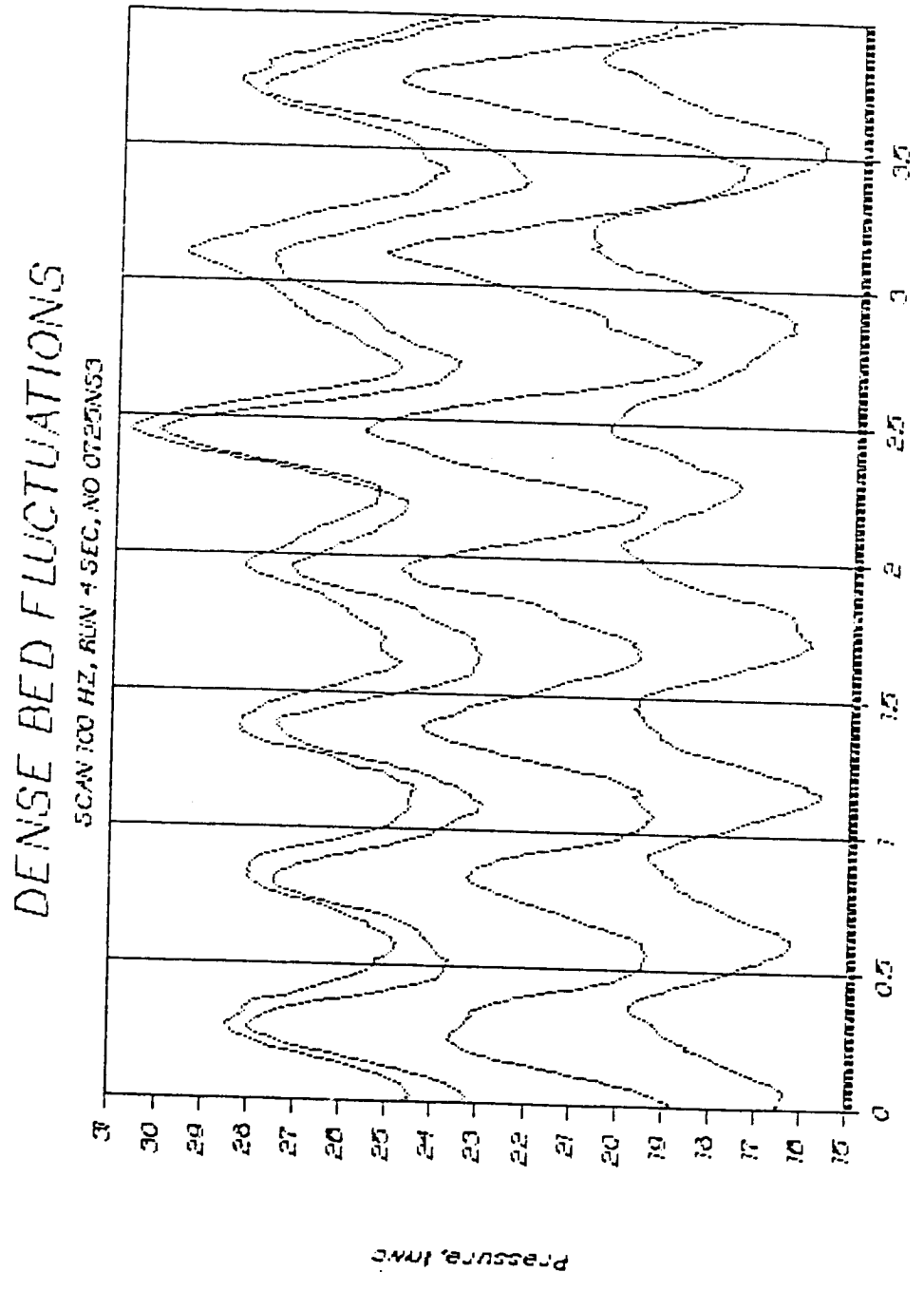

Figure 4.10: Typical Pressure Trace resulting from the Dense Bed Pressure Fluctuations

were similar. There was only one major difference in the overall experimental procedure; solids mass flow measurements in the Riley Stoker unit was conducted using an isokinetic sampling technique instead of following a particle down a specified section of the downcomer over a period of time. The latter technique is more accurate and it was possible to use this method in the UNH unit because the downcomer was clear acrylic. The isokinetic sampling method had to be used in the Riley Stoker pilot plant as the downcomer was primarily opaque except for a very short section.

The isokinetic sampling method is routinely used in the industry to measure solids flow rates in gas-solid suspensions. It consists of inserting a sampling probe into the unit containing the suspension flow, accurately aligning the mouth of the probe with the flow , and ajusting the sampling rate to the true suspension velocity. This adjustment is typically done by monitoring the vacuum on the sampling line. Thus solids flow rate can be estimated by weighing the sample using the following expression :

$$MassFlowrate_{solids} = \frac{(Weight_{sample})(Area_{column})}{(Area_{probemouth})(Time_{sampling})} \tag{4.2.1}$$

4.3 Residence Time Measurements at the UNH facility

The unit 0.102m (4") CFB unit was used to measure average residence times of the circulating fine particles in the dense bed. The defluidization method was adopted because of its simplicity, accuracy, and ease of operation. The technique consisted of starting the circulating system, attaining steady state, and then abruptly and instantaneously cutting off all air supplies (primary fluidizing air and L- valve motive and assist air). The solids in the riser would 'defluidize' and gravitate to the bottom. The solids were then removed from the column and the coarse dense bed particles were sieved out. The fines were weighed on an electronic balance. This experiment was subsequently repeated without the dense bed and using the same circulating solids mass flux. The difference in the weights of the two experiments gave the solids 'holdup' due to the dense bed . This weight (or more

appropriately , mass) difference divided by the mass flow rate of solids gave the average residence time of the fine particles due to the presence of the dense bed.

Chapter 5

RESULTS AND DISCUSSION

This chapter deals with the discussion of experimental results and the analysis of the mathematical model developed for the determination of residence times of fine particles in the dense bed section. The chapter is divided into three sections, namely, L-valve Characterization, Measurement of Bubble Properties in the Dense Bed of a CFB, and, Residence Time of Fine Particles in the Dense Bed of a CFB.

5.1 L-valve Characterization

The L-valve is a robust solids recirculating and measuring device often used in the combustion industry. It consists of a right angle elbow with a motive air port just above the bend. It also has an assist air tube, with holes along the tube axis, to keep the solids in the horizontal leg of the L-valve in a loosely suspended or 'fluidized' state (Fig.5.1). This facilitates movement of solids by the L-valve; control action (regulation of mass flux) comes primarily by adjusting the motive air flow rates. There is no solids flow with the motive air off.

The most attractive features of this solids recirculating and measuring device include ease of manufacture, absence of moving parts and simple operation. However, calibrating such a device accurately is a relatively difficult task.

The L-valve is, typically, one of the primary solids recirculating devices employed in loop fluidized beds. Hot and cold L-valves are used in transporting solids through various different sections of a circulating fluidized bed combustor. Hence it is important to gain

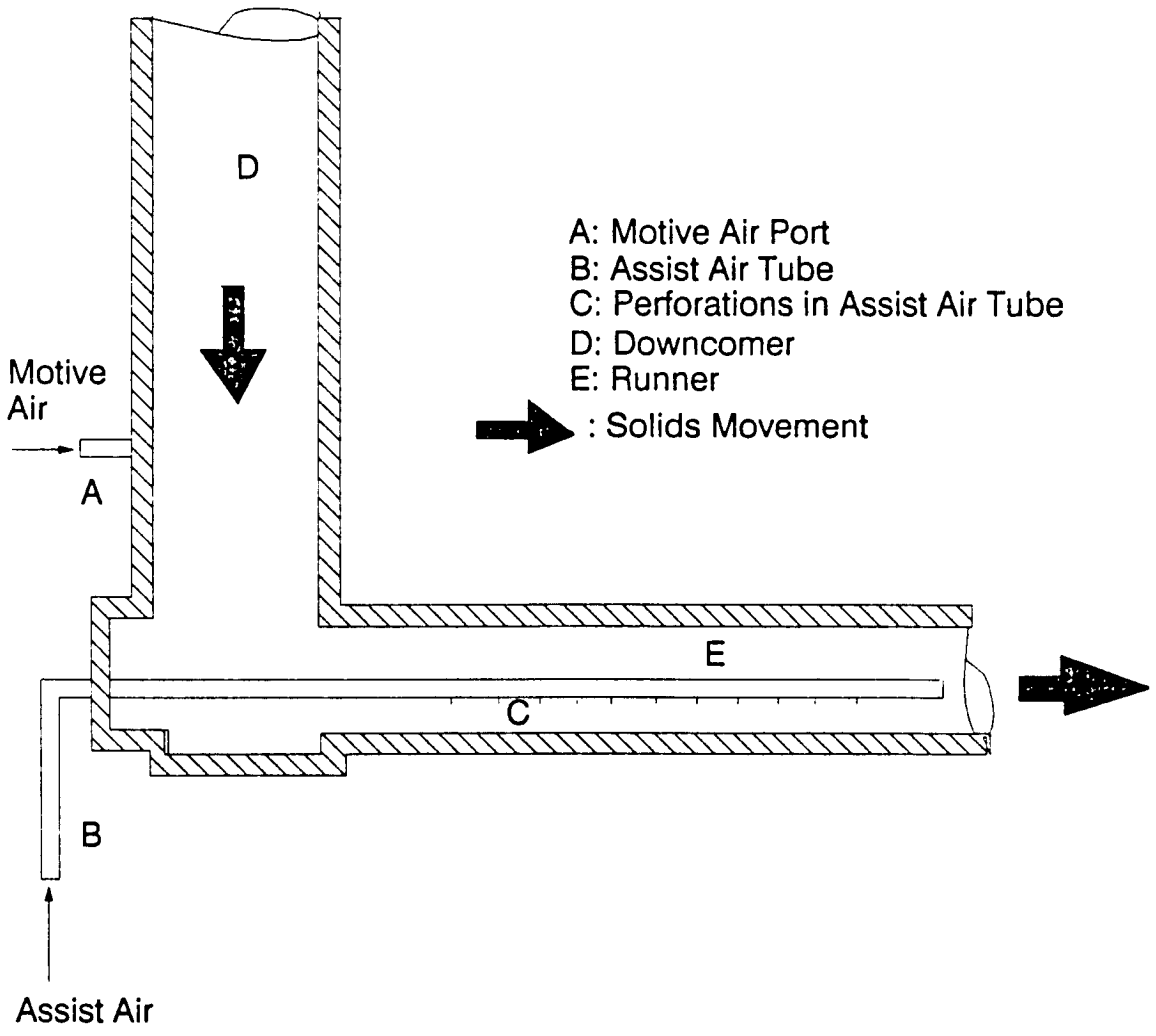

Figure 5.1: Schematic Diagram of an L-valve

an insight into the operation and mechanics of such a device. Unfortunately, very little information is currently available in the literature as regards characterizing the L-valve. Knowlton et al.[15] have done pioneering work in this area, presenting the important features and functions of such a device.

5.1.1 Measurement of Void Fraction Near an L-valve

In the present experimental study, efforts were made to characterize (including calibration) a 0.038m (n.d.) L-valve. Characterization consisted of measuring two critical parameters of an L-valve. The first was solids flow rate through the L-valve as a function of motive and assist air rates. The second was measuring void fraction near the bend of the L-valve , also as a function of motive and assist air rates. In the latter case, use was made of the Auburn solids monitor which employs a capacitance technique to measure solids fraction.

5.1.2 Discussion of Experimental Results

The solids feed and recirculating section of a circulating fluidized bed unit is of critical importance. Performance characteristics of a CFB including turndown, which is probably one of the most attractive features of a CFB, are controlled by this section. Thus an open loop segment of the recirculating section of a CFB was constructed and characterized for solids flow and void fraction. The following discussion pertains to the analysis of data from such a system. The first set of experiments were conducted on a short horizontal leg B-C of 0.41m (16") as shown in Fig 5.2. Results are discussed in the following section (part A). In Part B, experimental results obtained with a longer horizontal section of 0.914m (36") are described.

Part A: Experiments conducted with the 0.41m horizontal leg

The initial measurements were made of solids fraction in the vertical section AB, with increasing total air flow . Solids fractions were measured using the Auburn mass fraction

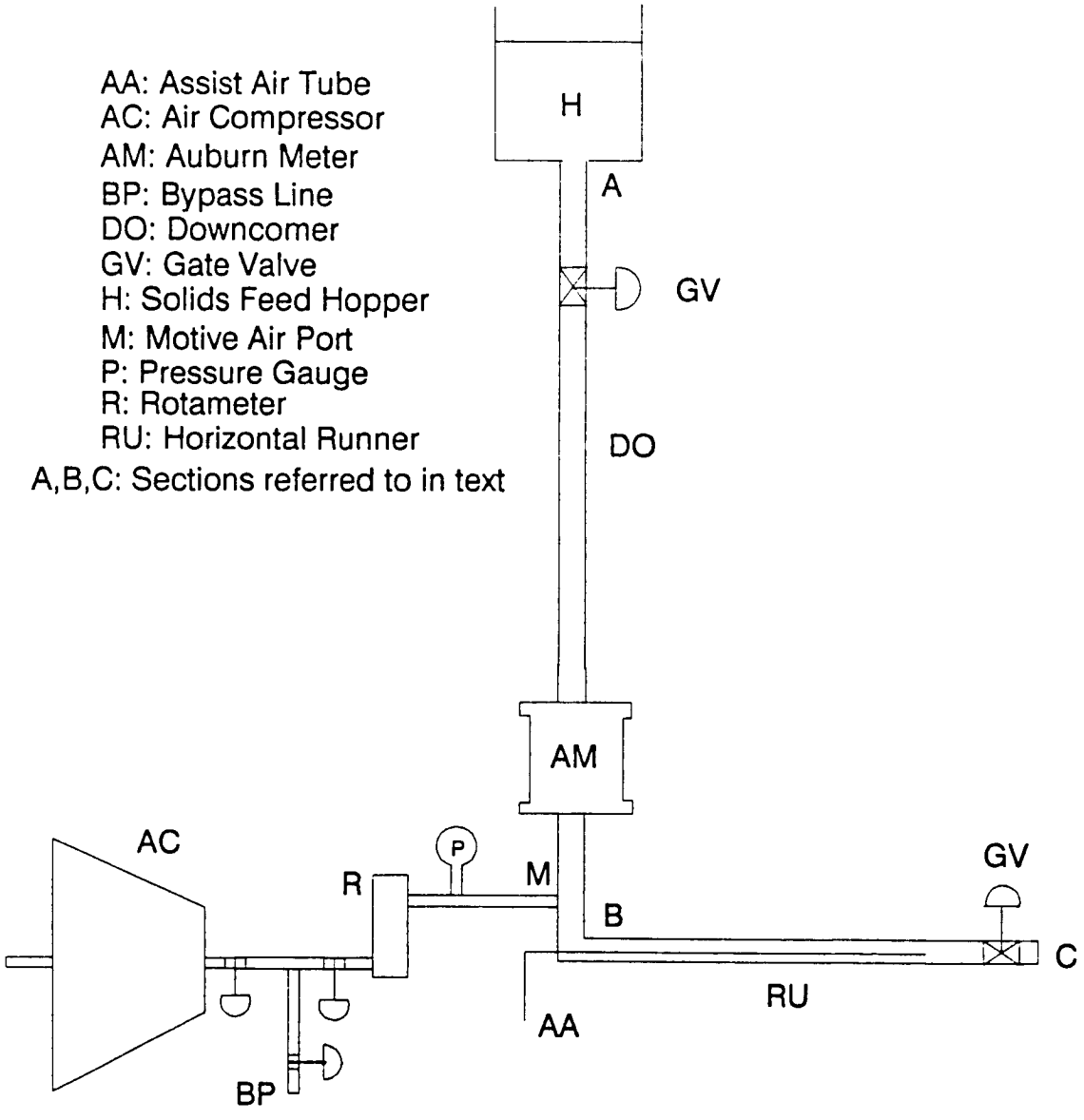

Figure 5.2: Experimental Assembly for L-valve Characterization

meter. Air flow rates were measured using a rotameter. Only the motive air flow rate was recorded ; the assist air rate, being about 1% of the total air rate was not metered. The procedure consisted of filling the downcomer AB with sand and introducing motive and assist air. Solids fractions were then recorded for various air rates. The values of solids fraction with increasing motive air flow rate are presented in Table 5.1.

Table 5.1: Experimental Data of Solids Fraction and Motive Air Flow Rate for 0.41m Runner

Serial No.	Rot.Reading	Air Flow Rate	Solids Fraction	Void Fraction
–	–	$Sm^3/s * 10^4$	–	–
1	3.0	2.32	0.520	0.480
2	5.5	3.46	0.480	0.520
3	8.5	4.29	0.400	0.600
4	10.0	4.58	0.340	0.660
5	13.5	5.05	0.260	0.740
6	16.0	5.29	0.120	0.880
7	23.5	5.62	0.040	0.960

The plot of solids fraction versus motive air rate , as shown in Fig. 5.3, shows a decrease in the solids fraction with increasing air flow rates. These data were recorded just before air back-flow up the downcomer occurred. The data were also plotted as void fraction versus motive air rate (Fig. 5.4). As mentioned earlier, all solids fraction measurements were made using the Auburn solids mass fraction meter. This meter gives an analog display of solids fraction in the tube, averaging over six diametrically placed capacitance probes.

Experimental runs were also made to obtain flow rates of solids at different motive air

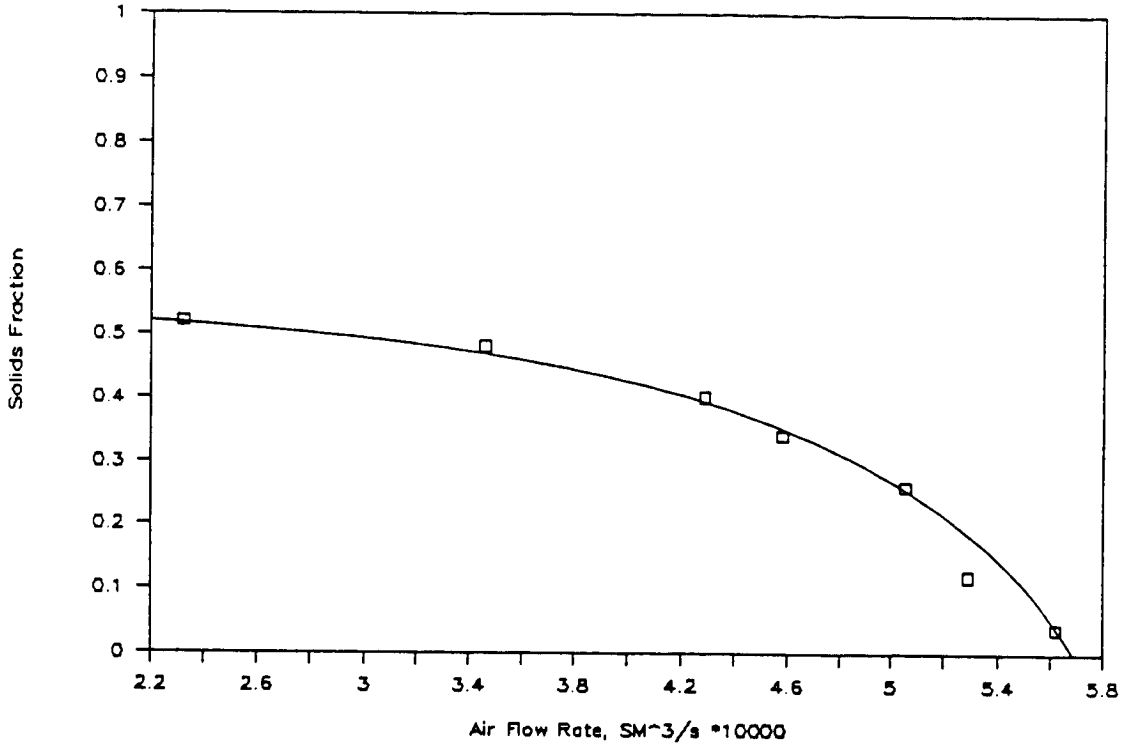

Figure 5.3: Solids Fraction vs Air Flow Rate, 0.41m Runner in L-valve Assembly

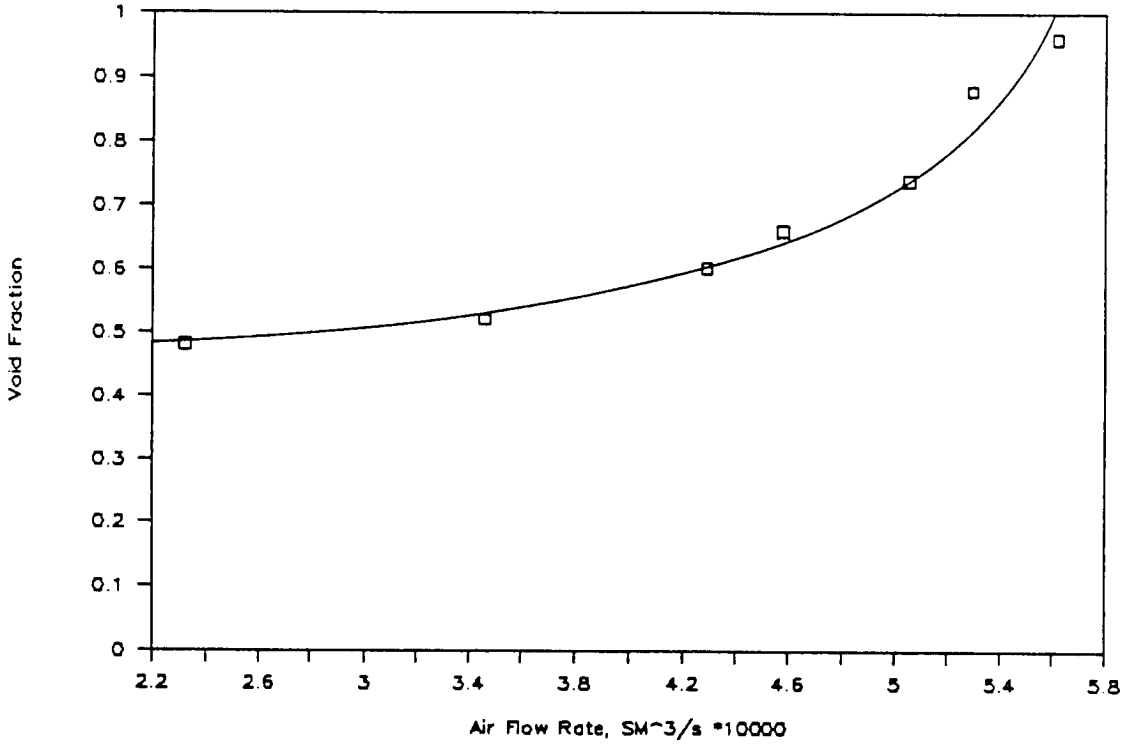

Figure 5.4: Void Fraction vs Air Flow Rate, 0.41m Runner in L-valve Assembly

rates (Table 5.2) .

Table 5.2: Experimental Data of Solids Flowrate and Motive Air Rate for 0.41m Runner

Serial No.	Air Flow Rate	Solids Flow Rate
–	$Sm^3/s * 10^4$	kg/s
1	1.700	0.308
2	3.920	0.376
3	4.719	0.611
4	5.498	0.792
1	1.36	0.132
2	2.59	0.508
3	3.68	0.641
4	4.39	0.786
5	4.81	0.614

Solids flow rates were measured by weighing sand collected over a fixed period of time in a bucket. As shown in Fig. 5.5, solids flow rates increased with increasing motive air rates. There is some scatter in the experimental data. However, there is a region of operation, between motive air rates of $1.42 * 10^{-4}$ to $4.72 * 10^{-4}$ Sm^3/s where it is possible to operate this device in a stable fashion. The scatter in the data is probably due to inaccuracies in the weighing system and the intrinsic difficulties associated with calibrating an L-valve in this fashion. These data were taken over a period of two days. A much larger effect (of different solids flow rates at the same air rates, when data was recorded on different days) was observed during the preliminary experiments conducted at an industrial facility; those data are not reported in this thesis.

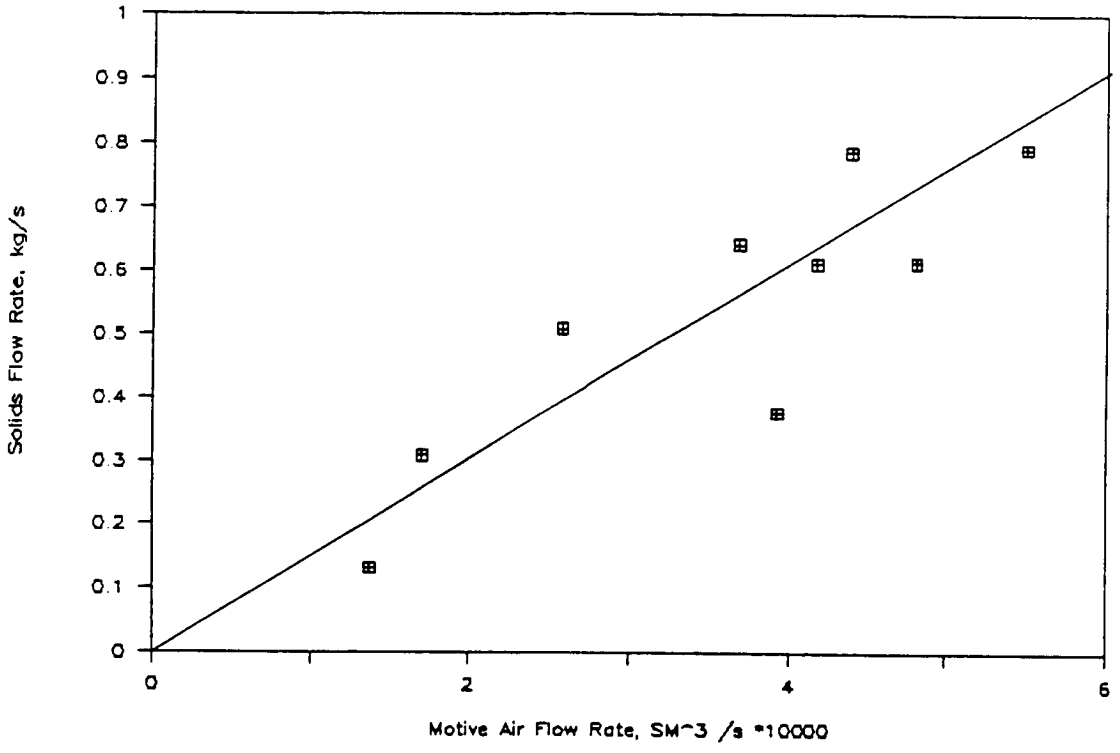

Figure 5.5: Solids Flow Rate vs Motive Air Flow Rate, 0.41m Runner in L-valve Assembly

In the second series of experiments, data were recorded with the downcomer filled to different initial heights with sand particles (Table 5.3).

Table 5.3: Experimental Data of Solids Fraction and Initial Height in Downcomer for 0.41m Runner, at Constant Air Flow Rate of $3.63 * 10^{-4}\ Sm^3/s$

Serial No.	Initial Height of Solids in downcomer	Solids Fraction in downcomer	Void Fraction in downcomer
–	m	–	–
1	0.762	0.626	0.374
2	0.838	0.630	0.370
3	0.889	0.630	0.370
4	0.965	0.628	0.372
5	1.016	0.630	0.370
6	1.092	0.625	0.375
7	1.143	0.630	0.370

These experiments were conducted to see if solids head in the downcomer had any effect on the void fraction (in turn, solids flow rate) near the bend of the L- valve. Flow was in the stick-slip regime. There were minor variations observed in the voidage with increasing initial height of sand particles in the downcomer . This is shown in Fig. 5.6.

Part B: Experiments with a 0.914m Horizontal Leg

The work described in this section was conducted primarily to observe further, the behavior of an L-valve under conditions similiar to that one would encounter in a closed loop circulating fluidized bed with a dense bed. The dense bed was simulated by throttling the

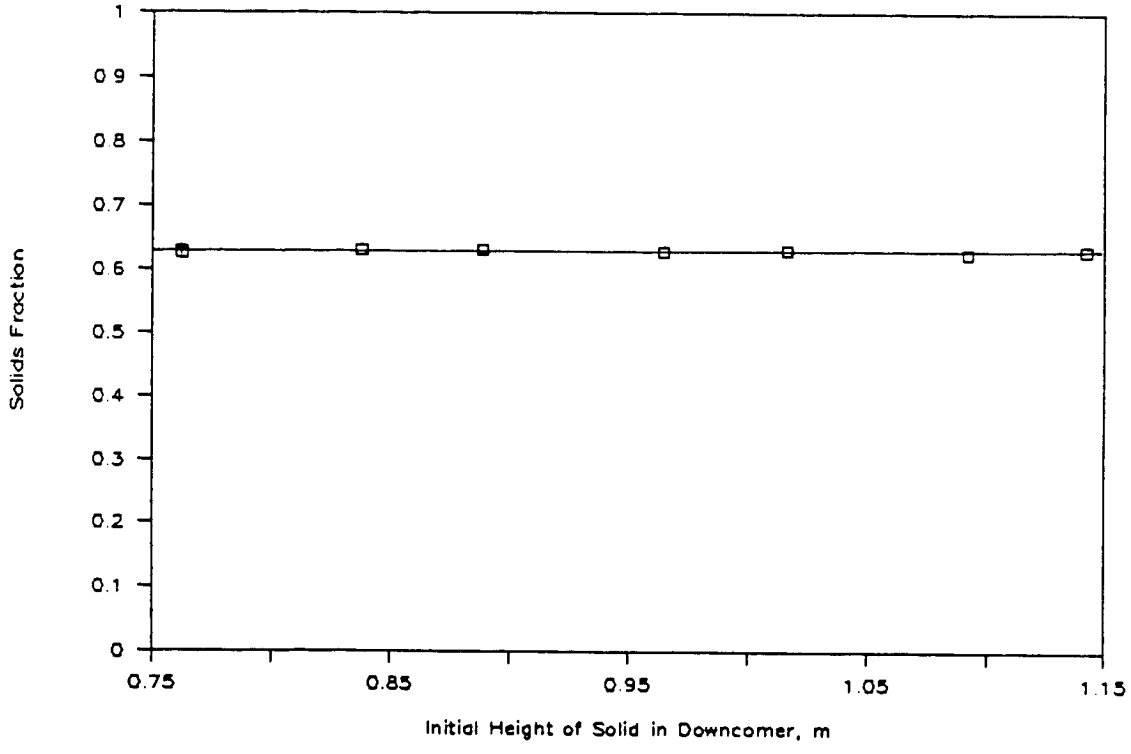

Figure 5.6: Solids Fraction vs Initial Height of Solids in Downcomer

gas through a gate valve at the end of the runner BC, which served as a major pressure drop unit in the circuit. The behavior was again characterized by measuring solids fraction near the bend and solids flow rates, with varying motive air flow rates. The experimental unit used in this investigation was a modified version of the one used in Part A. Details of the experimental apparatus and the procedure are available elsewhere in this thesis. Briefly, the procedure consisted of filling the downcomer with sand and varying the motive air pressure by throttling the gas at the downstream gate valve. Solids fraction values were recorded using the Auburn meter. This is tabulated in Table 5.4.

Table 5.4: Experimental Data of Solids Fraction and Air Flow for 0.91m Runner

Serial No.	Air Pressure near bend	Air Flow Rate	Solids Fraction
–	kPa	$Sm^3/s * 10^4$	–
1	104.8	1.746	0.520
2	108.3	2.313	0.440
3	111.7	2.926	0.375
4	117.2	3.634	0.330
5	119.3	4.058	0.300
6	124.8	4.648	0.220
7	130.3	5.403	0.150

Fig. 5.7 shows the variation of solids fraction versus motive air flow rate. There was a decrease in solids fraction with an increase in motive air flow rate . This was expected as higher amounts of air near the bend area increased the void fraction in that region. Compared to the results obtained with the 0.41m horizontal leg, the solids fractions for a given motive air flow rate are significantly lower. This can be explained by the fact that

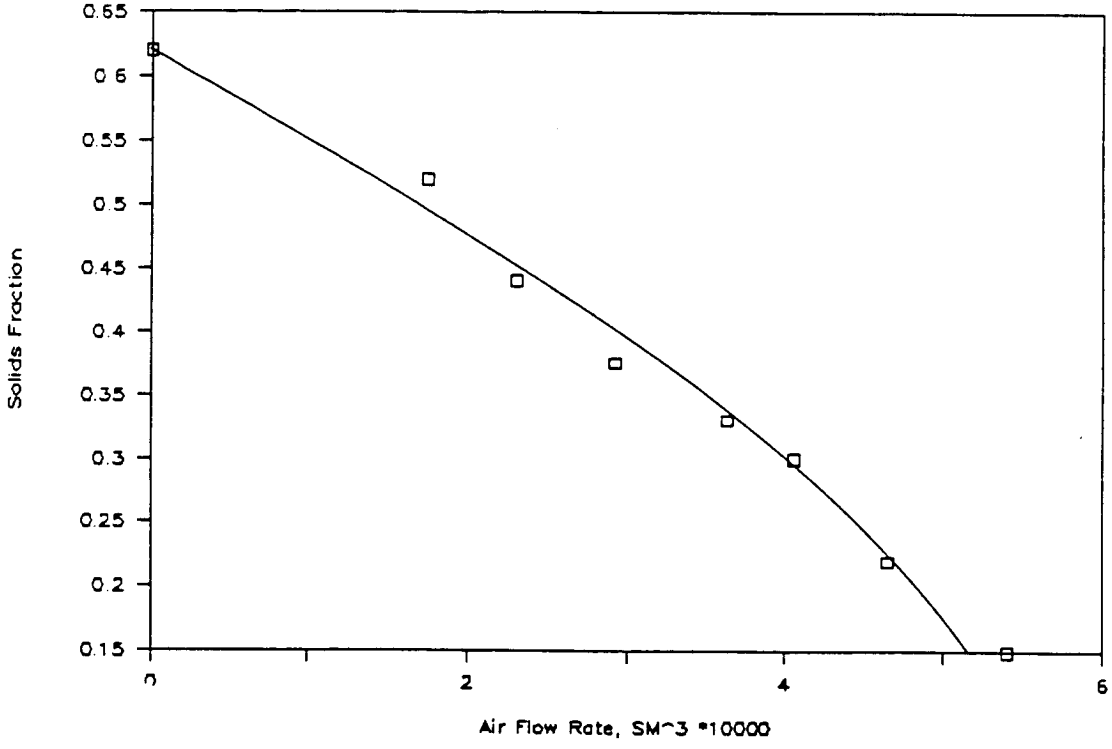

Figure 5.7: Solids Fraction vs Motive Air Flow Rate, 0.914m Runner in L-valve Assembly

a longer runner filled with moving solids created a greater flow resistance than a shorter section. This forced some of the motive air up the riser, accounting for the larger voidage (lower solids fraction) values.

Fig. 5.8 shows the variation of solids fraction with inlet air pressure. This relationship has the same behavior as the solids fraction versus air flow rate curve. As the air pressure increased , air flow rate also increased, thereby reducing solids fractions.

Solids fractions near the bend of the L-valve were measured with the Auburn solids meter. This parameter would be useful in understanding solids-air behavior near the L-valve reigon of the combustor in actual practice. The effect of changing the horizontal runner length showed that shorter ones results in greater solids fractions, hence greater solids flow rates. This is an important design criteria.

In short this study generated Fig. 5.1 through 5.8 which shows the behavior of the L-valve. This behavior is primarily characterized by solids flow rate and void fraction near the bend. The parameters that were varied independently were motive air flow rate and initial height of solids in the downcomer. One objective of this study was to have data that would help characterize any L-valve , especially one operating under 'hot' conditions. The figures 5.3 and 5.5 thus constitute 'calibration plots'. These calibration plots, particularly ones for solids flow rate versus motive air flow rate, and solids fraction versus motive air flow rate are of great significance in a hot industrial unit. In such a unit the solids flow rate and void fraction could be characterized by simply monitoring the motive air and reverting to the calibration charts. In-situ measurements of solids flow rate and void fraction in a CFB combustor are extremely difficult. A hot isokinetic sampling technique would have to be used in the riser section of the CFB to estimate solid mass flowrates.

5.1.3 Solids flux measurement technique used in this study

In this study, because the experimental apparatus was constructed of clear plexiglass, a different technique was used to measure solids flow rate. The downcomer was marked on a

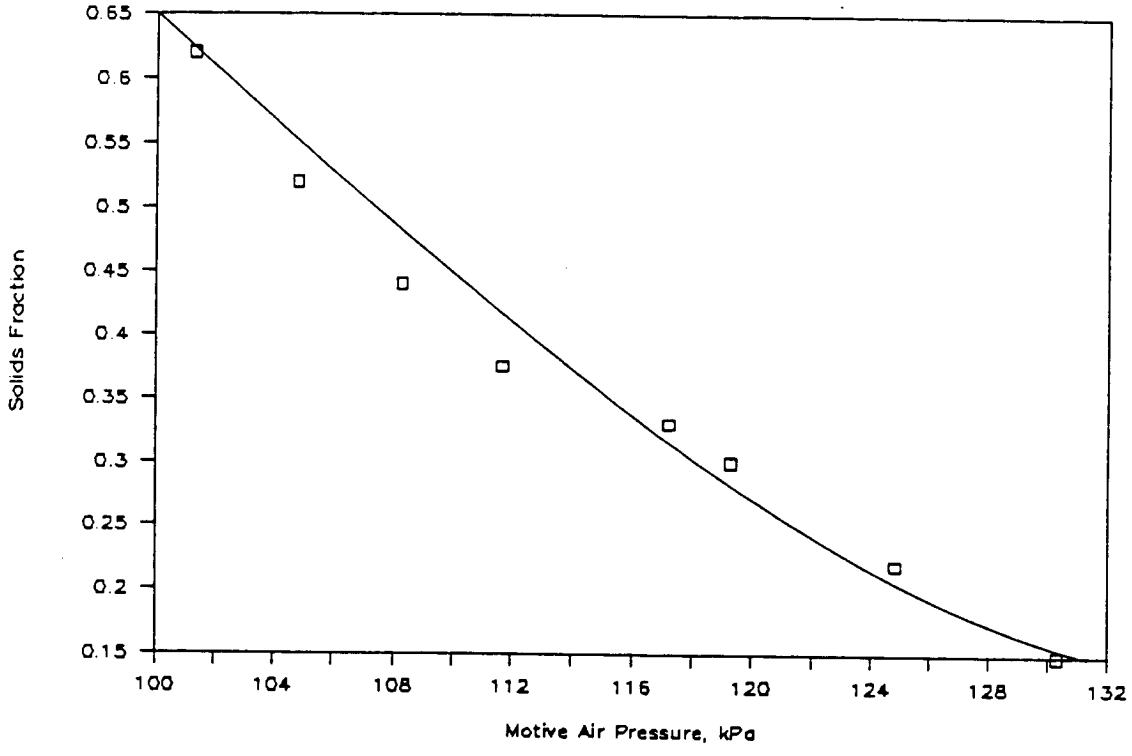

Figure 5.8: Solids Fraction vs Motive Air Pressure, 0.914m Runner in L-valve Assembly

linear scale, and solid particles were tracked visually over a specified distance to give particles velocities. This value when multiplied by the average bulk density in the downcomer yields solids mass flux. The average bulk density is given by the equation:

$$\rho_b = \epsilon\rho_g + (1-\epsilon)\rho_s \tag{5.1.1}$$

where ρ_b is the average bulk density,ϵ is the void fraction, ρ_g is the density of gas (air) and ρ_s is the density of solids. The void fraction, ϵ was the only parameter that was used in the subsequent determination of mass flux in this study. This is a more 'direct' method of obtaining solids flow rates or mass fluxes when the material of construction permits. Cold units typically are fabricated of clear acrylic or glass and hence a direct measurement is advisable.

5.2 Measurement of Bubble Properties in the Dense Bed of a CFB

The passage of gas bubbles causes pressure fluctuations in a fluidized bed. This property has been utilized to characterize the bubbles with respect to size, velocity and frequency. Size of a bubble has been defined as the 'pierced length of bubble', velocity as the 'rise velocity of the bubble' and frequency as the number of bubbles passing a given point in the bed per second. Details of the theory, pressure probes used in the measurements and the on-line data aquisition system have been presented earlier in this thesis.

Characteristics of the gas bubbles control the performance of the fluidized bed. Size, velocity and frequency control solids mixing, convection and diffusion of gas components (reactants and products), elutriation of fine particles and attrition of large particles. Hence, it is of utmost importance to measure bubble properties and establish their dependence on the major operating parameters. Large particles, when fluidized, typically give rise to slow moving bubbles; the passage of circulating fine particles through coarse solids however

changes bubble characteristics considerably. The objective of this part of the study was to quantify such changes in bubble properties with independent variables such as solids mass flux.

Data were collected from three experimental units - a 0.038m (1.5") diameter column at the UNH facility, a 0.102m (4") diameter column also built and operated at UNH, and a 0.229m (9") square fluidizing column at the Riley Stoker Corporation in Worcester, Mass. All three equipment were 'cold' circulating fluidized bed units. Two air-solids systems were primarily used in the three set-ups : copper dust circulating through steel pellets and sand circulating through rocks. The first system was based on a 'scaling law' analysis and simulated the conditions of a hot combustor when fluidized with air at room temperature. The second system consisted of materials actually used in a hot CFB, but operated at room temperature. Thus, data from the copper-steel system can be viewed as that resulting from the operation of a HOT unit, and the sand-rock system data as that from a $COLD$ unit using materials used in the combustor. Nicastro et al. [31] have shown using experiments and a statistical analysis technique that the 'scaling law materials' yield the pertinant data; this operation using scaling law materials in a cold unit is similar to the operation of a hot unit. If the hot bed materials are used in a cold flow unit, erroneous conclusions are inferred. Thus the copper-steel data of bubble characteristics and residence time of fines in the dense bed truly represent the behavior of an actual hot combustor. Additional rationale for the choice of these sytems is described in the theory chapter of this thesis.

5.2.1 Bubble Characteristics Data from the 0.038m UNH Experimental Unit

The bubble properties in the dense bed were measured using the pressure fluctuation technique, as described earlier. Bubble length in this study was estimated as ' the pierced length of bubble '; subsequently, pierced length of bubble will be simply referred to as 'bubble length' or 'length of bubble'. Bubble rise velocity was calculated from the pressure

signals as the time for the pressure signal from the bubble to traverse unit distance. Bubble frequency was the number of bubbles passing the pressure probe per unit time.

The bubble characteristics for the 0.038m UNH unit are shown in Table 5.5 as a function of circulating solids mass flux for the copper-steel system. Solids mass flux was

Table 5.5: Bubble Characteristics for the UNH 0.038m Unit, Copper-Steel System

Serial No.	Air Velocity	Air Flow rate	Solids Mass Flux	Bubble Length	Bubble Velocity	Bubble Frequency
–	m/s	$kg/s * 10^3$	$kg/sq.m - s$	m	m/s	s^{-1}
1	3.62	4.13	8.96	0.254	0.81	2.2
2	3.62	4.13	9.95	0.288	0.81	1.88
3	3.62	4.13	11.19	0.304	0.98	2.0
4	3.62	4.13	87.79	0.62	0.98	2.0
5	3.62	4.13	117.84	0.762	1.22	1.75
6	3.62	4.13	159.85	0.948	1.63	1.75
7	4.48	5.1	*Nosolids*	0.762	1.22	1.62
8	4.48	5.1	15.99	0.544	1.05	1.87
9	4.48	5.1	41.46	0.588	1.05	1.87
10	4.48	5.1	62.20	0.762	1.22	1.62
11	4.48	5.1	88.85	0.914	1.46	1.62
12	4.48	5.1	143.53	0.853	1.46	1.87
13	4.48	5.1	185.9	1.524	2.44	1.87

varied from about 8.96 kg/sq.m-s to about 185.9 kg/sq.m-s. For comparision purposes one data point was taken at a solids mass flux of zero. The pierced length of bubble is plotted

against solids mass flux in Fig. 5.9. There is an increase in bubble length from about 0.254 to 1.5 m as solids mass flux is increased from approximately 8.96 to 185.9 kg/sq.m-s. This is fairly easily explained if one analyzes the escape mechanism of air and fine particles from the dense bed. As the solids mass flux is increased the dense bed expands. More fluidizing air accumulates between regions of high concentrations of solids. Ultimately this region of increased fluidizing air (constituting a larger bubble) escapes out of the bed. Thus as solids mass flux increases bubble length increases. The rise velocity of bubbles as a function of solids mass flux is plotted in Fig. 5.10. The trend is the same as Fig. 5.9; as solids mass flux increases the bubble rise velocity increases. Values of rise velocity range from about 0.81 to 2.40 m/s as the solids mass flux is increased from 8.96 to 185.9 kg/sq.m-s. This occurs because solids rise faster as solids mass flux is increased (solids continuity). The regions of faster rising solids have accompanying regions of voids interspaced, that also rise with a greater velocity. Bubble frequency has also been tabulated in Table 5.5. This parameter remains fairly constant with increasing solids mass flux, at a value of about 1.75 bubbles/sec passing through the dense bed. This characteristic of the bubble appears to be set by the mode of fluidization, which is fixed by nature of the solids and fluidizing gas .

The sand-rock bubble characteristics data are presented in Table 5.6.

Solids mass flux was again the independent variable and ranged from 5.79 to about 39.5 kg/sq.m-s. Resulting bubble lengths ranged from 0.183 to 0.305 m and bubble rise velocites from 0.386 to 0.965 m/s. Bubble frequencies remained fairly constant at about 1.85 bubbles/s. The length of bubble versus solids mass flux is plotted in Fig. 5.11 and bubble velocity versus mass flux is shown in Fig. 5.12. The relationship is the same as that for the copper-steel system (Fig. 5.9). Bubble lengths increased with increasing mass flux. There were, however, two noticeably different features. The first, the solids circulating range, was considerably lower because of the circulating solids being much larger (300 micron sand as compared to 80 micron avg. diameter for copper). Secondly, there was more scatter in the data, particularly at the lower ranges of solids mass flux, between 5.79

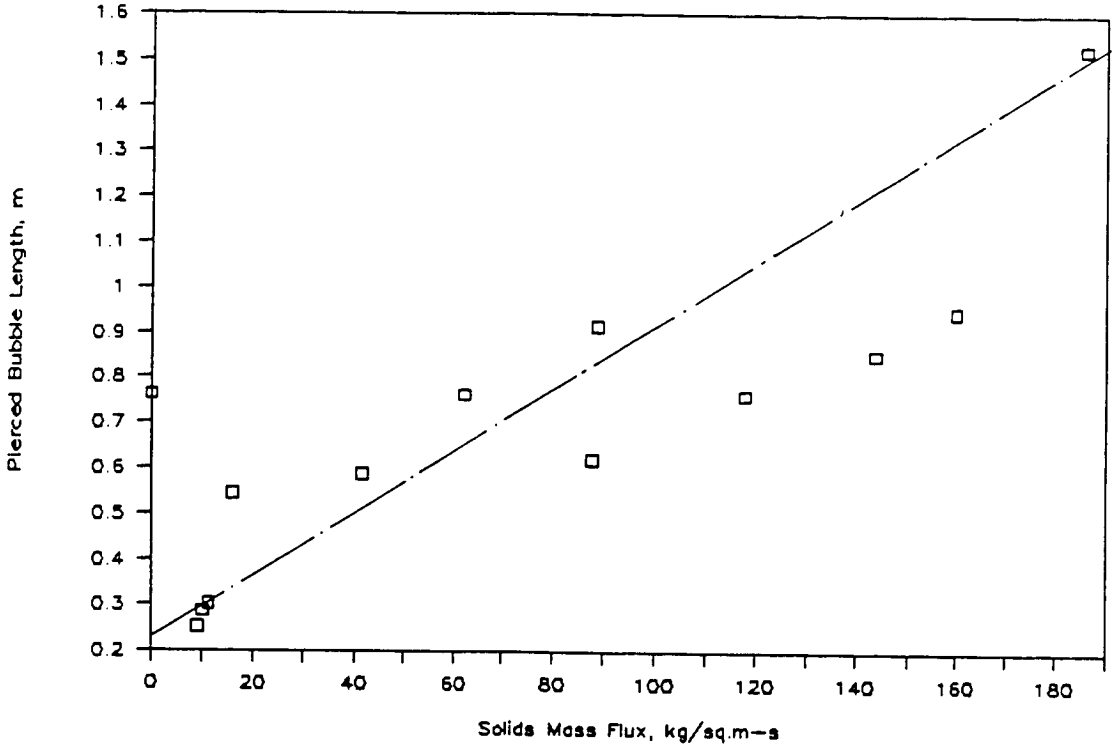

Figure 5.9: Pierced Bubble Length vs Solids Mass Flux, UNH 0.038m Unit, Copper- steel System

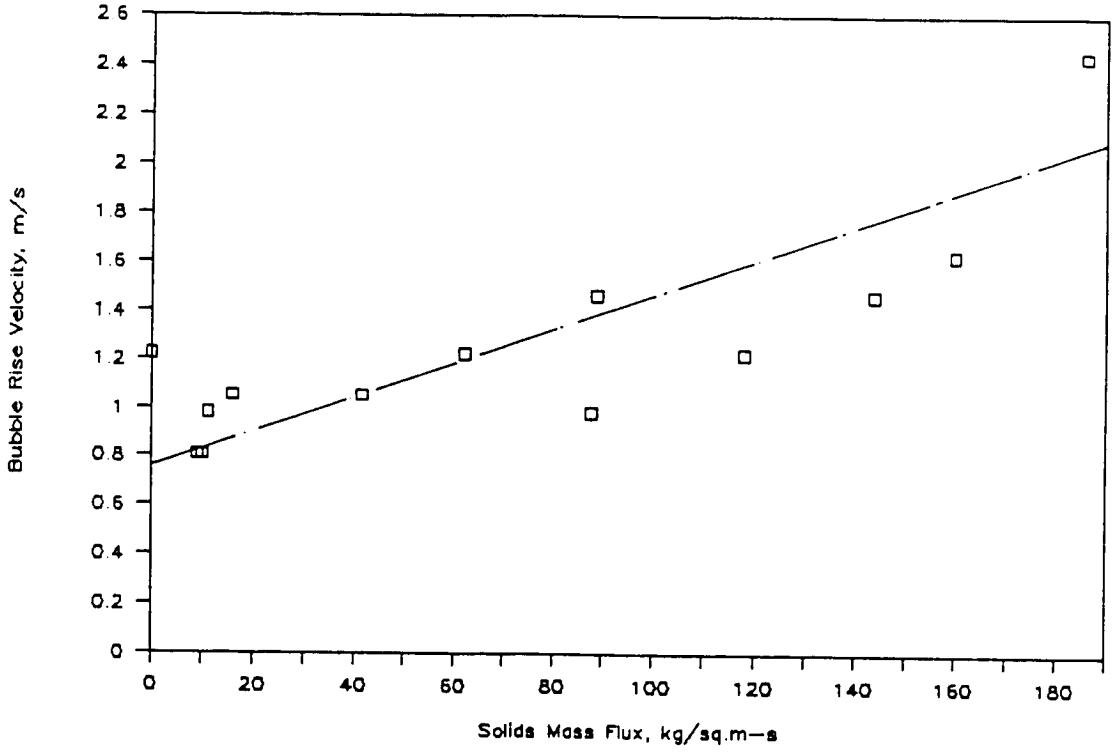

Figure 5.10: Bubble Rise Velocity vs Solids Mass Flux, UNH 0.038m Unit, Copper- steel System

Table 5.6: Bubble Characteristics for the UNH 0.038m Unit, Sand-Rock System

Serial Number –	Air Velocity m/s	Air Flow rate $kg/s * 10^3$	Solids Mass Flux $kg/sq.m - s$	Bubble Length m	Bubble Velocity m/s	Bubble Frequency s^{-1}
1	3.19	4.41	39.53	0.305	0.965	2.2
2	3.19	4.41	28.89	0.305	0.772	1.8
3	3.19	4.41	22.75	0.291	0.552	1.8
4	3.19	4.41	16.69	0.254	0.483	1.9
5	3.19	4.41	13.66	0.282	0.551	1.7
6	3.19	4.41	11.55	0.203	0.429	2.0
7	3.19	4.41	9.16	0.183	0.386	1.8
8	3.19	4.41	8.35	0.237	0.429	1.7
9	3.19	4.41	6.83	0.183	0.386	1.8
10	3.19	4.41	5.79	0.234	0.386	1.8
11	3.19	4.41	*NoSolids*	0.194	0.351	1.8

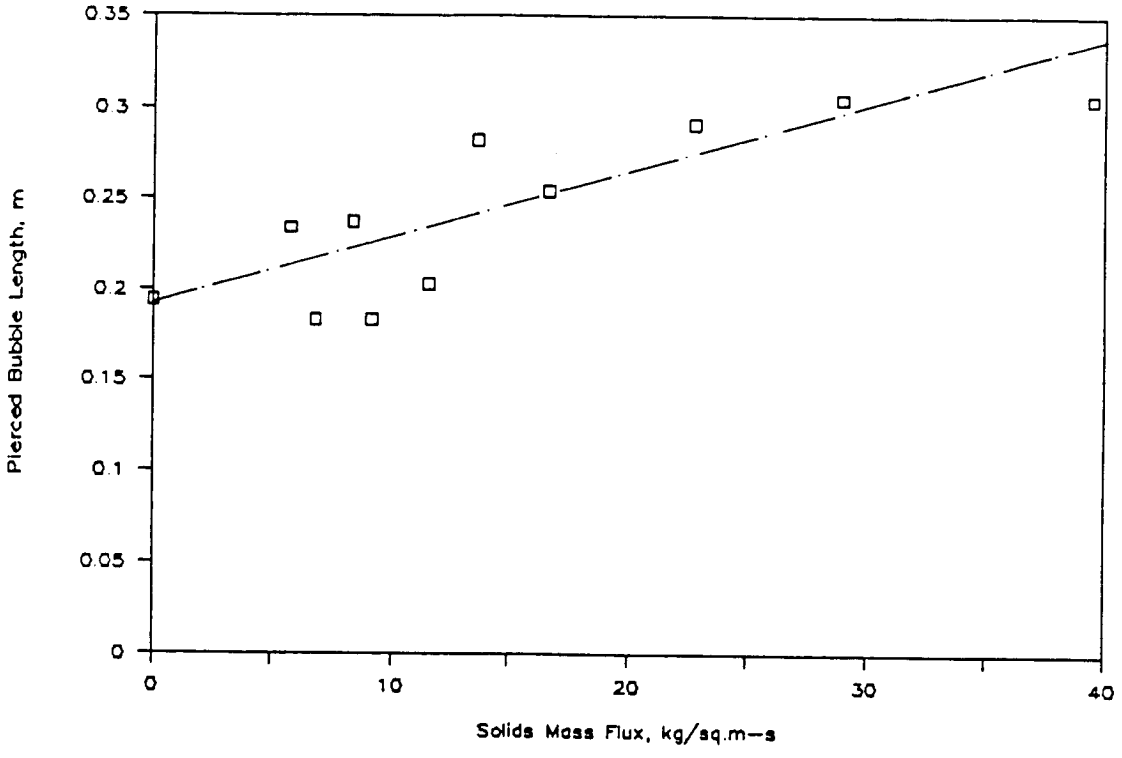

Figure 5.11: Pierced Bubble Length vs Solids Mass Flux, UNH 0.038m Unit, Sand-Rock System

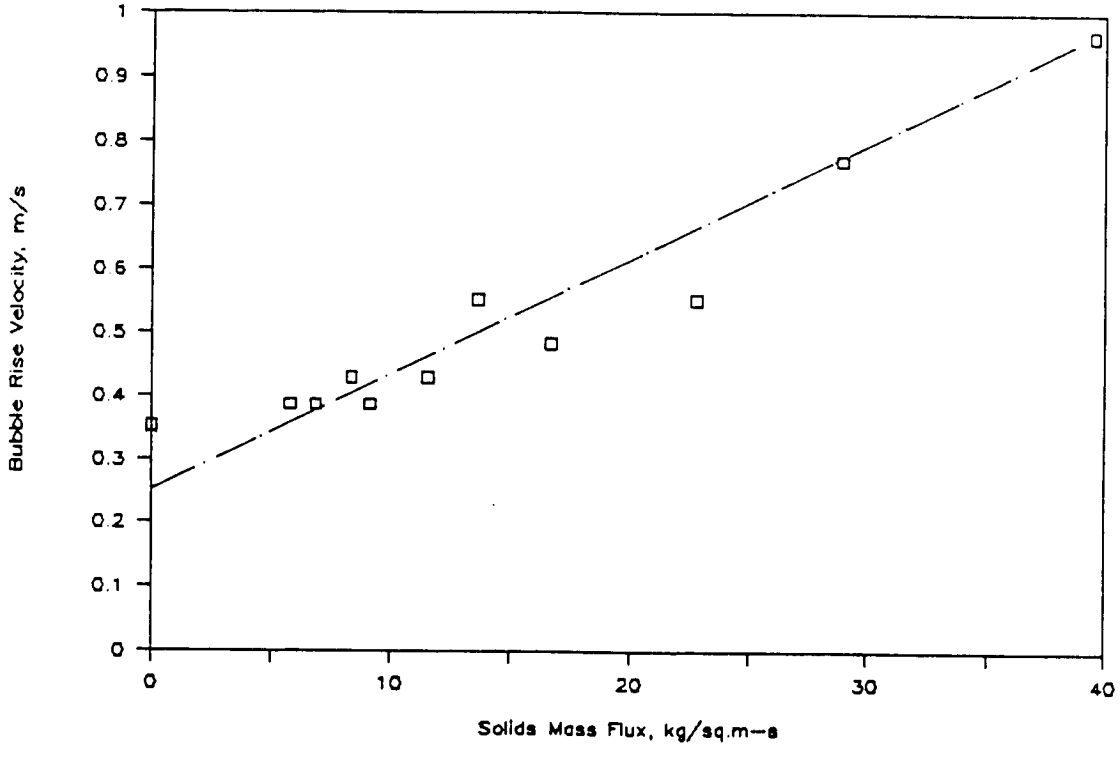

Figure 5.12: Bubble Rise Velocity vs Solids Mass Flux, UNH 0.038m Unit, Sand-Rock System

and 13.66 kg/sq.m-s. The explanations for the increase of length and rise velocity of the bubbles remain the same.

Finally, it may be mentioned that any transport process operated on a column diameter of less than 0.102m(4") suffers from wall effects. In the case of a circulating fluidized bed where sensitive pressure measurements were being made, these effects appear in certain typical ways. It was observed that the dense bed started 'slugging' almost immediately after the onset of fluidization. Hence the word 'bubble' should be more appropriately be replaced by 'slug' for the 0.038m unit. However, the term 'bubble' has been used to encompass elongated bubbles, flat nosed slugs and wall slugs all of which were observed. The flat nosed slugs were by far the most frequently seen.

5.2.2 Bubble Characteristics Data from the 0.102m UNH Experimental Unit

The 0.038m unit was replaced in part by a 0.102m (n.d)section. The riser, which had the dense bed at the bottom, was the section changed. The remainder of the experimental apparatus including pressure probes, pressure transducers, A/D boards and software associated with the data acquisition system were unchanged. Bubble characteristic data were collected in the form of pierced length of bubble, bubble rise velocity and bubble frequency. The independent variable was circulating solids mass flux. Again, two systems were tested - copper-steel and sand-rock.

Table 5.7 shows the bubble data for the copper-steel system. This is plotted as bubble properties versus solids mass flux in Fig. 5.13. Solids mass flux was varied from about 49.76 to 145.8 kg/sq.m-s. There was a very gradual increase in pierced length of bubble from 0.139 m to 0.353 m as the solids mass flux was increased from 49.76 to 145.8 kg/sq.m-s. The corresponding increase in bubble rise velocity was from 0.443 m/s to 1.06 m/s. Bubble frequency again remained fairly constant at about 3.6 bubbles/s. The bubble characteristic data for the sand-rock system is presented in Table 5.8 and plotted in Fig. 5.14. Here

Table 5.7: Bubble Characteristics for the UNH 0.102m Unit, Copper-Steel System

Serial no.	Air Velocity	Air Flow rate	Solids Mass Flux	Bubble Length	Bubble Velocity	Bubble Frequency
–	m/s	$kg/s * 10^3$	$kg/sq.m - s$	m	m/s	s^{-1}
1	4.54	43.5	*NoSolids*	0.142	0.488	3.5
2	4.54	43.5	49.76	0.139	0.443	3.5
3	4.54	43.5	59.70	0.165	0.609	3.5
4	4.54	43.5	80.44	0.203	0.697	3.8
5	4.54	43.5	111.95	0.229	0.813	3.3
6	4.54	43.5	145.80	0.353	1.06	4.0

Table 5.8: Bubble Characteristics for the UNH 0.102m Unit, Sand-Rock System

Serial no.	Air Velocity	Air Flow rate	Solids Mass Flux	Bubble Length	Bubble Velocity	Bubble Frequency
–	m/s	$kg/s * 10^3$	$kg/sq.m - s$	m	m/s	s^{-1}
1	4.08	38.9	*No Solids*	0.109	0.348	2.75
2	4.08	38.9	10.38	0.125	0.375	2.75
3	4.08	38.9	15.49	0.142	0.487	2.75
4	4.08	38.9	17.49	0.119	0.406	2.5
5	4.08	38.9	20.46	0.254	0.813	1.75
6	4.08	38.9	27.80	0.229	0.406	1.6
7	4.08	38.9	34.18	0.279	0.610	1.75

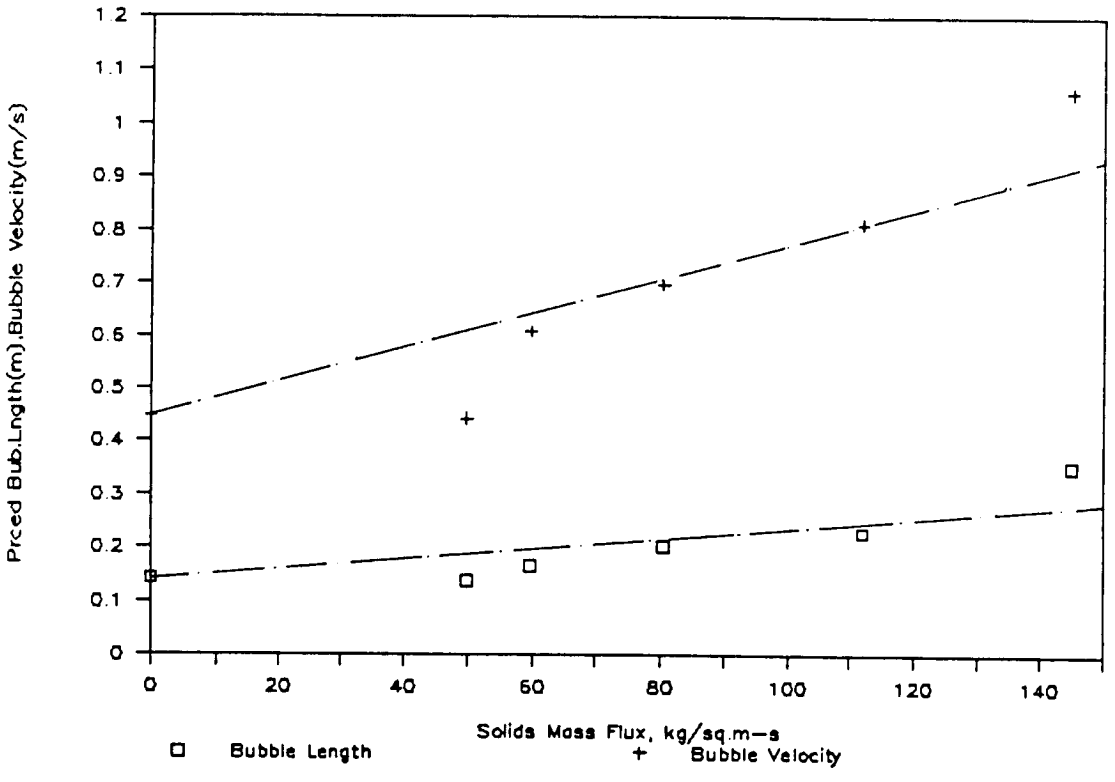

Figure 5.13: Bubble/slug Properties, UNH 0.102m Unit, Copper-steel System

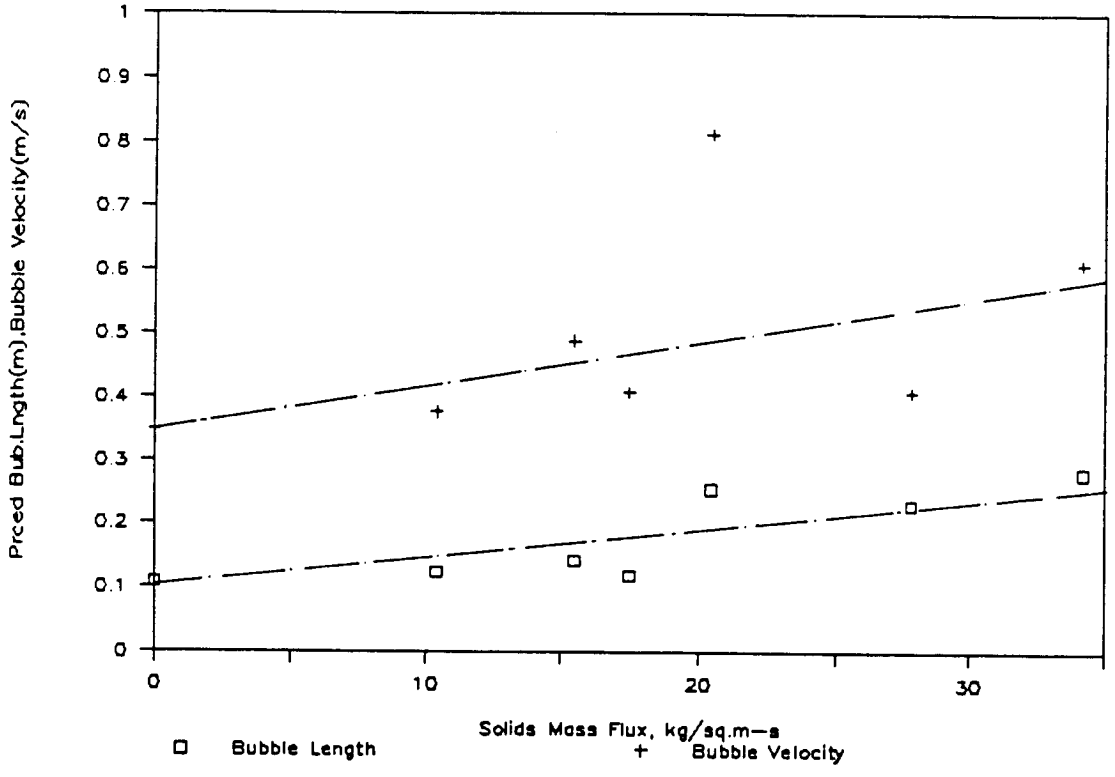

Figure 5.14: Bubble/slug Properties, UNH 0.102m Unit, Sand-rock System

the solids mass flux was increased from 10.38 to around 34.2 kg/sq.m-s. Bubble lengths increased from 0.125 m to 0.279 m. Bubble rise velocities also increased from 0.375 m/s to 0.813 m/s. Bubble frequencies decreased slightly from 2.75 to 1.75 bubbles/s.

5.2.3 Bubble Charactersitics Data from the 0.229m Riley Stoker Unit

The experimental data analysed in this section was obtained at the Riley Stoker facility in Worcester, Massachussetts. The unit essentially consisted of a 0.229m x 0.229m column where solids are fluidized with air. Circulating solids were captured by a cyclone and returned to the riser by L-valves. A hydrodynamic study of the flow of fine particles through the dense bed of large particles with respect to bubble characteristics was conducted, as in the earlier cases of experimentation at the UNH facility. Bubbles were characterized by their pierced length, rise velocity through the dense bed and frequency. Solid systems studied were copper fines circulating through steel shots and sand particles through rocks. The data are presented in Tables 5.9 and 5.10 and also shown in Fig.5.15 through 5.18.

The data on the copper-steel system is presented in Table 5.9 and plotted in Figs. 5.15 and 5.16. This system, as mentioned earlier, simulates the actual operation of a hot CFB. Fig 5.15 shows an increase in the bubble length of about 0.007 m for an increase in solids mass flux of 1 kg/sq.m-s. Fig 5.16 shows an increase in the bubble rise velocity of about 0.03m/s for an increase of 1.0 kg/sq.m-s of solids mass flux.

Figs. 5.17 and 5.18 are similar to Figs.5.15 and 5.16 respectively, except they pertain to the sand-rock system. For comparision, the ordinates of Fig.5.17 and 5.18 are maintained the same as Figs.5.15 and 5.16, respectively. This data represents the 'cold' operation of CFB using materials that are actually used in a hot combustor. The data have been taken at two sets of air superficial velocities of 3.69 and 4.12 m/s. This small variation in air superficial velocities does not show any significant effect. There is an increase of about 0.37 in elongated bubble length for an increase of 1 kg/sq.m-s of solids mass flux. Comparing this to the value of 0.007m/ 1 kg/sq.m-s as obtained in the copper-steel system, it is evident

Table 5.9: Bubble Characteristics for the Riley Stoker 0.229m Unit, Copper-Steel System

Serial no.	Air Velocity	Air Flow rate	Solids Mass Flux	Bubble Length	Bubble Velocity	Bubble Frequency
–	m/s	kg/s	$kg/sq.m-s$	m	m/s	s^{-1}
1	2.51	0.154	0.0	No	$Bubbles,$	$Min.Fluidzn$
2	3.13	0.193	0.0	0.214	0.363	1.75
3	3.76	0.231	0.0	0.295	0.508	1.81
4	4.38	0.269	0.0	0.36	0.635	1.94
5	3.61	0.222	5.89	0.171	0.318	2.3
6	3.61	0.222	11.69	0.085	0.423	3.0
7	3.61	0.222	15.59	0.085	0.282	2.5
8	3.61	0.222	16.17	0.217	0.417	2.0
9	3.61	0.222	22.22	0.163	0.508	2.3

Table 5.10: Bubble Characteristics for the Riley Stoker 0.229m Unit, Sand-Rock System

Serial no.	Air Velocity	Air Flow rate	Solids Mass Flux	Bubble Length	Bubble Velocity	Bubble Frequency
–	m/s	kg/s	$kg/sq.m-s$	m	m/s	s^{-1}
1	4.1	0.252	0.0	1.143	1.829	1.75
2	4.1	0.252	0.18	0.683	1.219	1.75
3	4.1	0.252	0.457	0.635	1.219	1.88
4	4.1	0.252	0.619	0.762	1.524	2.10
5	4.1	0.252	1.598	1.029	1.829	1.88
6	3.69	0.227	0.0	1.263	2.09	1.75
7	3.69	0.227	1.734	1.036	1.463	2.00
8	3.69	0.227	2.994	1.029	1.829	2.00
9	3.69	0.227	3.582	1.219	2.438	2.00

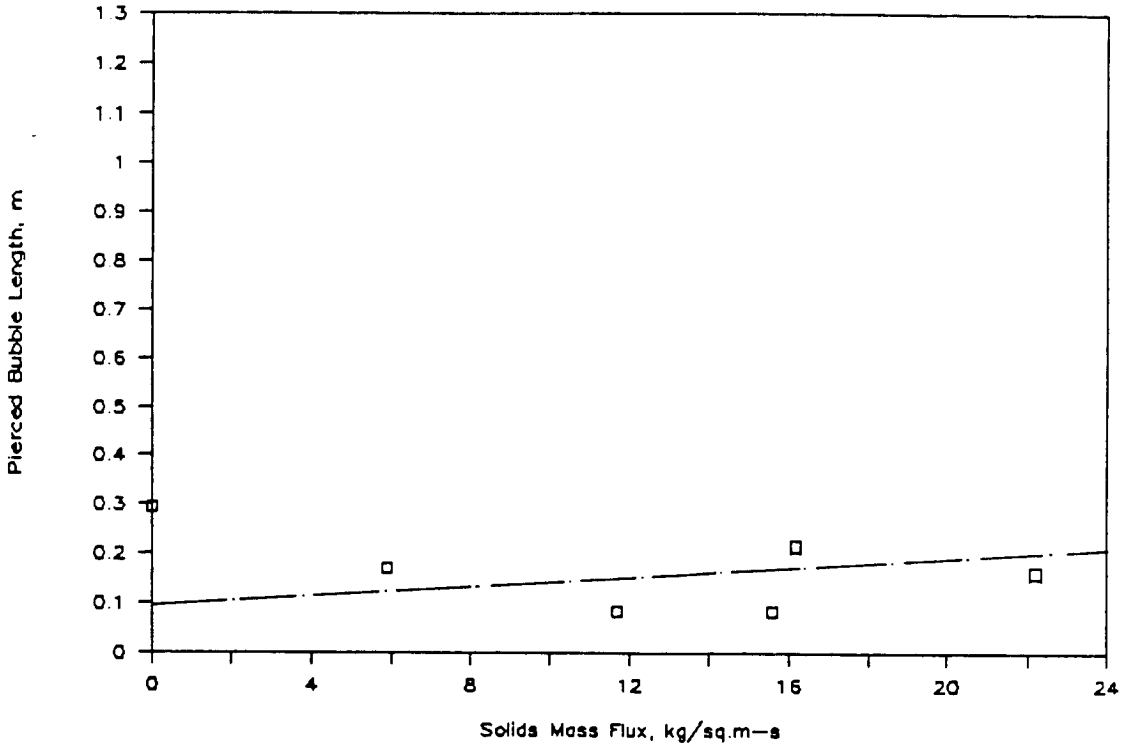

Figure 5.15: Pierced Bubble Length vs Solids Mass Flux, Riley 0.229m Unit, Copper- steel System

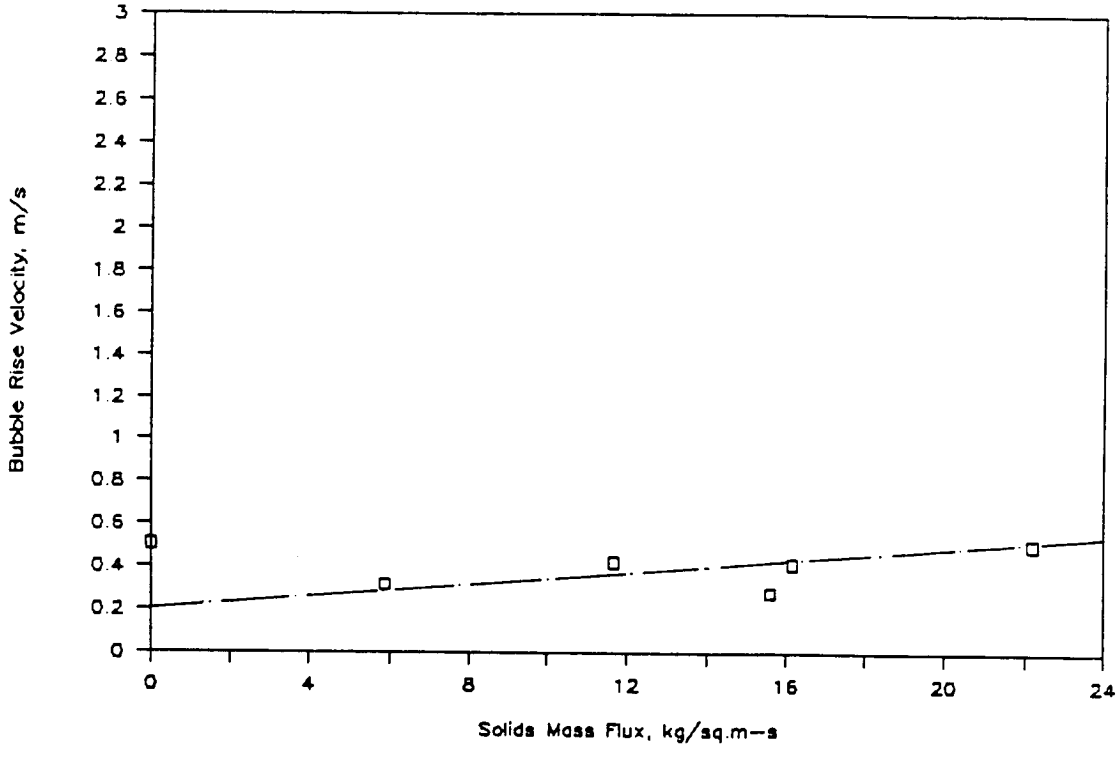

Figure 5.16: Bubble Rise Velocity vs Solids Mass Flux, Riley 0.229m Unit, Copper- steel System

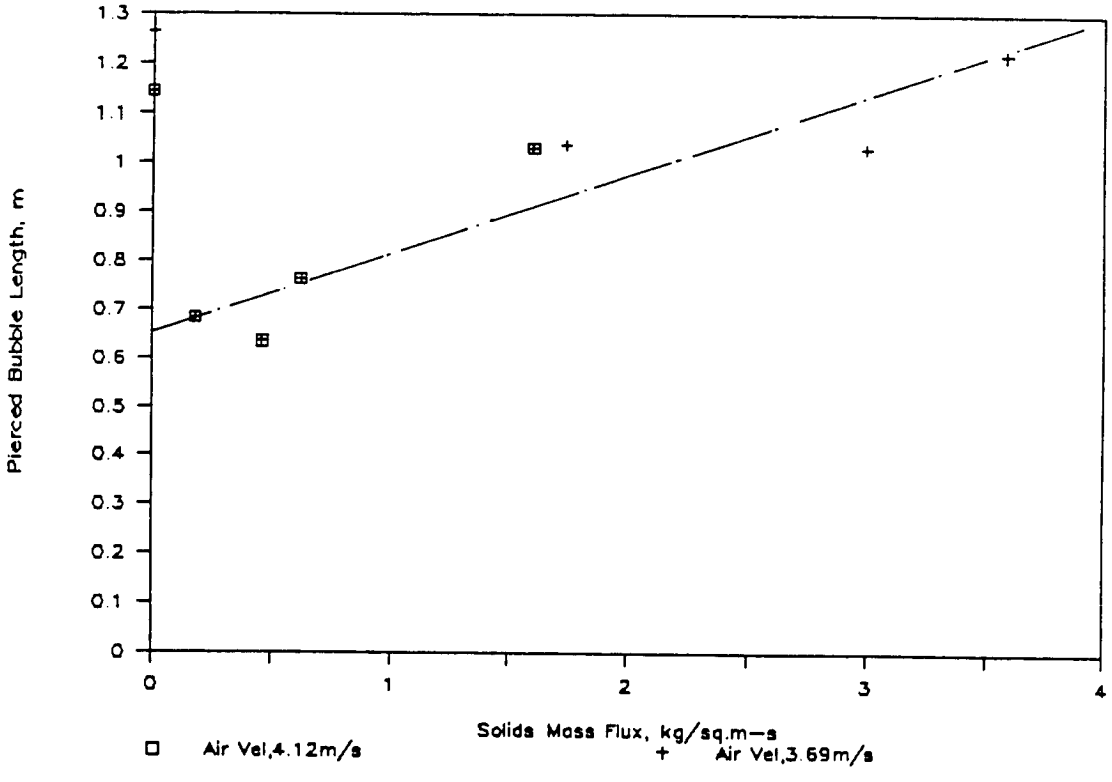

Figure 5.17: Pierced Bubble Length vs Solids Mass Flux, Riley 0.229m Unit, Sand- rock System

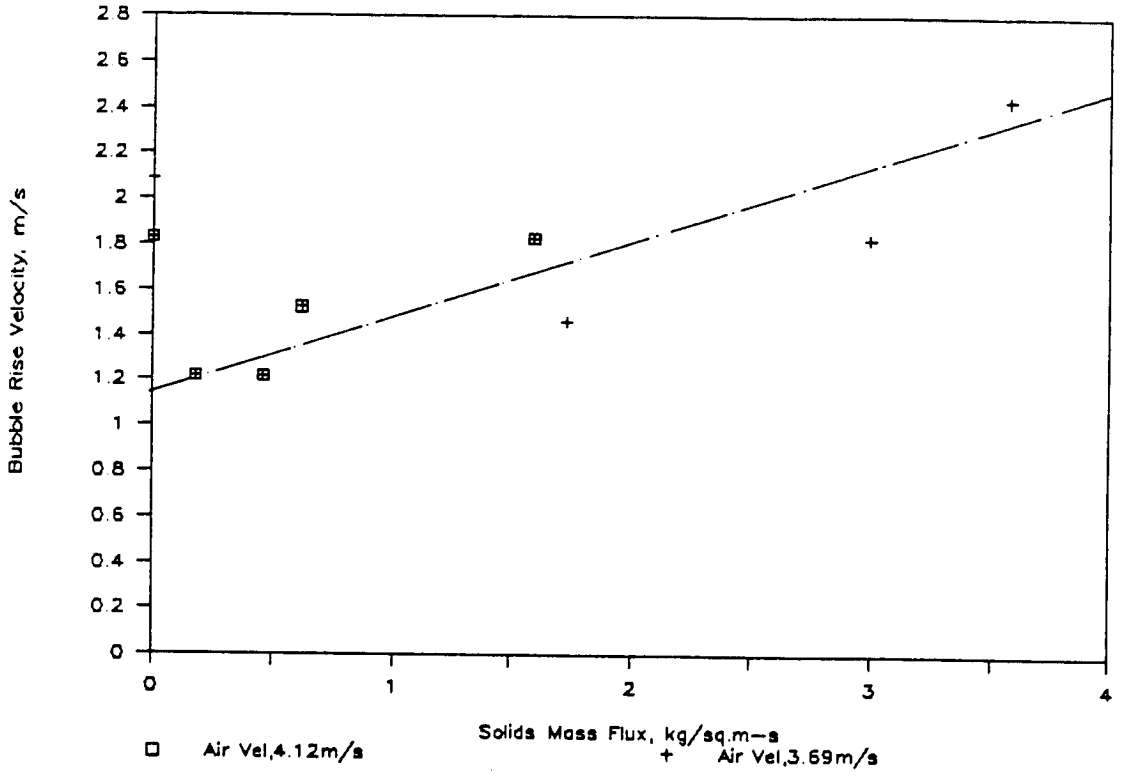

Figure 5.18: Bubble Rise Velocity vs Solids Mass Flux, Riley 0.229m Unit, Sand- rock System

that the growth of the bubble per pound of fines passing through the bed is much slower in the copper-steel system. This shows the existence of smaller bubbles in the copper-steel system. One can thus infer that the bubbles in the hot combustor would be smaller than the ones seen if the same materials are used in the cold unit at room temperature.

Figure 5.18 shows an increase in the bubble rise velocity of about 0.66 m/s for an increse of 1 kg/sq.m-s of solids mass flux. This value when compared to the one obtained in Fig. 5.16 (of 0.03 m/s per 1 kg/sq.m-s), shows that the rise velocity of the bubbles in the sand-rock system is about 22 times higher than in the copper-steel system, per unit solids mass flux.

Figures 5.19 through 5.22 are comparative plots of bubble length and bubble rise velocities for both solids systems from all three units. Figs.5.19 and 5.20 are bubble lengths and bubble velocities, respectively, for the copper-steel system. The data from the 0.038m UNH unit appears considerably high, both for the bubble length and rise velocity. The 0.038m data does lie beyond a 'banded' zone that can be drawn for the 0.102m and 0.41m data. Significant effects of the wall in terms of increased slug lengths (growth of the bubble in the radial direction was severely restricted because of the narrow diameter) and increased velocities are considered the cause for this deviation. Figures 5.21 and 5.22 (plots similar to Fig 5.19 and 5.20, for the sand-rock system) show that the 0.229m data are completely out of any banded zone of data fluctuations. The values of both bubble length and bubble rise velocity are an order of magnitude higher than those from the 0.038m and 0.102m units. The possible explanation for this can be that the data for the sand-rock system in the 0.229m unit was taken at an extremely low solids mass flux range. Sand mass flux values ranged from 0.18 to 3.58 kg/sq.m-s. Visual observation showed a freely bubbling regime of fluidization, quite different from the other modes of operation. The escape mechanism for the gas was primarily via bubbles and not slugs. This could be a faster process, since the time it takes for the bubbles to coalesce and form the slug over the entire diameter of the column, then expand and rise, is eliminated.

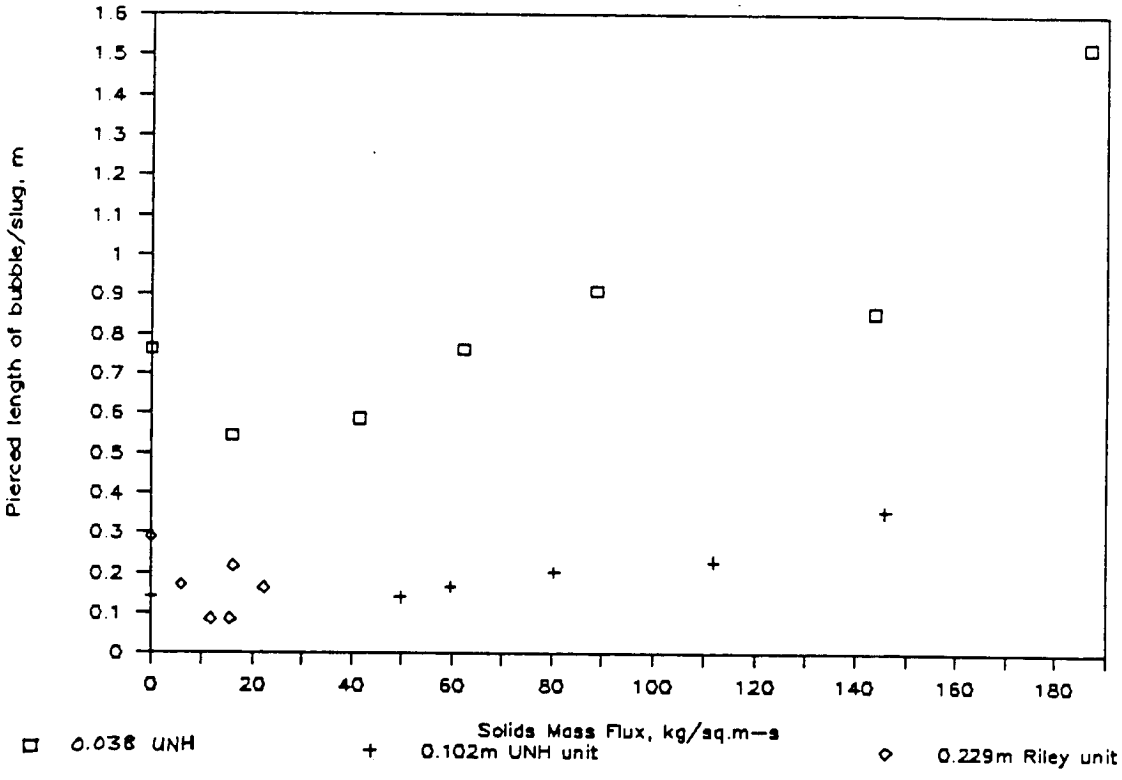

Figure 5.19: Bubble/slug Pierced Length, Copper-steel System : All Units

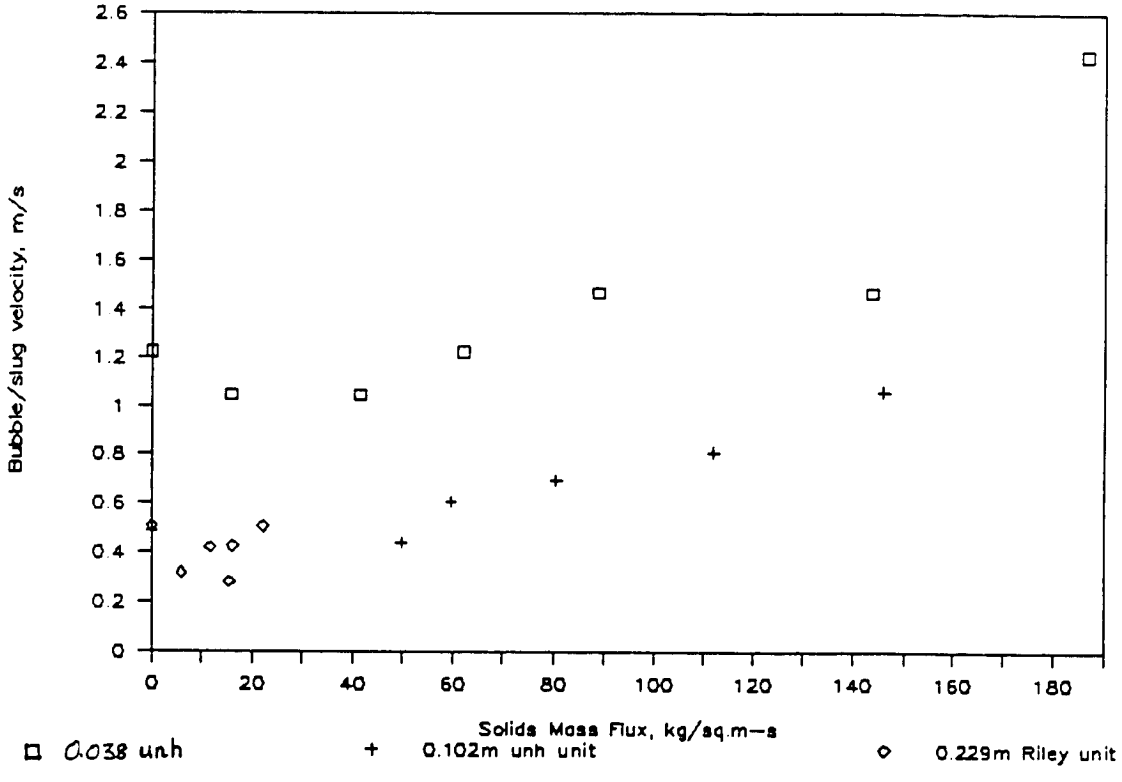

Figure 5.20: Bubble/slug Rise Velocity, Copper-steel System: All Units

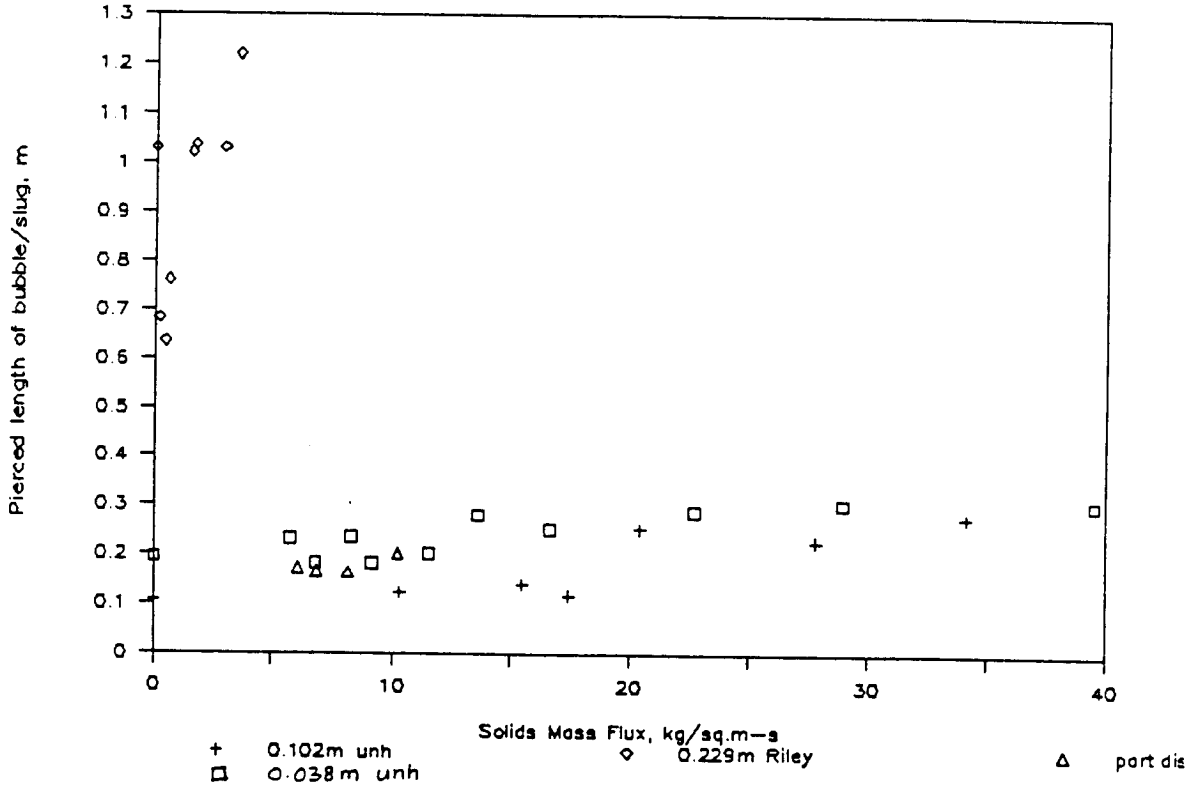

Figure 5.21: Bubble/slug Pierced Length, Sand-rock System : All Units

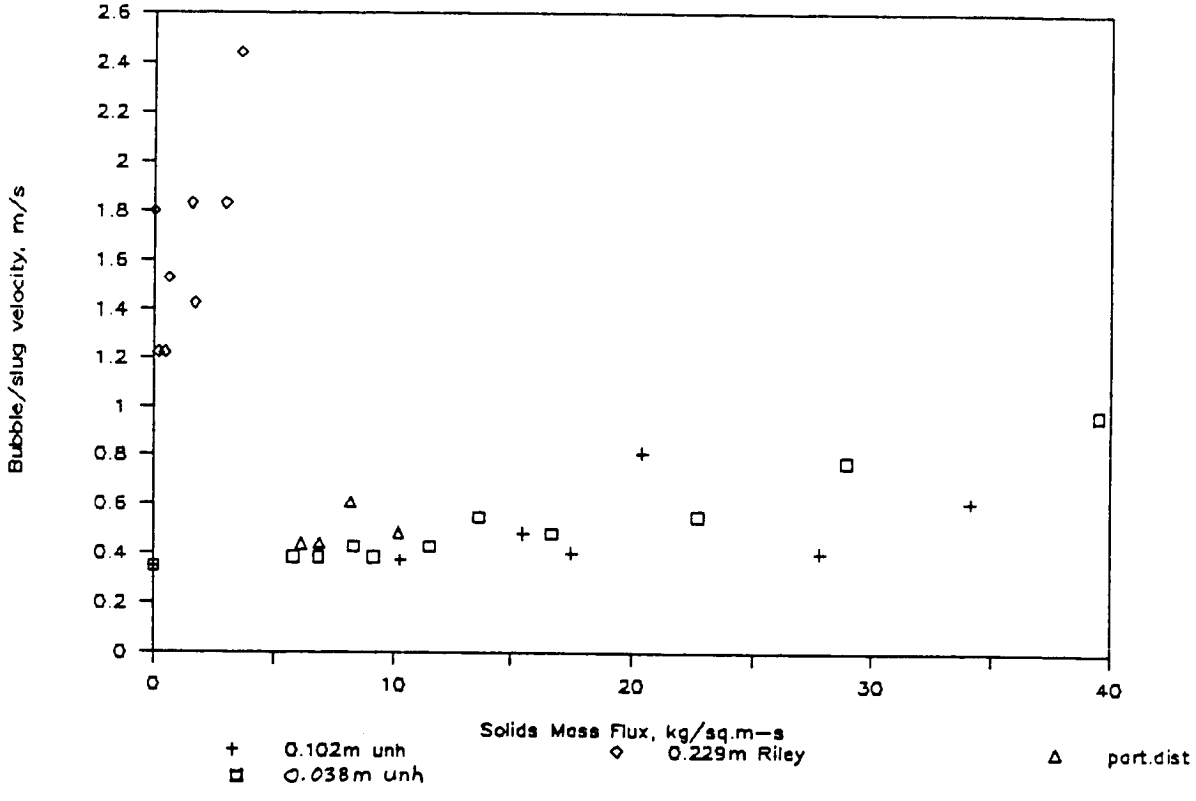

Figure 5.22: Bubble/slug Rise Velocity, Sand-rock System: All Units

All the pressure time traces for 0.038m, 0.102m, and 0.229m units, for both copper-steel and sand-rock systems, have been included in Appendix B. A sample calculation showing the procedure to evaluate bubble characteristics from a pressure-time trace is included in Appendix C.

5.3 Residence Time of Fine Particles in the Dense Bed and Proposed Model

One of the objectives of the present investigation is to examine the flow behavior of the fine particles in a circulating fluidized bed apparatus as they pass through the dense bed. Solids residence time and solids holdup are two parameters that are experimentally measured with varying dense bed void fraction and mass flux of circulating fine particles. Attempts are made to explain the findings based on the physical phenomena. A mechanistic model to reflect the flow behavior of the fine particles is proposed and verified against the experimental data. As mentioned earlier in this chapter, the residence time data resulting from the copper-steel system reflects the performance of a the dense bed section of an actual *hot* combustor in its ability to retain circulating fine particles. The sand-rock and sand-alumina systems are the materials used in a hot unit; however, when they are used in a cold fluidized bed set-up the resulting data does not simulate a hot operating unit. Data from all three systems have been taken and analysed in the subsequent sections.

5.3.1 Experimental Data Acquisition

Residence time data were obtained from the bench-scale circulating fluidized bed, using the defluidization technique as described in the experimental apparatus and procedure section. Three different systems were selected ; copper fines circulating through steel balls, sand through rocks and sand through alumina. The rationale for this choice is described elsewhere in the thesis. In all systems the fluidizing medium was air. The mass flux of circulating solids were varied by air inputs to the L-valve .Measurements of this mass flux

were made by timing the descent of particles in the downcomer. Dense bed void fraction was varied by changing the bed inventory of coarse solids and fluidizing them with a constant amount of air.

5.3.2 Experimental Residence Time Values

Tables 5.11 through 5.13 show the experimental residence time values of the circulating fine particles in seconds per foot of expanded dense bed.

Table 5.11: Effect of Bed Density and Mass Flux on Residence Time - Copper-steel System

Serial No	Solids Mass Flux	Expanded Bed Voidage	Solids Residence Time
–	$\frac{kg}{m^2 s}$	–	$\frac{sec}{m-bed}$
1	21.71	0.72	18.2
2	44.65	0.68	12.7
3	63.78	0.68	12.0
4	89.56	0.68	11.1
5	21.71	0.75	7.3
6	44.65	0.75	9.4
7	63.78	0.75	7.3
8	89.56	0.75	6.4
9	21.71	0.80	16.4
10	44.65	0.81	3.5
11	63.78	0.81	3.3
12	89.56	0.81	3.4

Table 5.12: Effect of Bed Density and Mass Flux on Residence Time - Sand-alumina System

Serial No	Solids Mass Flux	Expanded Bed Voidage	Solids Residence Time
–	$\frac{kg}{m^2 s}$	–	$\frac{sec}{m-bed}$
1	11.63	0.73	53.2
2	16.28	0.73	24.2
3	22.20	0.73	4.3
4	11.63	0.80	56.4
5	16.28	0.80	19.8
6	22.20	0.80	11.9
7	11.63	0.94	45.1
8	16.28	0.93	18.2
9	22.20	0.93	2.7
10	11.63	0.68	17.7
11	16.28	0.81	19.8
12	22.20	0.82	6.2

Table 5.11 shows residence time variation with mass flux and dense bed voidage for the copper-steel system. Table 5.12 and 5.13 show similar results for the sand- alumina and sand-rock systems respectively. These data are plotted in Figures 5.23 through 5.25.

Figure 5.23 shows the variation in residence time with expanded dense bed voidage for the copper-steel system, for three mass fluxes namely, 44.65, 63.78 and 89.56 kg/sq.m-s. In all three cases the residence time decreases from about 13.12 to 1.64 sec/m of expanded

Table 5.13: Effect of Bed Density and Mass Flux on Residence Time - Sand-rock System

Serial No	Solids Mass Flux	Expanded Bed Voidage	Solids Residence Time
–	$\frac{kg}{m^2 s}$	–	$\frac{sec}{m-bed}$
1	10.67	0.67	10.47
2	24.04	0.67	4.36
3	10.67	0.72	6.43
4	15.58	0.72	5.08
5	17.44	0.72	4.36
6	20.94	0.72	2.36
7	15.27	0.77	4.69
8	26.60	0.77	3.71

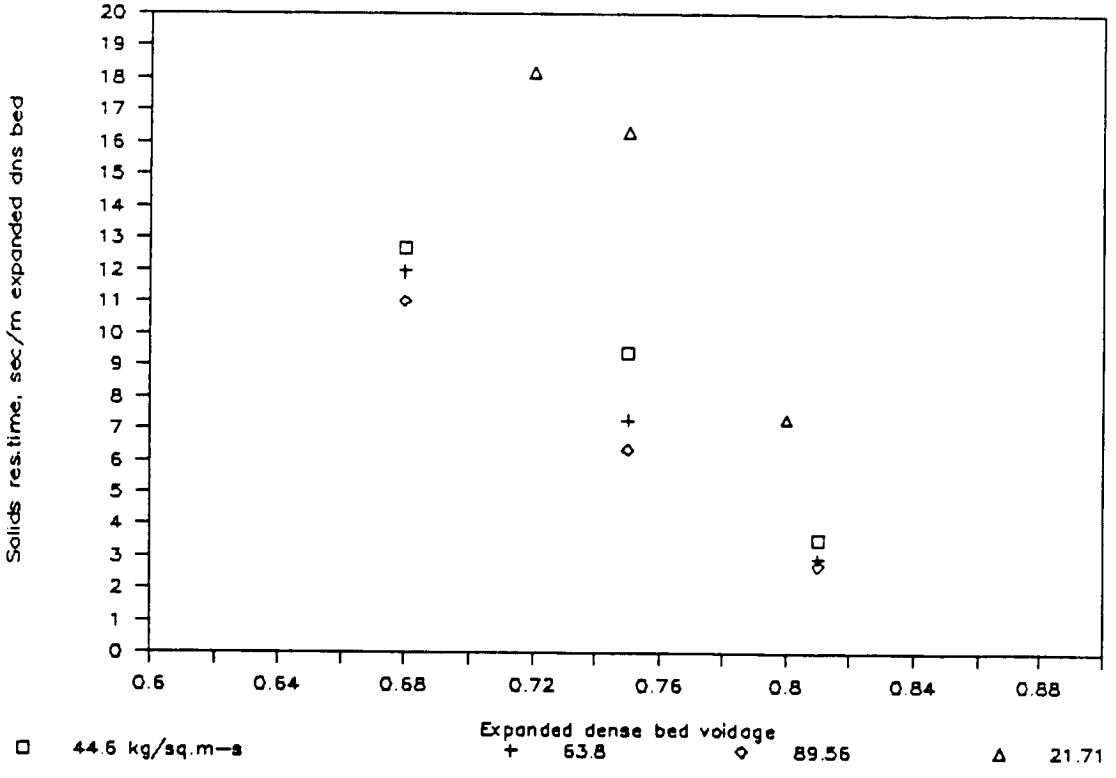

Figure 5.23: Dense Bed Solids Residence Time, 0.102m UNH Unit, Copper-steel System

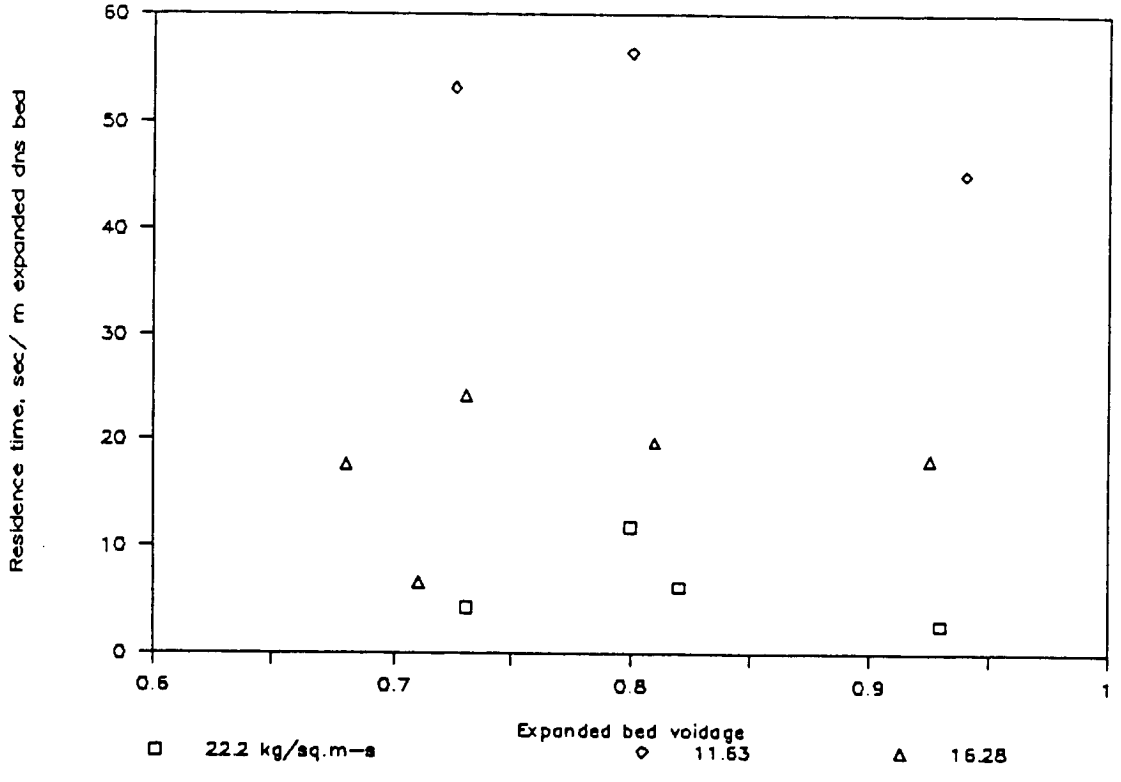

Figure 5.24: Dense Bed Solids Residence Time, 0.102m UNH Unit, Sand-alumina System

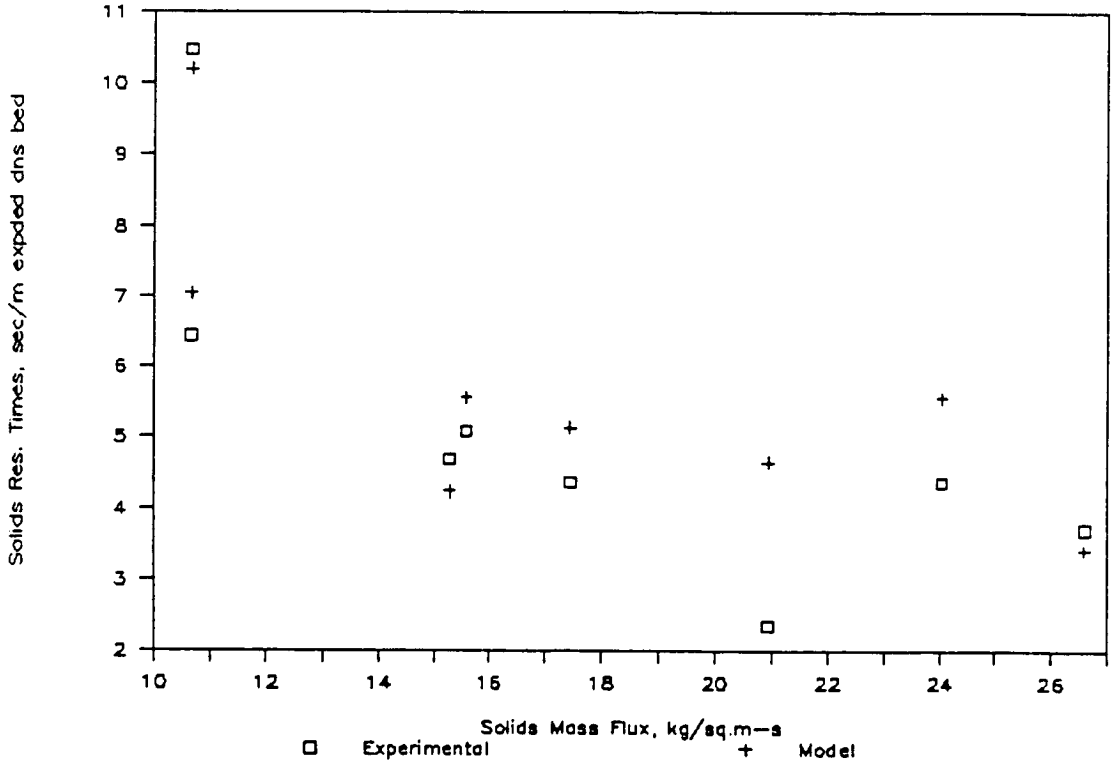

Figure 5.25: Dense Bed Solids Residence Time, 0.102m UNH Unit, Sand-rock System

bed, as the void fraction in the dense bed is increased from about 0.68 to 0.82. This decrease in residence time with increasing dense bed voidage is similar in all three systems. Figure 5.24 shows the variation of residence time as a function of dense bed voidage for the sand-alumina system. Here, also , the fine particle residence time decreases slightly for all three mass fluxes, as dense bed voidage is increased from about 0.65 to 0.92. This can be explained by the fact that there are fewer coarse particles per unit volume of bed at higher dense bed voidages. This lower number of large particles results in fewer collisions between the large and small particles, thereby resulting in the fine particles spending less time in the dense bed. The fine particle residence time also appears to decrease with increasing mass flux. The rate of decrease of residence time with increasing mass flux is, however, very different in the two systems. The dependence of residence time on circulating mass flux is less obvious in both systems. As the mass flux of the fine particles increases,the ability of unit volume of the dense bed to capture these particles decreases. Hence, for a fixed dense bed voidage, residence time decreases as mass flux increases. Fig. 5.25 shows the residence time values obtained in the sand-rock system. The residence time data are plotted against solids mass flux; this is because these data are taken to verify the proposed model, and both solids mass flux and expanded dense bed voidage values are varied in a fairly random manner. The sand-rock data are further explained in the following section.

5.3.3 Development and Verification of the Model

The model as discussed earlier describes a force balance on the fine particles as they pass through a bubbling bed of coarse solids. The drag force is the upward accelarating force, and gravity, friction and collision are the downward retarding forces. The solution of this steady-state force balance yields fine particle velocities. A certain degree of empiricity is introduced in this mathematical model. The friction term includes an empirical constant 'n' which has been evaluated for the three systems using a regression analysis; data used in the determination of 'n' was obtained experimentally and is presented in Tables 5.11, 5.12

and 5.13. The index 'p' to which the ratio of particle to air mass flux is raised, in both the friction and the collision terms, has also been determined using regression analysis of experimental data. It is found to be 0.25. As a result of this analysis the values of 'n' for the copper-steel, sand-alumina and rock- sand system are 2.9, 0.8 and 2.5, respectively. For this set of 'n' values and the mass flux ratio index of 0.25, the least values of AAPD are calculated. The Absolute Average Percentage Deviation (AAPD) is defined as:

$$AAPD = \frac{1}{n}\sum_{i=1}^{n}\left(\frac{|\ \tau_{r,exp} - \tau_{r,cal}\ |}{\tau_{r,exp}}\right) 100\%$$

Here, τ_r is the solids residence time in sec/m of dense bed. The AAPD values for the various systems are listed in Table 5.14.

The model generated curves for the copper-steel and the alumina-rock system are shown in Figures 5.26 and 5.27, respectively. In Fig. 5.26, the model traces for three mass fluxes are shown, as the solid lines, with increasing dense bed voidage. There is reasonable agreement between experimental data and model generated values with AAPD values ranging from 20 to 29.2. Fig. 5.27 shows a greater deviation between experimental and model values with AAPD values ranging from 24.8 to 85.2. This information is also presented in Table 5.14. The AAPD values for the copper-steel system range from 20 to 29.2; for the sand- alumina system the variation is more pronounced , ranging from 22.7 to 85.2. The sand-rock data has been used as an independent check for the model. This is presented in Fig. 5.25 which shows reasonable agreement between experimental data and model generated values. AAPD values for this system range from 2.59 to 97.03. This appears to validate the mathematical model, since these data were not used in the model development. The high value of 97.03 may be an experimental error.

5.3.4 Development of Empirical Equation for Predicting 'n' Values

The empirical constant 'n' of the model previously described together with the other variables such as sphericity, density of particles, particle size, it employs , is summarized in this section. The relevant variables used in the model are listed in Table 5.15.

Table 5.14: AAPD Values for Copper-steel, Sand-alumina and Sand-rock Systems

Serial No	System	Solids Mass Flux	Expanded Bed Voidage	AAPD
–	–	$\frac{kg}{m^2 s}$	–	%
1	Cu-steel	21.71	0.72-0.80	20.0
2	Cu-steel	44.65	0.68-0.81	29.2
3	Cu-steel	63.78	0.68-0.81	24.4
4	Cu-steel	89.56	0.68-0.81	21.5
5	Alu-sand	11.63	0.73-0.94	24.8
6	Alu-sand	16.28	0.73-0.93	22.7
7	Alu-sand	22.20	0.73-0.93	85.2
8	Roc-sand	10.67	0.67	2.59
9	Roc-sand	24.04	0.67	27.5
10	Roc-sand	10.67	0.72	9.48
11	Roc-sand	15.58	0.72	9.45
12	Roc-sand	17.44	0.72	17.89
13	Roc-sand	20.94	0.72	97.03
14	Roc-sand	15.27	0.77	9.59
15	Roc-sand	26.6	0.77	8.47

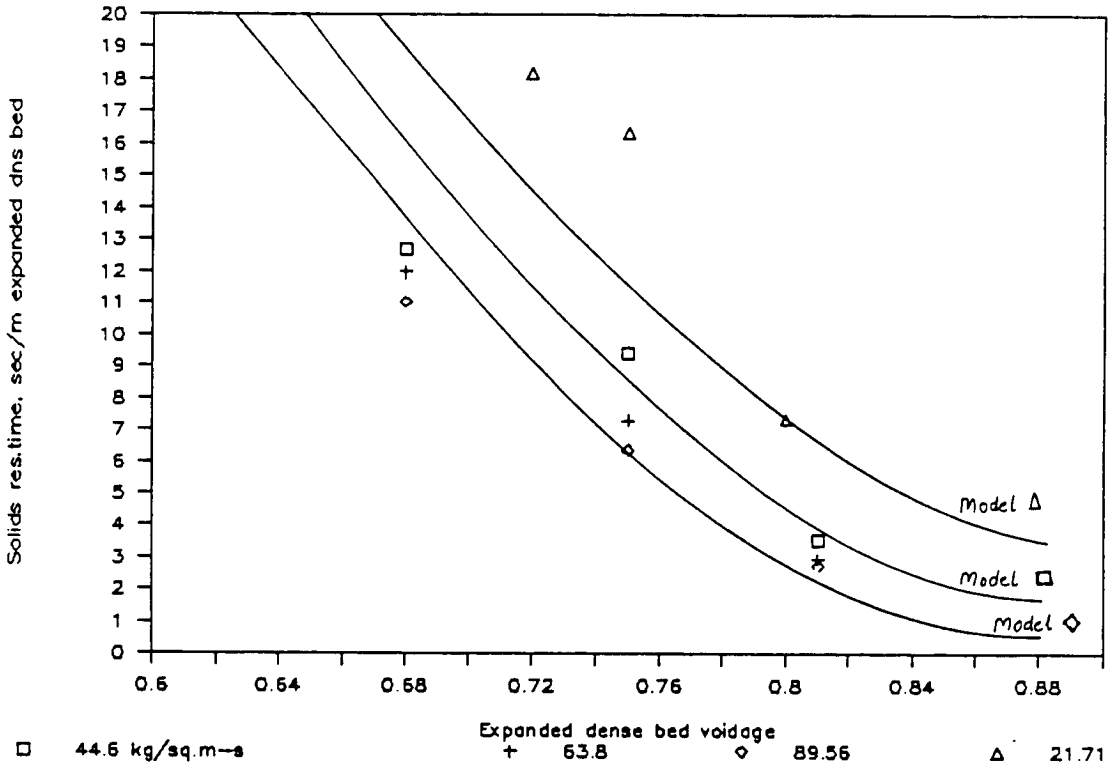

Figure 5.26: Model Traces of Residence Time Values, UNH 0.102m Unit, Copper-steel System

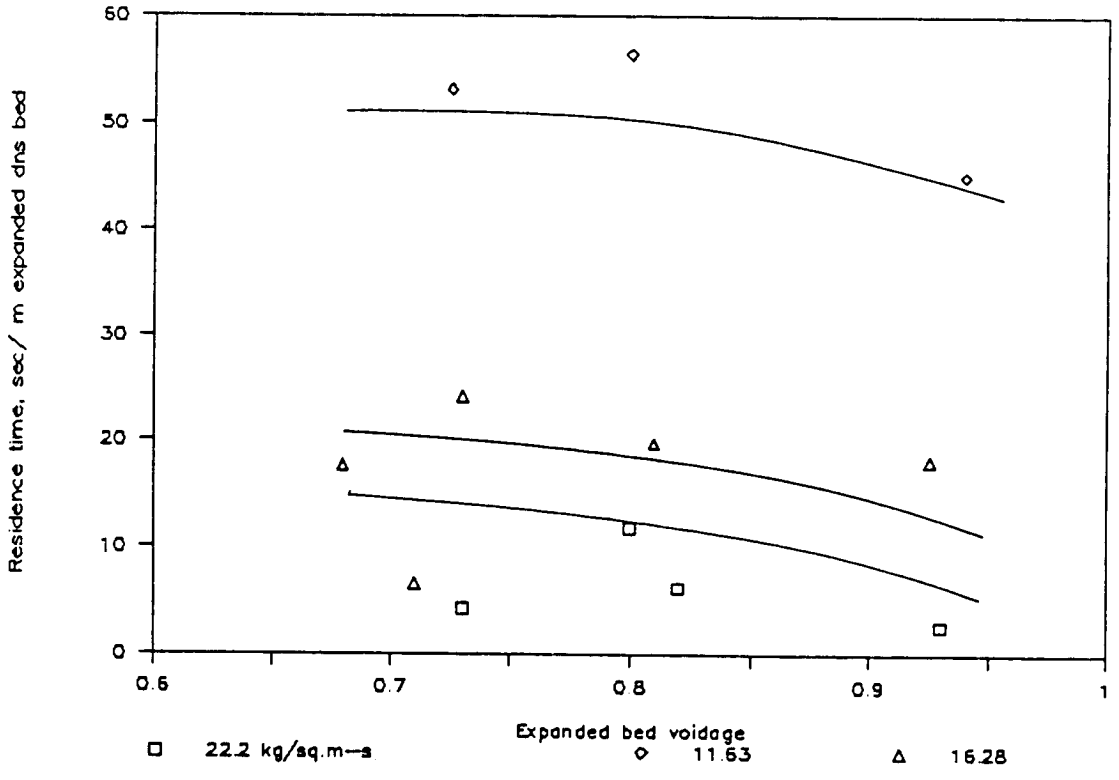

Figure 5.27: Model Traces of Residence Time Values, UNH 0.102m Unit, Sand-alumina System

Table 5.15: Variables Used in the Model and Resulting 'n' Values

Variable	Copper-steel	Sand-alumina	Sand-rock
ϕ_1	1.0	0.95	0.6
$\rho_1\ [kg/m^3]$	7900	3400	2800
$\rho_2\ [kg/m^3]$	8900	2600	2600
$d_{p_1}\ [m]$	$3.175 * 10^{-3}$	$6.35 * 10^{-3}$	$9.525 * 10^{-3}$
$d_{p_2}\ [m]$	$80 * 10^{-6}$	$300 * 10^{-6}$	$300 * 10^{-6}$
n	2.9	0.8	2.5
p	0.25	0.25	0.25

The overall mathematical model thus becomes:

$$\begin{aligned}\frac{\frac{3}{4}C_{D,}\epsilon_f^{-4.7}\rho_a(U_a - U_{p_2})^2}{\rho_{p_2}d_{p_2}} &= g(1 - \frac{\rho_a}{rho_{p_2}}) \\ &+ 10(\frac{1-\epsilon}{\epsilon})^n\frac{U_{p_2}}{D}\frac{1}{\phi_1 d_{p_1}}(\frac{W_g}{W_{p_2}})^{0.25} \\ &+ \frac{6(U_{p_1} - U_{p_2})^2(1-\epsilon)}{\phi_1 d_{p_1}}(\frac{W_g}{W_{p_2}})^{0.25}\end{aligned}$$

The usefulness of such a model is enhanced if the model can be applied to any independent system operating under different conditions and parameters than those used in this study. An attempt has been made to correlate the empirical constant 'n' with such system-dependent parameters like particle diameters, particle densities etc. Some of these relevant parameters that influence the empirical constant 'n' have been collected in dimensionless groups and a regression analysis has been performed. The results of analysis are tabulated in Table 5.16 and presented in graphical form in Fig. 5.28. A linear variation of 'n' with the diameter-to- density ratio of fine particle/large particle is observed. The resulting expression for 'n' in terms of the fine and coarse particle characteristics is:

$$n = -32\frac{\frac{\phi_2 d_{p_2}}{\rho_2}}{\frac{\phi_1 d_{p_1}}{\rho_1}} + 3.6 \qquad (5.3.2)$$

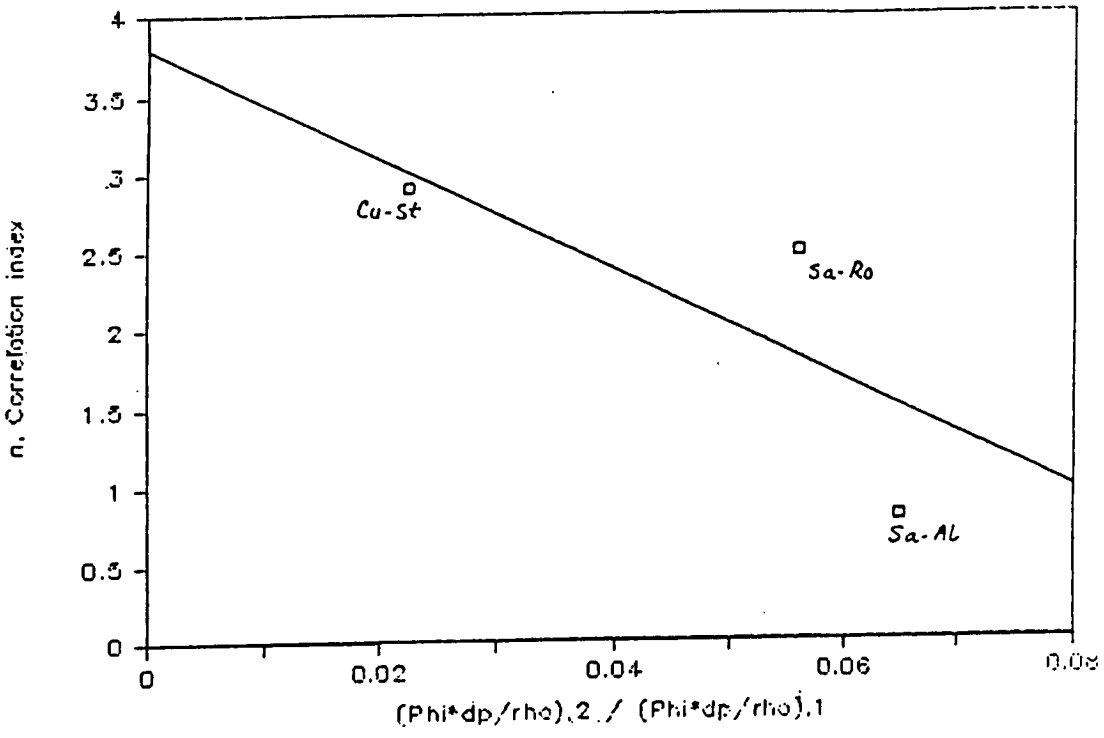

Figure 5.28: Empirical Correlation for 'n' Based on UNH Data

Table 5.16: Characteristics Groups and 'n' Values

System	Fine Particle Characteristic Group $\frac{\phi_2 d_{p_2}}{\rho_2}$	Coarse Particle Characteristic Group $\frac{\phi_1 d_{p_1}}{\rho_1}$	Dimensionless Group Ratio $\frac{\frac{\phi_2 d_{p_2}}{\rho_2}}{\frac{\phi_1 d_{p_1}}{\rho_1}}$	n Values
–				–
Copper – steel	$8.988 * 10^{-9}$	$4.0189 * 10^{-7}$	0.0224	2.9
Sand – alumina	$1.154 * 10^{-7}$	$1.774 * 10^{-6}$	0.065	0.8
Sand – rock	$1.154 * 10^{-7}$	$2.041 * 10^{-6}$	0.056	2.5

This linearity will facilitate the use of the model. If the system parameters are known, 'n' can be determined from the correlation. Hence, fine particle residence time can be calculated using the model.

5.4 Comparision with Existing Model(s)

There are only very few studies on the flow of fine particles through a bed of coarse solids. The holdup of fine particles through a bed of coarse solids have been studied by Fan et al.[17,18] for two different cases. In the first case a bed of coarse solids was packed, and in the second case it was a bubbling fluidized bed. A mechanistic model was developed from fundamental principles to account for the behavior of these fine particles as they percolated through the packed/fluidized bed of coarse solids. Fig. 5.29 shows the variation of solids holdup (volume fraction of fines in the dense bed) as a function of fine particle flow rate. This relationship has been reported by Fan et al. using a fluidized bed of coarse solids. Fig. 5.30 is a graphical representation of the solids holdup in the dense bed as a function of loading ratio, for the copper-steel system as studied in this research. The three different traces correspond to the three dense bed voidages that were varied independently. Comparing this with Fig. 5.29 of Fan et al.[18] we see that the trends are very similar : as fine particle mass flux increases the solids holdup increases. A direct comparision is difficult because of the fact that dense bed voidage, an important parameter in this study, was not measured by Fan et al. Fig. 5.31 is essentially the same as Fig. 5.30 except that the solids holdup is plotted as a function of void fraction instead of loading ratio. It is presented here since all the earlier data (of residence times) were plotted as a function of void fraction. Another important difference between the model proposed by Fan et al. and the one developed in this investigation is that the collision term and friction term in their study have been lumped together in one term as an 'interaction coefficient' . Figure 5.32 as reported by Fan et al.[18] shows the variation of interaction coefficient with the ratio of fine particle-to-air mass flux. It is claimed by the authors, as is evident from the horizontal lines, that interaction coefficient (hence , residence time) is independent of mass flux of fine particles. The scatter in their data is quite substantial to make such a conclusive finding. In the study of holdup of fines using a packed dense bed, however, Fan et al. [17] reported a decrease in interaction coefficient with increasing rate of fine particle flow, at a fixed air rate.

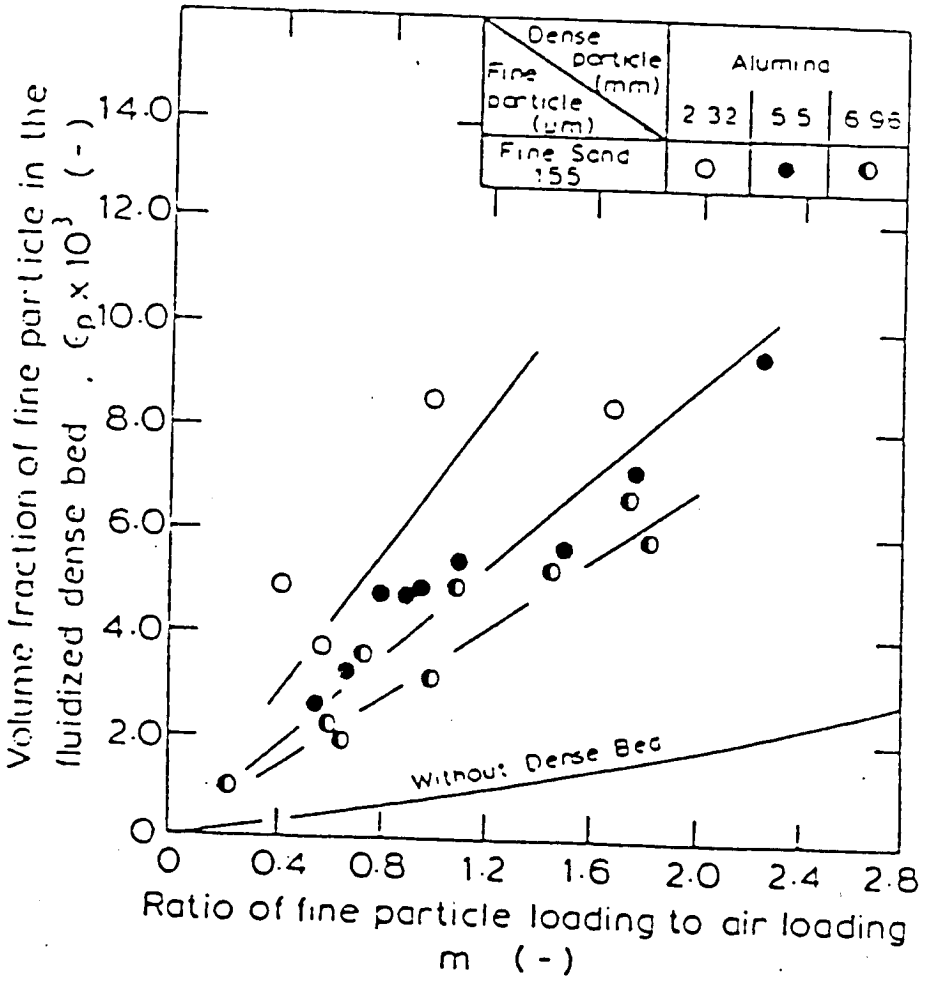

Figure 5.29: Variation of Fine Particle Holdup with the Loading Ration, 155μm Fine Sand and Various Sizes of Alumina [18]

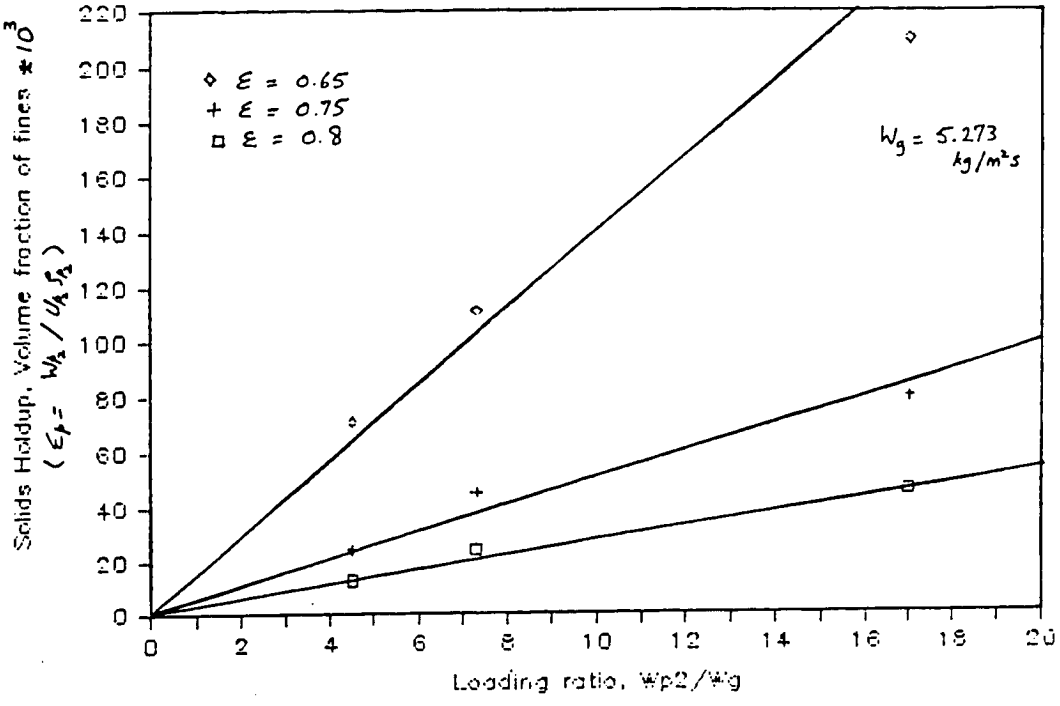

Figure 5.30: Solids Holdup vs Loading Ratio, Model Values of Copper-steel System

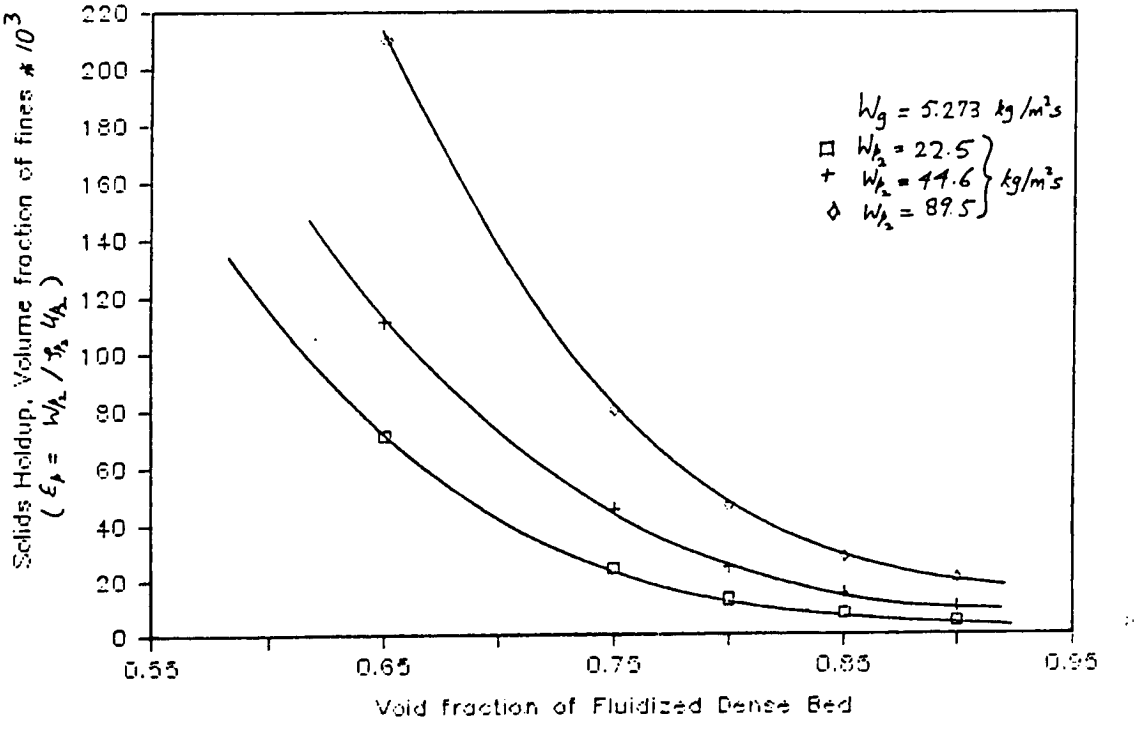

Figure 5.31: Solids Holdup vs Void Fraction, Model Values of Copper-steel System

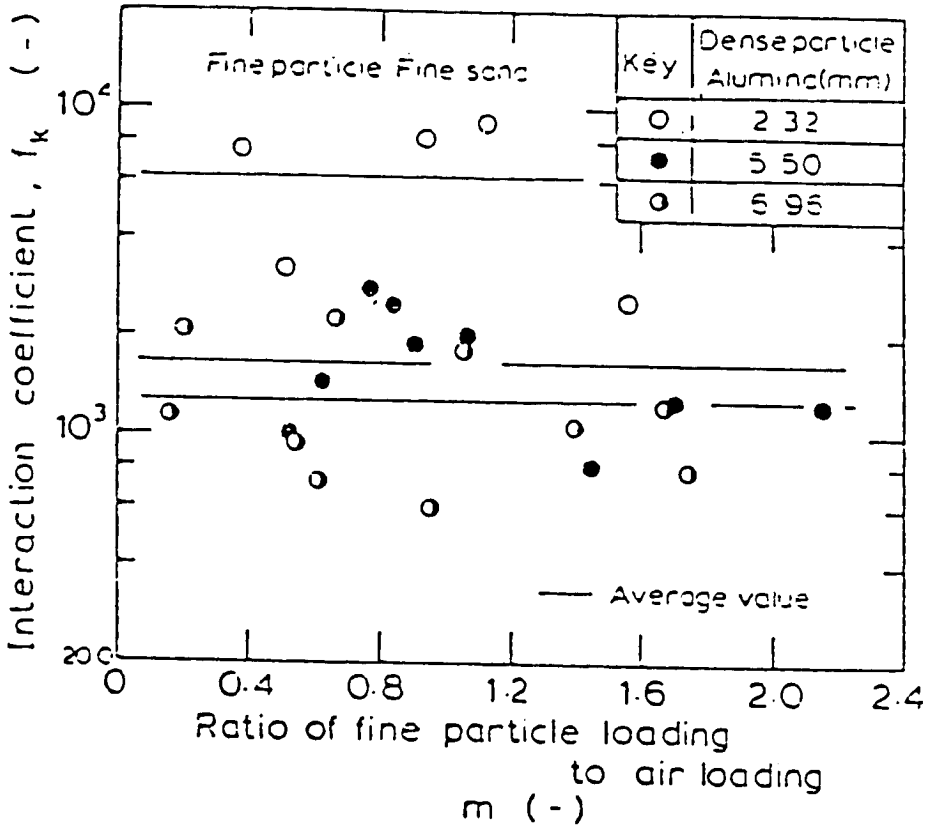

Figure 5.32: Variation of the Interaction Coefficient in the Slugging Dense Bed Regime with the Loading Ratio for 155 μm Fine Sand and Various Sizes of Alumina [18]

This is shown in Fig. 5.33, adapted from Fan et al. A decrease in interaction coefficient with increasing solids rate implies a decrease in residence time , which is in accordance with our results. A careful review of Fig. 5.33 shows that at zero value of m (no particles circulating) the interaction coefficient is maximum. This is contrary to the reasoning that at zero mass flux of solids (fine circulating particles) there is no interaction between fine and coarse particles. Thus the 'interaction coefficient' which combines together frictional and collison effects of the fine and large particles should be zero at zero particle mass flux.

Another study on a circulating fluidized bed with a dense bed has been conducted by Nack et al.[19]. Part of the investigation has been directed towards solids residence time estimation. Using a defluidization technique, similar to the one used in this study, Nack et al. have determined solids residence times. Their findings are shown in Fig. 5.34. The relevant trace to be compared with this study is the one for an air velocity of 15 ft/sec (4.7m/s). This trace shows that the solids residence time increases with increasing mass flux. This is contrary to our findings showing an opposite trend, that solids residence time decreases with increasing mass flux. Unfortunately, a very few details are given by Nack et al. This prevents an in-depth analysis of the discrepancy. Efforts to obtain more information on this study from the authors did not prove fruitful.

5.5 Gross Behavior of the Dense Bed Section of the MSFB

As mentioned earlier in this thesis, the behavior of any fluidized bed can be divided into two broad groups - its gross (or macroscopic) behavior and its fine (or microscopic) behavior. The gross behavior of a fluidized bed is characterized by easily measurable parameters such as the pressure drop per unit height of bed, the average bed voidage, and the bed expansion. Such information gives an overview of the nature of the fluidized bed and may be used to estimate bed dimensions, solids inventory, and power requirements. From an industrial viewpoint the macroscopic parameters are of immediate interest. However, the gross behavior of a fluidized bed gives little or no insight into the actual flow patterns of

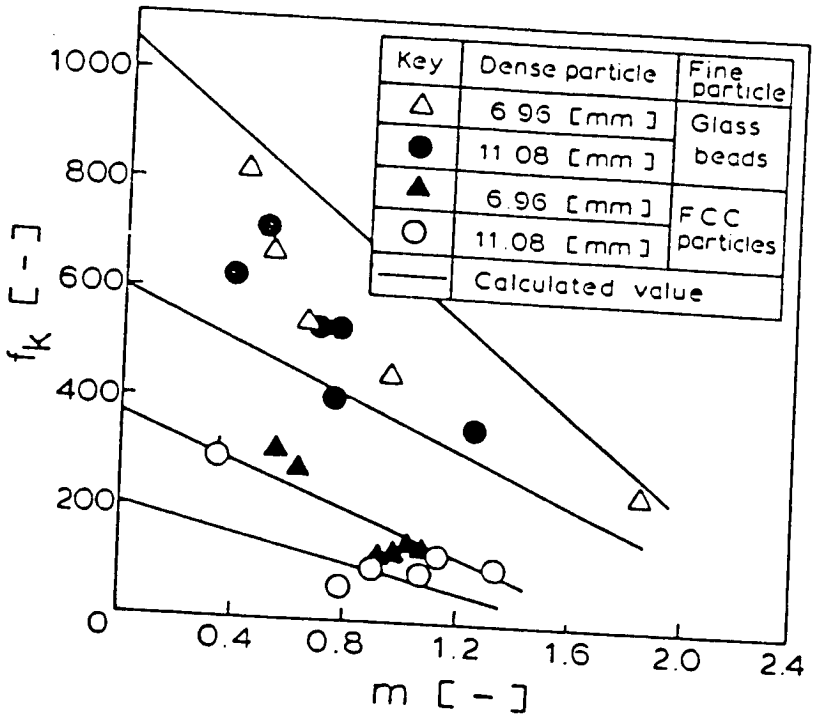

Figure 5.33: Variation of the Interaction Coefficient with the Loading Ratio for Air-Glass Beads and Air-FCC Particles Flows through a Packed Bed of Various Dense Particles[17]

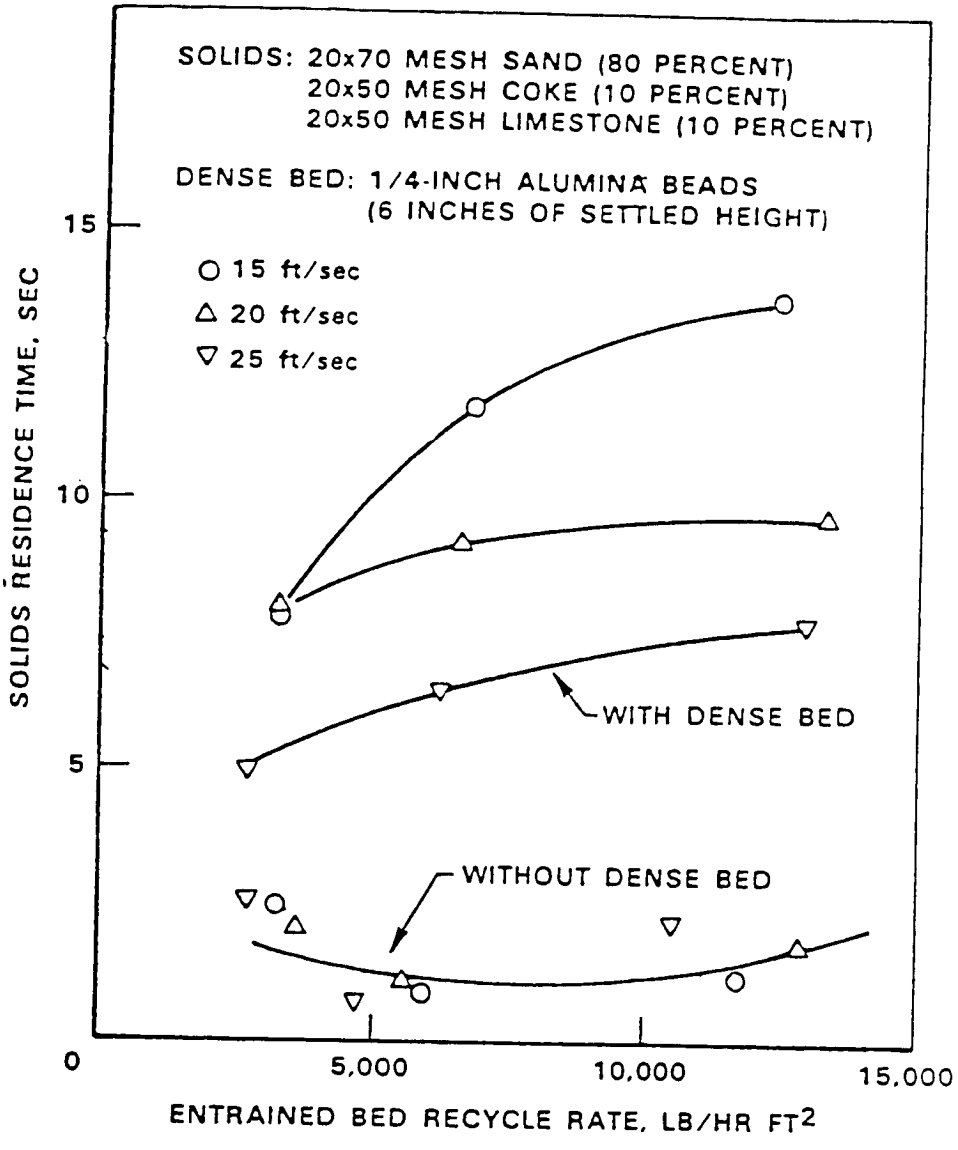

Figure 5.34: Solids Residence Time Test [19]

gas and solids, their mixing characteristics, and the escape mechanism of gas and solids. If detailed information is desired, the microscopic behavior needs to be studied.

Bubble characteristics (length, rise velocity and frequency) are most important in quantifying the microscopic behavior of a fluidized bed. In the dense bed section of the MSFB, in addition to bubble characteristics, the residence time of fines are another important microscopic parameter. All these microscopic parameters have been studied thoroughly , and an exhaustive amount of bubble characteristic and residence time data have been presented and analyzed in earlier sections. However, no description of any fluidized bed process is complete without the inclusion of macroscopic parameters such as pressure drop. Thus a limited amount of data on the pressure drop across the dense bed of an MSFB, the average bed voidage in the dense bed , and the bed expansion is presented and analyzed in the subsequent section.

5.5.1 Pressure Drop and Associated Gross Characteristics of the Dense Bed

The pressure drop per unit height of the expanded bed was estimated from the pressure time traces. This was done by averaging each pressure signal (the averaging process actually performed by the software Notebook) with time to get a trace of average pressure versus time. The final pressure drop was the mean of the differences of two averaged pressure time traces. Since the distance between the pressure probes was known, the pressure drop per unit height of expanded bed was calculated by dividing the pressure drop by the separation distance. Mathematically,

$$\frac{\Delta P}{\Delta L} = \frac{\overline{< P_1 > - < P_2 >}}{L} \tag{5.5.3}$$

where $\frac{\Delta P}{\Delta L}$ is the pressure drop per unit height of the expanded bed, $< P_1 >$ and $< P_2 >$ are the time averaged top and bottom pressures respectively, and L is the distance of separation between the pressure probes. The overbar indicates the mean of the difference between the

two time averaged pressures. The expanded bed height was recorded visually, and the bed height at minimum fluidization condition was measured before the introduction of fine particles. Thus, from a force balance on the bubbling bed of coarse material,

$$\begin{aligned} \Delta P A_t = A_t L_{mf}(1-\epsilon_{mf})(\rho_s - \rho_g)\frac{g}{g_c} &\approx A_t L_f(1-\epsilon_f)(\rho_s-\rho_g)\frac{g}{g_c} \\ \Rightarrow L_f(1-\epsilon_f) &\approx L_{mf}(1-\epsilon_{mf}) \end{aligned}$$

where A_t is the cross-sectional area of the bed, L_{mf} and L_f are the bed heights at minimum fluidization and expanded bed condition respectively, ϵ_{mf} and ϵ_f are the void fractions at mininum fluidization condition and expanded bed condition respectively, ρ_s and ρ_g refer to the solid and gas density, and g is the acceleration due to gravity. The approximate nature of the above relationship is due to the fact that the fluidized bed height is of an oscillatory nature, and at best time-averaged values of the bed height may be obtained.

Some pressure drop data taken by the averaging technique mentioned above is presented here in Table 5.17. The raw, average pressure trace data, is attached in appendix D. This data are also plotted as pressure drop per meter of the dense bed versus solids mass flux in Fig.5.35. Three systems were tested; sand circulating through alumina spheres using a perforated plate distributor (serial numbers 1 through 5), sand through alumina spheres in a single nozzle distributor (as used by Batelle, numbers 6 and 7) and sand through rock using a perforated plate distributor (numbers 8 through 12). In all three systems the variation of pressure drop with solids mass flux is minimal. Interestingly, however, the maximum pressure drop occured when there were no solids circulating through, and then levelled off as solids mass flux was increased. This phenomena seems akin to the phenomena of 'drag reduction by the addition of fines to a gas' [33]. The drag force on the dense solids by the air is more than the drag force on the dense solids by the two-phase mixture of air and fine particles, resulting in a lesser pressure drop in the latter case.

The pressure drop data analyzed and presented here are by no means exhaustive. A separate study may be undertaken to determine pressure drop and its dependence on

Table 5.17: Effect of Solids Mass Flux on Dense Bed Pressure Drop

Serial No	Solids Mass Flux	Pressure Drop	Pressure Drop/ Meter
–	$\frac{kg}{m^2 s}$	$Inwc$	$\frac{inwc}{m-expandedbed}$
1	0	2.62	51.56
2	14.66	1.92	37.79
3	22.90	2.46	48.41
4	31.86	2.38	46.84
5	34.89	2.23	43.89
6	0	3.46	68.09
7	31.86	2.00	39.36
8	0	3.53	69.47
9	7.71	2.77	54.51
10	15.27	2.30	45.26
11	17.44	3.08	62.58
12	20.94	2.69	52.94

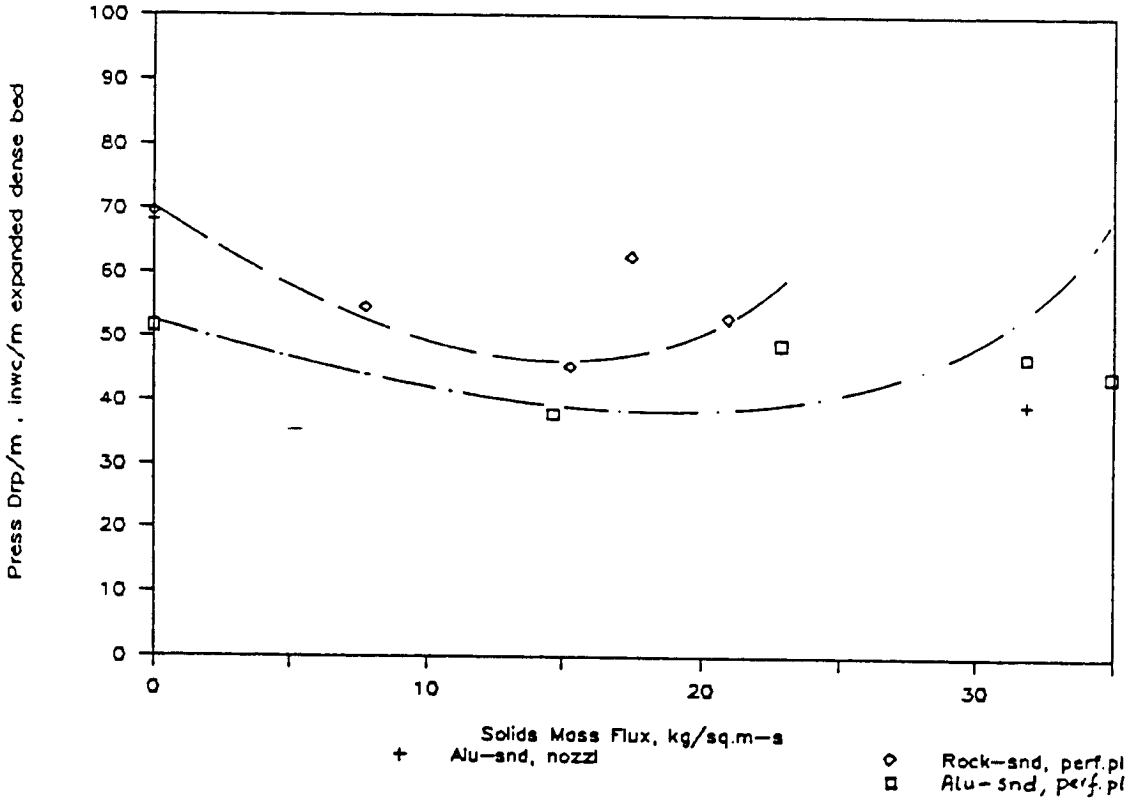

Figure 5.35: Dense Bed Pressure Drop, UNH 0.102m Unit, Sand-alumina and Sand-rock Systems

the various independent parameters. Since pressure drop is a 'gross' characteristic of a fluidized bed its omission is noticeable. However in this study as the primary focus was the microscopic behavior of the fine particles as seen from the pressure traces, the overall pressure drop data presents little additional information.

Chapter 6

CONCLUSIONS

During the past several years CFB combustion systems have gained considerable popularity. The CFB boiler has demonstrated superior carbon burnout efficiencies, better turndown and fuel flexibility, improved sulfur capture performance and lowered NO_x emission levels. It is therefore no surprise that boiler manufacturers worldwide have joined this technological race, resulting in several competing designs. The Ahlstrom/Pyropower CFB boiler, the Lurgi CFB system, the Keeler/Dorr-Oliver CFB boiler, the Studsvik CFB system, and the Battelle MSFB technology are at the forefront of this race. However, as it has happened with conventional bubbling fluidized bed systems, large gaps in knowledge of the fundamental processes that occur in a CFB, still remain. This investigation concentrated at bridging such a gap in the hydrodynamic aspects of the Batelle MSFB system. The area focussed upon was the dense bed section at the bottom of the riser of the MSFB. The major findings of this study are:

(1) The two-dimensional model of a dense bed of coarse particles with injection of fines gives a visual image of the bubble-structure and behavior of such a sytem.

(2) Two CFB systems have been built and operated at the UNH facility, and a large scale model was operated at the Riley Stoker facility. All units are 'cold'. The three units are 0.038m, 0.102m, and 0.229m in effective diameter, respectively. These three units were successfully used to collect data of bubble length, bubble rise velocity and bubble frequency.

(3) An on-line data acquisition system was successfully used to obtain pressure-time signals (traces). The pressure-fluctuation technique was used to analyze these signals. The technique essentially consisted of estimating bubble characteristics (length, velocity and frequency) from the separation distance of the peaks and troughs of the sinusoidal signals. It is found to be a robust technique and accurately describe the bubble dynamics of the dense bed, that can be used for a wide range of solid loadings and a variety of materials (including conducting powders).

(4) It was found that bubble properties, are dependent on the column diameter, with the smallest typically giving rise to the longest and fastest bubbles. Bubble frequency remained almost independent of column diameter. The bubble data from the 0.038m UNH unit suffers from 'wall effects'.

(5) The materials chosen for study were based on the scaling law hypothesis. As a comparision, the actual materials used in the combustor were also used. This resulted in the use of copper-steel, sand-rock, and sand-alumina systems. These systems were used for the bubble characteristic and/or the residence time studies. An analysis of bubble data shows a striking difference between the values obtained from the different systems. Since the copper-steel system actually simulates the materials in a hot combustor, those data may be used to design a coal-burning MSFB.

(6) A mathematical model to predict the residence time of the fines in the dense bed was developed from first principles, based on a momentum balance approach. The friction and collision terms appear separately. The effect of solids mass flux is incorporated, improving upon existing model(s). The following model has been proposed for predicting the residence time of fine particles flowing through a bubbling fluidized bed of coarse solids:

$$\frac{\frac{3}{4}C_D\epsilon_f^{-4.7}\rho_a(U_a - U_{p_2})^2}{\rho_{p_2}d_{p_2}} = g(1-\frac{\rho_a}{\rho_{p_2}}) + 10(\frac{1-\epsilon}{\epsilon})^n U_{p_2} D \frac{1}{\phi d_{p_1}}(\frac{W_g}{W_{p_2}})^{0.25} + \frac{6(U_{p_1} - U_{p_2})^2}{\phi d_{p_1}}(\frac{W_g}{W_{p_2}})^{0.25}$$

(7) The model developed here employs a semi-empirical constant, n. An empirical equation is developed relating n and system dependent parameters such as fine and coarse particle properties. Thus, once a physical system is chosen the n may be evaluated, and the model may be used to predict residence time values of the fine particles in the dense bed. The empirical equation for estimating n is :

$$n = -32\frac{(\phi d_p/\rho)_2}{(\phi d_p/\rho)_1} + 3.6$$

(8) The solids residence times are determined by a defluidization technique for various gas-solids systems in the 0.102m UNH unit. Residence time values are compared with those predicted by the model. The AAPD values range from 20 to 29.2 for the copper-steel system, from 22.7 to 85.2 for the sand-alumina system, and from 2.59 to 97.03 for the sand-rock system.

(9) The operation of an L-valve is studied both as a solids recirculating device as well as a device for controlling solids flow rates. Solids fractions near the bend are found to be independent of initial height of solids in the downcomer, and are inversely proportional to motive air flow rates. Solids flow rates are directly proportional to motive air flow rates. Calibration plots of an L-valve are prepared; these included plots of solids flow rate versus motive air flow rates.

Chapter 7

RECOMMENDATIONS

This study was conducted on three experimental units, with the objective of understanding the mechanism of fine particle flow behavior through a fluidized bed of coarse particles. Two bench scale CFB systems were built and operated at the UNH facility, and a large scale model was operated at an industrial facility. From an experimental standpoint these units covered practically the entire size range - from bench scale units to small pilot plant. A mathematical model to predict the residence time of fines in the dense bed was developed, which provides results in agreement with the experimental data. All the data have been presented in the form of graphs, charts, tables or mathematical equations.

Even though this investigation has met its objective, there are areas which need further study. The following recommendations are made:

(1) A better picture may emerge if more sophisticated high-speed photography is employed in a two-dimensional setup. The images of bubbles erupting, of the fines short circuiting through the slow-rising bubbles and the nature of gas-solids mixing, may be recorded and analyzed to give further insight into the dense bed dynamics.

(2) The pressure fluctuation technique is a robust method for obtaining bubble dynamics in a fluidized bed. The data collected in this study were from cold units using scaling law materials. Efforts should be made to acquire bubble data from a hot operating MSFB using the pressure fluctuating technique, and the signals should be compared to those obtained from a cold flow unit using both scaling law materials and actual

materials used in the hot combustor. The comparisons may be made based on statistical properties of the signal. This would also verify the validity of scaling law materials in a MSFB.

(3) As of this date, no model exists that predicts bubble behavior in a coarse particle system with fines passing through it. Models should be developed to predict bubble length, bubble velocity and bubble frequency in such a system. Data from the present study may be used to validate the models.

(4) Efforts should be made to obtain residence time data from a hot pilot-plant scale combustor, and compare them with data from the present study, to further prove the validity of the scaling laws. Data from a hot unit may also be used to further validate the mathematical model developed in this study.

(5) The mechanism of gas-mixing and solids-mixing in a coarse particle system is not well understood. Efforts should be made to gain a better understanding of such processes, both by designing experiments and by mathematical modelling of the physical phenomena.

(6) There is a certain degree of empiricity in the model developed here for the prediction of residence time of fine particles. Efforts should be made to understand and incorporate all the effects in the dynamics of the dense bed; this would include electrostatic effects, attrition, agglomeration of particles etc. If these effects are included the empiricity may be avoided.

(7) As industrial units are currently in operation using this technology, efforts should be made to obtain operating data and use it for further verification of the present residence time model.

(8) Only two sections of the MSFB process are studied in detail in this investigation - the dense bed section and the solids recirculating device. The dynamics of solids

flow in the freeboard region above the dense bed and the gas-solids separation device (cyclone) need to be studied; a knowledge of hydrodynamics of the dense bed,the freeboard region, and the cyclone would enhance the understanding of the gas-solids flow behavior in the entire loop.

(9) A fairly sophisticated data acquisition software is used in data collection. However, machine capabilities limited other functions such as performing on line FFTs, as large amounts of data are continuously collected in the high speed mode. It is recommended that a faster machine be used in conjunction with the software to enable one to perform on-line statistical and other data manipulations. A computer with a 386/486 Intel chip or equivalent would be adequate.

(10) The pressure drop studies of the dense bed as part of its gross characterization should be extended to include more data. Such data are available as a result of the current study, but need to be analyzed to get a more complete picture of the dependency of pressure drop on various independent parameters.

(11) As a natural extention of any hydrodynamic study, the associated heat transfer aspects need to be investigated. Combustion is a phenomenon in which the hydrodynamics and heat transfer are coupled. Once the hydrodynamics are thoroughly understood , efforts should be made to understand the heat transfer process. Such an understanding can be attained both by designing experiments and by modelling the physical phenomena.

NOMENCLATURE

A, A_t	Cross-Sectional Area of the Empty Bed, m^2
Ar	Archemides Number
C_D	Drag Coeffcient for a Single Sphere
C_{DM}	Multi-Particle Drag Coeffcient
d_b	Bubble Diameter, m
d_p	Particle Diameter, m
d_{p_1}	Coarse Particle Diameter, m
d_{p_2}	Fine Particle Diameter, m
D	Bed Diameter, m
f	Bubble Frequency, $\frac{1}{s}$
f_k	Interaction Coefficient in Fan et al. Model, $\frac{s^2}{m}$
Fr	Froude Number
g	Acceleration due to Gravity, $\frac{m}{s^2}$
G_g	Gas Mass Flux, $\frac{kg}{m^2 s}$
G_s	Solid Mass Flux, $\frac{kg}{m^2 s}$
L	Bubble Probe Separation Distance, m
L_b	Bubble Rise Velocity, $\frac{m}{s}$
L_f	Height of Bubbling Fluidized Bed, m
L_{mf}	Height of Bed at Minimum Fluidization Condition, m
m	Mass of Particles, kg
n	System Dependent Parameter used in Model
p	Fitting Parameter of Model
Pr	Prandtl Number

Nomenclature, Continued

ΔP	Pressure Drop in the Fluidized Dense Bed, kPa
$\overline{\Delta P}$	Ensemble Average Pressure Drop, kPa
$< P >$	Time-Averaged Pressure from Fluctuating Pressure Signal, kPa
Re	Reynolds Number
Re_p	Particle Reynolds Number
S_{xx}	Power Spectral Density Function of a Fluctuating Pressure Signal
t	time, s
T	Total Elapsed Time of Signal in Statistical Functions, s
U, U_o	Superficial Gas Velocity, $\frac{m}{s}$
U_a, U_f	Actual (Interstitial) Gas Velocity, $\frac{m}{s}$
U_b	Bubble Rise Velocity, $\frac{m}{s}$
U_{br}	Bubble Rise Velocity of a Single Bubble, $\frac{m}{s}$
U_{mb}	Miminum Bubbling Velocity, $\frac{m}{s}$
U_{mf}	Minimum Fluidization Velocity, $\frac{m}{s}$
U_{p_1}	Coarse Particle Velocity, $\frac{m}{s}$
U_{p_2}	Fine Particle Velocity, $\frac{m}{s}$
U_t	Terminal Falling Velocity, $\frac{m}{s}$
W_a	Mass Flux of Air, $\frac{kg}{m^2 s}$
W_g	Mass Flux of Gas (Fluidizing Medium), $\frac{kg}{m^2 s}$
W_{mp}	Solids Mass Flow Rate of Fine Particles, $\frac{kg}{s}$
W_{p_1}	Solids Mass Flux of Coarse Particles, $\frac{kg}{m^2 s}$
W_{p_2}	Solids Mass Flux of Fine Particles, $\frac{kg}{m^2 s}$
$x(t)$,$y(t)$	Fluctuating Pressure Signals from Two Pressure Probes

Greek Symbols

Δm	Infinitesmal Amount of Fine Particles in Section ΔL of the Dense Bed, kg
ϵ	Average Bed Void Fraction
ϵ_f	Voidage of the Fine Particle Phase
ϵ_p	Average Fine Particle Holdup
ω	Frequency Domain
μ_a	Viscosity of Air, $\frac{kg}{m-s}$
μ_x	Mean of a Fluctuating Pressure Signal
ϕ_1	Sphericity of Coarse Particles
ϕ_2	Sphericity of Fine Particles
ϕ_{xx}	Auto-correlation Function of a Fluctuating Pressure Signal
ϕ_{xy}	Cross-correlation Function of a Fluctuating Pressure Signal
ρ_a	Density of Air (Fluidizing Medium), $\frac{kg}{m^3}$
ρ_b	Average Bulk Density of Solids, $\frac{kg}{m^3}$
ρ_{p_1}	Density of Coarse Particles, $\frac{kg}{m^3}$
ρ_{p_2}	Density of Fine Particles, $\frac{kg}{m^3}$
ρ_s	Density of Solids, $\frac{kg}{m^3}$
σ_x	Variance of a Fluctuating Pressure Signal
τ	Time Needed for a Bubble to Pass a Single Probe, s
τ_m	Mean Lag Time between Two Pressure Traces, s
τ_r	Average Residence Time of Fine Particles in the Dense Bed, $\frac{s}{m}$

Subscripts

1 Referring to the Coarse Particles

2 Referring to the Fine Particles

REFERENCES

1) Kunii, D. and O. Levenspiel, *Fluidization Engineering*, John Wiley and Sons, New York, 1969.

2) Geldart, D., Types of Fluidization, Powder Technology, Vol. 7, 1973.

3) Davidson, J.F., *Fluidized Particles*, Cambridge University Press, London, 1963.

4) Davidson, J.F., Clift, R. and D. Harrison, *Fluidization*, 2nd. Ed., Academic Press, 1985.

5) Cheremisinoff, N.P. and P.N. Cheremisinoff, *Hydrodynamics of Gas-Solids Fluidization*, Gulf Publishing Co., 1984.

6) Cranfield, R.R. and D. Geldart, Large Particle Fluidization, Chemical Engineering Science, Vol. 29, 1974, 935.

7) McGrath, L. and R.E. Streatfield, Bubbling in Shallow Gas- Fluidized Beds of Large Particles, Transactions of the Institute of Chemical Engineers, Vol. 49, 1971, 70.

8) Glicksman, L.R. and G. McAndrews, The Effect of Bed Width on the Hydrodynamics of Large Particle Fluidized Beds, Powder Technology, Vol. 42, 1985, 159.

9) Yerushalmi J., Turner, D.H. and A.M. Squires, The Fast Fluidized Bed, Ind. Eng. Chem., Proc. Dev., Vol. 15, No. 1, 1976, 47.

10) Avidan, A. and J. Yerushalmi, Bed Expansion in High Velocity Fluidization, Powder Technology, Vol. 32, 1982, 223.

11) Geldart, D. and M.J. Rhodes, From Minimum Fluidization to Pneumatic Transport - A Critical Review of the Hydrodynamics, in *Circulating Fluidized Bed Technology (Ed. Basu, P)*, Pergamon Press, 1986, 21.

12) Brereton, C. and L. Stromberg, Some Aspects of the Fluid Dynamic Behaviour of Fast Fluidized Beds, in *Circulating Fluidized Bed Technology (Ed. Basu, P)*, Pergamon Press, 1986, 133.

13) Glicksman, L.R., Scaling Relationships for Fluidized Beds, Chemical Engineering Science, Vol. 39, No. 9, 1984, 1373.

14) Breault, R.W., Hydrodynamic Characteristics and Coal Combustion Modeling of a High Velocity Fluidized Bed, Ph.D. Dissertation, University of New Hampshire, 1985.

15) Knowlton, T.M. and I. Hirsan, L-Valves Characterized for Solids Flow, Hydrocarbon Processing, March 1978, 57.

16) Dry, R.J. and R.D. La Nauze, Combustion in Fluidized Beds, Chemical Engineering Progress, July, 1990, 31.

17) Fan, L.S., Toda, M. and S. Satija, Hold-up of Fine Particles in the Packed Dense Bed of the Multisolid Pneumatic Transport Bed, Powder Technology, Vol. 36, 1983, 107.

18) Kitano, K., Wisecarver, K.D., Satija, S. and L.S. Fan, Holdup of Fine Particles in the Fluidized Dense Bed of the Multisolid Pneumatic Transport Bed, Ind. Eng. Chem. Res, Vol. 27, 1988, 125.

19) Nack, H., Litt, R.D. and B.C. Kim, Multisolid Fluidized-Bed Combustion, Chemical Engineering Progress, January, 1984,

20) Lirag, R. and H. Littman, Statistical Study of the Pressure Fluctuations in a Fluidized Bed, AIChE Symposium Series, Vol. 67, No. 11, 1971, 116.

21) Fan, L.T., Ho, T.C., Hiraoka, S. and W.P. Walawender, Pressure Fluctuations in a Fluidized Bed, AIChE Journal, Vol. 27, No. 3, 1981, 388.

22) Fan, L.T., Ho, T.C. and W.P. Walawender, Measurements of the Rise Velocities of Bubbles, Slugs and Pressure Waves in a Gas-Solid Fluidized Bed Using Pressure Fluctuation Signals, AIChE Journal, Vol. 29, No. 1, 1983, 33.

23) Wisecarver, K., Kitano, K. and L.S. Fan, Pressure Fluctuation in a Multisolid Pneumatic Transport Bed, in *Circulating Fluidized Bed Technology (Ed. Basu, P)*, Pergamon Press, 1986, 145.

24) Liu, K.T., Martin, J.C. and H. Nack, On Some Fundamentals of Multisolid Fluidized Bed, Presented at the AIChE 86th National Meeting, Houston, Texas, 1979.

25) van Deemter, J.J., Mixing, in *Fluidization (Ed. Davidson, J.F. et al.)*, Academic Press, 1985, 331.

26) Lee, G.S. and S.D. Kim, Gas Mixing in Slugging and Turbulent Fluidized Beds, Chem. Eng. Comm., Vol. 86, 1989, 91.

27) Ake, T.R. and L.R. Glicksman, Scale Model and Full Scale Test Results of a Circulating Fluidized Bed Combustor, Presented at the Seminar of Fluidized Bed Combustion Technology for Utility Applications, Palo Alto, California, 1988.

28) Swinehart, F.M., A Statistical Study of Local Wall Pressure Fluctuations in Gas Fluidized Columns, Ph.D. Dissertation, University of Michigan, 1966.

29) Kang, W.K., Sutherland, J.P. and G.L. Osberg, Pressure Fluctuations in a Fluidized Bed with and without Screens Cylindrical Packings, I & EC Fundamentals, Vol 6, 1967, 449.

30) Ishii, H., Nakajima, T. and M. Horio, The Clustering Annular Flow Model of Circulating Fluidized Beds, Journal of Chem. Eng. of Japan, Vol. 22, No. 5, 1989, 484.

31) Nicastro, M.T. and L.R. Glicksman, Experimental Verification of Scaling Relationships for Fluidized Bed, Chem. Eng. Sci., Vol. 39, No. 9, 1984, 1381.

32) Mathur, V.K., Technical Report to Riley Stoker Corporation, Worcester, MA, 1989.

33) Boothroyd, R.G., *Flowing Gas-Solids Suspensions*, Chapman and Hall, London, 1971.

34) Klinzing, G.E., *Gas-Solid Transport*, McGraw Hill Book Company, 1981.

35) Yang, W.C., Mathematical Definition of Choking Phenomenon and Mathematical Model for Predicting Choking Velocity and Choking Voidage, AIChE Journal, Vol. 21, No. 5, 1975, 1013.

36) Marble, F.E., Mechanism of Particle Collision in the One- Dimensional Dynamics of Gas-Particle Mixtures, The Physics of Fluids, Vol. 7, No. 8, 1964, 1270.

APPENDICES

This Appendix has been divided into four parts, A, B, C, and D. Appendix A contains a sample program listing used to evaluate residence time of the fine particles in the dense bed. It is a FORTRAN-coded version of the mathematical model developed in this study.

Appendix B contains the raw bubble characteristic data, taken in the UNH 0.038m and 0.102m diameter units, and in the Riley Stoker 0.229m unit. These raw data are in the form of pressure-time traces, with pressure in inches of water column (inwc) and time in seconds. Each set of bubble characteristic data contains an 'identification' relating the Serial No. which appears in the text, and the Run No. which appears with the raw data.

Appendix C contains a sample calculation of bubble length, bubble rise velocity and bubble frequency from a raw pressure-time trace.

Appendix D contains the averaged pressure-time traces used in the pressure drop studies.

APPENDIX A : SAMPLE PROGRAM TO EVALUATE FINE PARTICLE RESIDENCE TIME IN THE DENSE BED

```
C       THIS PROGRAM CALCULATES PARTICLE VELOCITIES IN A MULTI-SOLIDS
C       FLUIDIZED BED, WITH FINE PARTICLES CIRCULATING THROUGH
C
C       S.I. UNITS ARE USED THROUGHOUT, EXCEPT IN TAU [sec/ft]
C       SUBSCRIPT 1 refers to large particles (dense bed material)
C       SUBSCRIPT 2 refers to fine particles ( recirculating material)
C
C
C
C       INITIALIZE DATA
C
        REAL RHOA,RHOP2,DP2,DP1,D,U0,UA,UP2,MUA,G,CDS,EPS,EPSF,EPS2,REP
        REAL DRAGF,GRAVF,C,PHI1,PHI2
C
C
        RHOA = 1.177          ! Density of fluidizing medium
        RHOP2 = 8900          ! Density of small particles
        DP2 = 80.E-6         ! Diameter of small particles
        DP1 = 3.175E-3        ! Diameter of large particles
        D = 0.1016            ! Diameter of column
        U0 = 4.48             ! Superficial air velocity
        MUA = 1.8462E-5       ! Viscosity of air
        G = 9.807             ! Acceleration due to gravity
        WG = 5.27             ! Gas mass flux, kg/sqm-s
        WP2 = 44.6            ! Recirc. fine particle mass flux, kg/sqm-s
        EPSF = 0.99           ! Void fraction in fine particle phase
        PHI1 = 1.00           ! Sphericity of large particle
C
C
C       Open files to write output
        OPEN(UNIT=21,FILE='COPSTL.OUT',STATUS='NEW')
        WRITE(21,999)
999     FORMAT(4X,'EPSIL',4X,'TAU',5X,'UP2',5X,'DRAGF',4X,'FRICF',4X,
     1  'COLLIF',3X,'HOLDUP',2X//)
C
C       Start void fraction loop
C
        DO 30 I=65,90,1
         EPS = I/100.0        ! EPS, dense bed void fraction
         UA = U0/EPS          ! Interstitial air velocity
C
C       Start fine particle velocity loop ( iteration)
C
 10     DO 25 J = 10,2000,1
         UP2 = J/1000.0
        REP = RHOA * DP2 * (UA)/MUA   !  Particle Reynold's Number
        CDS = 18.5/( REP**0.6)  ! Drag coeff. for a single small particle
        CDM = CDS*(EPSF**-4.7)  ! Drag coeff for all small particles
        TAU = 1./(UP2*3.28) ! TAU = Residence time, sec/ft of dense bed
C
C
C       Calculate forces acting on fine particles
C
        DRAGF = 0.75* CDM*RHOA*((UA-UP2)**2)/(RHOP2*DP2)  !Drag Force
        GRAVF = G * (1.-RHOA/RHOP2) ! Net gravitational force
        FRICF =10.*((1-EPS)**2.9/EPS**2.9)*(UP2/D)*(1./(PHI1*DP1)**1.0)
     1                *(WG/WP2)**0.25
C
C       FRICF = Frictional force ; Breault's correlation has been modified
C               for friction between small particles and the wall and between
C               small particles and large particles
```

```
C
C
C       FRICF = 2*((0.0285 * (G*D)**0.5)/UP2)*UP2**2/D ! KONNO & SAITO
C       FRICF = 2*(0.021*( UA**-0.9)*UP2**2)/D ! KLINZING, pg 94, for dNS PHASE
C
C               The above expressions were also tried in this situation
C               but proved inaccurate
C
        COLLIF = 6 * ((UP2)**2) *((1.-EPS)**1.0/(PHI1*DP1))*(WG/WP2)**0.25!Col.
C                                                                        Force
        NETF = DRAGF - ( GRAVF + FRICF + COLLIF) ! Net force; should be close
        ABSNET = ABS(NETF)                       ! to zero at steady state
        IF (ABSNET.LT.0.1) THEN
C
C        Also calculate "Solids Holdup"  EPS2 =  WP2/(RHOP2*UP2) to compare
C        with L.S.Fan's model
C
          EPS2 = WP2/(RHOP2 * UP2)
C
        WRITE(21,1000) EPS,TAU,UP2,DRAGF,FRICF,COLLIF,EPS2
1000    FORMAT(3X,F6.3,3X,F5.2,3X,F6.3,3X,F6.2,3X,F6.2,3X,F6.2,3X,F5.3)
        ELSE
        CONTINUE
        ENDIF
25      CONTINUE
30      CONTINUE
        STOP
        END
```

APPENDIX B : BUBBLE CHARACTERISTICS DATA: PRESSURE TIME TRACES

Bubble Data, UNH 0.038m (1.5",n.d.) unit

Table B1 :Copper-steel System Identification Key, UNH 0.038m Unit

Run Number	Serial Number,Table 5.5 in TEXT
$01S1$	10
$01S2$	11
$01S3$	12
$01S4$	13
$01S5$	8
$01S6$	9
$01NS$	7
$2S1$	3
$2S2$	2
$2S3$	1
$2S4$	4
$2S5$	5
$2S6$	6

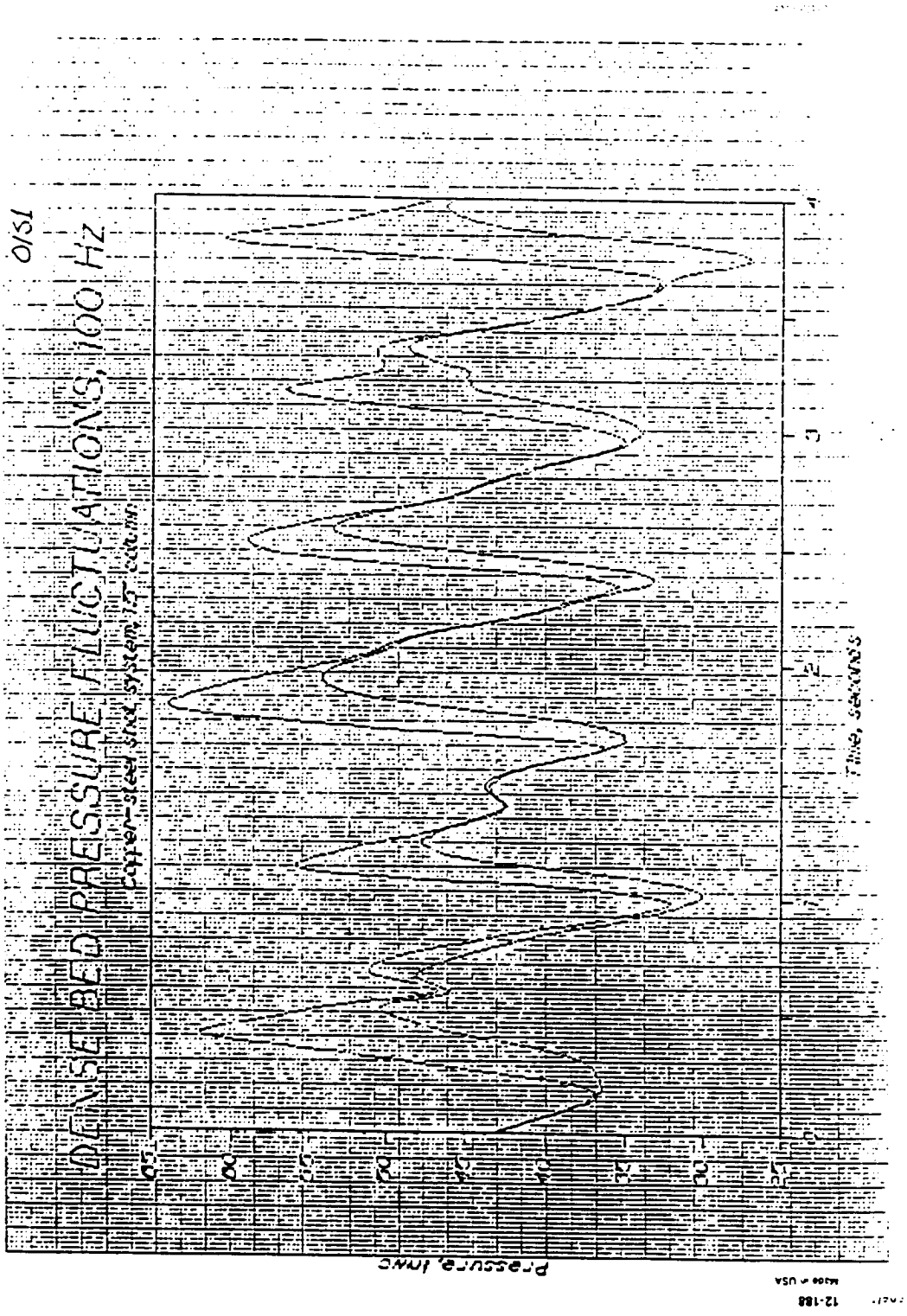

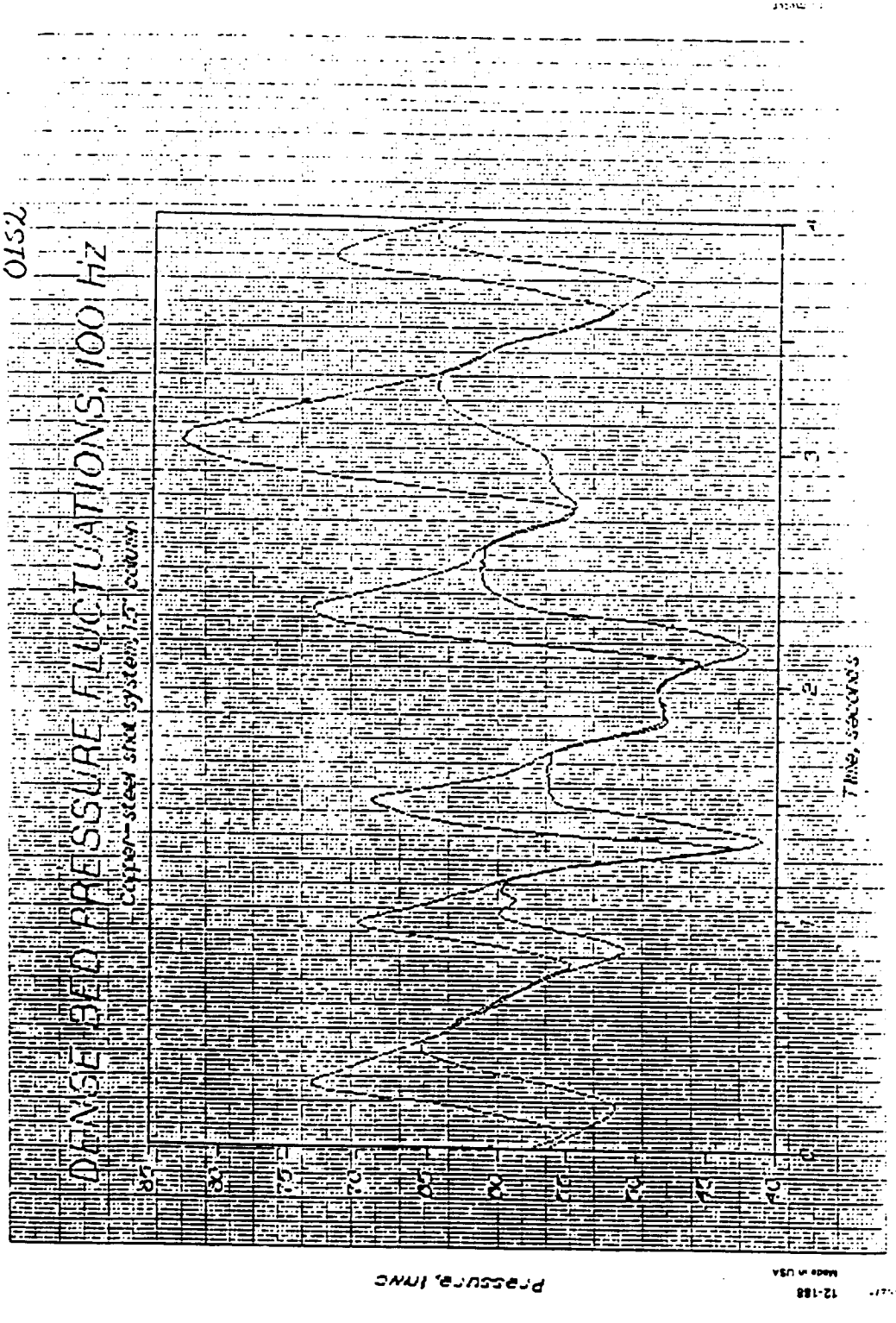

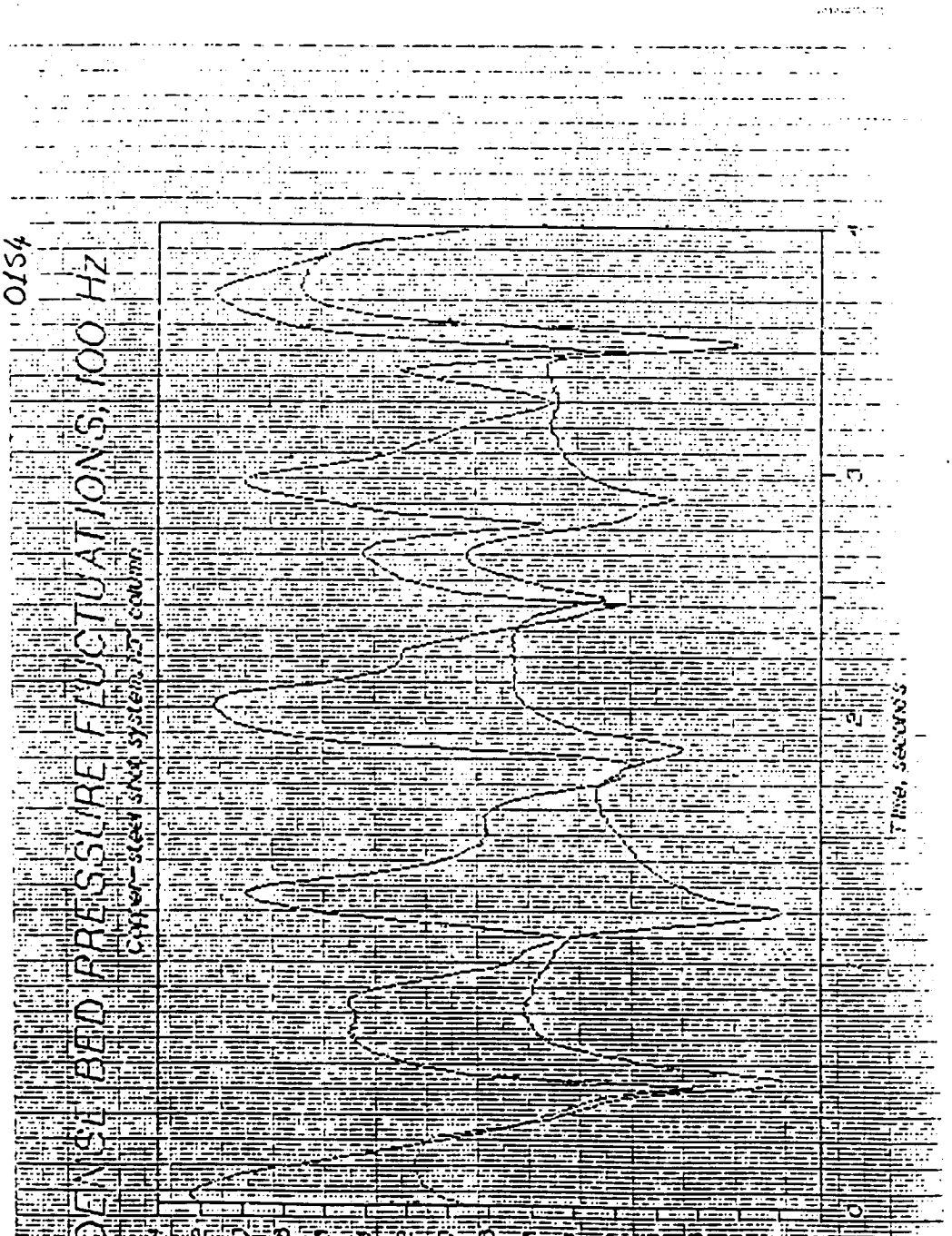

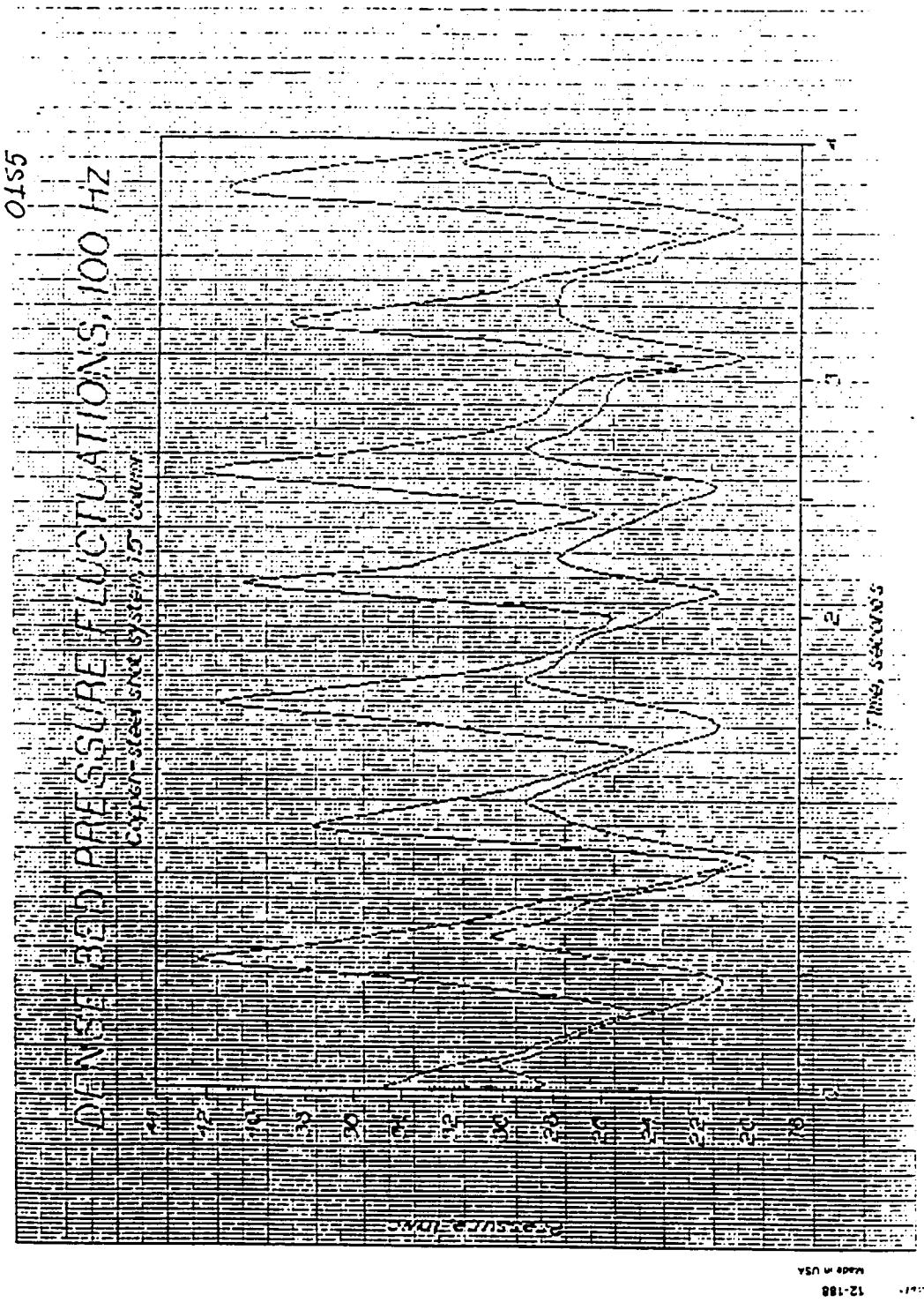

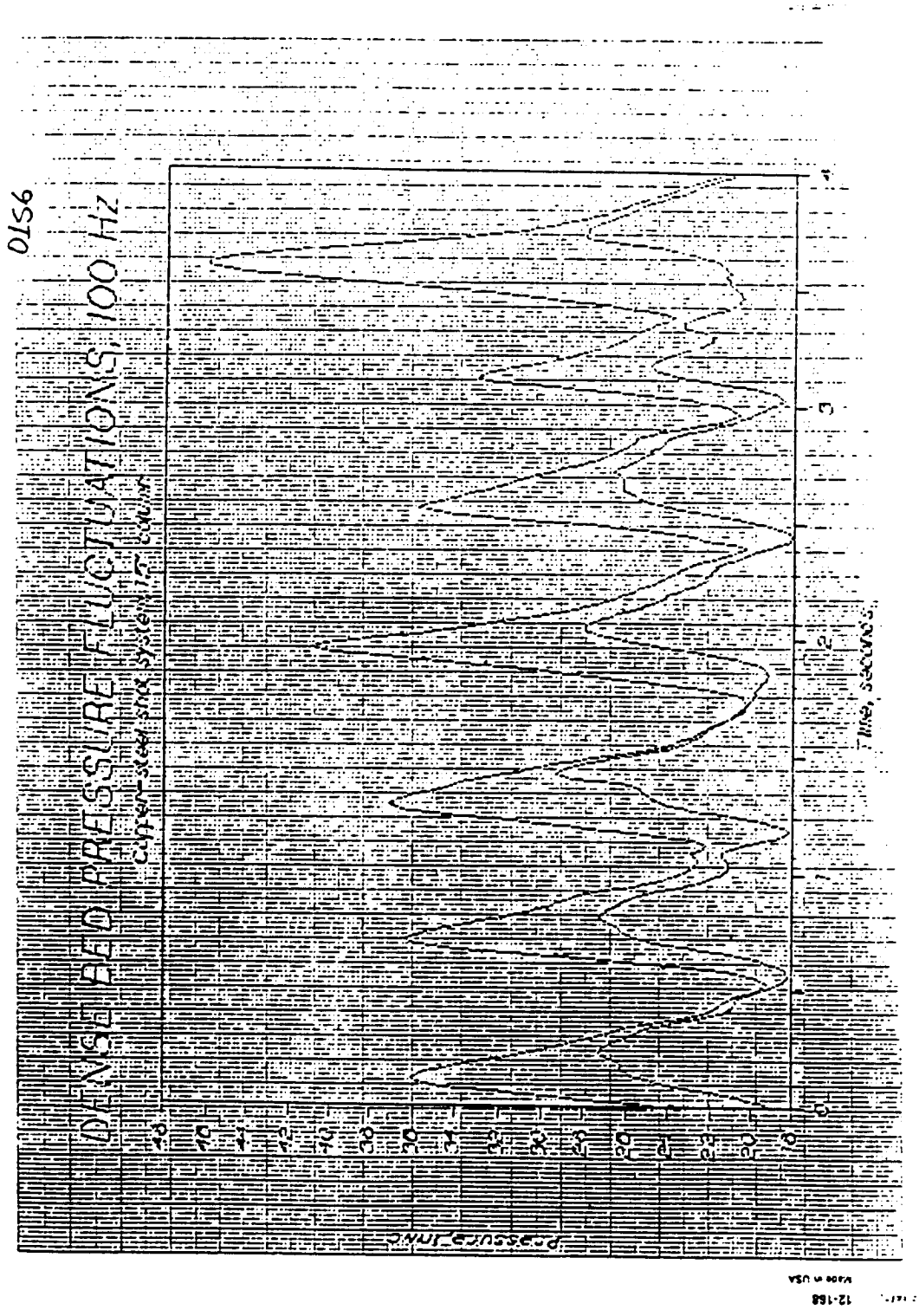

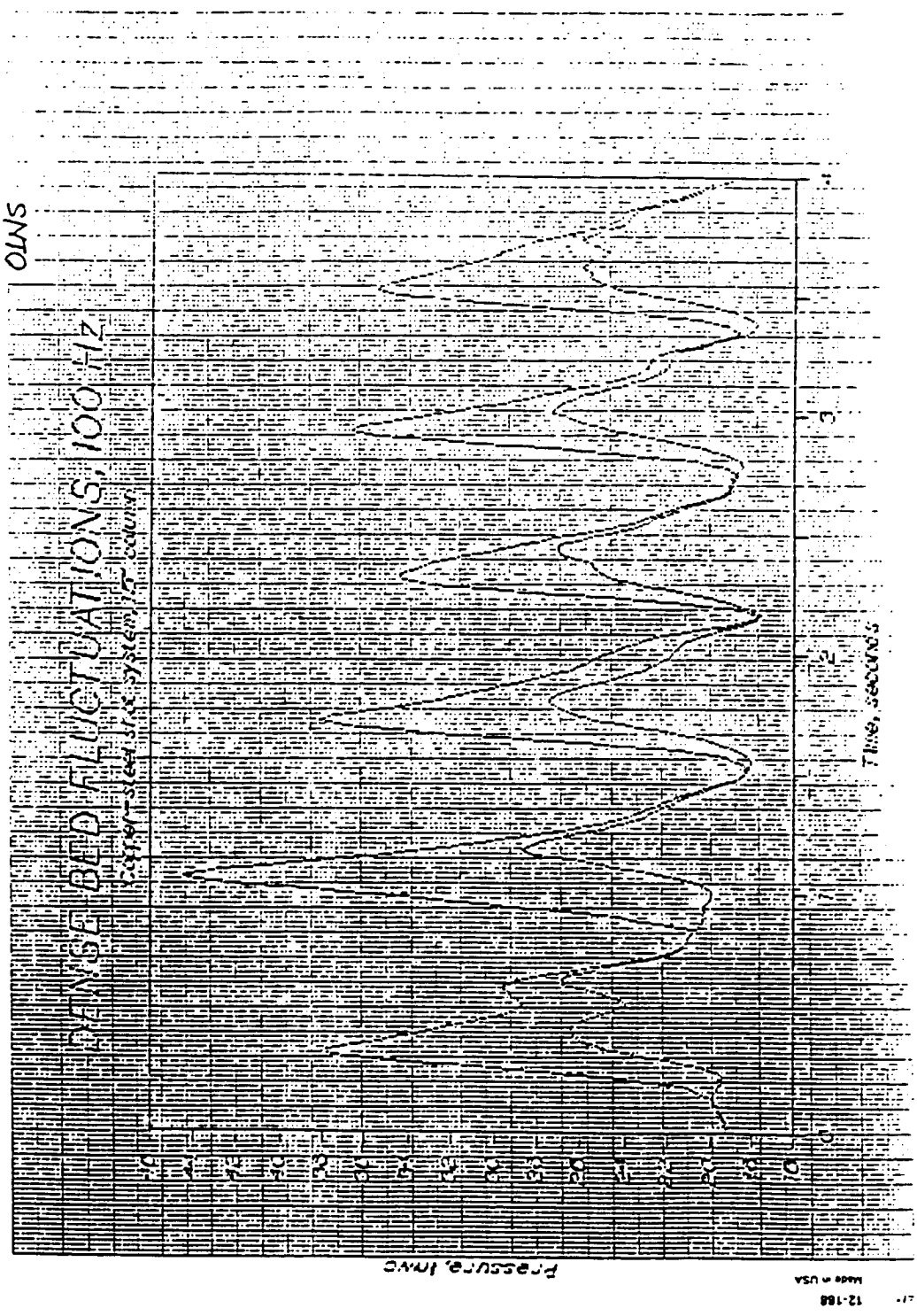

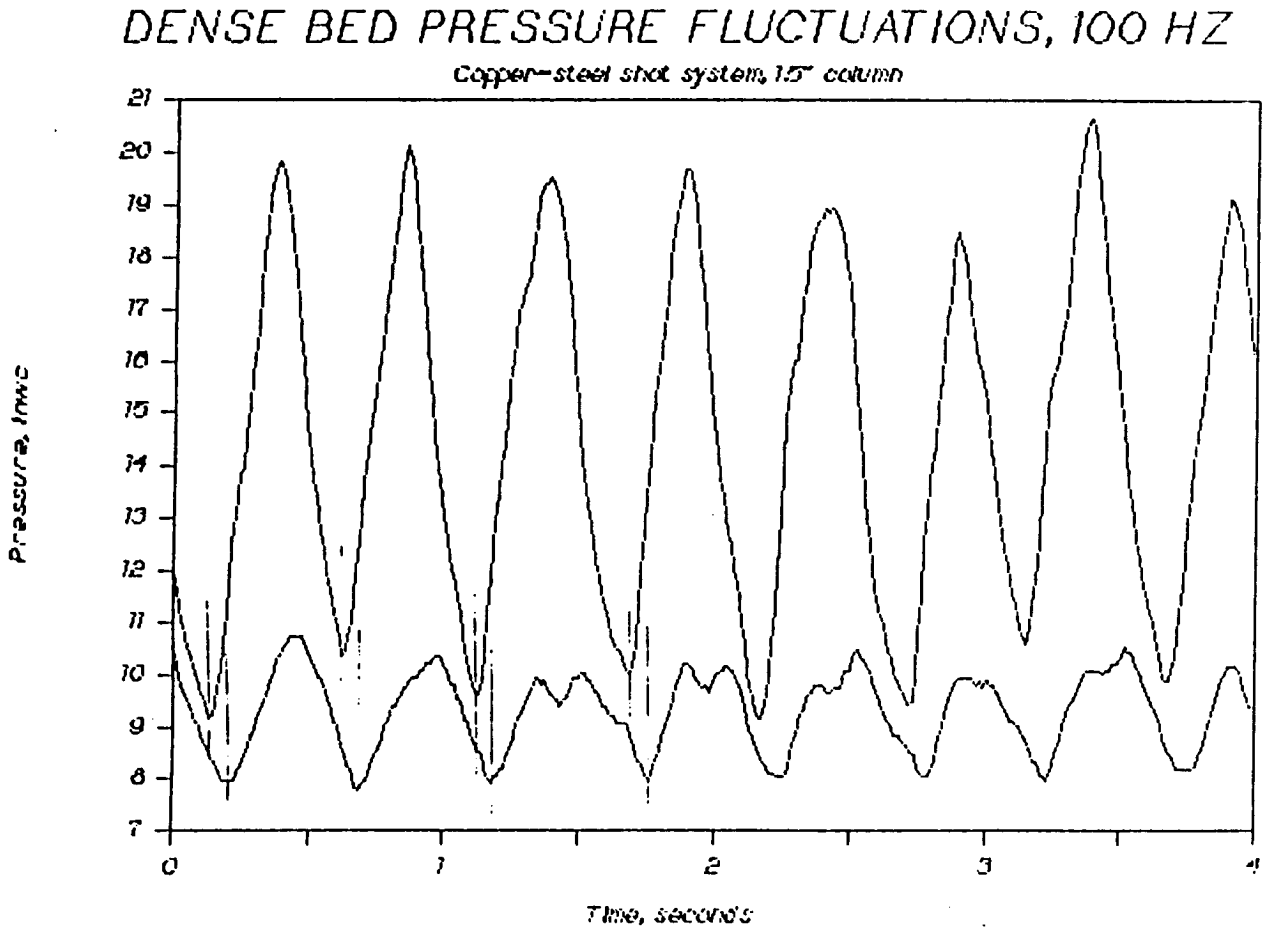

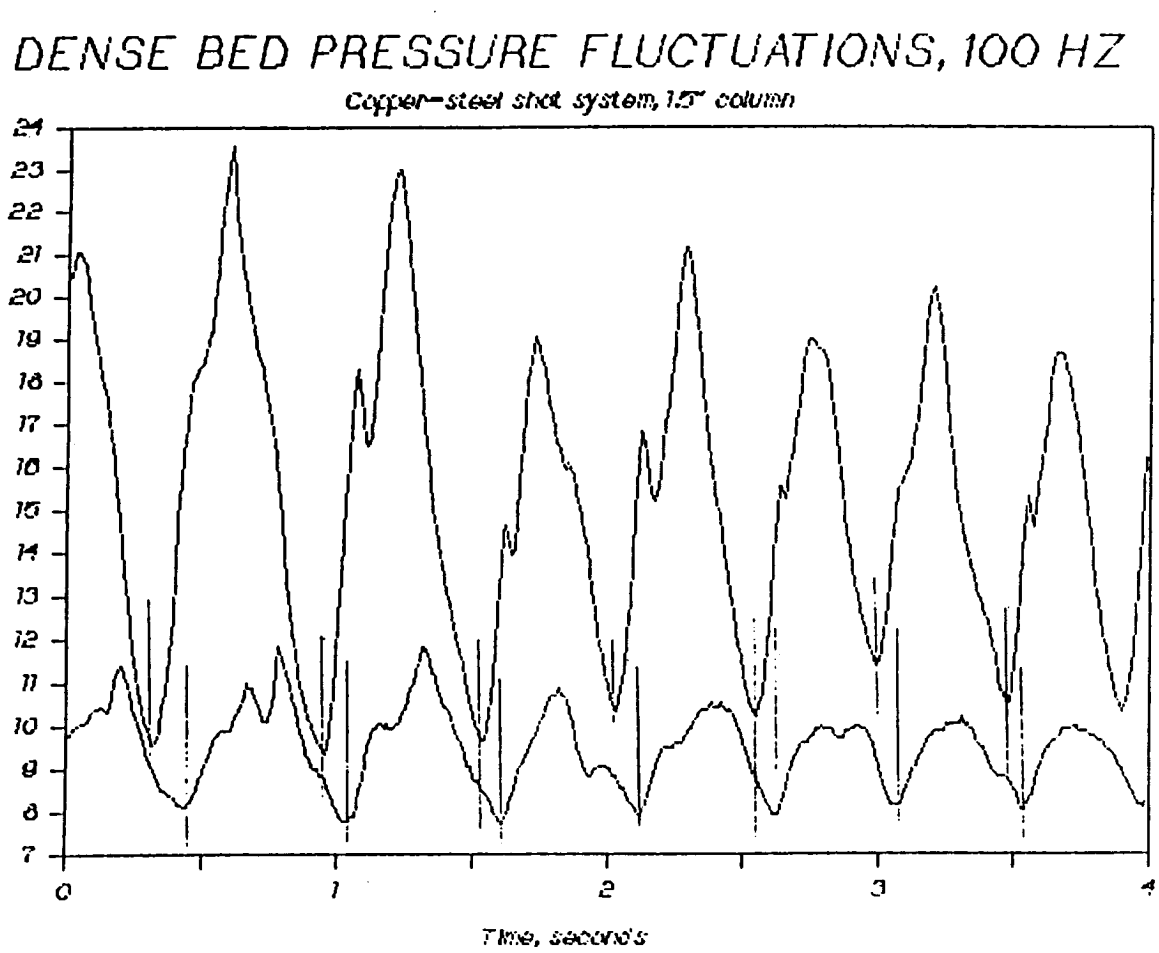

253

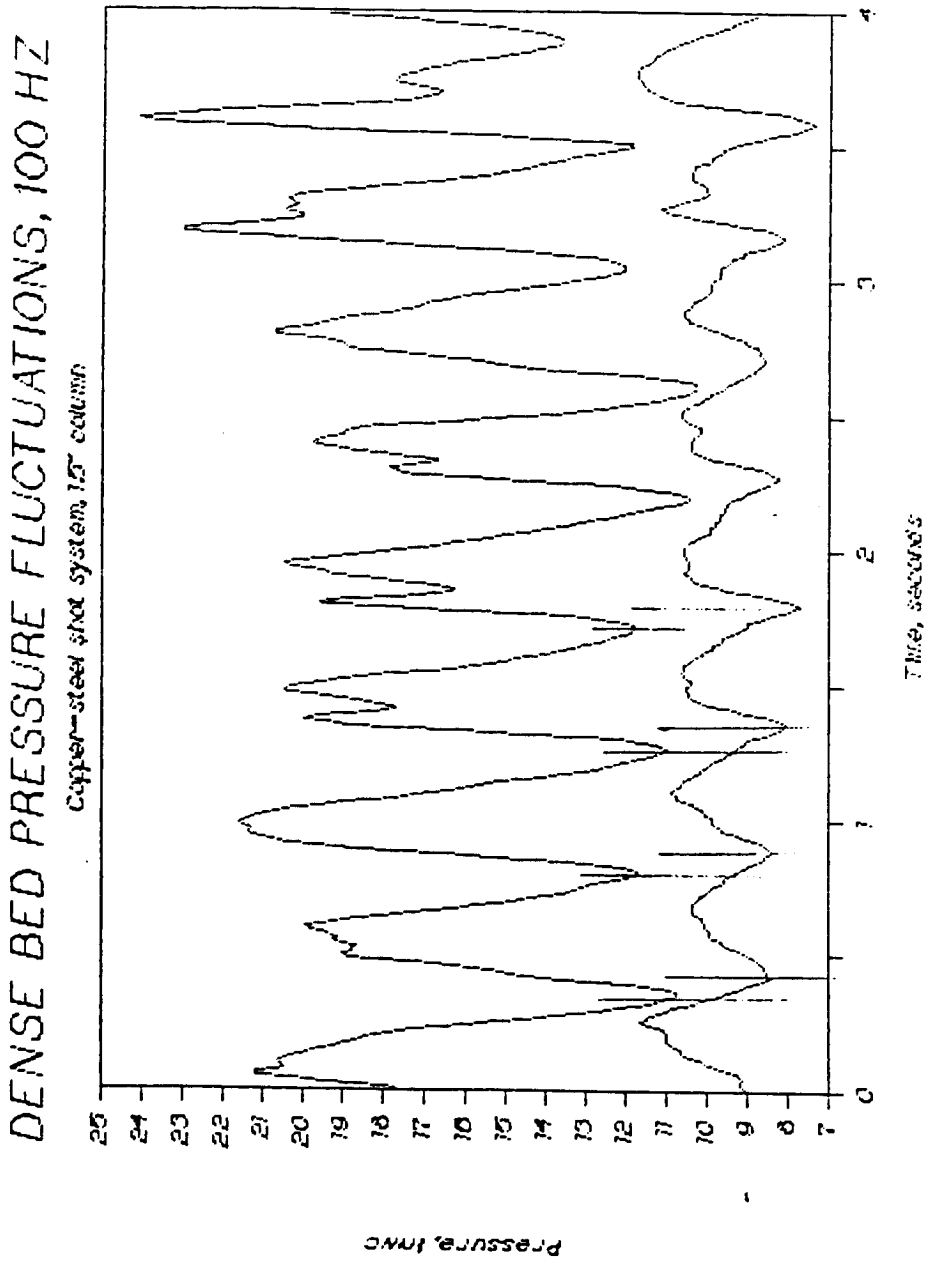

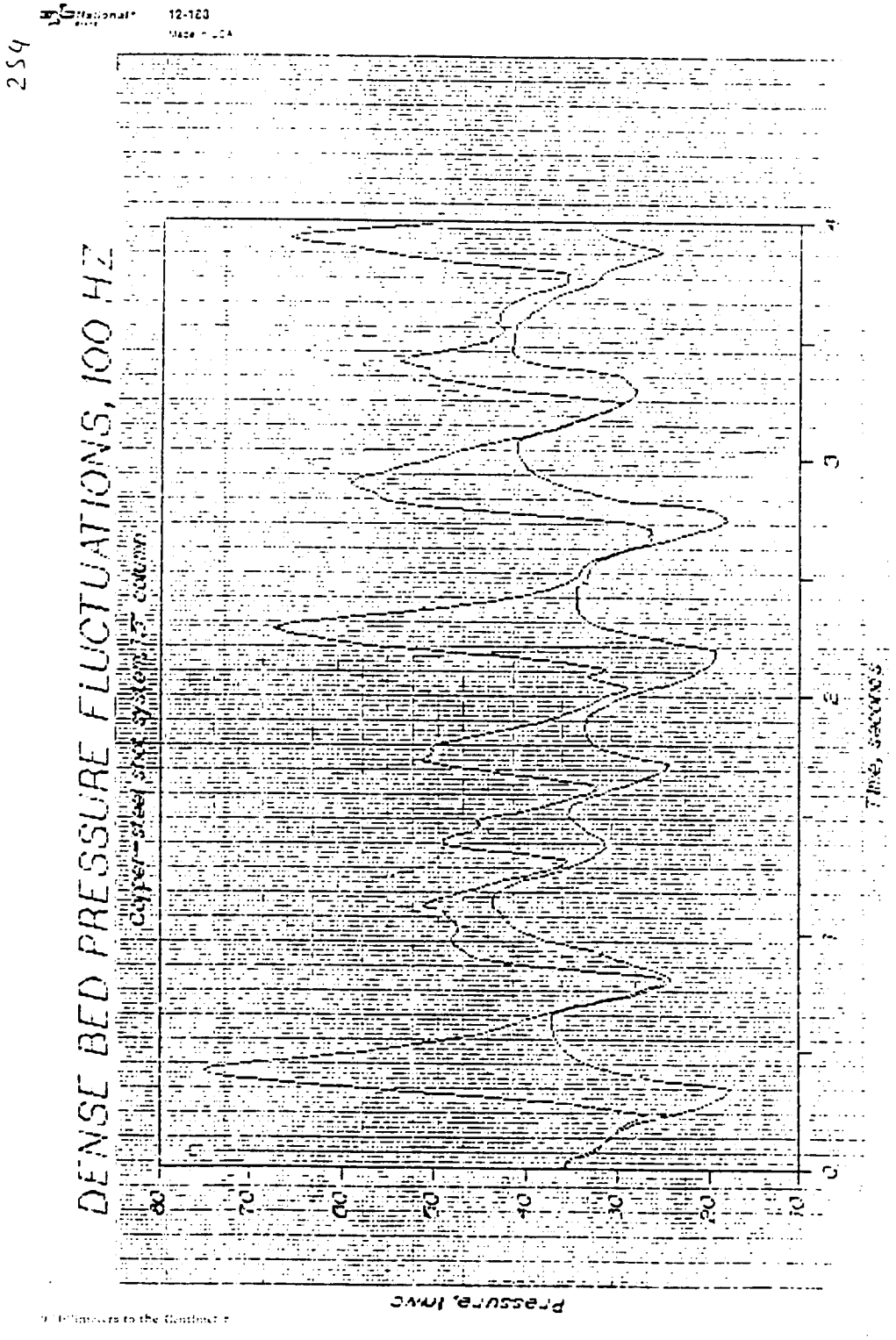

255

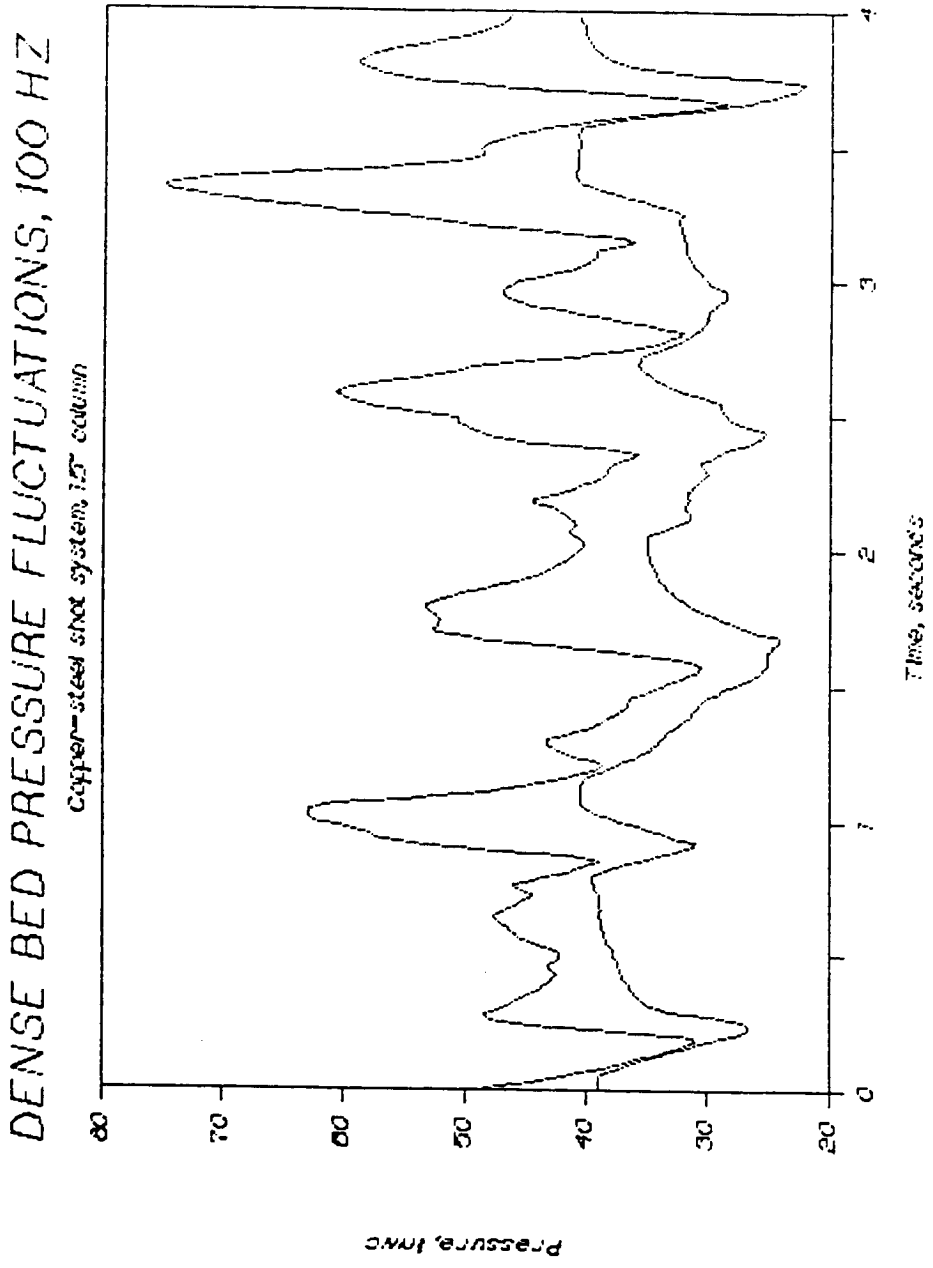

256

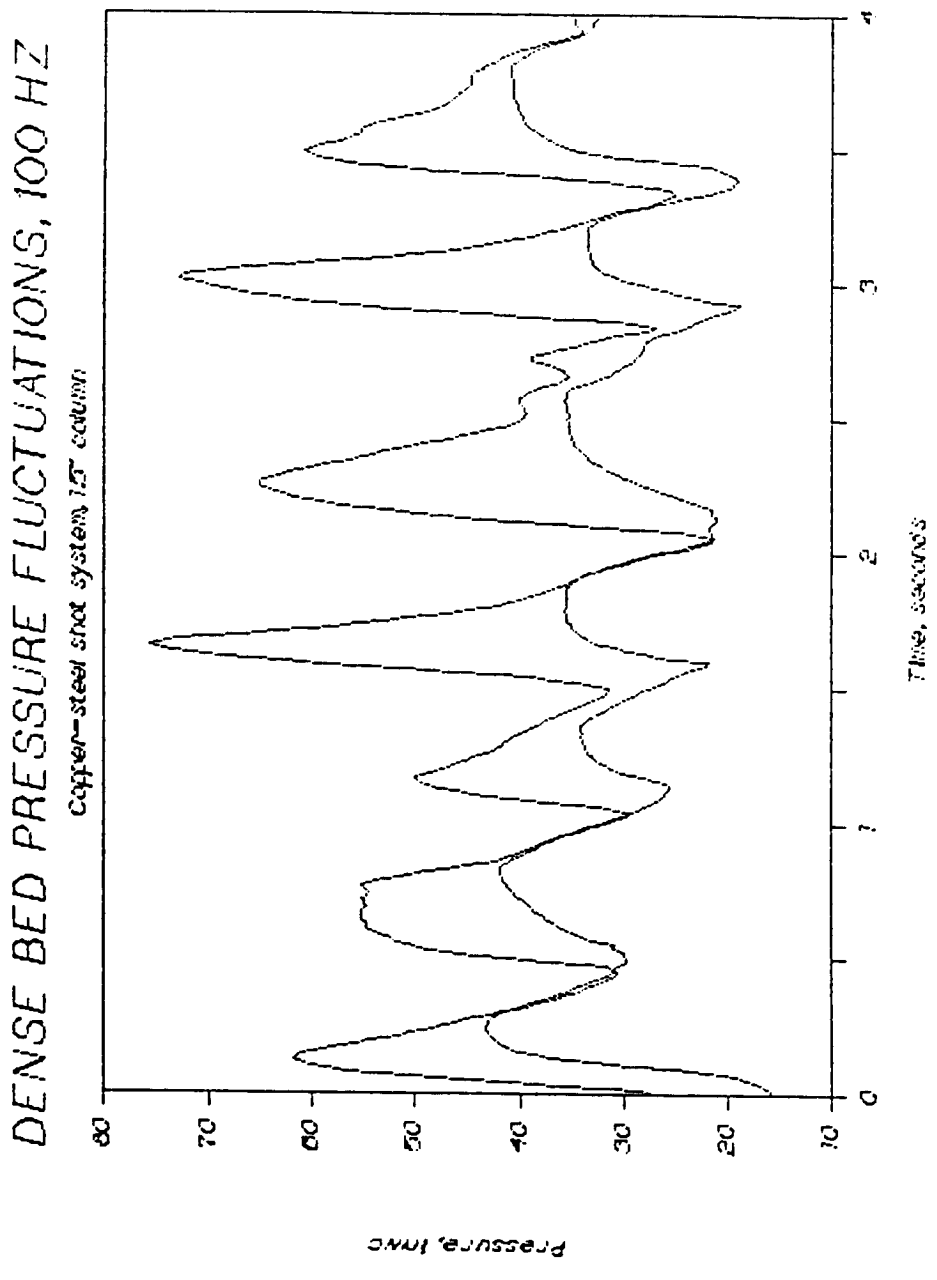

Table B2: Sand-rock System Identification Key, UNH 0.038m Unit

Run Number	Serial Number,Table 5.6 in TEXT
$11S1$	2
$11S2$	3
$11S3$	4
$11S4$	5
$11S5$	6
$11S6$	7
$11S7$	8
$11S8$	9
$11S9$	10
$11S10$	1
$11NS$	11

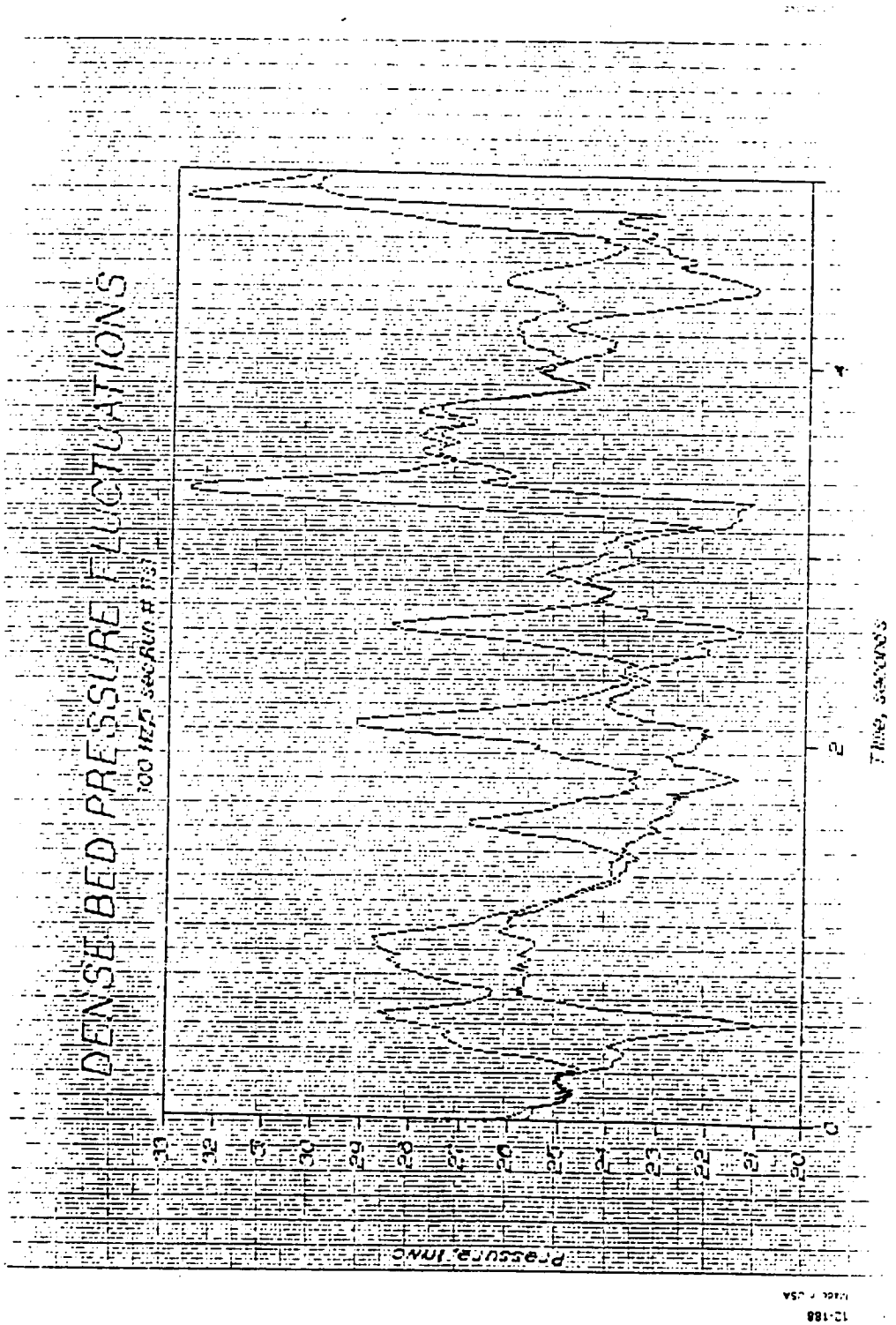

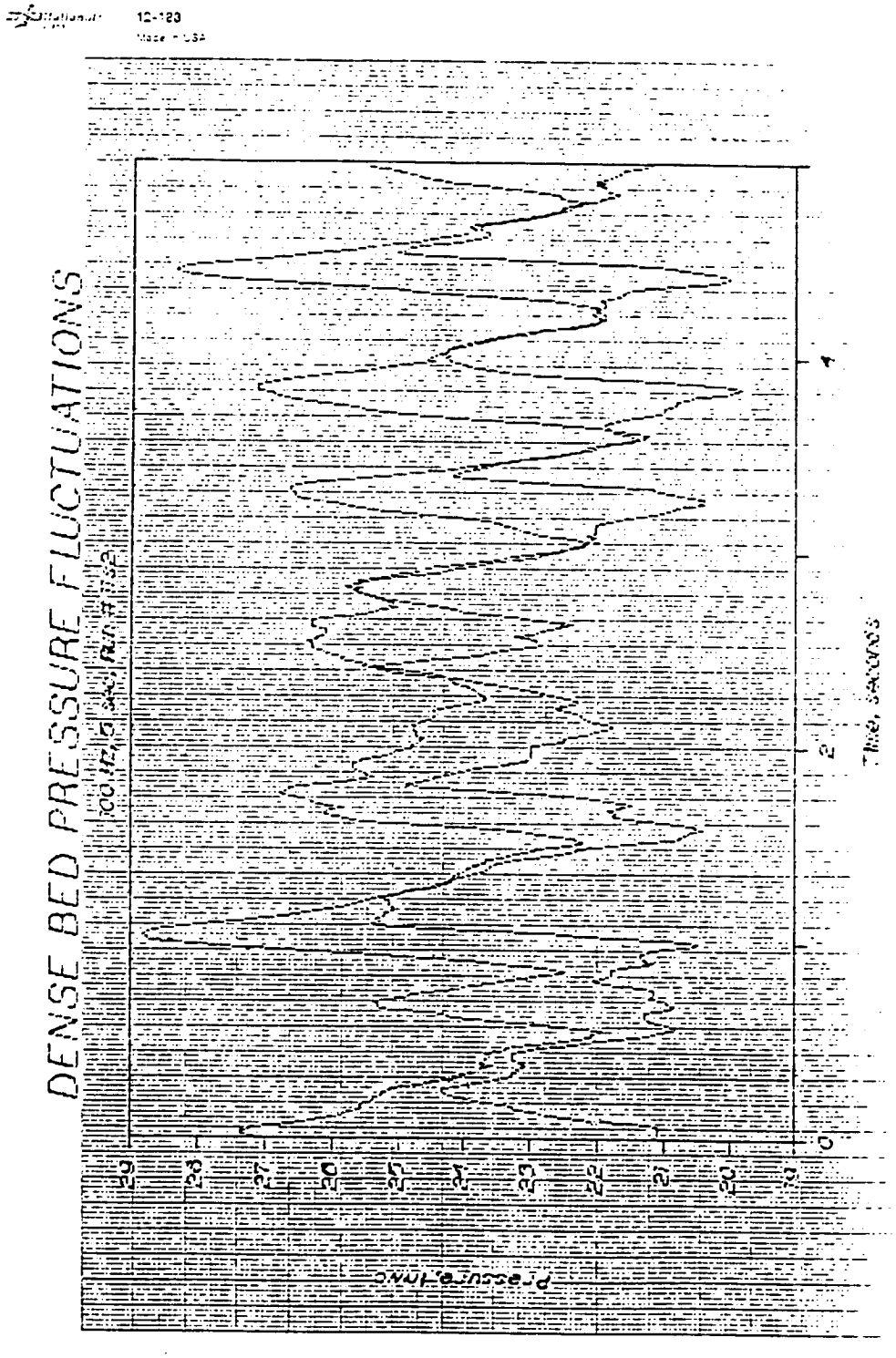

10 Millimeters to the Centimeter

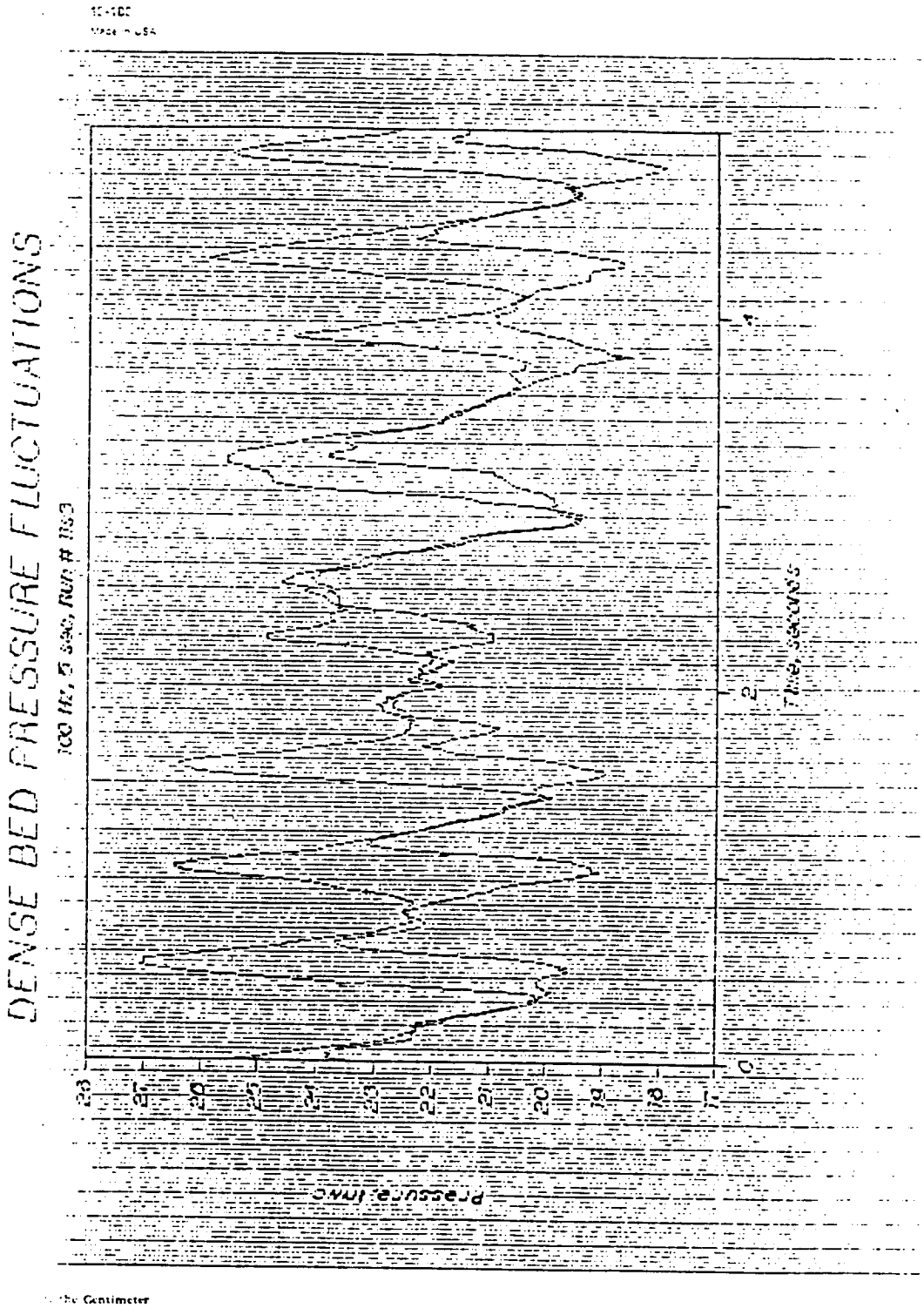

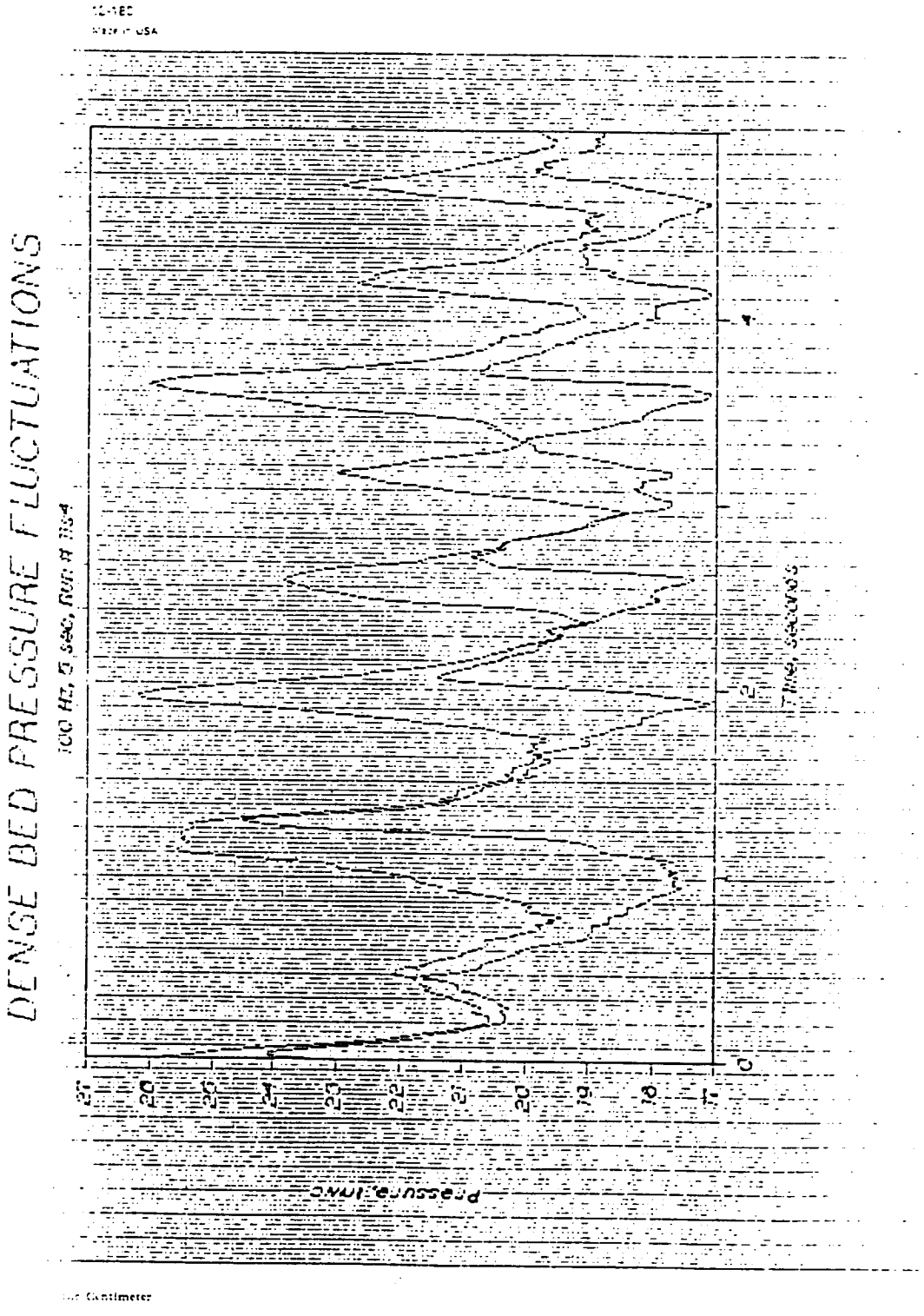

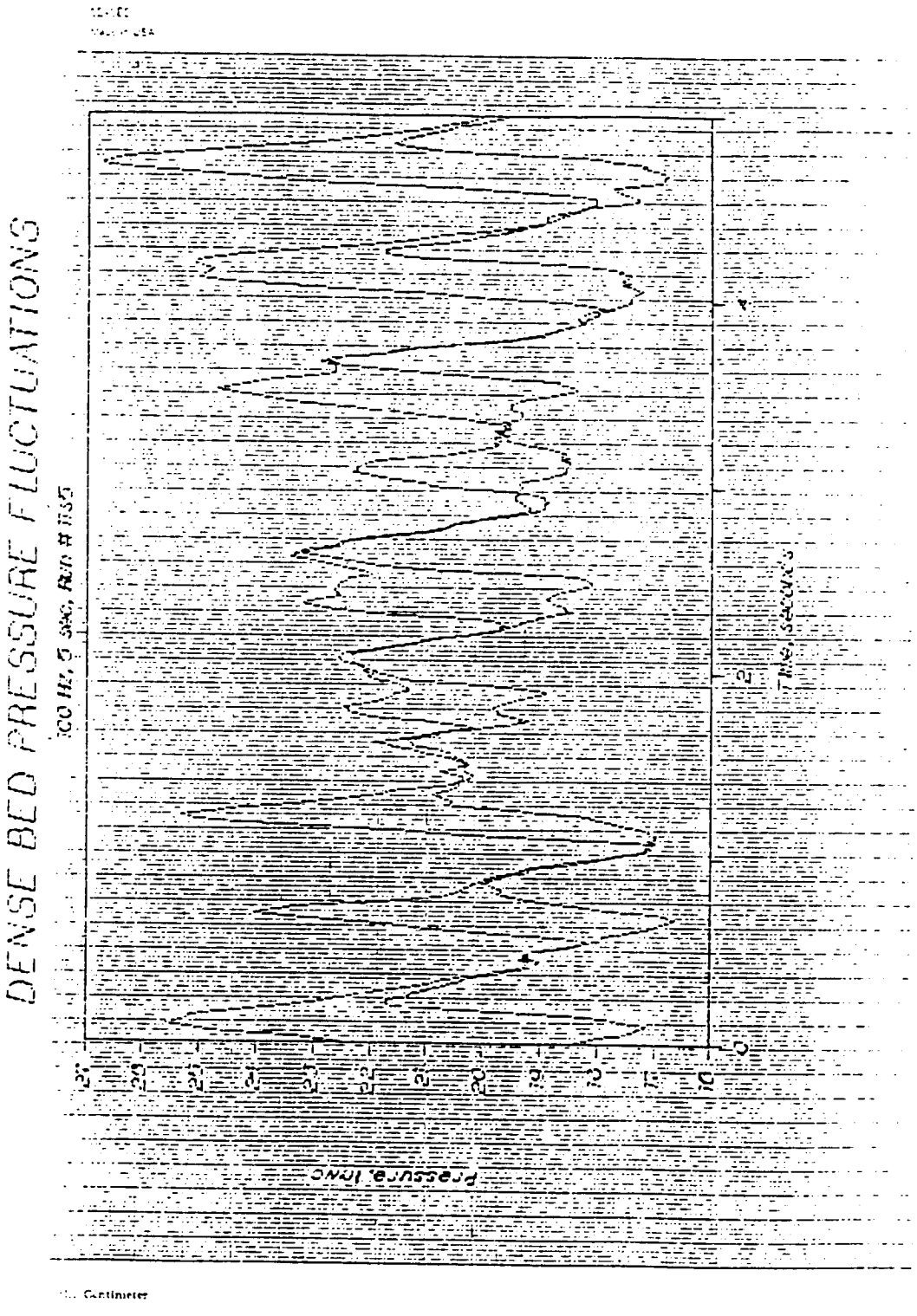

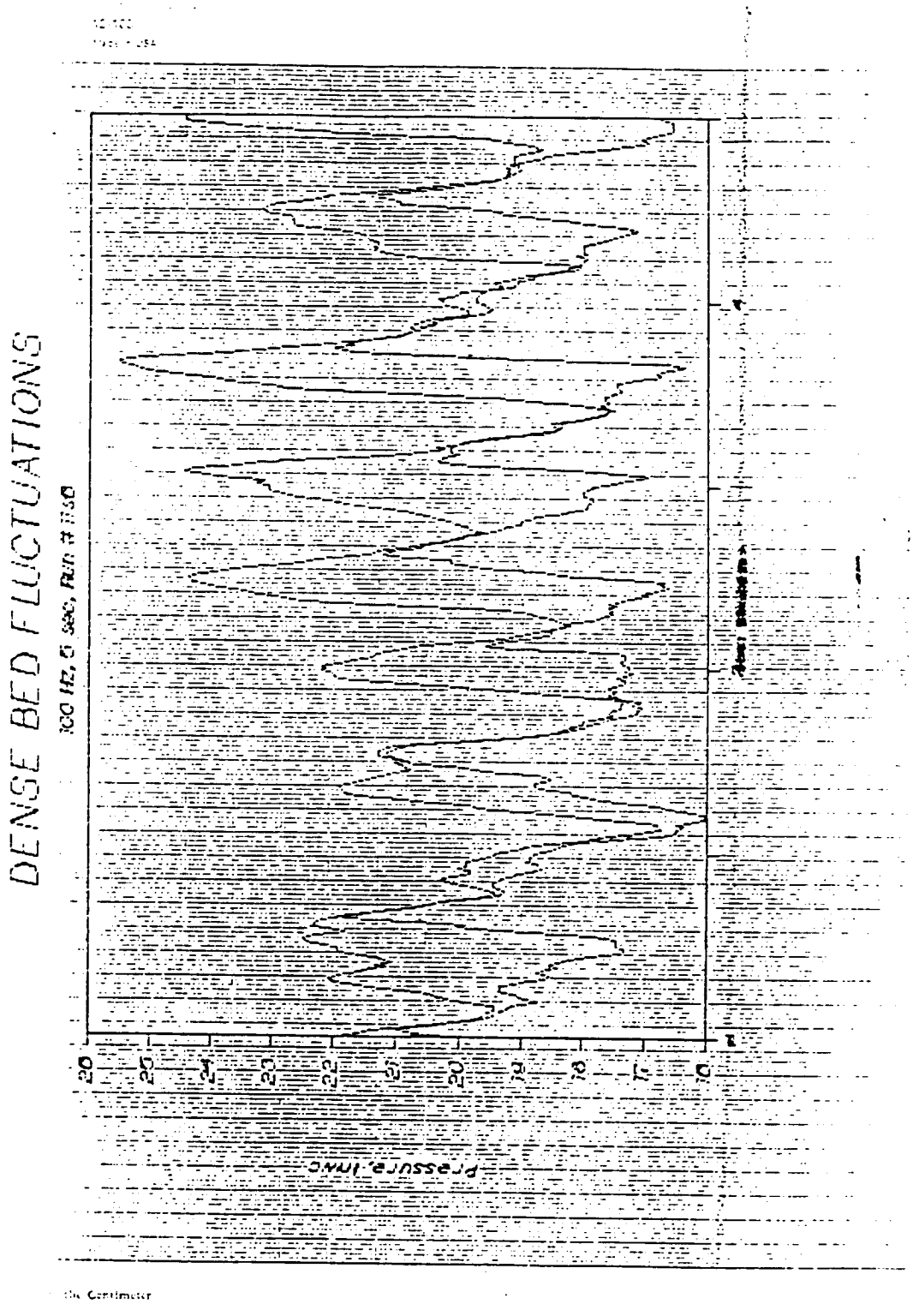

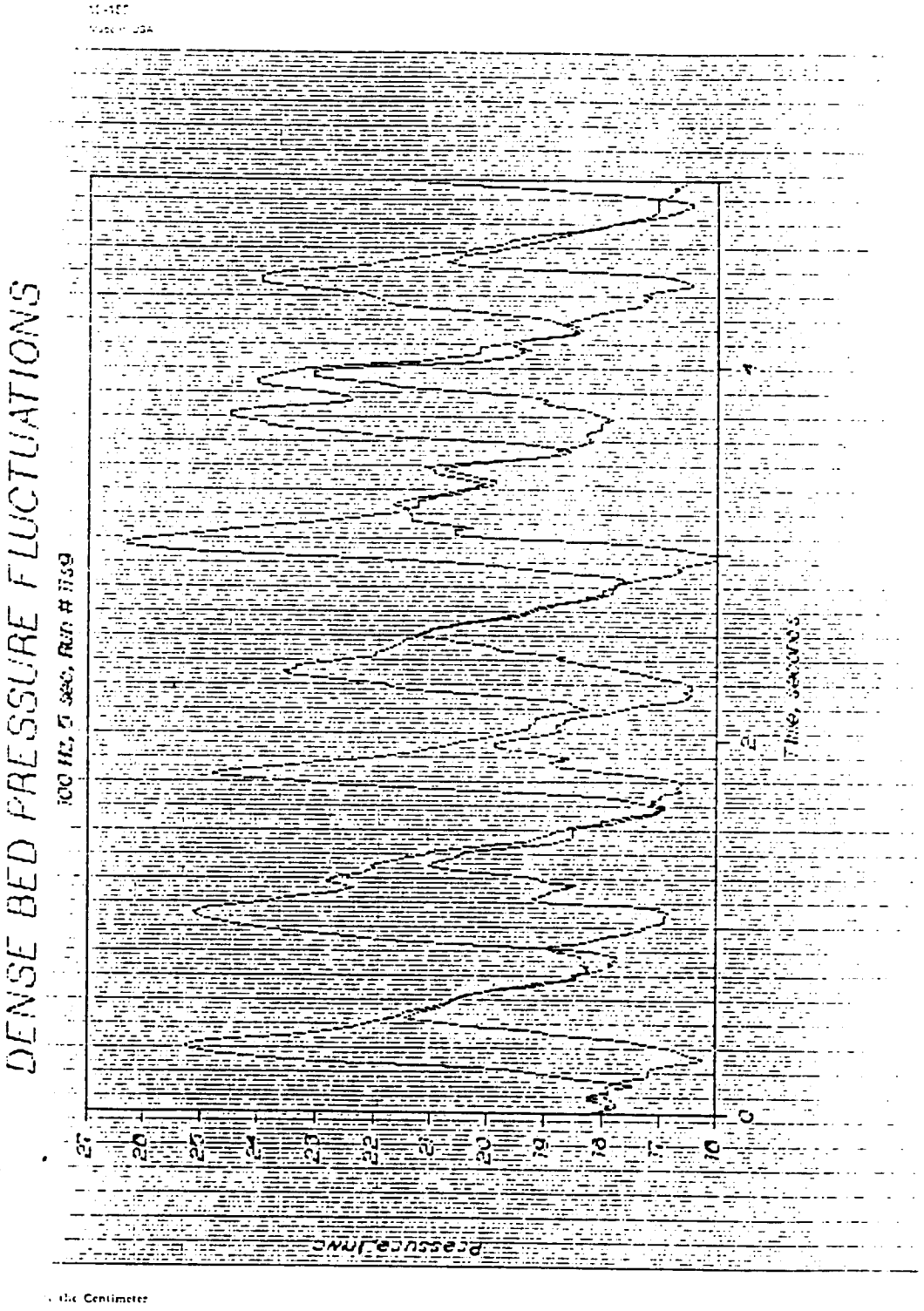

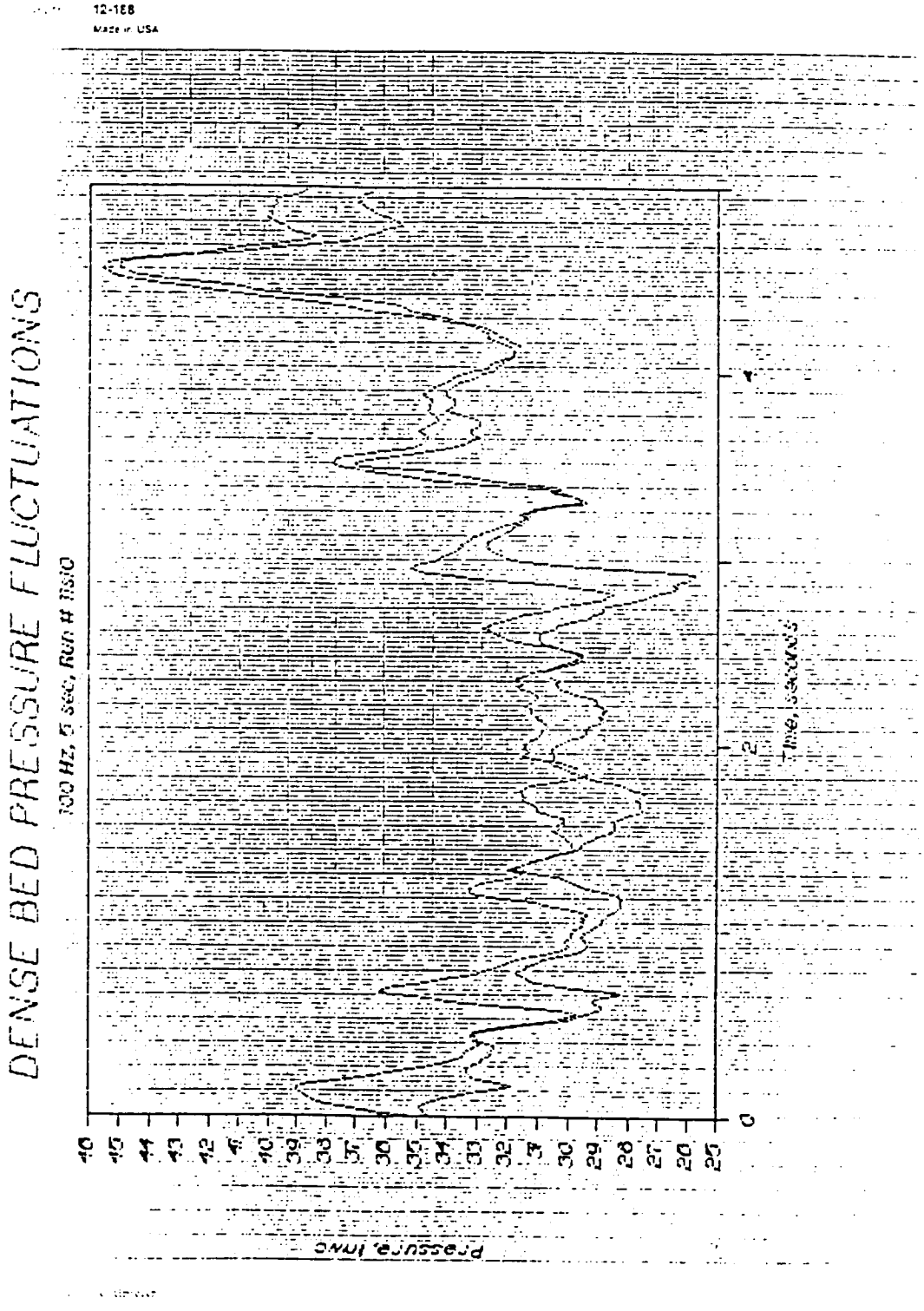

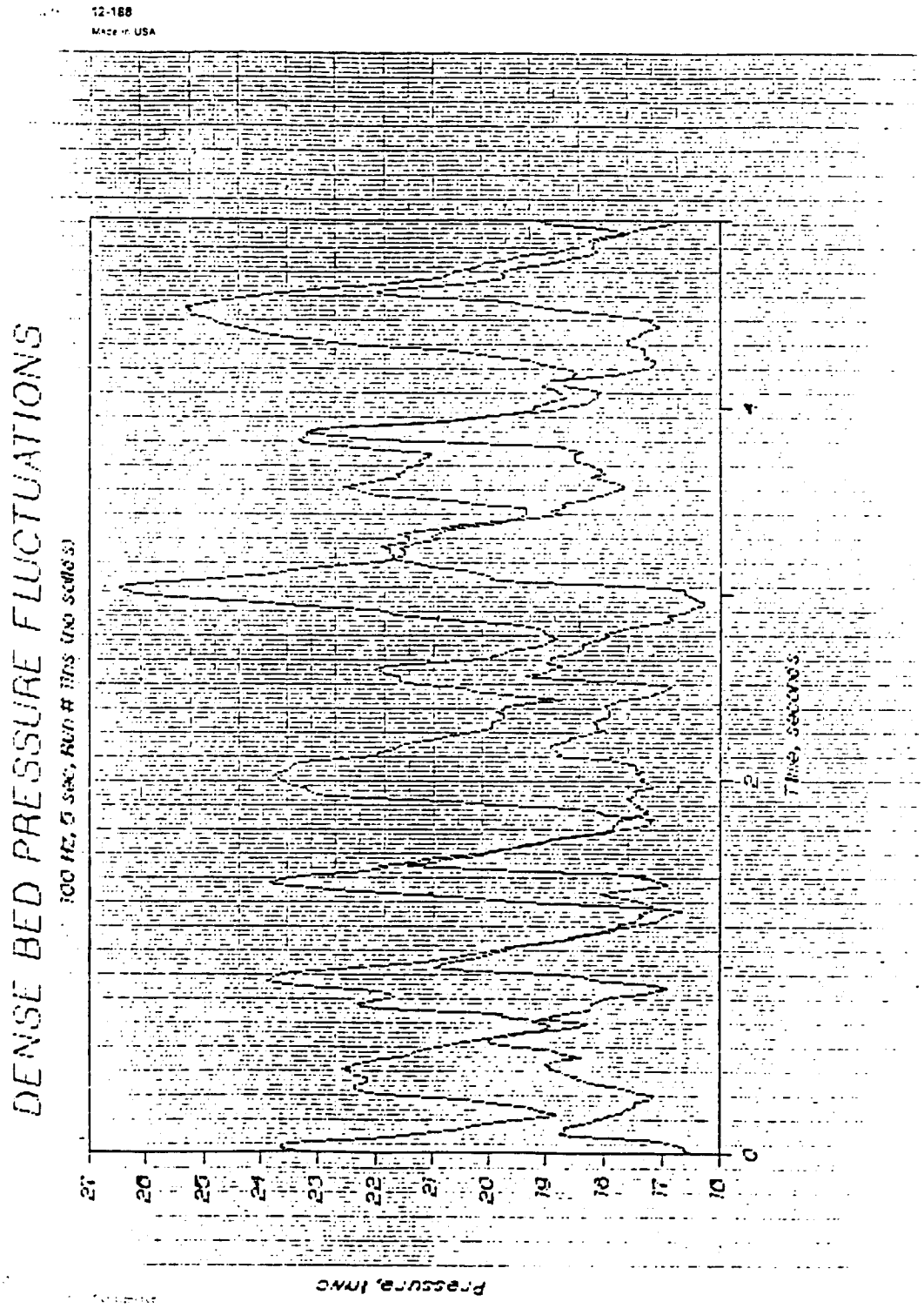

Table B3: Copper-steel System Identification Key, UNH 0.102m Unit

Run Number	Serial Number,Table 5.7 in TEXT
04$S1$	4
04$S2$	5
04$S3$	3
04$S4$	2
04$S5$	6
04NS	1

Table B4: Sand-rock System Identification Key, UNH 0.102m Unit

Run Number	Serial Number,Table 5.8 in TEXT
04$R1$	7
04$R2$	5
04$R3$	6
04$R4$	4
04$R5$	3
04$R6$	2
04RNS	1

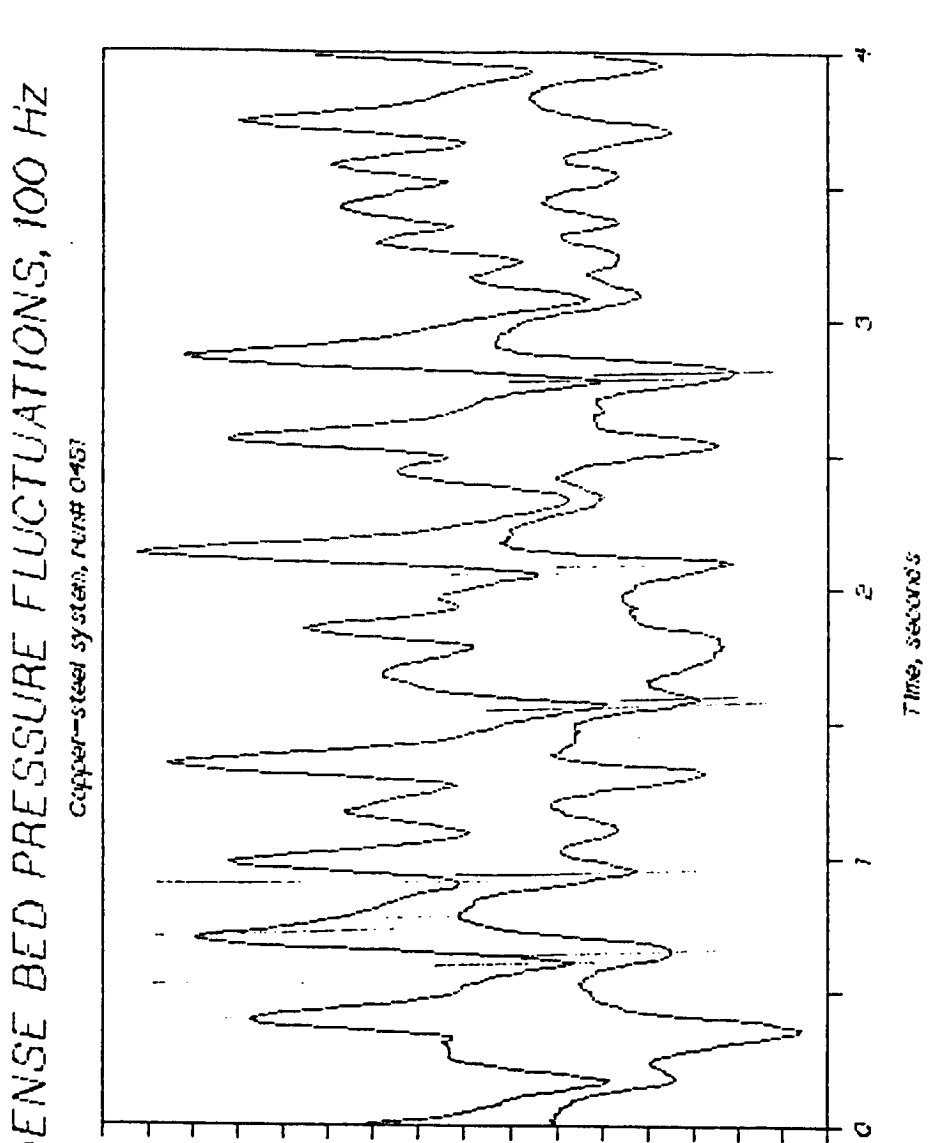

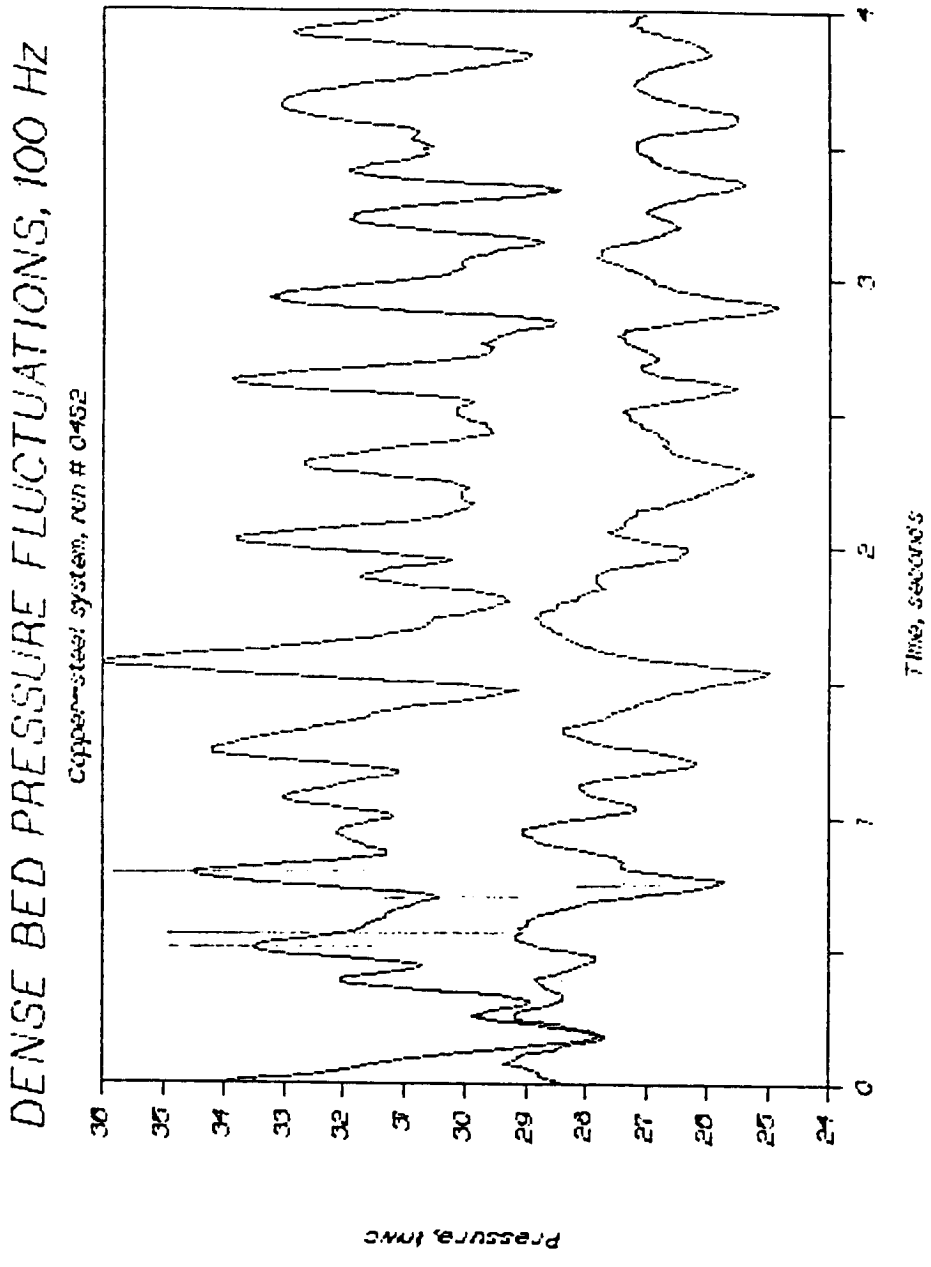

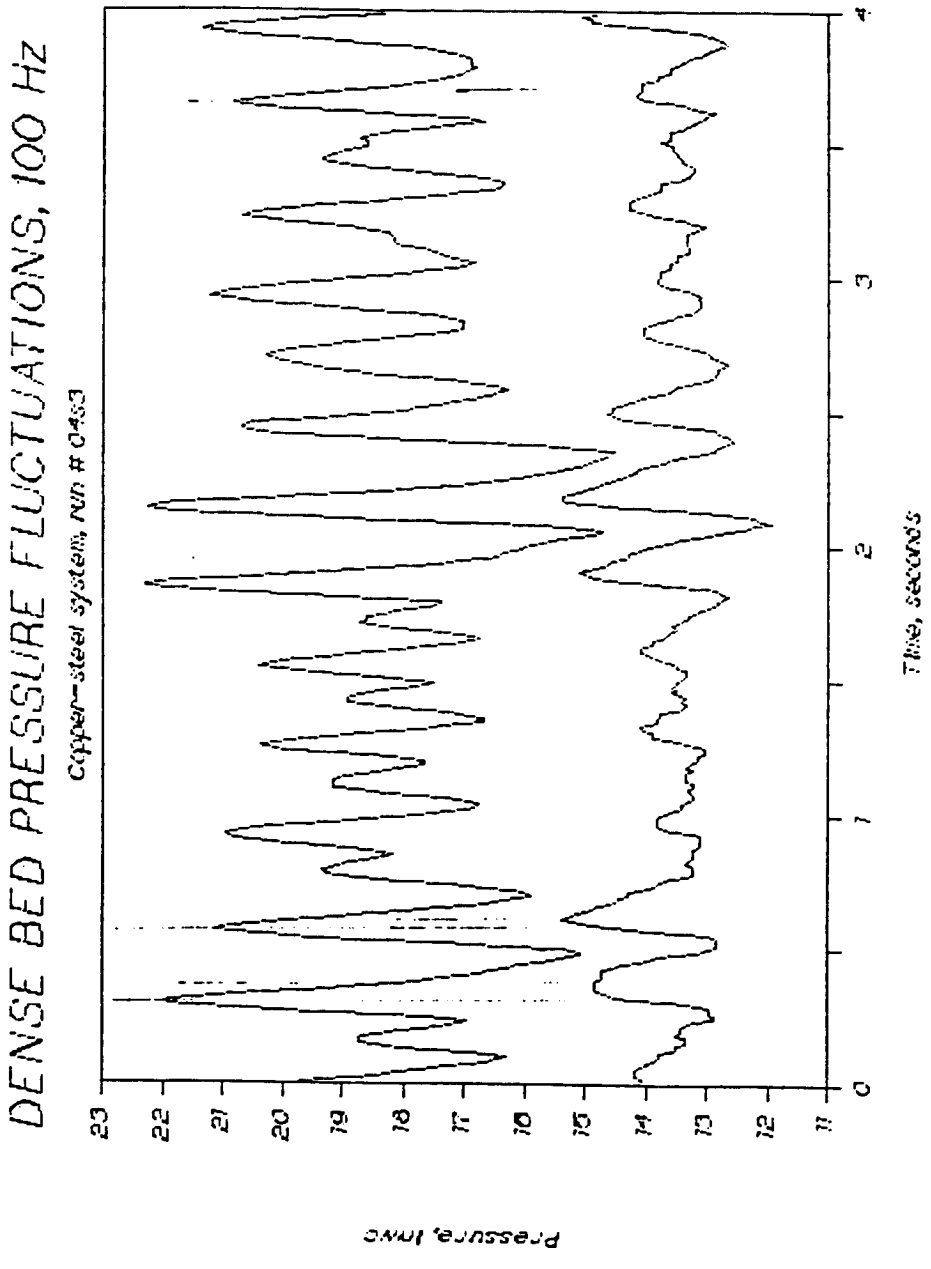

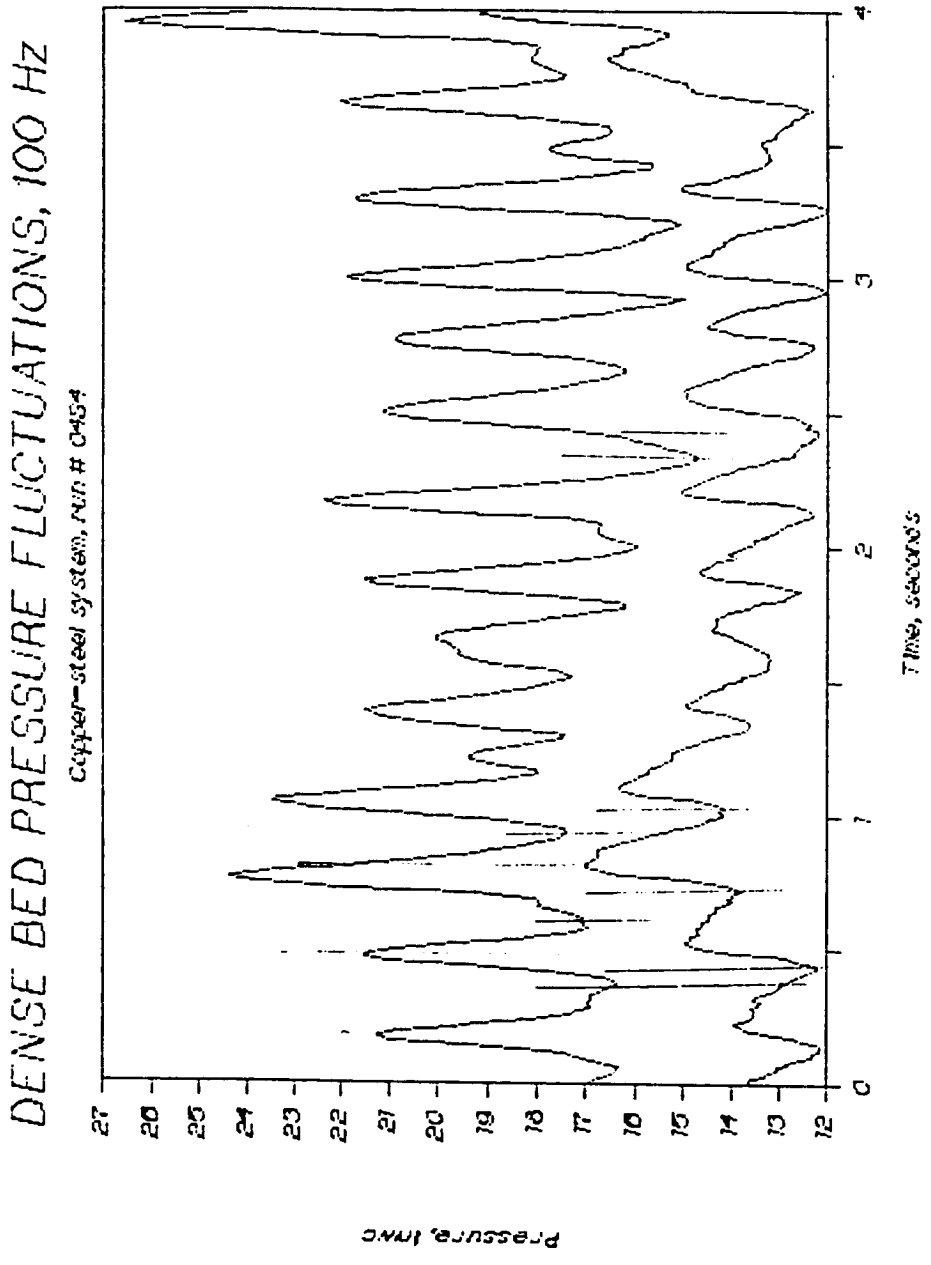

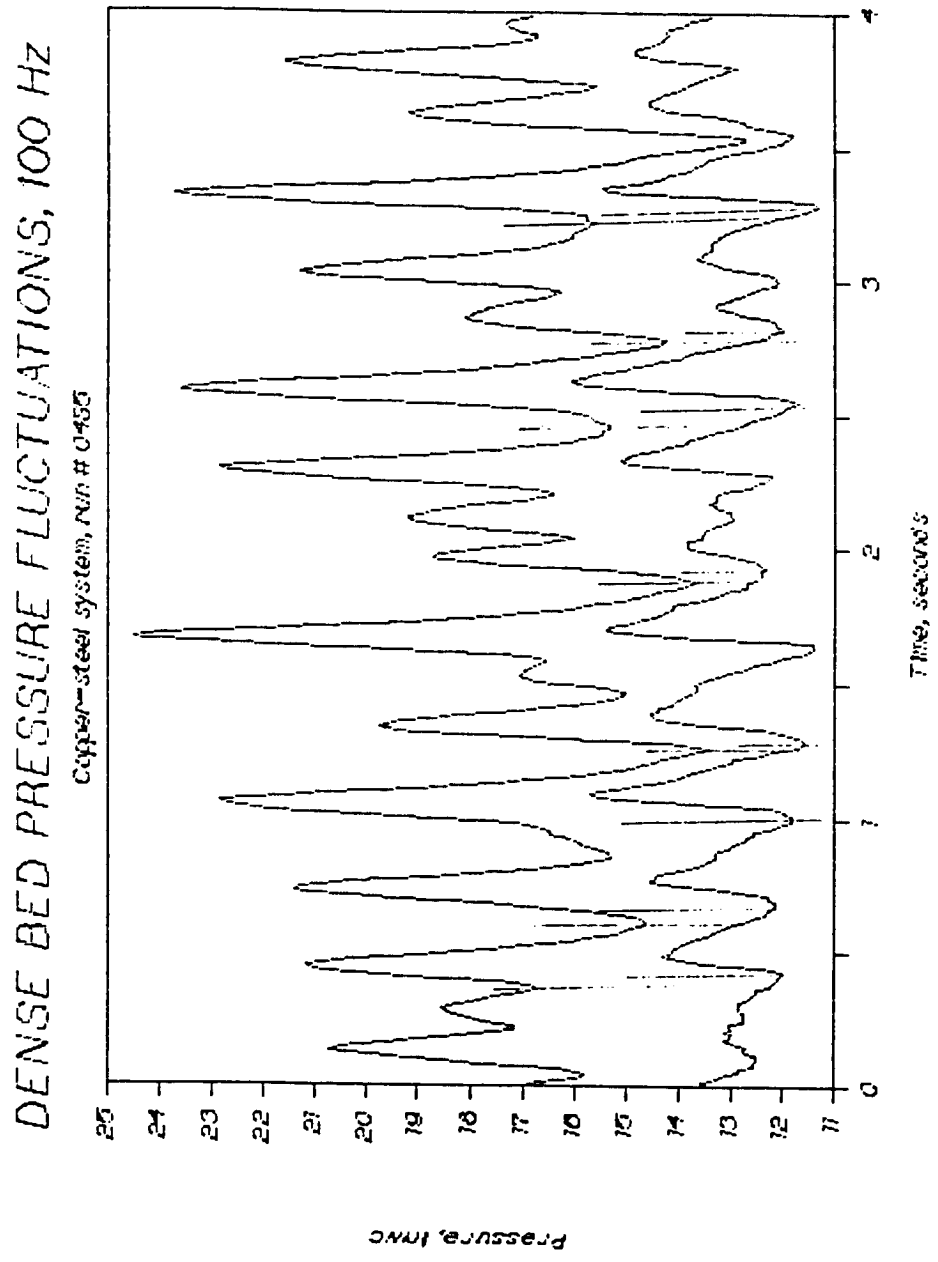

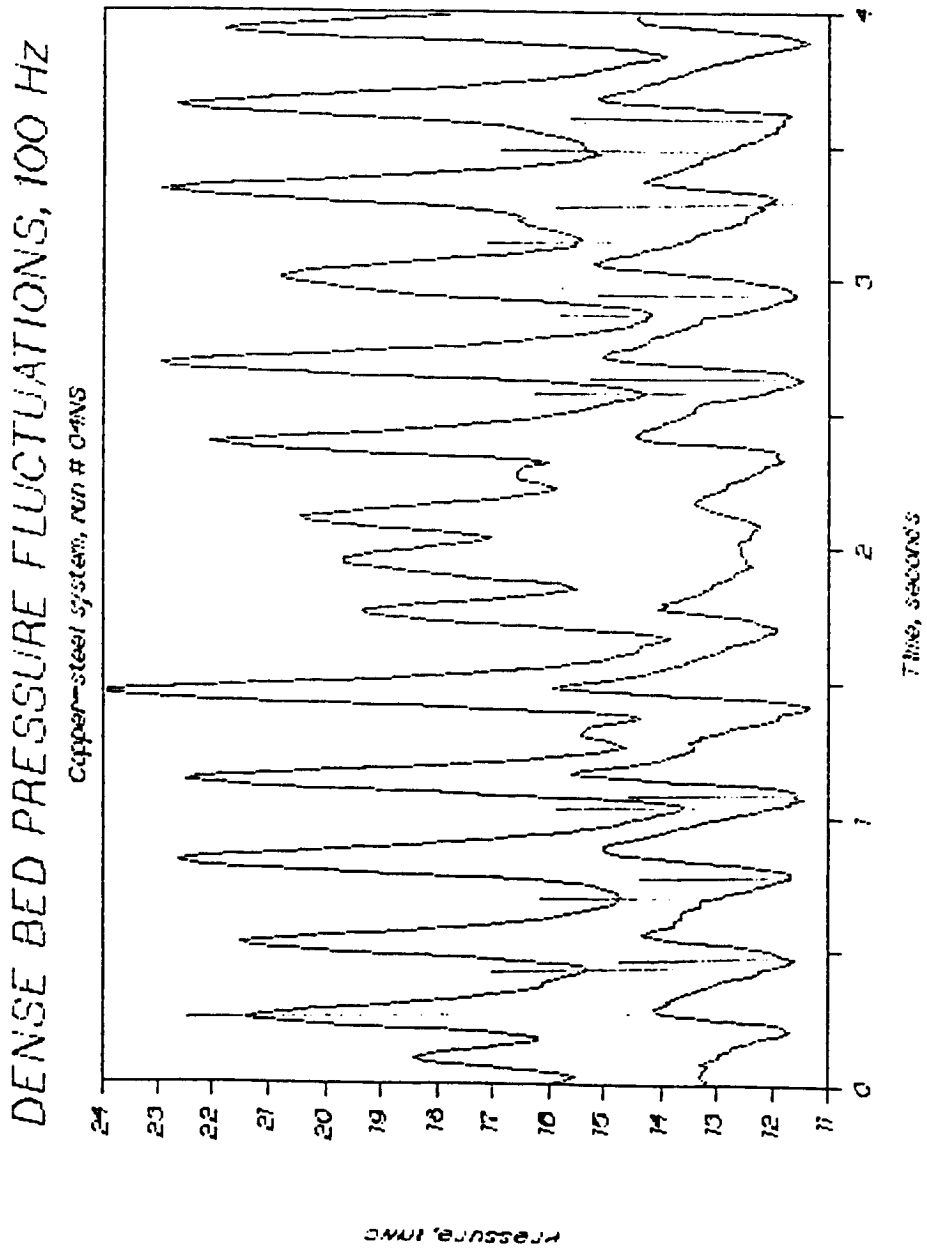

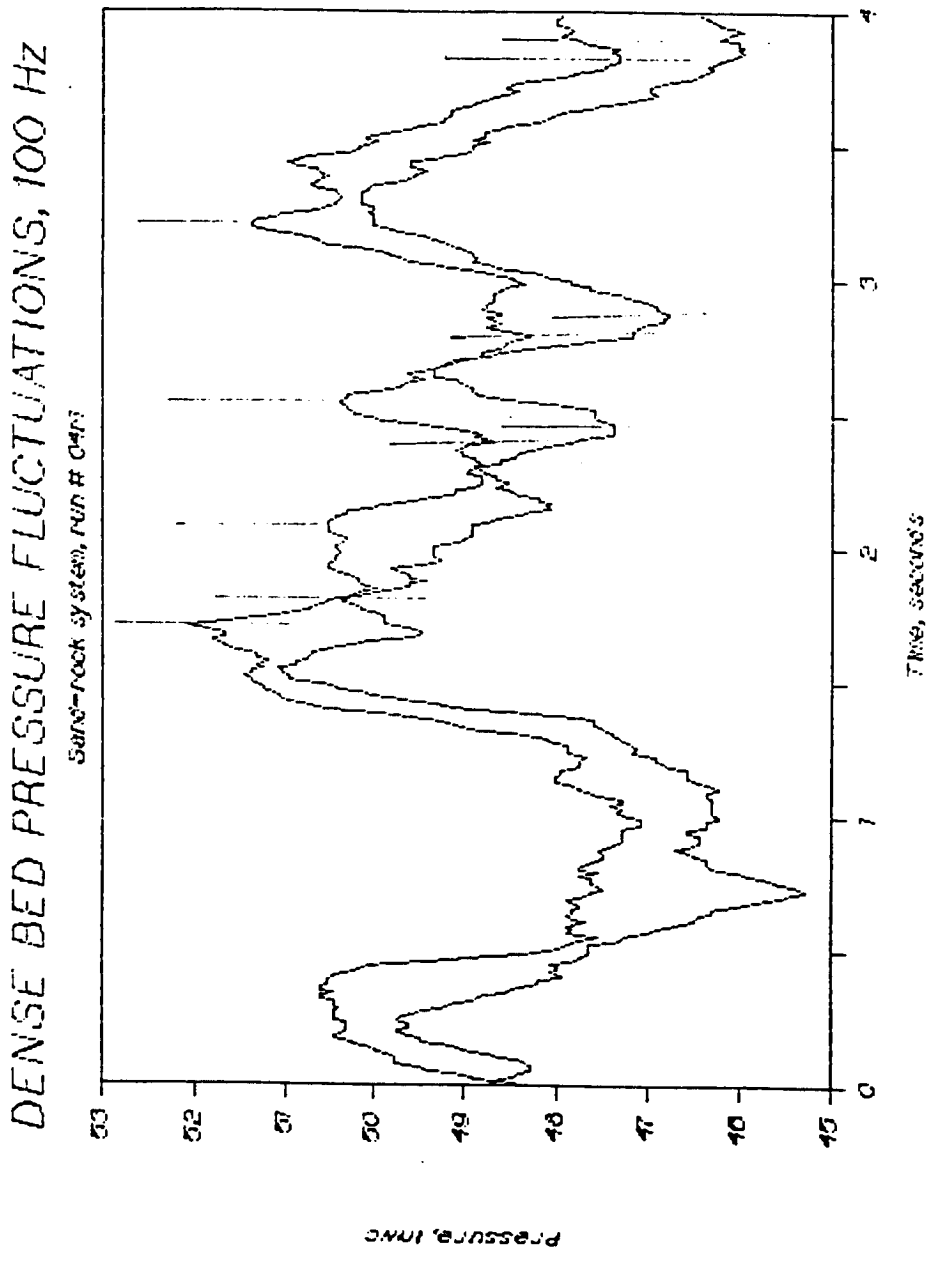

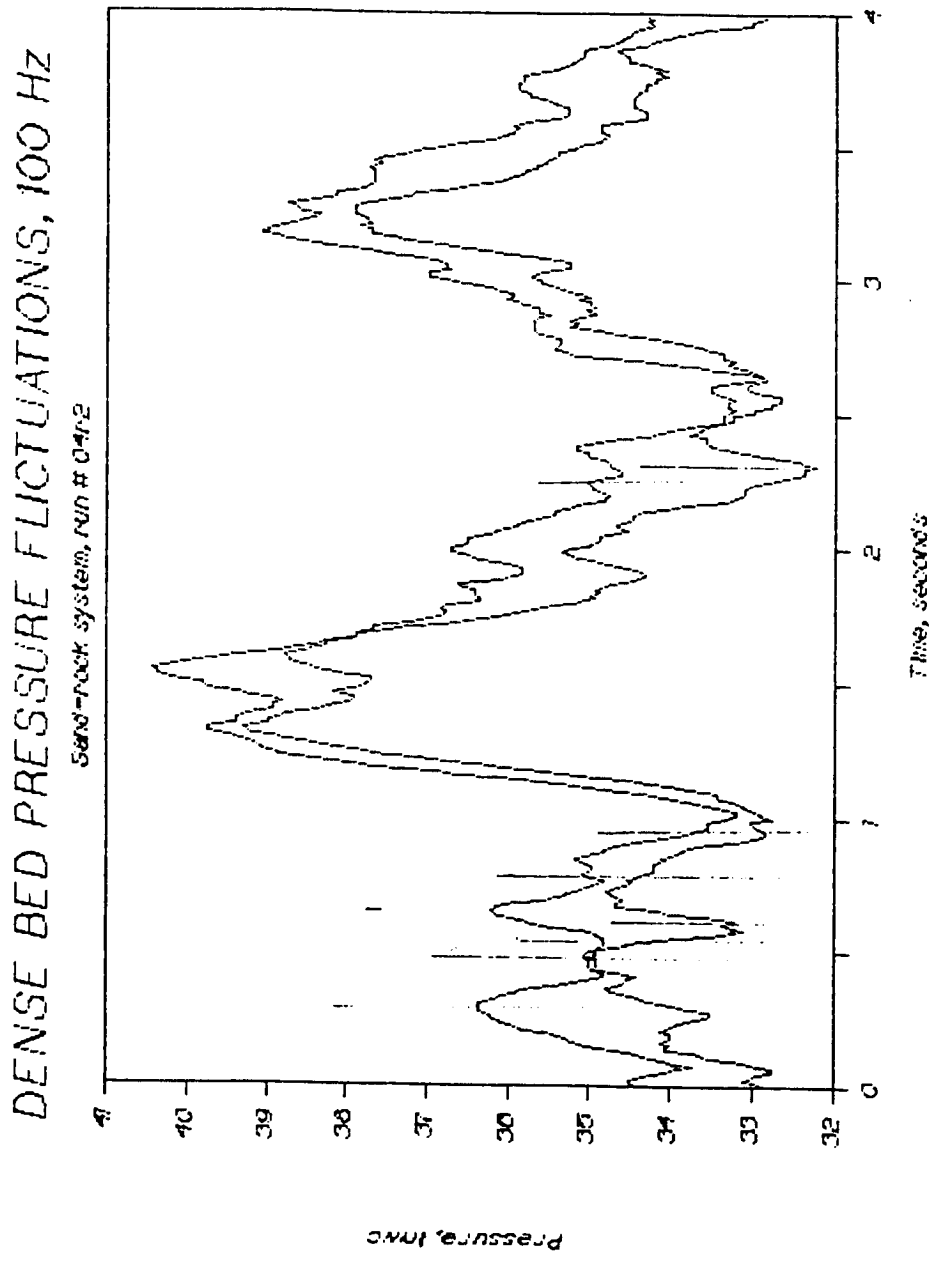

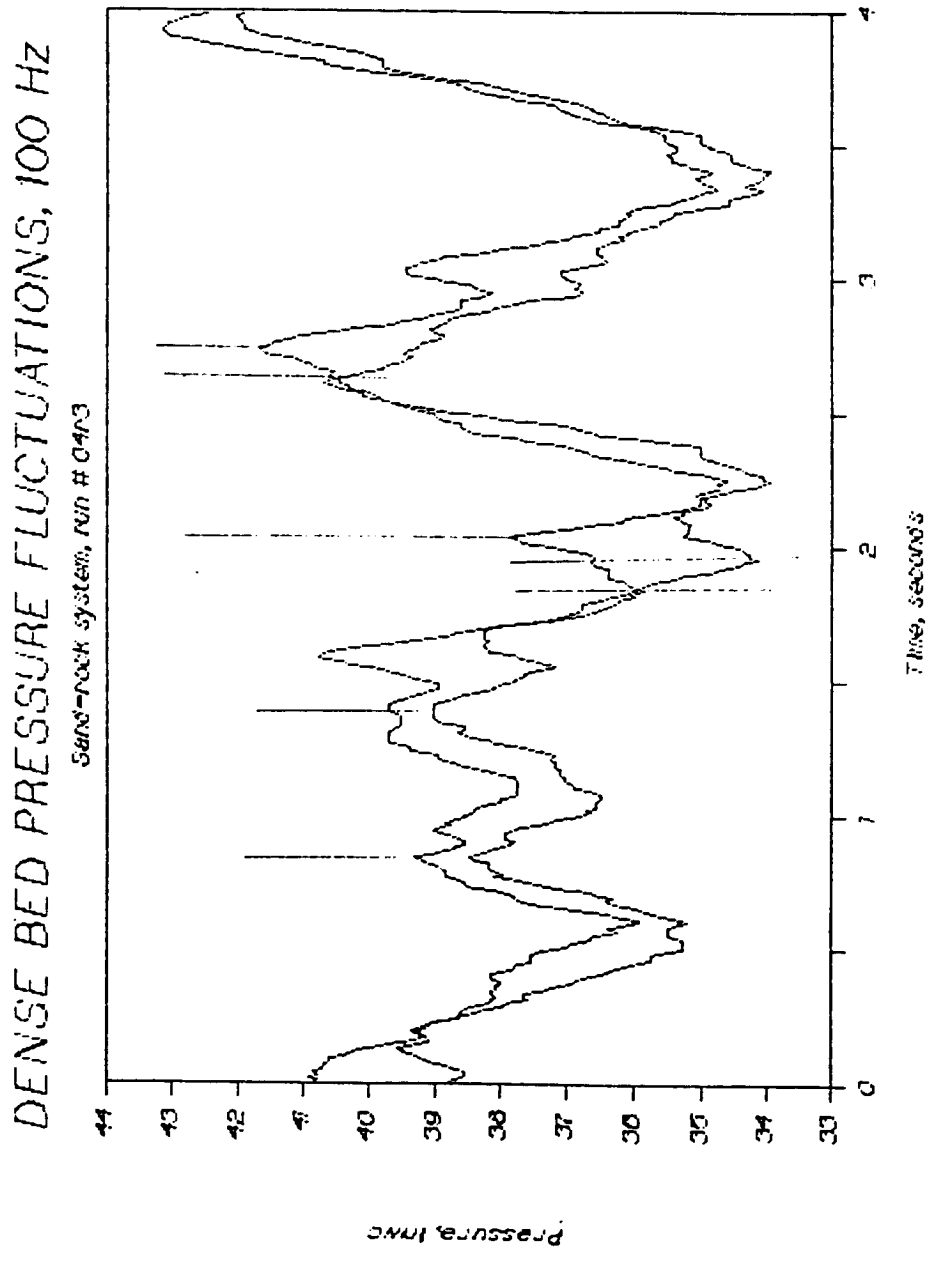

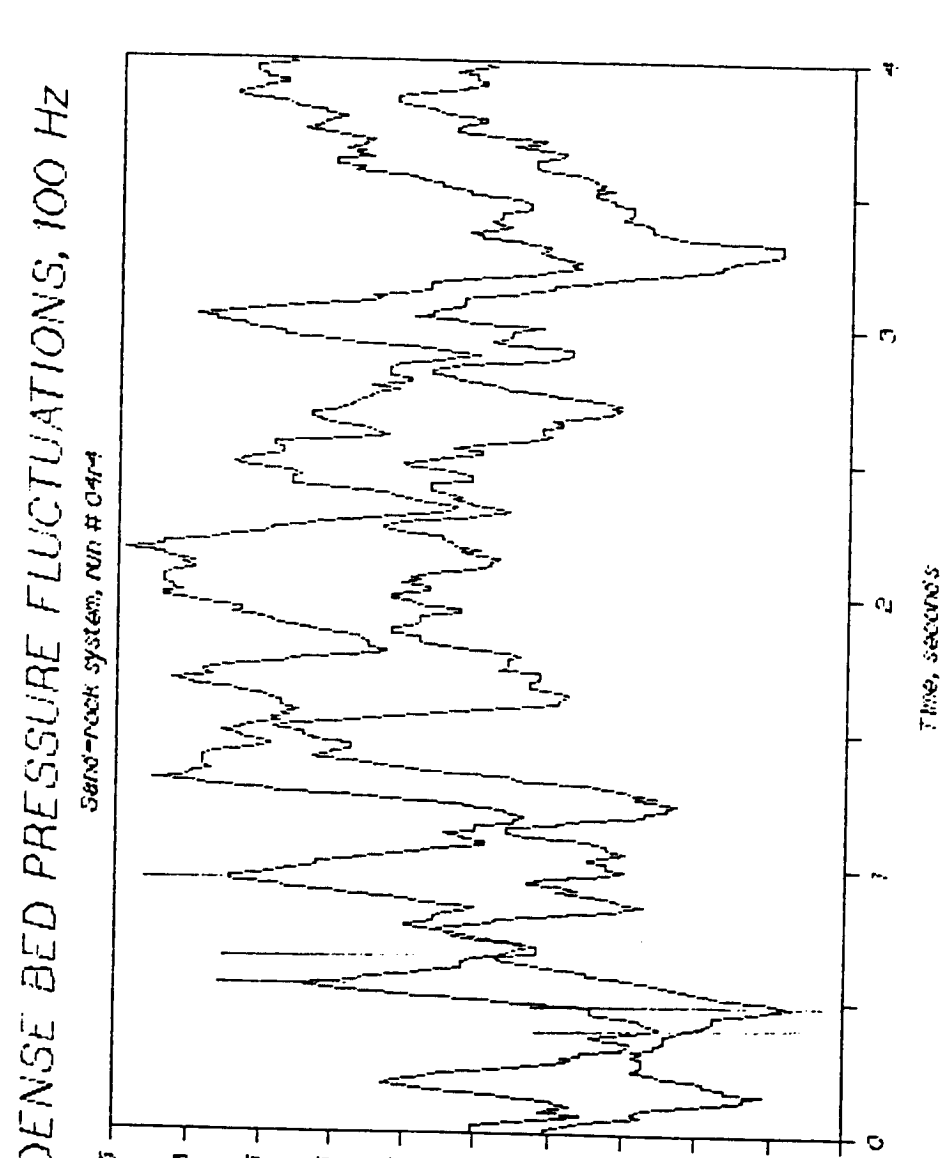

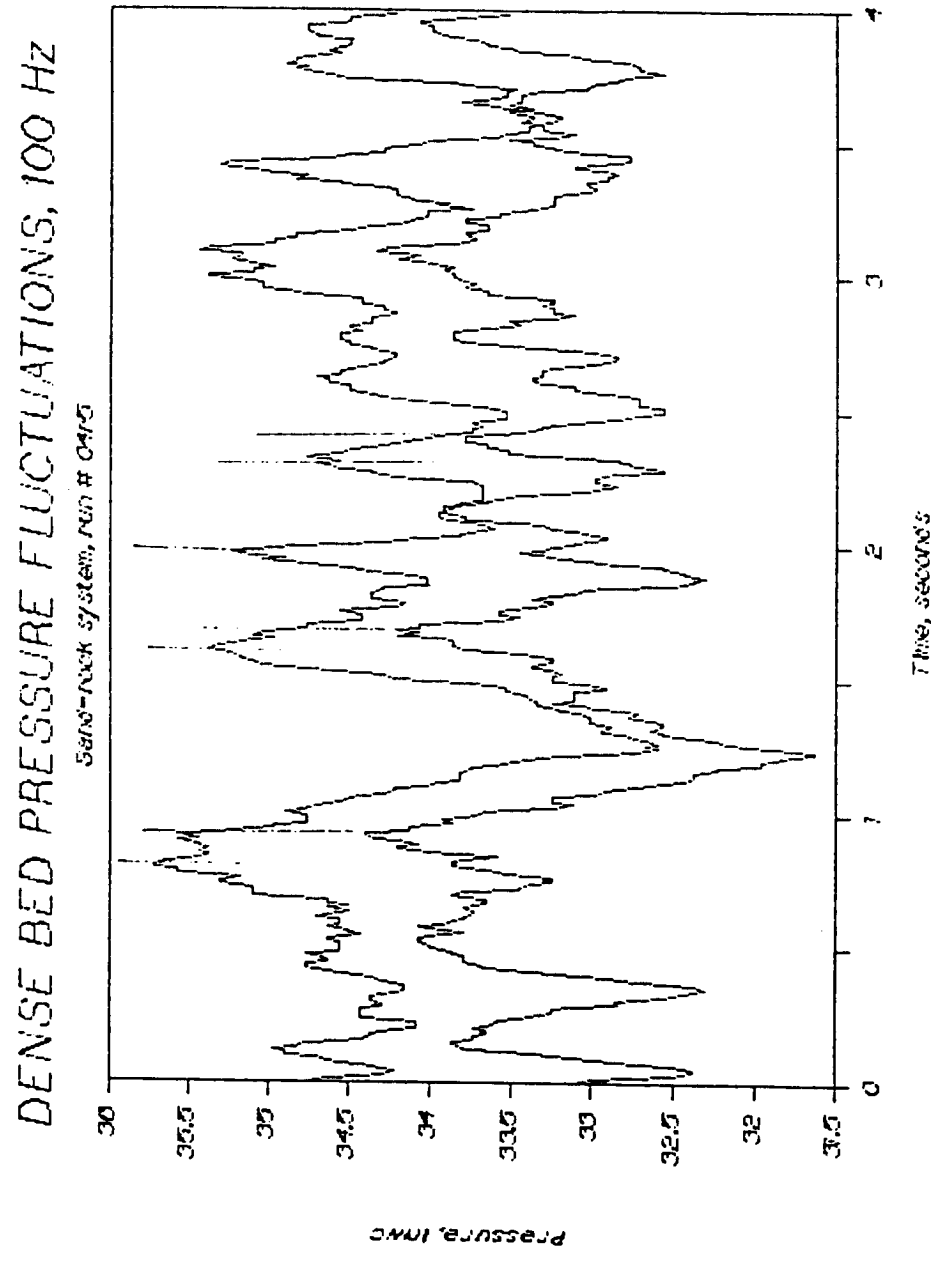

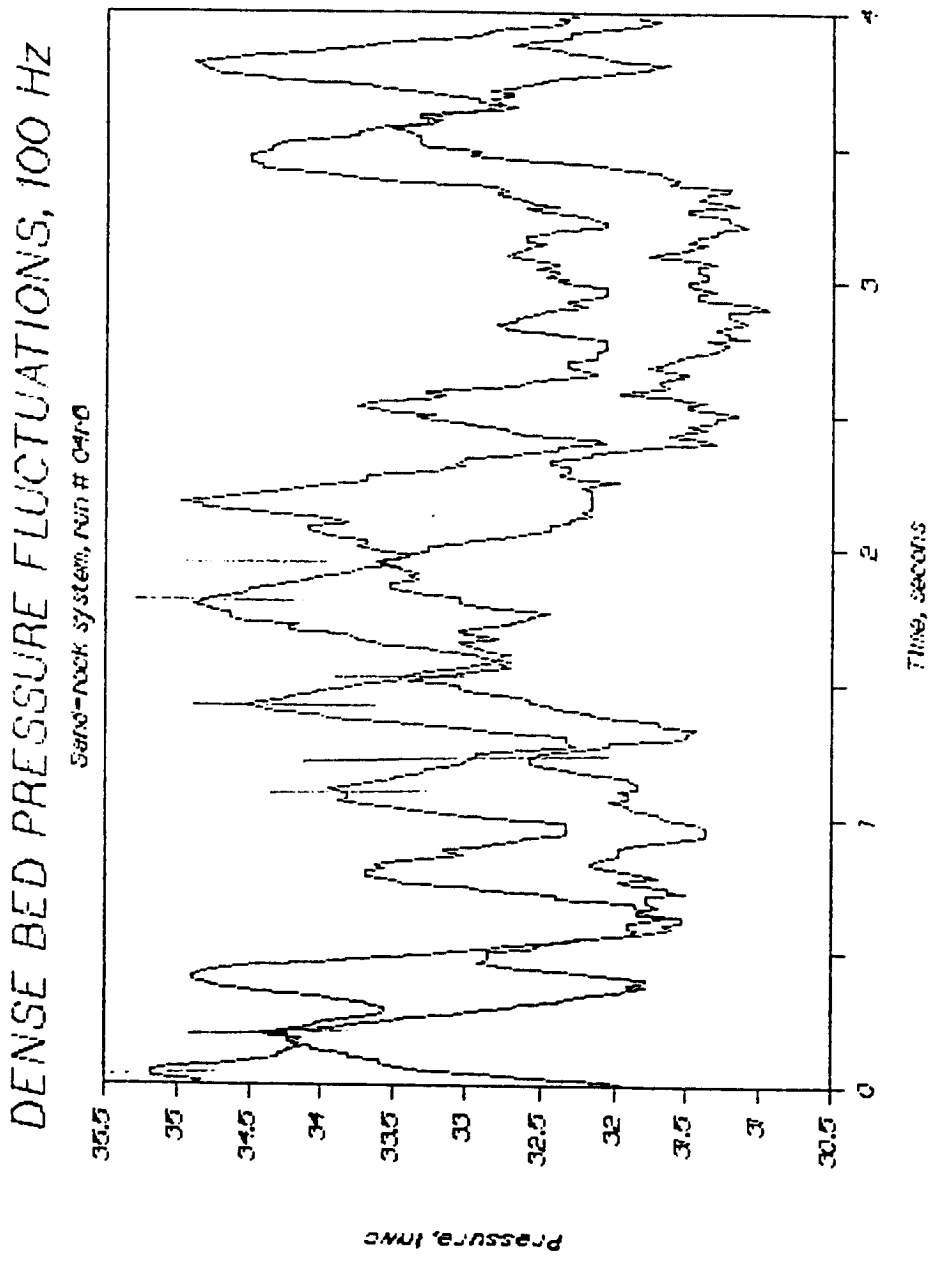

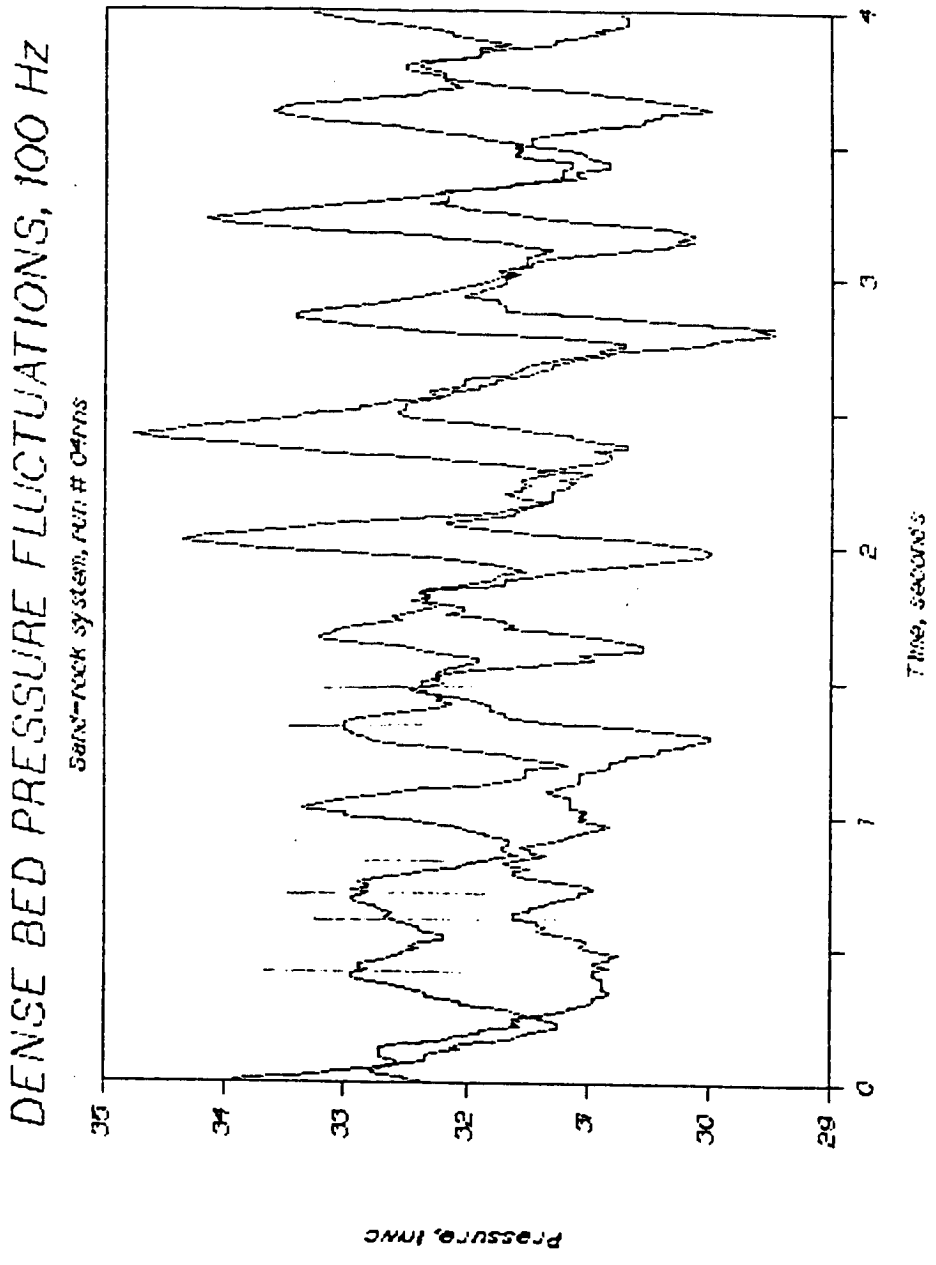

Bubble Data, Riley Stoker 0.229m (9",n.d.) Unit

Table B5: Copper-steel System Id. Key, Riley Stoker 0.229m Unit

Run Number	Serial Number,Table 5.9 in TEXT
07	1
09, 10	2
01, 12	3
13, 14	4
04	5
03	6
05	7
17, 18, 19, 20	8
06	9

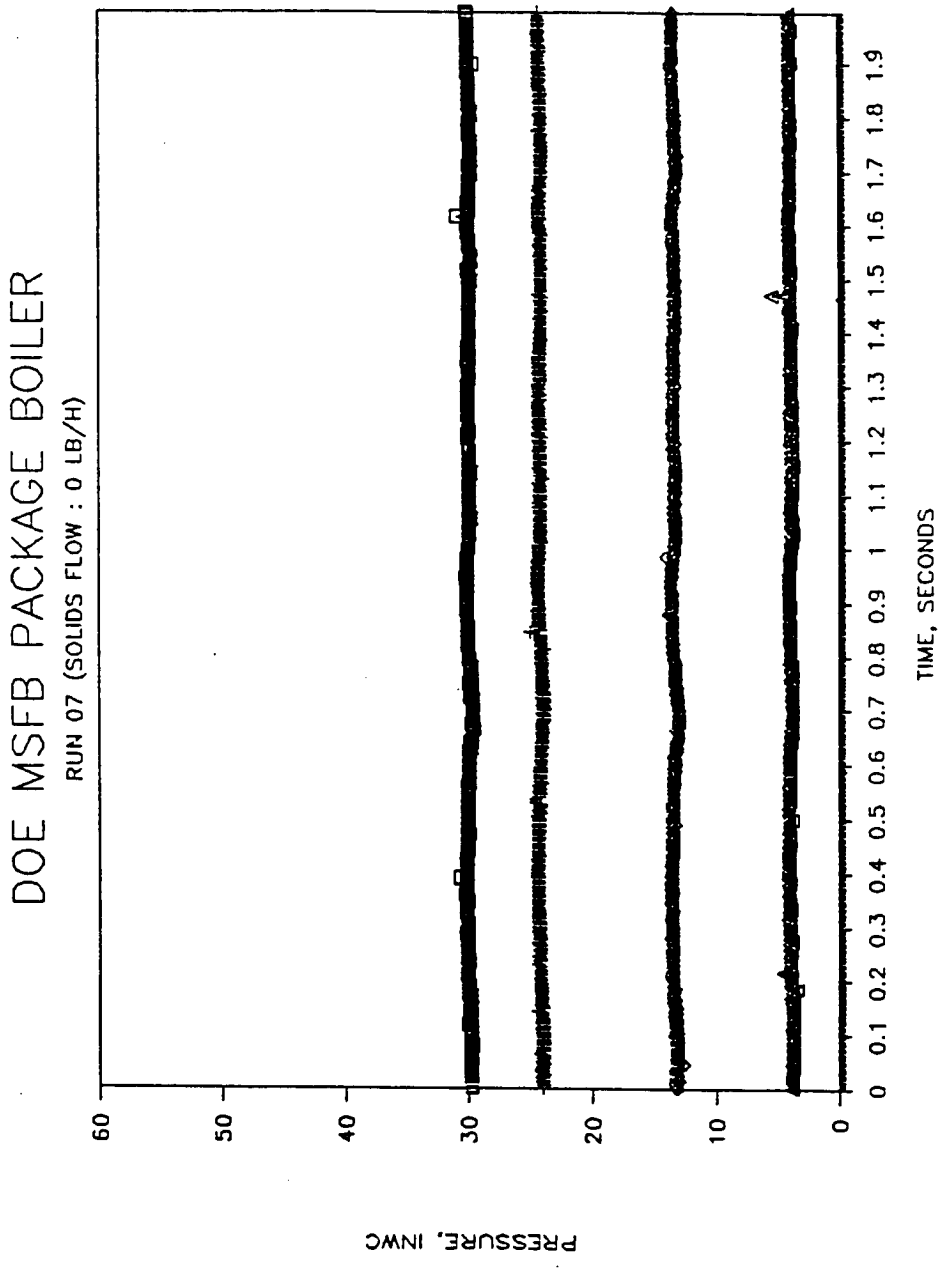

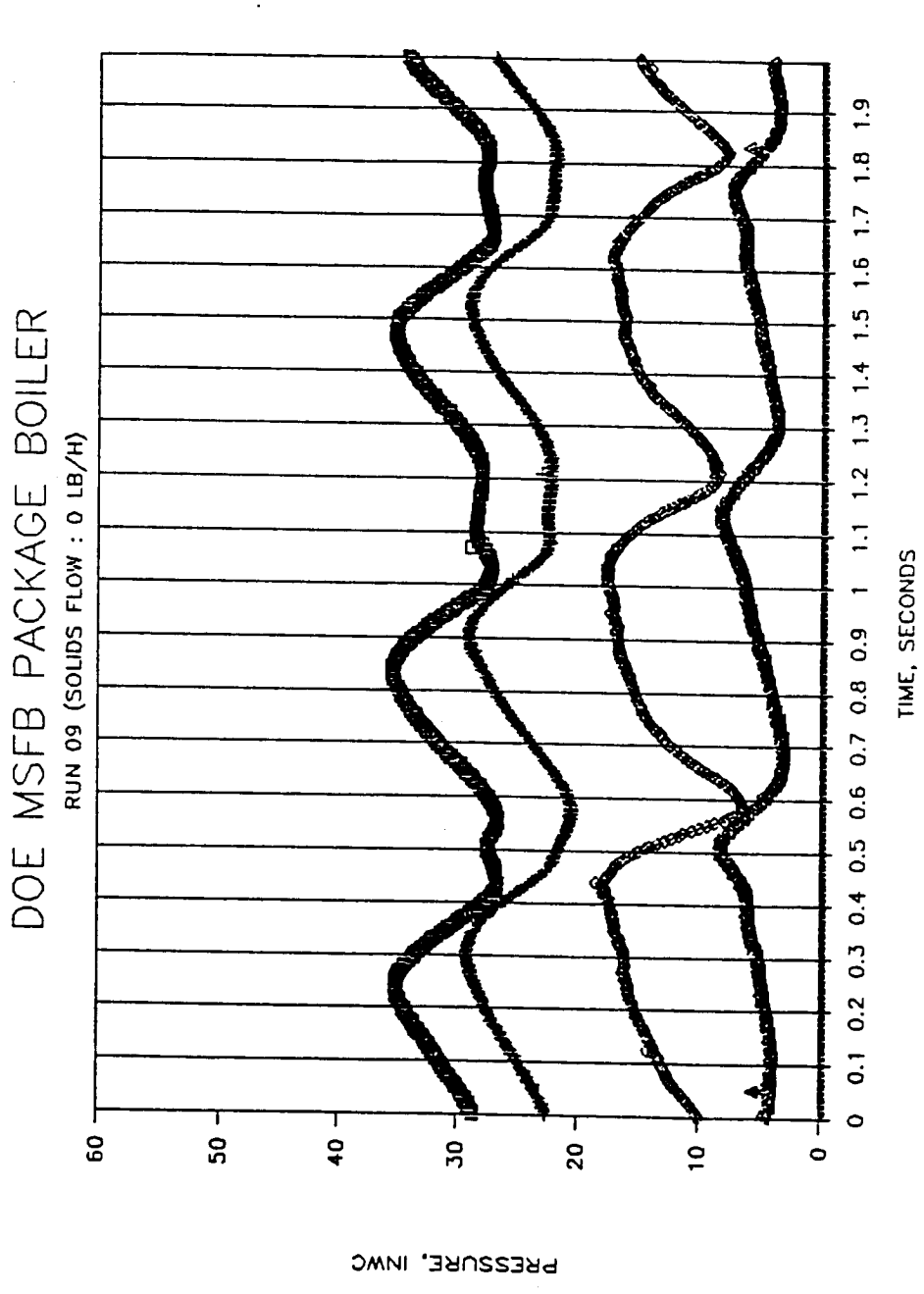

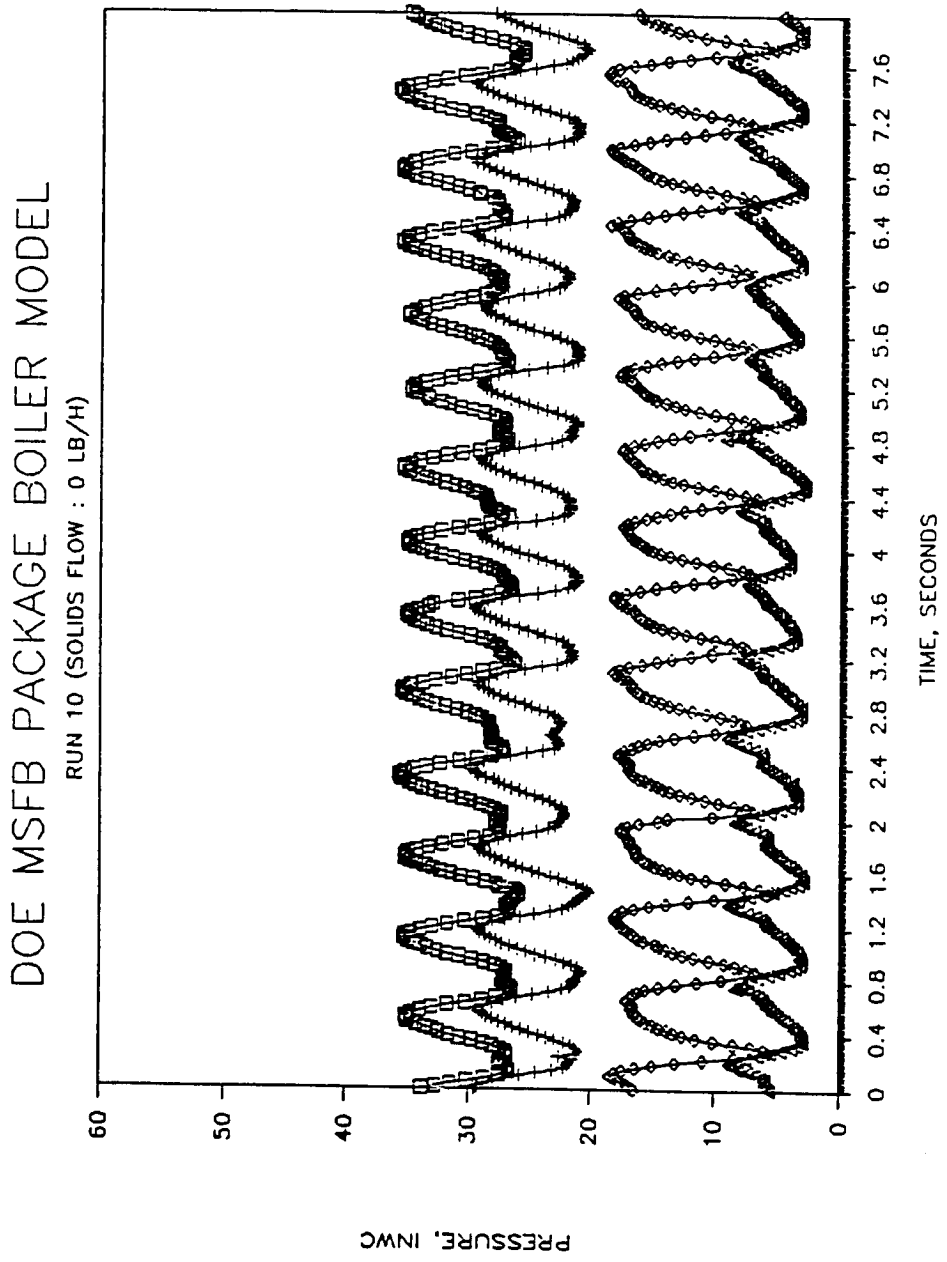

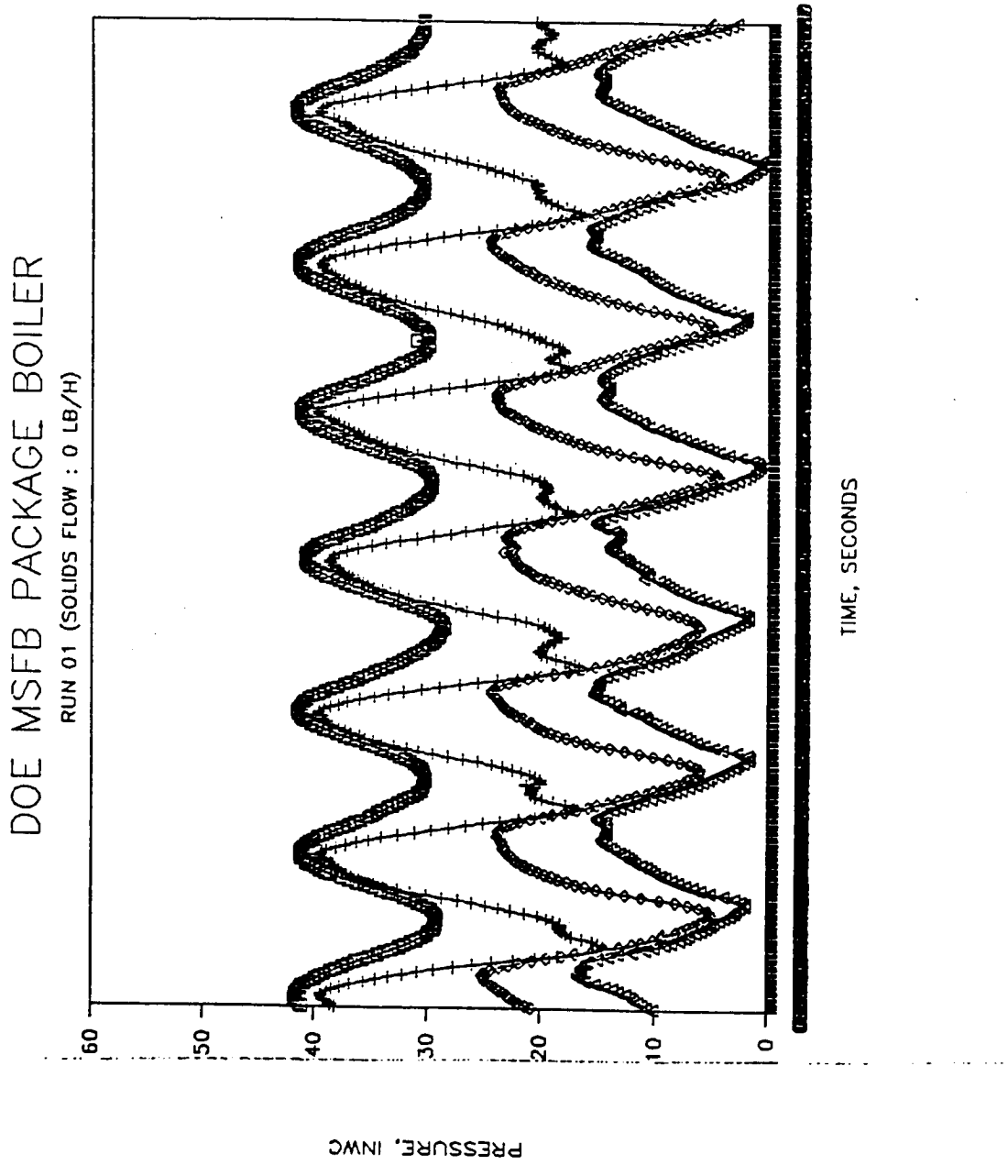

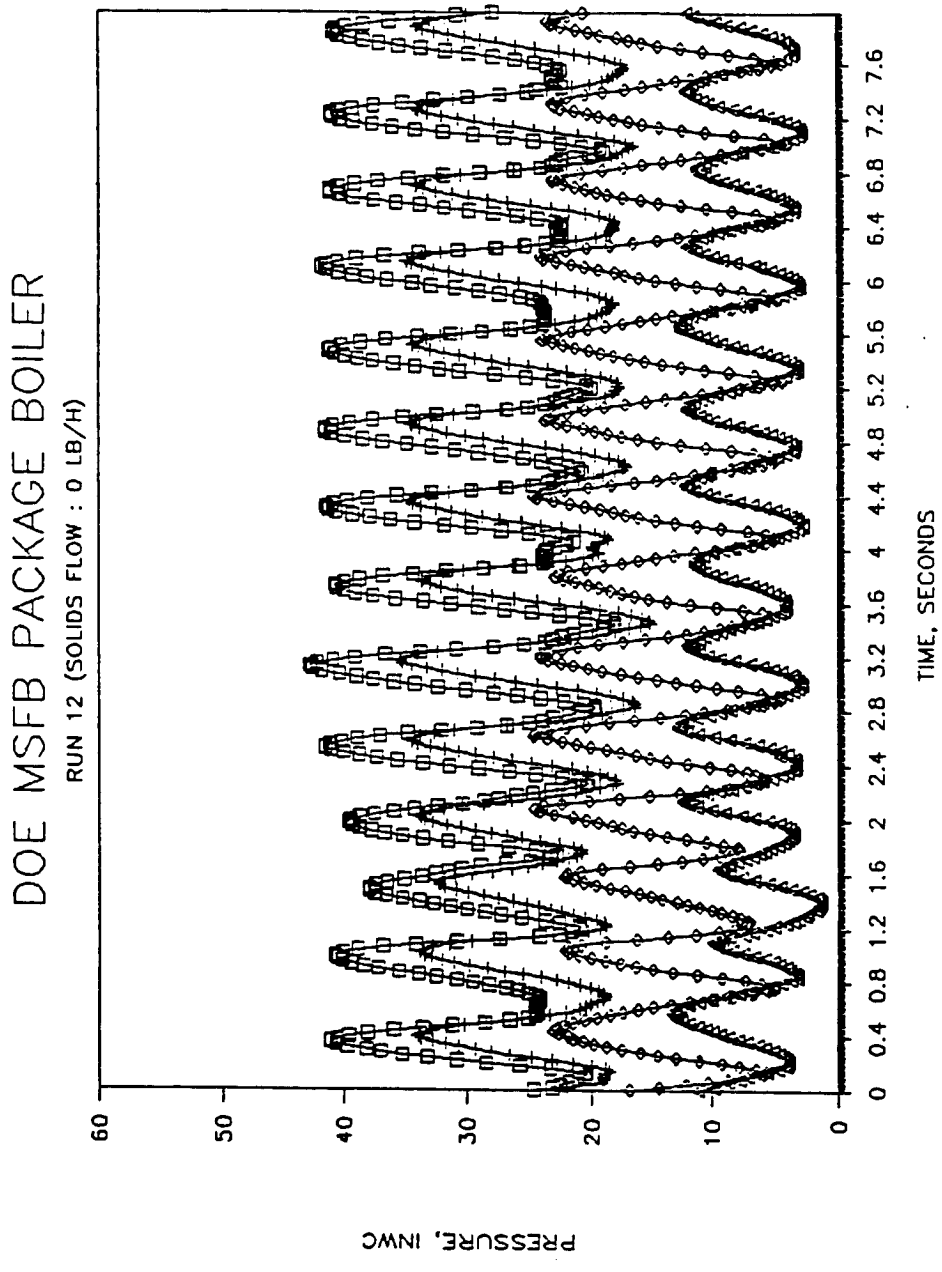

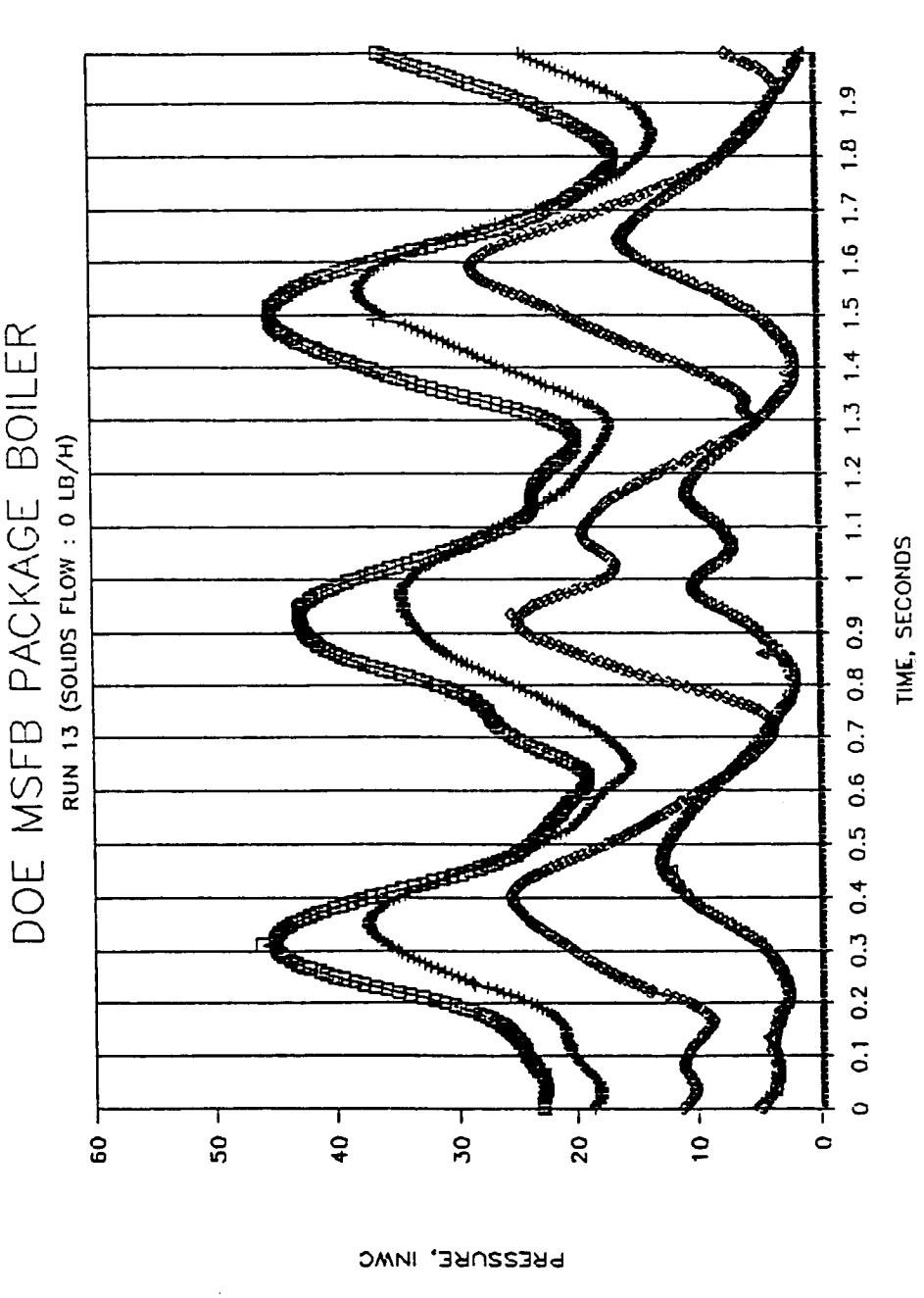

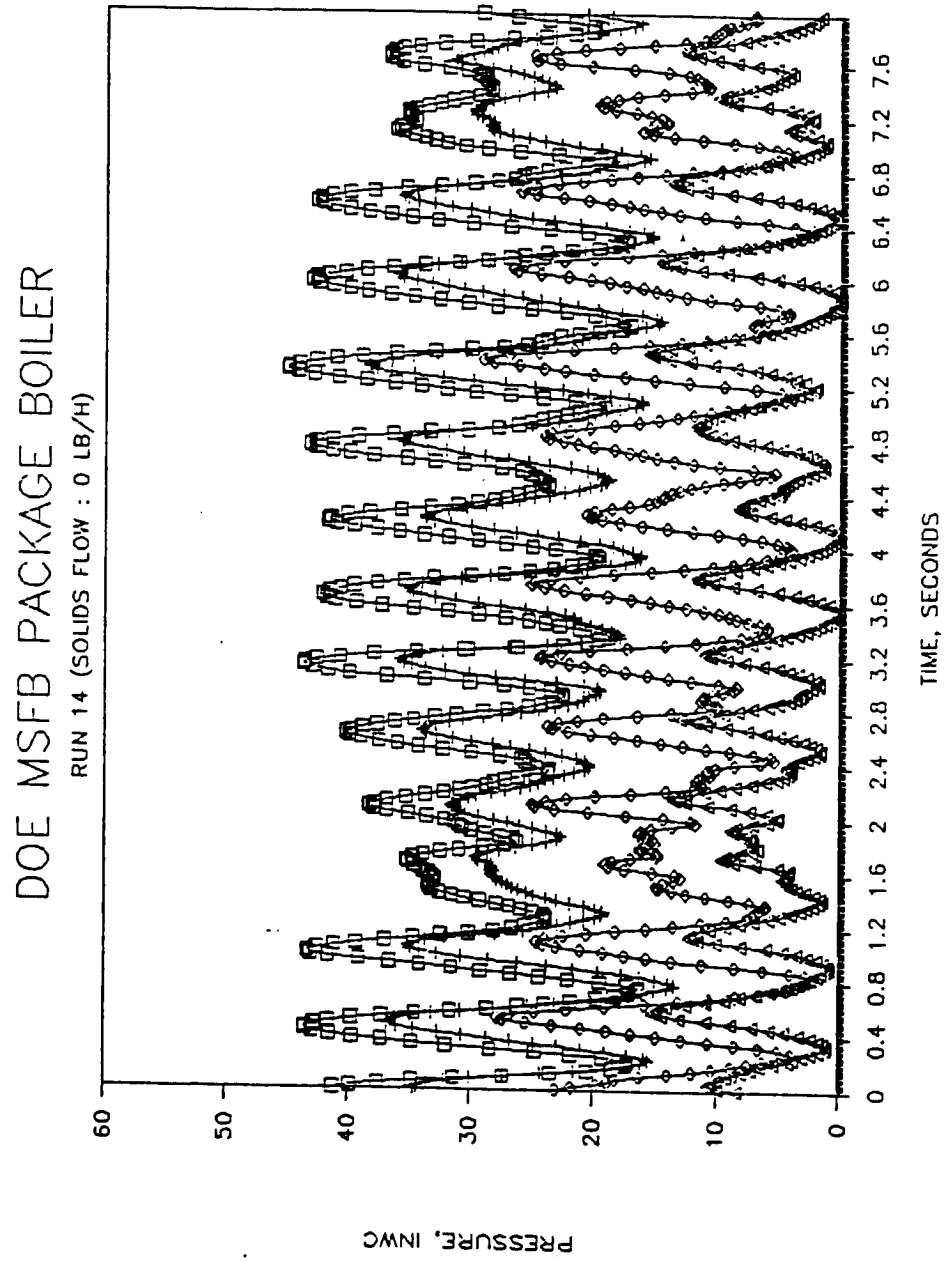

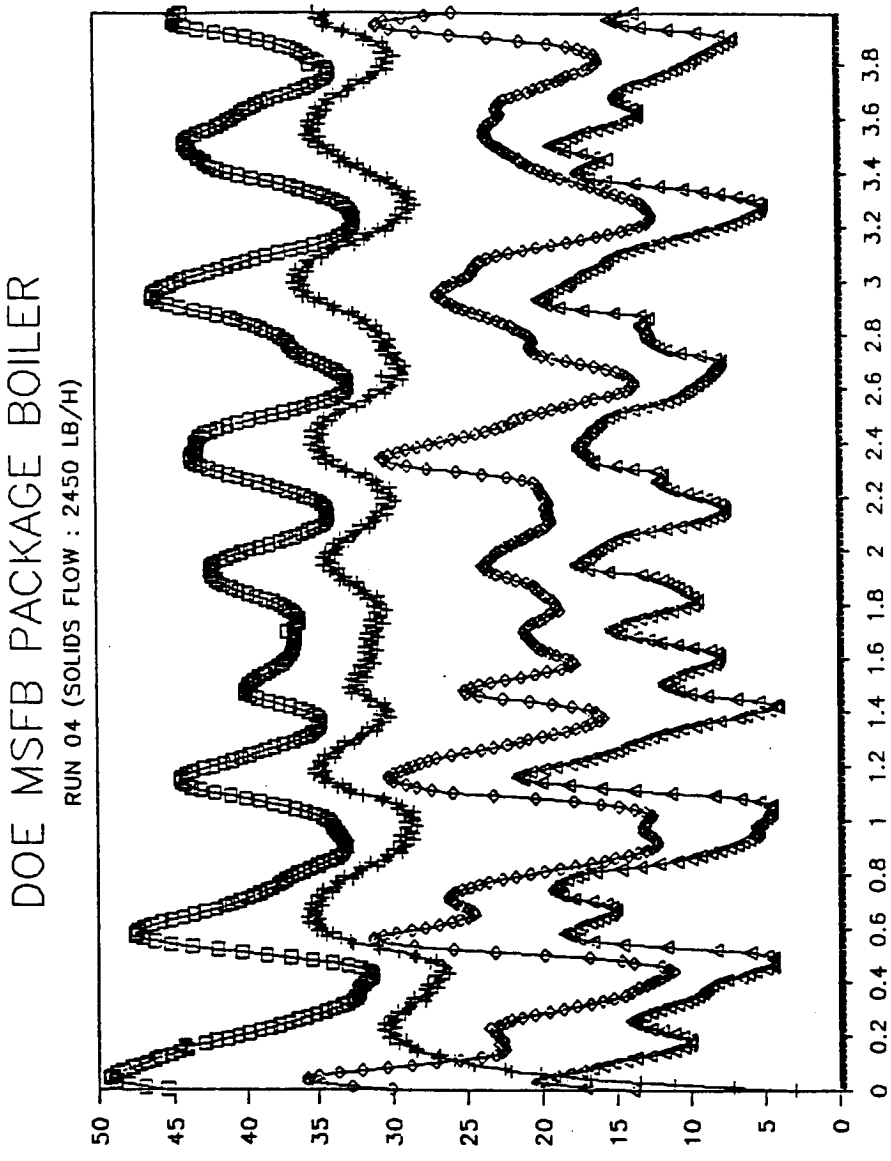

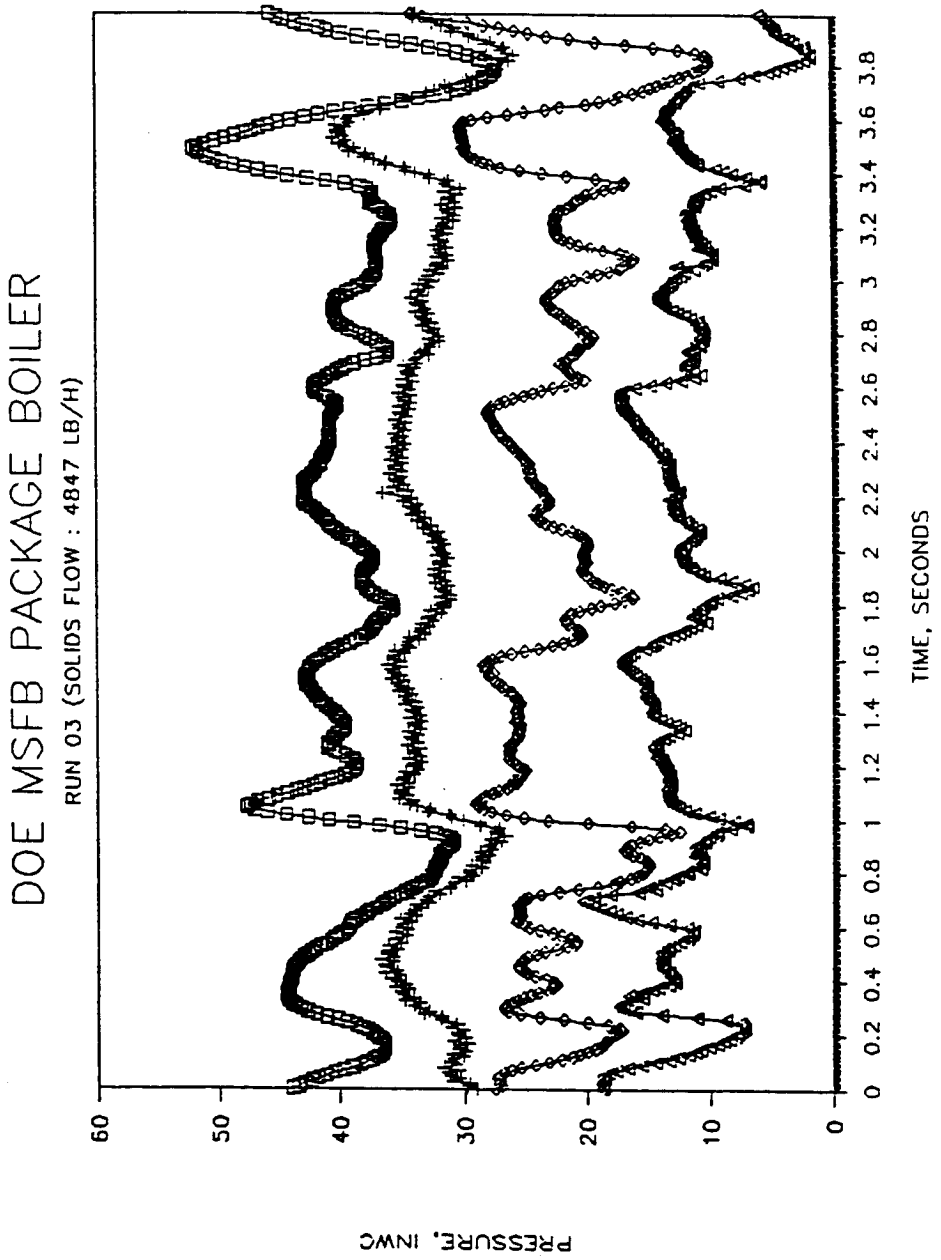

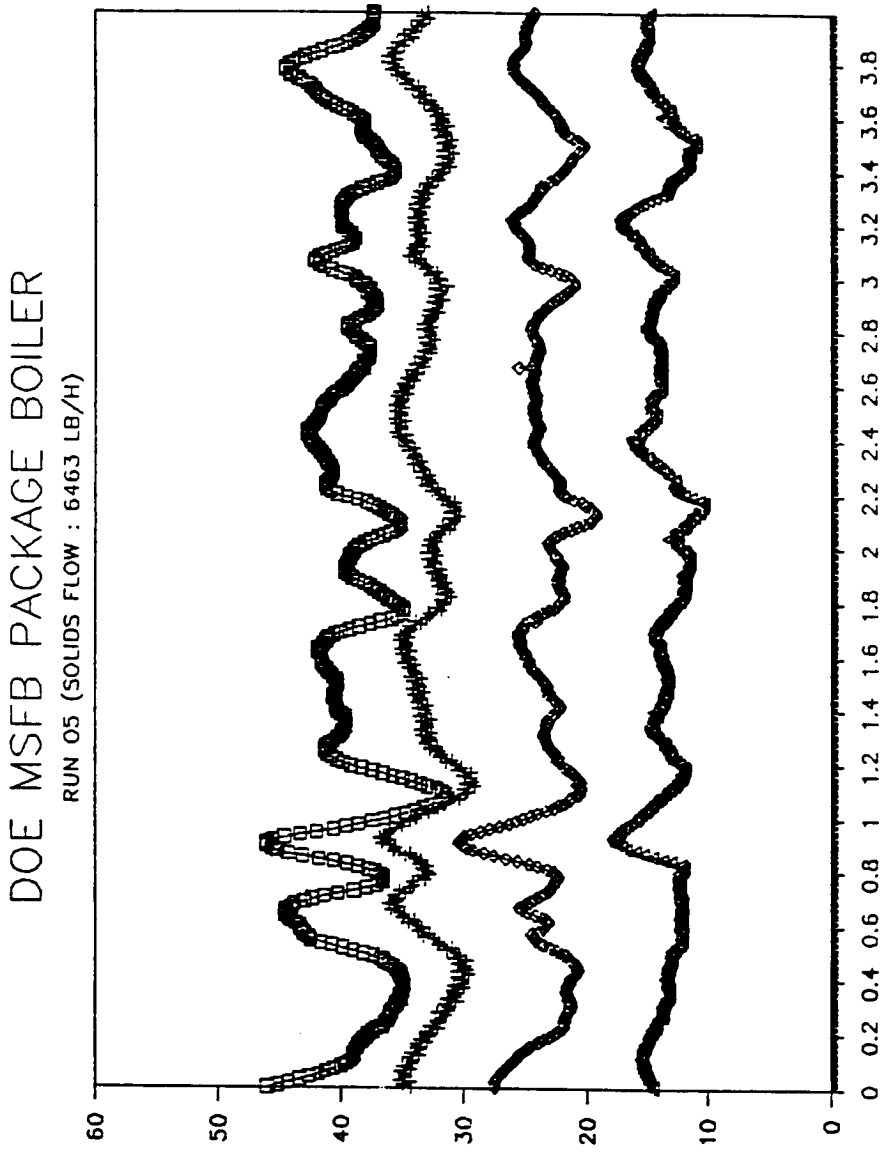

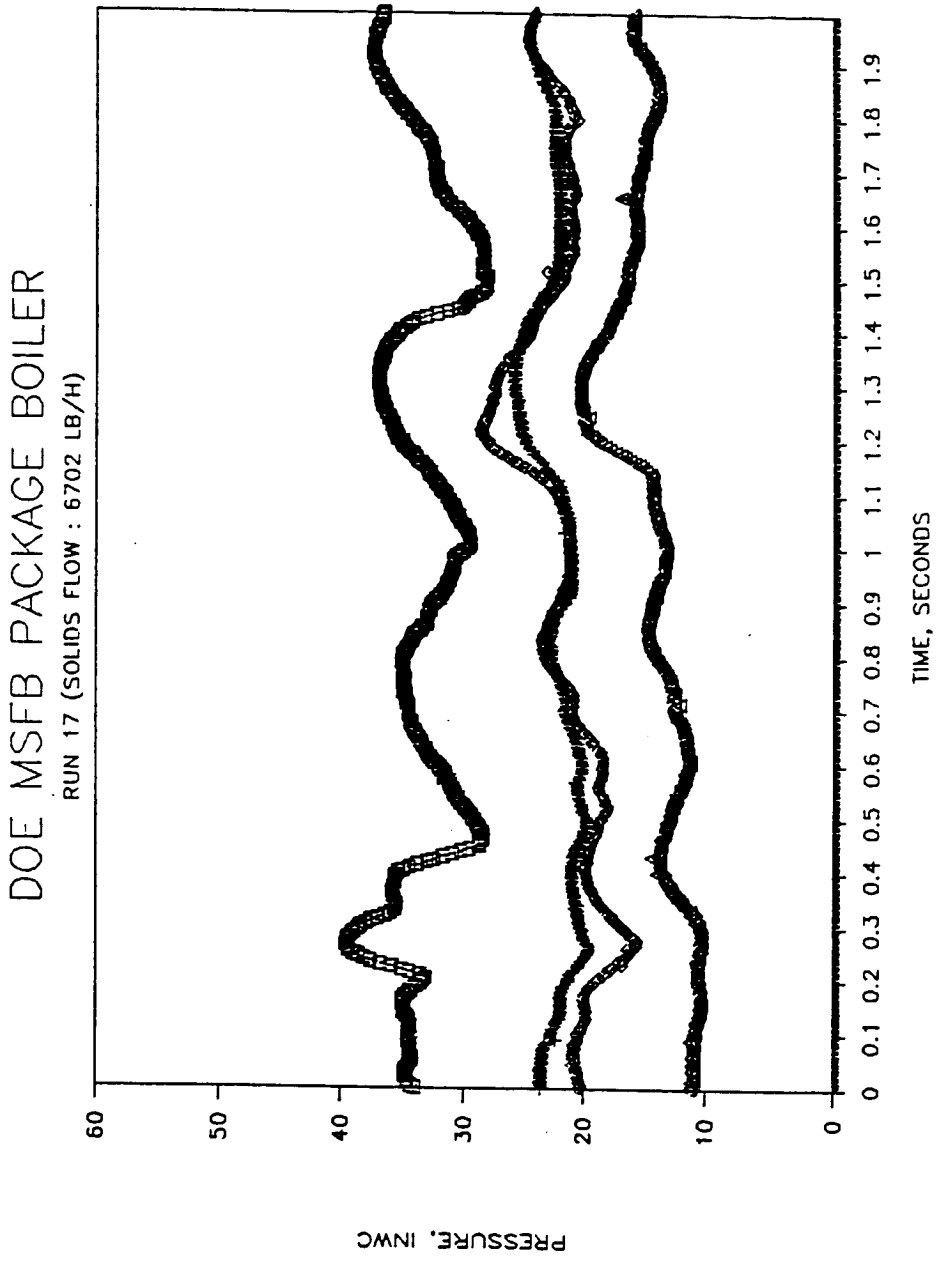

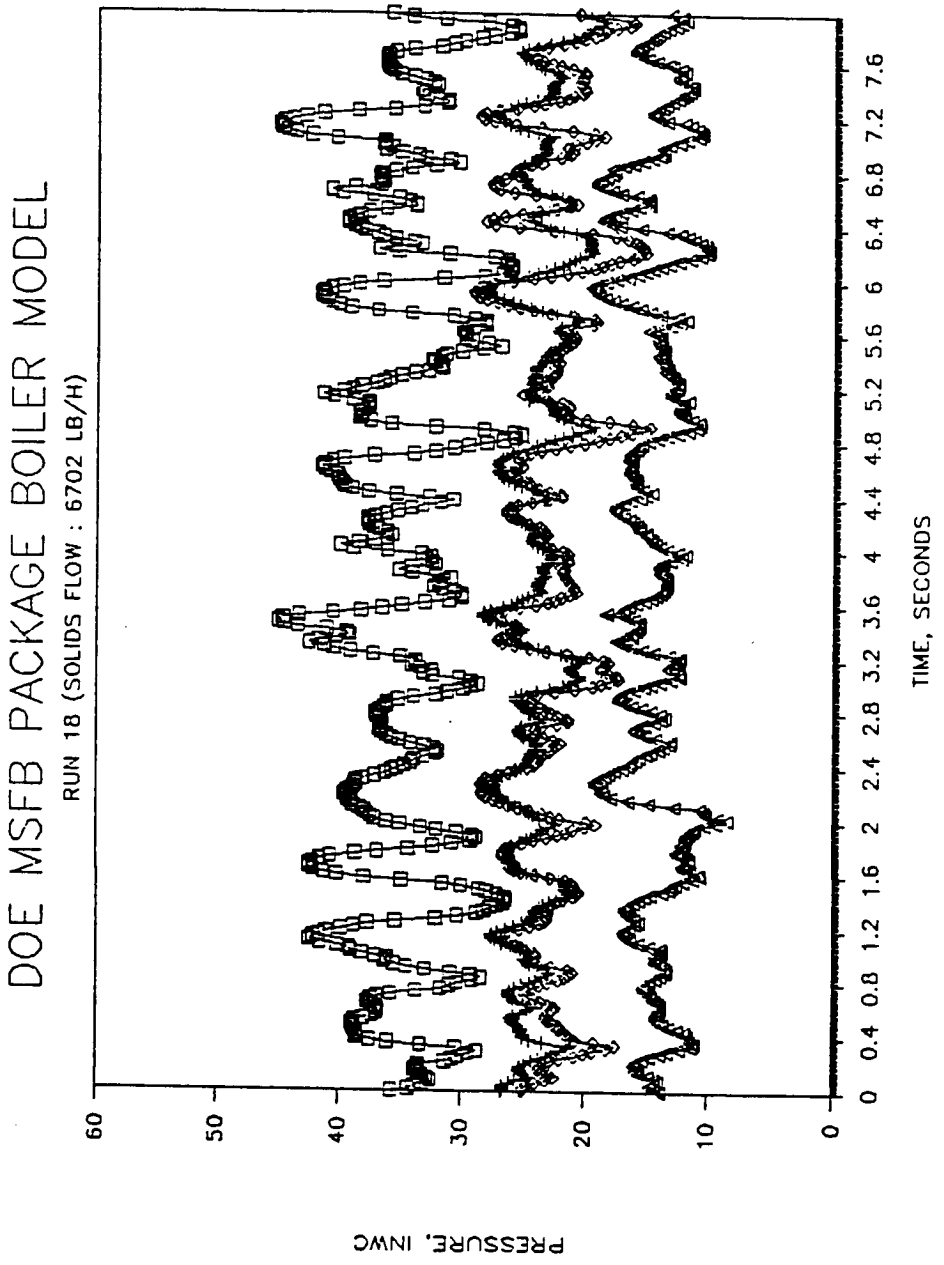

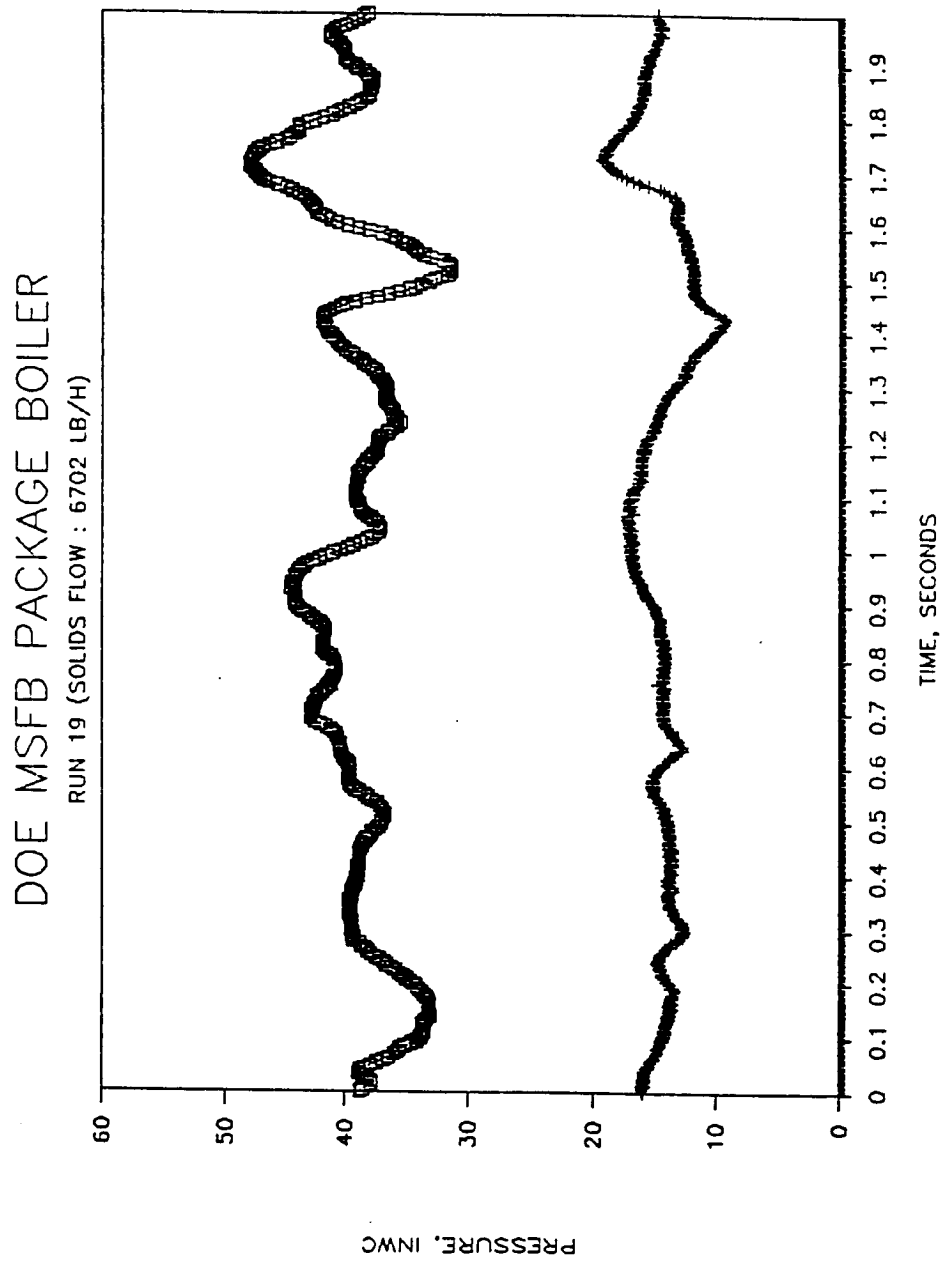

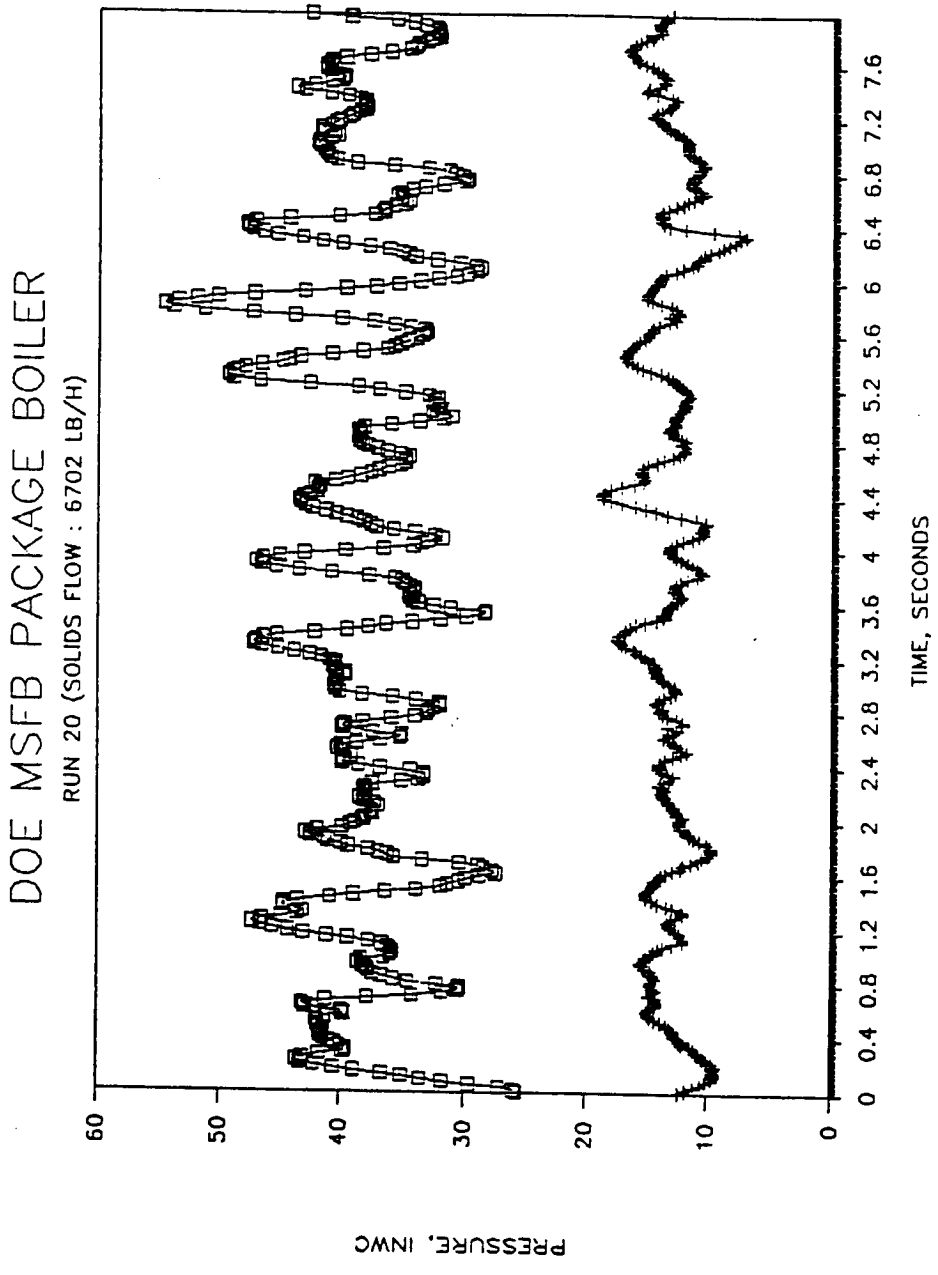

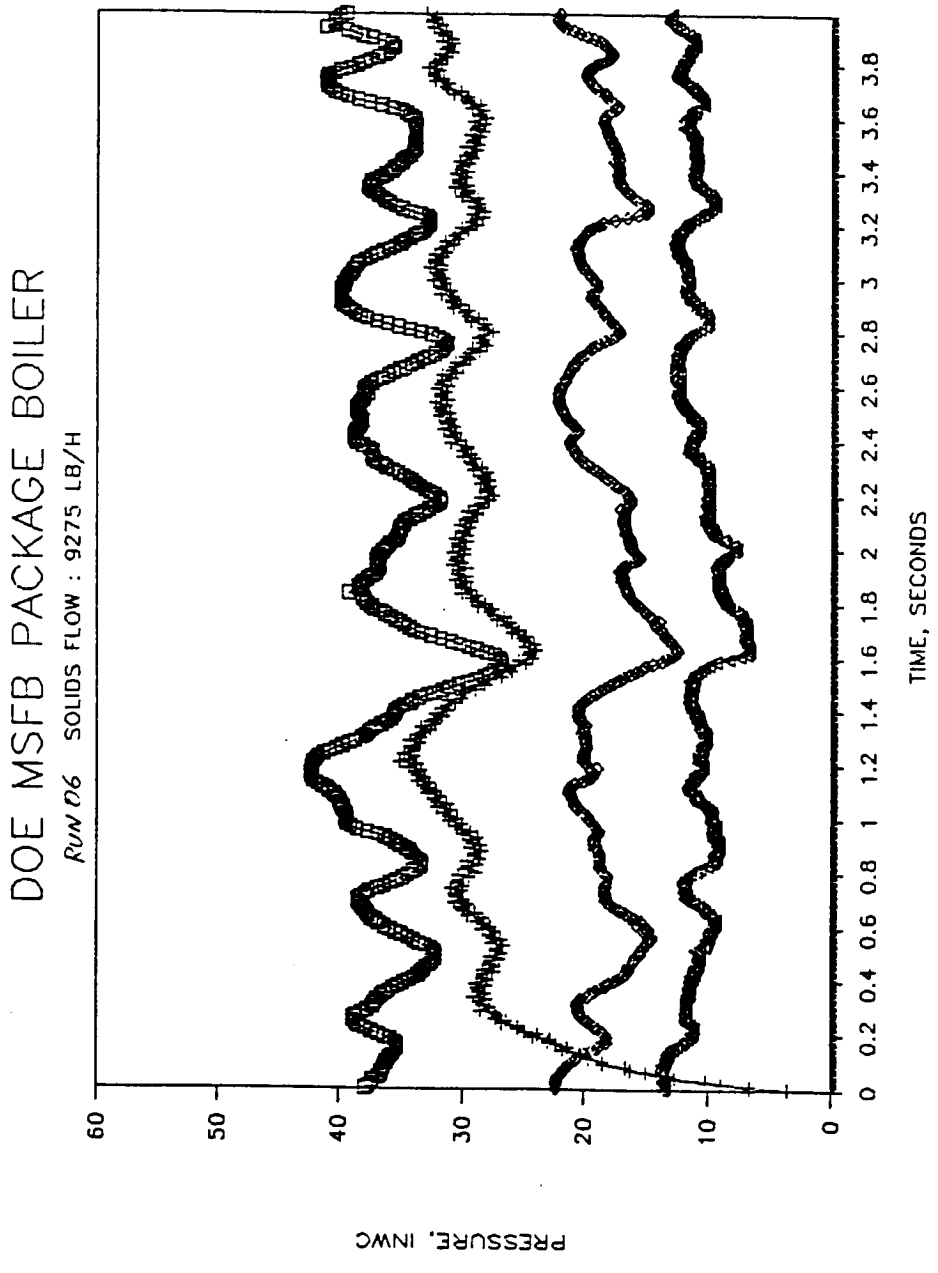

Table B6: Sand-rock System Id. Key, Riley Stoker 0.229m Unit

Run Number	Serial Number,Table 5.10 in TEXT
$0721S1$	2
$0721S2$	3
$0721S3$	4
$0721S4$	5
$0721NS$	1
$0725S1$	7
$0725S2$	8
$0725S3$	9
$0725NS3$	6

46 1510

46 1510

46 1510

APPENDIX C : SAMPLE CALCULATION FROM A PRESSURE TIME TRACE

Bubble Measurements

Distance between top and bottom probes: 6"

Bubble velocity:

$$U_b = \frac{6}{12 * \tau_m}$$

$$U_b = \frac{0.5}{\tau_m}$$

where U_b is the bubble velocity in ft/s and τ_m is the lag time in seconds.

Thus, referring to the figure in the following page,

$$U_b = \frac{0.5}{0.067}$$

$$U_b = 7.46$$

The 'pierced length of bubble', L_b, in feet, is thus the bubble rise velocity times the time it takes for the bubble to pass a single probe, τ. Mathematically,

$$L_b = U_b * \tau$$

$$L_b = 7.46 * 0.47$$

$$L_b = 3.5$$

APPENDIX D : AVERAGED PRESSURE-TIME TRACES , PRESSURE DROP STUDIES OF THE DENSE BED